

Performance Assessment of Passive Gaseous Provisions (PGAP)

*Report of the International Project on Innovative
Nuclear Reactors and Fuel Cycles (INPRO)*



IAEA

International Atomic Energy Agency

PERFORMANCE ASSESSMENT OF PASSIVE GASEOUS PROVISIONS (PGAP)

The following States are Members of the International Atomic Energy Agency:

AFGHANISTAN	GUATEMALA	PANAMA
ALBANIA	HAITI	PAPUA NEW GUINEA
ALGERIA	HOLY SEE	PARAGUAY
ANGOLA	HONDURAS	PERU
ARGENTINA	HUNGARY	PHILIPPINES
ARMENIA	ICELAND	POLAND
AUSTRALIA	INDIA	PORTUGAL
AUSTRIA	INDONESIA	QATAR
AZERBAIJAN	IRAN, ISLAMIC REPUBLIC OF	REPUBLIC OF MOLDOVA
BAHRAIN	IRAQ	ROMANIA
BANGLADESH	IRELAND	RUSSIAN FEDERATION
BELARUS	ISRAEL	RWANDA
BELGIUM	ITALY	SAUDI ARABIA
BELIZE	JAMAICA	SENEGAL
BENIN	JAPAN	SERBIA
BOLIVIA	JORDAN	SEYCHELLES
BOSNIA AND HERZEGOVINA	KAZAKHSTAN	SIERRA LEONE
BOTSWANA	KENYA	SINGAPORE
BRAZIL	KOREA, REPUBLIC OF	SLOVAKIA
BULGARIA	KUWAIT	SLOVENIA
BURKINA FASO	KYRGYZSTAN	SOUTH AFRICA
BURUNDI	LAO PEOPLE'S DEMOCRATIC REPUBLIC	SPAIN
CAMBODIA	LATVIA	SRI LANKA
CAMEROON	LEBANON	SUDAN
CANADA	LESOTHO	SWAZILAND
CENTRAL AFRICAN REPUBLIC	LIBERIA	SWEDEN
CHAD	LIBYA	SWITZERLAND
CHILE	LIECHTENSTEIN	SYRIAN ARAB REPUBLIC
CHINA	LITHUANIA	TAJIKISTAN
COLOMBIA	LUXEMBOURG	THAILAND
CONGO	MADAGASCAR	THE FORMER YUGOSLAV REPUBLIC OF MACEDONIA
COSTA RICA	MALAWI	TOGO
CÔTE D'IVOIRE	MALAYSIA	TRINIDAD AND TOBAGO
CROATIA	MALI	TUNISIA
CUBA	MALTA	TURKEY
CYPRUS	MARSHALL ISLANDS	UGANDA
CZECH REPUBLIC	MAURITANIA	UKRAINE
DEMOCRATIC REPUBLIC OF THE CONGO	MAURITIUS	UNITED ARAB EMIRATES
DENMARK	MEXICO	UNITED KINGDOM OF GREAT BRITAIN AND NORTHERN IRELAND
DOMINICA	MONACO	UNITED REPUBLIC OF TANZANIA
DOMINICAN REPUBLIC	MONGOLIA	UNITED STATES OF AMERICA
ECUADOR	MONTENEGRO	URUGUAY
EGYPT	MOROCCO	UZBEKISTAN
EL SALVADOR	MOZAMBIQUE	VENEZUELA
ERITREA	MYANMAR	VIETNAM
ESTONIA	NAMIBIA	YEMEN
ETHIOPIA	NEPAL	ZAMBIA
FIJI	NETHERLANDS	ZIMBABWE
FINLAND	NEW ZEALAND	
FRANCE	NICARAGUA	
GABON	NIGER	
GEORGIA	NIGERIA	
GERMANY	NORWAY	
GHANA	OMAN	
GREECE	PAKISTAN	
	PALAU	

The Agency's Statute was approved on 23 October 1956 by the Conference on the Statute of the IAEA held at United Nations Headquarters, New York; it entered into force on 29 July 1957. The Headquarters of the Agency are situated in Vienna. Its principal objective is "to accelerate and enlarge the contribution of atomic energy to peace, health and prosperity throughout the world".

PERFORMANCE ASSESSMENT OF PASSIVE GASEOUS PROVISIONS (PGAP)

REPORT OF THE INTERNATIONAL PROJECT ON INNOVATIVE
NUCLEAR REACTORS AND FUEL CYCLES (INPRO)

COPYRIGHT NOTICE

All IAEA scientific and technical publications are protected by the terms of the Universal Copyright Convention as adopted in 1952 (Berne) and as revised in 1972 (Paris). The copyright has since been extended by the World Intellectual Property Organization (Geneva) to include electronic and virtual intellectual property. Permission to use whole or parts of texts contained in IAEA publications in printed or electronic form must be obtained and is usually subject to royalty agreements. Proposals for non-commercial reproductions and translations are welcomed and considered on a case-by-case basis. Enquiries should be addressed to the IAEA Publishing Section at:

Marketing and Sales Unit, Publishing Section
International Atomic Energy Agency
Vienna International Centre
PO Box 100
1400 Vienna, Austria
fax: +43 1 2600 29302
tel.: +43 1 2600 22417
email: sales.publications@iaea.org
<http://www.iaea.org/books>

For further information on this publication, please contact:

INPRO Group
International Atomic Energy Agency
Vienna International Centre
PO Box 100
1400 Vienna, Austria
Email: Official.Mail@iaea.org

© IAEA, 2013
Printed by the IAEA in Austria
July 2013

IAEA Library Cataloguing in Publication Data

Performance assessment of passive gaseous provisions (PGAP)

– Vienna : International Atomic Energy Agency, 2013.

p. ; 30 cm. – (IAEA-TECDOC series, ISSN 1011-4289 ; no. 1698)

ISBN 978-92-0-139010-3

Includes bibliographical references.

1. Nuclear engineering – Congresses. 2. Nuclear power plants – Design and construction – Congresses. 3. Nuclear reactors – Cooling – Computer simulation. I. International Atomic Energy Agency. II. Series.

FOREWORD

The International Project on Innovative Nuclear Reactors and Fuel Cycles (INPRO) was launched in 2000 on the basis of IAEA General Conference resolution GC(44)/RES/21. INPRO helps to ensure the availability of sustainable nuclear energy in the 21st century and seeks to bring together all interested Member States — both technology holders and technology users — to consider joint actions to achieve desired innovations.

To contribute to an international consensus on the definition of the reliability of passive systems that involve natural circulation, and on a methodology to assess this reliability, INPRO initiated a collaborative project on Performance Assessment of Passive Gaseous Provisions (PGAP) in 2007.

Advanced nuclear reactor designs incorporate several passive systems in addition to active ones, not only to enhance the operational safety of the reactors but also to mitigate the consequences of a severe accident should one occur. However, the reliability of passive safety systems is crucial and must be assessed before they are used extensively in future nuclear power plants. Several physical parameters affect the performance of a passive safety system, and their values at the time of operation are a priori unknown. The functions of many passive systems are based on thermohydraulic principles, which until recently were considered as not being subject to any kind of failure. Hence, large and consistent efforts are required to quantify the reliability of such systems.

Three participants from three INPRO Member States were involved in this collaborative project. Reliability methods for passive systems (RMPS) and assessment of passive system reliability (APSRA) methodologies were used by the participants to assess the performance and reliability of the passive decay heat removal system of the French gas cooled fast reactor design for station blackout and a loss of coolant accident combined with loss of off-site power, respectively. This publication presents the results and conclusions of this collaborative project and suggests further R&D activities.

The IAEA officers responsible for this publication were F. Lignini, H. Khartabil and K. Qureshi of the Division of Nuclear Power.

EDITORIAL NOTE

This publication (including the figures, tables and references) has undergone only the minimum copy editing considered necessary for the reader's assistance.

The views expressed do not necessarily reflect those of the IAEA, the governments of the nominating Member States or the nominating organizations.

The use of particular designations of countries or territories does not imply any judgement by the publisher, the IAEA, as to the legal status of such countries or territories, of their authorities and institutions or of the delimitation of their boundaries.

The mention of names of specific companies or products (whether or not indicated as registered) does not imply any intention to infringe proprietary rights, nor should it be construed as an endorsement or recommendation on the part of the IAEA.

The authors are responsible for having obtained the necessary permission for the IAEA to reproduce, translate or use material from sources already protected by copyrights.

The IAEA has no responsibility for the persistence or accuracy of URLs for external or third party Internet web sites referred to in this book and does not guarantee that any content on such web sites is, or will remain, accurate or appropriate.

CONTENTS

1.	INTRODUCTION.....	1
1.1.	Scope	2
2.	OBJECTIVES.....	3
3.	DESCRIPTION OF RELIABILITY EVALUATION METHODOLOGIES	3
3.1.	Reliability methods for passive safety functions (RMPS)	3
3.1.1.	Definition of accident scenario(s)	6
3.1.2.	System characterizations	6
3.1.3.	System modelling	7
3.1.4.	Identification of sources of uncertainty	7
3.1.5.	Identification of relevant parameters.....	7
3.1.6.	Uncertainty quantification	8
3.1.7.	Sensitivity analysis	8
3.1.8.	Reliability evaluations	10
3.1.9.	Integration of passive system reliability in PSA	11
3.1.10.	Conclusions and open questions.....	12
3.2.	Assessment of passive system reliability (APSRA).....	13
4.	DESCRIPTION OF PROCESS USED TO COMPARE METHODOLOGIES	17
4.1.	Overview of 2400 MW(th) GFR features	17
4.2.	DHR system description and function	20
4.3.	Scenarios selected for NCDHR reliability evaluation.....	22
5.	SIMULATION RESULTS.....	23
5.1.	CEA, France	23
5.1.1.	Modelling	23
5.1.2.	Reference results of transient I (LOFA)	23
5.1.3.	Reference results of transient II (LOCA)	24
5.1.4.	Identification and quantification of uncertainties.....	24
5.1.5.	Failure probabilities evaluations.....	28
5.1.6.	Global sensitivity analysis.....	32
5.2.	BARC, India.....	35
5.2.1.	GFR RELAP5 modelling	35
5.2.2.	Performance analysis.....	35
5.2.3.	Sensitivity analysis	36
5.2.4.	Prediction of failure surface	36
5.2.5.	Evaluation of reliability	36
5.3.	SCK-CEN, Belgium.....	37
5.3.1.	Highlights of transient I results	37
5.3.2.	Highlights of transient II results	38
6.	DISCUSSION AND CONCLUSIONS.....	39
6.1.	Comparison of results for transient I.....	39
6.1.1.	Deterministic results	39
6.1.2.	Reliability results.....	42
6.2.	Comparison of results for transient II	42

6.2.1.	Deterministic results	42
6.2.2.	Reliability results	44
6.3.	Insights from the application of two methodologies	45
6.3.1.	Similarities	45
6.3.2.	Differences	45
6.4.	Proposal for unified definition of reliability	47
6.5.	Merging of two methodologies	47
6.6.	Future R&D	47
6.7.	Conclusions	47
APPENDIX I: BENCHMARK SPECIFICATIONS AND TRANSIENT DEFINITIONS		49
APPENDIX II: TRANSIENT I RESULTS		58
APPENDIX III: TRANSIENT II RESULTS		142
REFERENCES		187
LIST OF ABBREVIATIONS		189
CONTRIBUTORS TO DRAFTING AND REVIEW		191

1. INTRODUCTION

Advanced nuclear reactor designs incorporate several passive systems in addition to active ones, not only to enhance the operational safety of the reactors but also to eliminate the possibility of hypothetical severe accidents. Unlike the active systems, the passive system does not need external input such as energy to operate. Passive systems are simpler in design besides avoiding human intervention in their operation, which increases their reliability as compared to the active ones. However, their performance is always correlated with the system geometry and the operating parameters. Normally, the driving head of passive systems is small, which can be easily influenced even with a small change in operating condition. This is particularly true for the passive systems classified as “type B” by the IAEA [1], i.e. those with moving working fluid; for example a natural circulation system. Such systems rely on natural forces arising due to gravity or buoyancy. The driving force is created by the buoyancy action due to change in density of fluid across the heated/cooled sections. For steady state operation, the buoyancy force is balanced by the resistive frictional force in the system. Since the driving force is due to buoyancy, its magnitude can be easily altered due to any disturbance either in operating parameters or geometry. Because of this, there has been growing concern amongst the nuclear engineers about their reliability not only at normal operation but also during transients and accidents.

Due to the low driving force of passive systems, sometimes the flow is not fully developed and can be multi-dimensional in nature. Besides, there can be existence of thermal stratification particularly in large diameter vessels wherein heat addition or rejection takes place. In such systems, the high density of fluid may settle at the bottom of the vessel and the low density fluid sits at the top allowing kettle type boiling when heat addition takes place. Besides, the heat transfer and pressure loss laws for natural convection systems may be quite different from that of forced convection systems. In the absence of plant data or sufficient experimental data from simulated facilities, the designers have to depend on existing ‘best estimate codes’ such as RELAP5 or TRACE or CATHARE, etc. for analyzing the performance of these systems. However, it is difficult to model accurately the characteristics of these passive systems using the above codes. As a result, there could be large scale uncertainties in simulation of several phenomena of these systems, particularly:

- Low flow natural circulation;
- Natural circulation flow instabilities;
- Critical heat flux under oscillatory condition;
- Condensation in presence of non-condensable gases;
- Thermal stratification in large pools, etc.

In view of the above, assessment of reliability of passive safety systems is a crucial issue to be resolved for their extensive use in future nuclear power plants. Several physical parameters affect the performance of a passive safety system, and their values at the time of operation are a priori unknown. The functions of many passive systems are based on thermohydraulic principles, which have been until recently considered as not subject to any kind of failure. Hence, large and consistent efforts are required to quantify the reliability of such systems.

In late 1990s, a methodology known as REPAS (reliability evaluation of passive safety system) has been developed cooperatively by ENEA [2], the University of Pisa, Milan Polytechnic University and the University of Rome. This methodology is based on the evaluation of a failure probability of a system to carry out the desired function from the

epistemic uncertainties of those physical and geometric parameters which can cause a failure of the system. The REPAS method recognizes the model uncertainties of the codes. The uncertainties in code predictions are evaluated by calculations of sensitivities to input parameters and by code-to-code comparisons.

However, it was later identified that to assess the impact of uncertainties on the predicted performance of the passive system, a large number of calculations with best estimate codes were needed. If all the sequences where the passive system involved are considered, the number of calculations could be prohibitive. In view of this, another methodology known as RMPS (reliability methods for passive safety functions) was developed within the fifth framework programme of the EU [3]. This method considered the identification and quantification of uncertainties of variables and their propagation in thermal hydraulic models, and assessment of thermal hydraulic passive system reliability. The RMPS approach adopts a probability density function (PDF) to treat variations of the critical parameters considered in the predictions of codes. Similar approach is followed by Pagani et al [4] to evaluate failure probability of the gas cooled fast reactor (GFR) natural circulation system. A methodology known as APSRA (assessment of passive system reliability) was developed by Nayak et al [5] for evaluation of reliability of passive systems. In this approach, the failure surface is generated by considering the deviation of all those critical parameters, which influence the system performance. Then, the causes of deviation of these parameters are found through root diagnosis. It is attributed that the deviations of such physical parameters occur only due to a failure of mechanical components such as valves, control systems, etc. Then, the probability of failure of a system is evaluated from the failure probability of these mechanical components through classical probabilistic safety assessment (PSA) treatment. Moreover, to reduce the uncertainty in code predictions, in-house experimental data from integral facilities as well as separate effect tests can be used.

As shown by the IAEA CRP "Natural circulation phenomena, modelling and reliability of passive systems that utilize natural circulation" and the IAEA technical meeting on "Status of validation and testing of passive systems for small and medium sized reactors (SMRs)" (June 2006, Vienna), different definitions for the thermal hydraulic passive system reliability and different assessment methodologies exist and are in operation, as for example:

- 5th PCRD of the EC: Reliability Methods for Passive Systems;
- MIT/CANES methodology with application to GFR;
- APSRA (India).

During the aforementioned meeting, the participants failed to find a consensus on the definition of the reliability of a thermohydraulic passive system. In spite of the differences in the points of view and in the assessment methodologies, the French atomic energy commission (CEA) thought that certain parts of some methodologies (RMPS and APSRA) could be merged in order to obtain a more complete methodology.

1.1. SCOPE

The scope of PGAP (Performance Assessment of Passive Gaseous Provisions) collaborative project was to reach a consensus on the definition of reliability of thermal hydraulic passive systems as well as a methodology to assess it, in coordination with the IAEA and other international initiatives on the subject. This project was built on the results of a benchmark

exercise modelling decay heat removal (DHR) transients with the French CEA gas cooled fast reactor (GFR) design in order to evaluate the reliability of the DHR system after assessing their ability to satisfy selected mission success criteria.

The Benchmark was comprised of two phases:

- "Deterministic calculations": simulation of selected transients taking into account nominal values of design and operation parameters;
- "Reliability calculations": multiple simulations of the same selected transients with determined variations of design or operation parameters having an impact on the success of the DHR mission.

For each phase, two transients were simulated to assess the performance of the DHR System:

- Station blackout (SBO);
- Loss of coolant accident (LOCA) combined with loss of forced circulation with two DHR loops available.

Different simulation codes (CATHARE, RELAP) and different existing assessment methods (RMPS and APSRA) were used by the participants. Consequently, the project was based on a comparative analysis of the definitions of the thermohydraulic passive system reliability, a comparison of the assessment methodologies and a comparison of computational results.

2. OBJECTIVES

Although risk informed safety approaches are increasingly considered, especially for innovative reactors, there is currently neither internationally recognized definition for the reliability of a thermal hydraulic passive system, nor methodology to estimate such reliability. The overall objective of this collaborative project was to contribute to an international consensus on the definition of the reliability of passive systems that involves natural circulation, and on a methodology to assess this reliability. This will help treating both active and passive systems in common PSA for innovative reactors with passive systems.

Keeping in view the above objectives, INPRO initiated an international collaborative project to evaluate the performance and reliability of the passive decay heat removal system of the French GFR design using the reliability methodologies available in Member States. Under this framework RMPS and APSRA methodologies were used to assess the performance and reliability of passive decay heat removal system of the French GFR design for two transients, namely station blackout (SBO) and loss of coolant accident (LOCA) combined with a loss of forced circulation with two DHR loops available.

3. DESCRIPTION OF RELIABILITY EVALUATION METHODOLOGIES

3.1. RELIABILITY METHODS FOR PASSIVE SAFETY FUNCTIONS (RMPS)

Innovative reactor concepts make use of passive safety features to a large extent in combination with active safety or operational systems. According to the IAEA definitions [1], a passive system does not need external input, especially energy to operate. That is why passive systems are expected to combine among others, the advantages of simplicity, a

decrease in the need for human interaction and a reduction or avoidance of external electrical power or signals.

Besides the open feedback on economic competitiveness, special aspects like lack of data on some phenomena, missing operating experience over the wide range of conditions, and driving forces which are smaller in most cases than in active safety systems, must be taken into account.

This remark is especially applicable to category B or C passive systems (i.e. implementing moving working fluid, following the IAEA classification [1]) and in particular to the passive systems that utilize natural circulation. These passive safety systems in their designs rely on natural forces to perform their accident prevention and mitigation functions once actuated and started. These driving forces are not generated by external power sources (e.g. pumped systems), as is the case of operating and evolutionary reactor designs. Because the magnitude of the natural forces, which drive the operation of passive systems, is relatively small, counter forces (e.g. friction) can be of comparable magnitude and cannot be ignored as it is generally the case with systems including pumps. Moreover, there are considerable uncertainties associated with factors, which depend on the magnitude of these forces and counter forces (e.g. values of heat transfer coefficients and pressure losses). In addition, the magnitude of such natural driving forces depends on specific plant conditions and configurations, which could exist when a system is called upon to perform its safety function. All these uncertainties affect the thermohydraulic (T-H) performance of the passive systems.

To assess the impact of uncertainties on the predicted performance of a passive system, a large number of calculations with best estimate T-H codes are needed. If all the sequences involving a passive system are considered, the number of calculations can be prohibitive. For all these reasons, it appeared necessary to create a specific methodology to assess the reliability of category B or C passive systems. The methodology has been developed within the framework of a project called reliability methods for passive safety functions (RMPS), performed under the auspices of the European 5th Framework Programme [3]. The methodology addresses the following issues:

- Identification and quantification of the sources of uncertainties and determination of the important variables;
- Propagation of the uncertainties through T-H models and assessment of T-H passive system unreliability;
- Introduction of passive system unreliability in the accident sequence analysis.

The proposed methodology consists of several steps, which are shown in Fig. 1 and are detailed as follows:

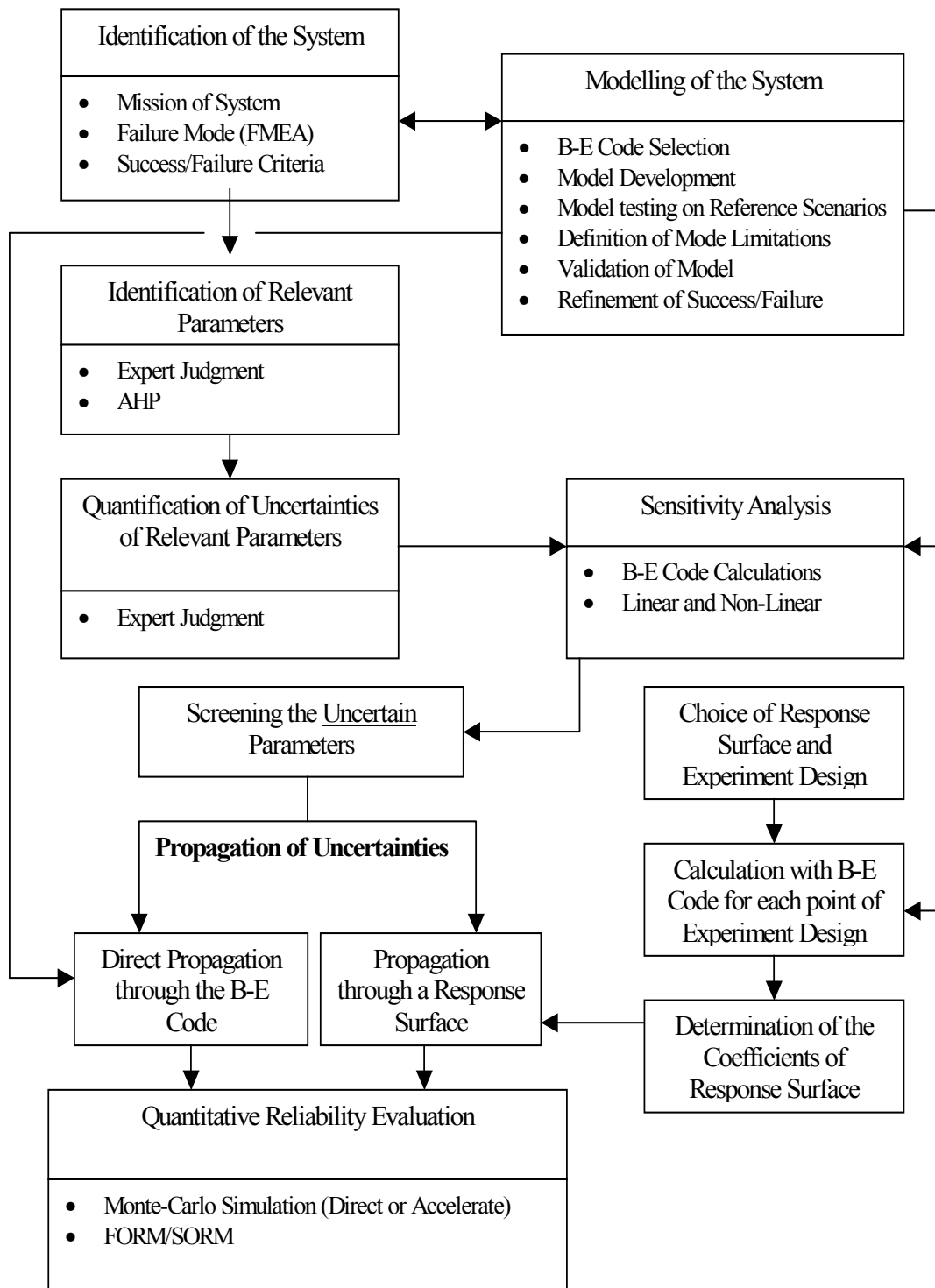


FIG. 1. RMPS methodology roadmap.

3.1.1. Definition of accident scenario(s)

The first step of the methodology is the definition of the accident scenario(s) in which a passive system is expected to operate. Knowledge of each scenario helps identifying the specific failure criteria and relevant parameters and the specific quantification of uncertainties. The results obtained in the reliability and sensitivity analyses of a passive system are thus specific to each scenario. A global evaluation of a passive system is obtained by the integration of its unreliability in a probabilistic safety assessment, in which all the sequences involving a passive system are considered. This approach is preferred to conservative analyses, which evaluate the system reliability for the worst scenario considered or by integrating the larger variability of the uncertain parameters covering all the scenarios involving the system.

3.1.2. System characterizations

The purpose of this analysis is to obtain information on the behaviour of a passive system in an accident scenario occurring during the life of a nuclear reactor, and to identify the failure zones and conditions if it exists. Therefore, the missions of the system, its failure modes and the failure criteria must be defined.

3.1.2.1. *Mission(s) of the system*

The missions of the system are the goals for which a passive system has been designed and located within the overall system. For instance, the mission of a passive system can be decay heat removal, vessel cooling, pressure decrease of the primary circuit, etc. In some cases, a passive system can be designed to fulfil several missions at the same time or different missions depending on the considered scenario.

3.1.2.2. *Failure mode*

Due to the complexity of T-H phenomena, and complex interaction between the passive system and the overall system, it is not always obvious to associate a failure mode to the mission of the system. A qualitative analysis is often necessary so as to identify potential failure modes and their consequences, associated with a passive system operation. A hazard identification qualitative method such as the FMEA (failure mode and effect analysis) can be used to identify the parameters judged critical for the performance of a passive system and to help associate failure modes and corresponding indicators of a failure cause. This method can necessitate the introduction of a “virtual” component, in addition to mechanical components of the system (piping, drain valve, etc.). This component is identified as natural circulation and is evaluated in terms of potential “phenomenological” factors (such as non-condensable gas build up, thermal stratification, surface oxidation, cracking, etc.), whose consequences can affect a passive system performance.

3.1.2.3. *Success/failure criteria*

Knowledge of system missions and failure modes allows the evaluation of failure criteria. The failure criteria can be established in terms of exceeding/not exceeding given thresholds set on relevant physical quantities over given time periods (e.g. mission times). Some examples include: exceeding a limit pressure in the primary system during the first 24 hours after the beginning of the scenario, or not removing more than a given fraction of residual energy produced during the same time period. In some cases, it is better to define a global failure criterion for the whole system instead of a specific criterion for a passive system. For

instance, the failure criterion can be based on the peak cladding temperature during a specified period. In this case, it will be necessary to model the complete system and not only a passive system.

3.1.3. System modelling

Due to the lack of suitable experimental databases for passive systems in operation, the evaluation must rely on numerical modelling. The system analysis must be carried out with a qualified T-H system code and performing best estimate calculations. Indeed, there is an increasing interest in computational reactor safety analysis to replace the conservative evaluation model calculations by best estimate calculations supplemented by a quantitative uncertainty analysis [6]. Particularly in the present methodology, where the objective is the passive system reliability evaluation, it is important to simulate a passive system performance in a realistic and not conservative way. At this stage, calculations have to be carried out on the reference case with nominal values of the system characteristic parameters. The results have to be compared with experimental data if exists. During the characterisation process, the modelling and the evaluation of the passive system, new failure modes can be identified (such as flow oscillations, plug phenomena due to non-condensable gases, etc.), which must also be taken into account.

3.1.4. Identification of sources of uncertainty

First of all, the method requires the identification of the potentially important contributors to uncertainty. These contributors are:

- Approximations in modelling physical process: for instance, the treatment of a liquid–steam mixture as a homogeneous fluid, the use of empirical correlations, etc.;
- Approximations in modelling system geometry: simplification of complex geometry features and approximation of three dimensional systems;
- The input variables: initial and boundary conditions such as plant temperatures, pressures, water levels and reactor power, dimensions, physical properties such as densities, conductivities, specific heats, and thermohydraulic parameters such as heat transfer coefficients or friction factors.

This identification of the relevant parameters must be based on expert opinions. Different methodologies have been developed to evaluate the overall uncertainty in the physical model predictions and some efforts have been made for the internal uncertainty assessment capacity of T-H codes [7]. In real applications, the reliability assessment should also include this type of uncertainty.

3.1.5. Identification of relevant parameters

The evaluation of the reliability of a passive system requires the identification of the relevant parameters, which really affect the system goal accomplishment. The tool initially chosen for this task was the analytic hierarchy process [8–9]. This method consists of three major steps i.e. building of a hierarchy to decompose the problem at hand, the input of pairwise comparison judgments regarding the relevance of the considered parameters, and the computation of priority vectors to obtain their ranking. Other deductive approaches have been used within the framework of the applications concerning new concepts of reactors under development [10].

3.1.6. Uncertainty quantification

A key issue in this methodology is the selection of distributions for the input parameters. The main objective is that the selected distribution for each input parameter must quantify the state of knowledge and express the reliable and available information about a parameter. The choice of distribution may highly affect the reliability evaluations of a passive system. The following points have to be considered for this quantification:

3.1.6.1. The amount of data

When the data on a parameter are abundant, statistical methods can be used such as the maximum likelihood method or the method of moments to adjust analytical density functions. Different goodness-of-fit tests can be used (Chi square, Kolmogorov, etc.) to find the best analytical fit to the data. When the data are sparse or non-existent, which is generally the case when we consider the uncertainties affecting a passive system performance, the evaluation of the probability functions of the uncertain parameters must be based on expert judgement. In the case where no preferences can be justified, a uniform distribution can be specified, i.e. each value between minimum and maximum is equally likely. These distributions are quantitative expressions of the state of knowledge and can be modified if there is new evidence. If suitable observations become available, they can be used consistently to update the distributions.

3.1.6.2. Dependence between parameters

If parameters have common contributors to their uncertainty, the respective states of knowledge are dependent. As a consequence of this dependence, values of different parameters cannot be combined freely and independently. Instances of such limitations need to be identified and the dependencies need to be quantified, if judged to be potentially important. If the analyst knows dependencies between parameters explicitly, multivariate distributions or conditional probability distributions may be used. The dependence between the parameters can also be introduced by covariance matrices or by functional relations between the parameters.

3.1.7. Sensitivity analysis

3.1.7.1. Objectives

An important feature of the methodology is to evaluate the sensitivity of reliability driving output variables (pressure, removed power, etc.) with respect to input uncertain parameters. The sensitivity measures give a ranking of input parameters. This information provides guidance as to where to improve the state of knowledge in order to reduce the output uncertainties most effectively. If experimental results are available to be compared with calculations, the sensitivity measures provide guidance as to where to improve the models of the computer code.

3.1.7.2. Qualitative sensitivity analysis

Sometimes the lack of operational experience and significant data concerning the passive system performance forces the analysis to be performed in a qualitative way aiming at the identification, for each failure mode, of both the level of uncertainty associated with the phenomenon and the sensitivity of failure probability to that phenomenon [11]. For example, even if a phenomenon is highly uncertain because of deficiencies in the physical modelling,

this may not be important for the overall failure probability. On the other hand, a phenomenon may be well understood (therefore the uncertainty is small), but the failure probability may be sensitive to small variation in this parameter. The worst case is characterized by "high" rankings relative to sensitivity or uncertainty (e.g. presence of non-condensable gas or thermal stratification), making the corresponding phenomena evaluation a critical challenge.

3.1.7.3. *Quantitative sensitivity analysis*

The quantitative sensitivity analysis necessitates T-H calculations. It consists of ranking the parameters according to their relative contribution on the overall code response uncertainty and quantifying this contribution for each parameter. To apportion the variation in the output to the different input parameters, many techniques can be used [12], each yielding different measures of sensitivity.

A common approach is to base the sensitivity analysis on a linear regression method, which is based on the hypothesis of a linear relation between response and input parameters. This, in case of passive systems is obviously restrictive. However, the method is simple and quick, and provides useful insights in case of a restricted number of sampling. Three different sensitivity coefficients have been considered and each one providing slightly different information on the relevance of a parameter: standardized regression coefficients (SRC), partial correlation coefficients (PCC) and correlation coefficients (CC). Small differences between the different coefficients may be due to a certain degree of correlation between the inputs and to the system's non-linearity. These occurrences should be analysed, the first one possibly through the examination of the correlation matrix and the second one by calculating the model coefficient of determination R^2 .

Depending on the nature of the model representing the passive system operation and calculating its performances, the use of sensitivity methods developed for non-monotonous or non-linear models are considered to be more accurate.

In case of non-linear but monotonous models, we perform rank transformations and calculate associated indices i.e. standardized rank regression coefficients (SRRCs) and partial rank correlation coefficients (PRCCs). The rank transformation is a simple procedure, which involves replacing the data with their corresponding ranks. We can also calculate a determination coefficient based on the rank R^{2*} . The R^{2*} will be higher than the R^2 in case of non-linear models. The difference between R^2 and R^{2*} is a useful indicator of non-linearity of the model. For non-linear and non-monotonous models, two methods exist i.e. the Fourier amplitude sensitivity test (FAST) and the Sobol method.

The main idea of these methods is to decompose the total variance of the response to express sensitivity through variance, and to evaluate how the variance of such an input or group of inputs contributes into variance of the output. The Sobol indices are calculated by Monte-Carlo simulation. The problem of these methods, and specially the Sobol method, is that a good estimation of these indices requires a great number of calculations (i.e. 10,000 simulations). Thus, it is necessary first to calculate a response surface validated in the domain of variation of the random variables (see Section 3.1.8.4). Thus, if the model is really not linear, nor monotonous, we propose to:

- Adjust non-linear models on the data;
- Test the validity of the model (e.g. in calculating R^2 , residues, predictive robustness);
- Use the model as a response surface in order to evaluate the Sobol or FAST indices.

3.1.8. Reliability evaluations

Different methods can be used to quantify the reliability of a passive system once a best estimate T-H code and a model of the system are given. The failure function of a passive system according to a specified mission is given by:

$$M = \text{relevant output variable} - \text{threshold} = g(X_1, X_2, \dots, X_n) \quad (1)$$

where X_i ($i=1, \dots, n$) are the n basic random variables (input parameters), and $g(\cdot)$ is the functional relationship between the random variables and the failure of the system. The failure function can be defined in such a way that the limit state, or failure surface, is given by $M = 0$. The failure event is defined as the space where $M \leq 0$, and the success event is defined as the space where $M > 0$. Thus a probability of failure can be evaluated by the following integral:

$$P_f = \int \int \dots \int f_X(x_1, x_2, \dots, x_n) dx_1 dx_2 \dots dx_n \quad (2)$$

where f_X is the joint density function of X_1, X_2, \dots, X_n , and the integration is performed over the region where $M \leq 0$. Because each of the basic random variables has a unique distribution and because they interact, the integral (Eq. 2) cannot be easily evaluated. Two types of methods can be used to estimate the failure probability i.e. Monte Carlo simulation with or without variance reduction techniques, and first and second order reliability methods (FORM/SORM).

3.1.8.1. Direct Monte Carlo

Direct Monte Carlo simulation techniques [13] can be used to estimate the failure probability defined in Eq. 2. Monte Carlo simulations consist in drawing samples of the basic variables according to their probabilistic characteristics and then feeding them into the failure function. An estimate $\overline{P_f}$ of the probability of failure P_f can be found in dividing the number of simulation cycles in which $g(\cdot) \leq 0$, by the total number of simulation cycles N . As N approaches infinity, $\overline{P_f}$ approaches the true failure probability. It is recommended to measure the statistical accuracy of the estimated failure probability by computing its variation coefficient (ratio of standard deviation to average of estimations). The smaller the variation coefficient, the better will be the accuracy of the estimated failure probability. For a small number of simulation cycles, the variance of $\overline{P_f}$ can be quite large. Consequently, it may take a large number of simulation cycles to achieve a good accuracy. The computational time needed for the direct Monte Carlo method will then be high, since each simulation cycle involves a long calculation (several hours) performed by a T-H code.

3.1.8.2. Variance reduction techniques

Variance reduction techniques offer an increase in the efficiency and accuracy of the simulation based assessment of passive system reliability for a relatively small number of simulation cycles [12–13]. Different variance reduction techniques exist, such as importance sampling, stratified sampling, Latin hypercube sampling (LHS), conditional expectation, directional simulation, etc.

3.1.8.3. *FORM/SORM*

An alternative to the Monte Carlo simulation is the use of first/second order reliability methods (FORM/SORM) [14–16]. They consist of 4 steps:

- Transformation of space of basic random variables X_1, X_2, \dots, X_n into a space of standard normal variables;
- Searching for the point of minimum distance from the origin to the limit state surface (this point is called the design point);
- Approximation by a first/second order surface of the real failure surface near the design point;
- Computation of the failure probability corresponding to the approximated failure surface.

FORM and SORM apply only to problems where the set of basic variables are continuous. For small probabilities FORM/SORM are extremely efficient when compared to other simulation methods. The drawbacks of these methods come from the difficulty in identifying the design point when the failure surface is not sufficiently smooth, and from the fact that, contrary to Monte Carlo method, there is no direct way to estimate the accuracy of the provided estimation.

3.1.8.4. *Response surface methods*

To avoid the problem of long computational times in the previous methods, it is interesting to approximate the response $Y=g(X)$ given by the T-H code, in the space of the input random variables, by a simple mathematical model $\tilde{g}(X)$ known as response surface. Experiments are conducted with the basic random variables X_1, X_2, \dots, X_n for a sufficient number of times to define the response surface to the level of accuracy desired. Each experiment can be represented by a point with coordinates $x_{1j}, x_{2j}, \dots, x_{nj}$ in an n-dimensional space. At each point, a value of y_j is calculated by the T-H code and the unknown coefficients of the response surface $\tilde{g}(X)$ are determined in such a way that the error is minimum in the region of interest. When a response surface has been determined, the passive system reliability can be easily assessed by using the Monte Carlo simulation. Different types of response surfaces can be fitted such as polynomial, thin plate splines, neural networks, generalized linear model, partial least squares regression, etc. The type of response surface will be chosen depending on the problem [17]. In any case, the response surface is just an approximation to the real model, and the error committed in such approximation should be taken into account in the final reliability estimate.

3.1.9. **Integration of passive system reliability in PSA**

The objective of this part of the methodology is the development of a consistent approach for introducing passive system reliability in an accident sequence in a PSA. So far, in existing innovative nuclear reactor PSAs, only passive system components failure probabilities are taken into account, disregarding the physical phenomena on which the system is based, such as the natural circulation. In fact, the inclusion of this aspect of the passive system failure in the PSA models is a difficult and challenging task and no commonly accepted practices exist. In a first approach, we have chosen an event tree (ET) representation of the accident sequences. ET techniques allow the identification of all accident sequences deriving from an initiating event. The initiating event is an event (e.g. equipment failure, transient) that can

lead to the accident if no protective action is taken by safety systems. Each sequence of the ET represents a certain combination of events corresponding to the failure or to the success of safety systems. Therefore, ET provides a set of alternative consequences. The consequences in the case of Level 1 PSA of nuclear reactors are usually defined as degrees of reactor core damage, including 'safe' state and 'severe' accident state. These consequences are generally evaluated by T-H calculations carried out in a conservative way.

This choice of the event tree representation might seem unsuitable because it does not appear to consider the dynamic aspects of the transient progression including dynamic system interactions, T-H induced failure, and operator actions in response to system dynamics. In fact, we have treated examples where the overall reactor, including the safety systems and in particular the passive system, is modelled by the T-H code. This results in the fact that the dynamic system interactions are taken into account by the T-H calculations itself. In addition, we have not considered human intervention during the studied sequences, which is coherent with the usual utilization of the passive systems in innovative reactors. So, as a first approach, the event tree representation seems a good and simple representation for the assessment of accident sequences, including the passive systems.

For the sequences where the definition of envelope cases are impossible, events corresponding to the failure of the physical process are added to the event tree and uncertainty analyses are carried out to evaluate the corresponding failure probability. For this purpose, the T-H code is coupled to a Monte-Carlo simulation module. The failure probabilities obtained by these reliability analyses are fed into the corresponding sequences.

3.1.10. Conclusions and open questions

The developed methodology participates to the safety assessment of reactors equipped with T-H passive systems and is an indispensable tool for the designers who define the architecture of safety systems and for the regulatory authorities in the safety evaluation of passive system.

During the RMPS project, the methodology was successfully applied to several passive systems, such as the Isolation Condenser System of Boiling Water Reactor [18], the Hydro-Accumulators of the VVER, and RP2 (Residual Passive heat Removal system on the Primary circuit) system [3]. More recent applications concern the PRHRS of the CAREM-like reactor developed by CNEA [19] and the DHR of the 2400 MW(th) GFR developed by CEA [20].

The results of the analyses made show that, in spite of the inherent characteristics of passive systems, which are a priori considered as advantages (simplicity, decrease of the need for human interaction, reduction or avoidance of external electrical power or signals), the decision for the designers to replace an active safety system by a passive system is not easy from a safety point of view.

Some points which have not been addressed within the framework of the RMPS project, due to limited time and resources, have to be studied in future work. The objectives of this future work can be divided into two parts: i) improvement of the method, ii) extension of the subject of investigations in order to solve the issue of active versus passive systems.

- (i) About the improvement of the RMPS methodology, two items of the methodology roadmap deserve closer attention: the identification of the relevant parameters and the quantification of uncertainties. In RMPS, the identification of the input parameters is not based on strict rules. Rules, which guarantee a rational approach to the problem and, which demonstrate that the procedure is based on realistic assumptions, would justify

the choice of the uncertain parameters and should convince the designer. In the selection of the relevant input parameters, a clear distinction between the different kinds of uncertainties should be introduced i.e. distinguishing between modelling uncertainties on one side and uncertainties dealing with the state of knowledge about the passive systems and their characteristic parameters on the other side. Another important item of improvement is the integration of the passive systems reliability in the PSAs. The first attempts performed within the framework of RMPS have taken into account the failures of the components of the passive system as well as the impairment of the physical process involved like basic events in static event trees. However, in order to generalize the methodology, it is important to take into account the dynamic aspects differently than by their alone modelling into the T-H code. Indeed, in complex situations where several safety systems are competing and where the human operation cannot be completely eliminated, this modelling should prove to be impossible or too expensive in terms of computing times. Therefore, there is a need to explore other solutions already used in the dynamic PSA like the method of the dynamic event trees.

- (ii) In addition to the improvement of different topics of the RMPS methodology and in order to answer the question of the choice between active and passive systems, it is necessary to take into account the facts other than the reliability, such as efficiency, simplicity, robustness, human factor and economic evaluations, and to develop a tool for helping the systems design's optimization. Human factors are important, since these might affect deeply the reliability of a passive system. Indeed, the periodic maintenance and inspection of such systems introduce particular constraints unlike an active system that can be more easily isolated or inspected during the shutdown periods. A passive system requires to be tested under its real physical conditions of utilization and this can generate new specific implementation in the global architecture and safety problems. In addition, the question of whether it is an advantage or a disadvantage that passive systems do not allow operator intervention during its operation, should be investigated. Technical–economical evaluations of the systems must be carried out to provide information that is essential for the comparison between passive and active systems. Before comparing a passive and an active system on the same mission, it is necessary to make sure that the passive system design is optimized in terms of performance. Methods have to be developed to ensure the optimization.

3.2. ASSESSMENT OF PASSIVE SYSTEM RELIABILITY (APSRA)

In the APSRA methodology, the passive system reliability is evaluated from the probability that the system fails to carry out the desired function. In principle, in a natural circulation system, the operational mechanism of buoyancy driven pump should never fail as long as there is a heat source and sink with an elevation difference between them. However, even though the mechanism does not fail, it may not be able to drive the required flow rate whenever called in, if there is any fluctuation or deviation in the operating parameters even though the system geometry remains intact. In the case of a mechanical pump, the head vs. flow characteristics is not so much susceptible to a slight change or fluctuation in operating parameter to cause the failure of the system unless there is any mechanical failure of the pump itself. Hence, its performance characteristics are well known and can be simulated accurately while assessing the overall safety of the plant. On the other hand, the characteristics of buoyancy driven pump cannot be accurately predicted under all operational conditions or transients due to the inherent complex phenomena associated with natural convection systems. Since applicability of the best estimate codes to passive systems are neither proven nor understood enough, hence, APSRA relies more on experimental data for various aspects

of natural circulation. APSRA compares the code predictions with the test data to evaluate the uncertainties on the failure parameter prediction, which is later considered in the code for prediction of failure conditions of the system. Figure 2 shows the steps followed in APSRA methodology.

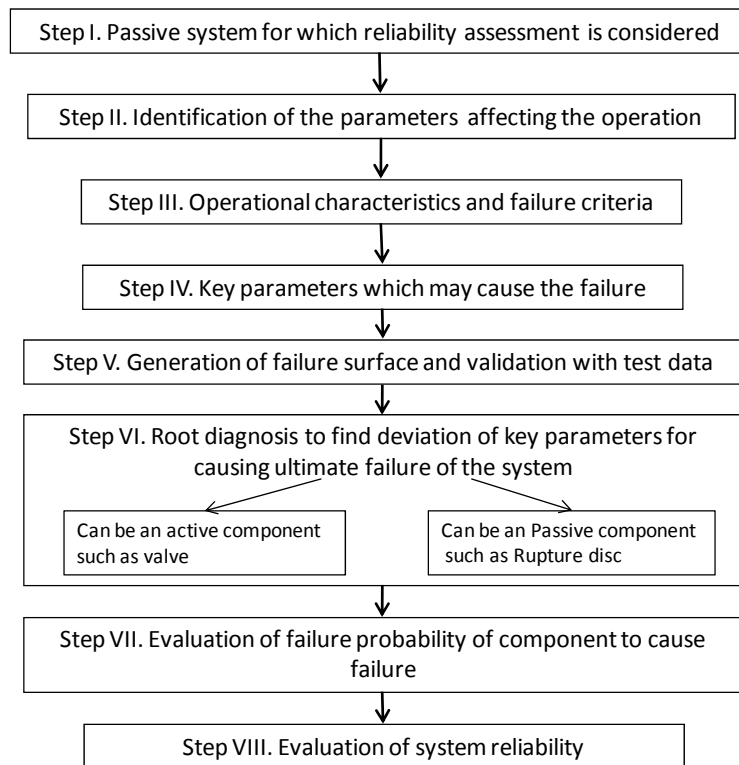


FIG. 2. APSRA methodology.

The steps of the methodology are discussed below in detail.

Step I: Passive system for which reliability assessment is considered

In step I, the passive system for which reliability will be evaluated is considered.

Step II: Identification of parameters affecting the operation

The performance characteristics of the passive system are greatly influenced by some operating parameters. For example, some of the critical operating parameters which influence the natural circulation flow rate in a boiling two phase natural circulation system are:

- System pressure;
- Heat addition rate to the coolant;
- Water level in the steam drum;
- Feed water temperature or core inlet sub-cooling;
- Presence of non-condensable gases.

Step III: Operational characteristics and failure criteria

In step III, APSRA requires the designer to have a clear understanding of the operational mechanism of the passive system and its failure, i.e. characteristics of the passive system. To judge its failure, the designer has to define its failure criteria. The characteristics of the system can be simulated even with simpler codes which can generate the passive system performance data qualitatively in a relatively short period. In this step, the purpose is just to understand the system operational behaviour but not to predict the system behaviour accurately. For this, the designer has to use the parameters identified in step II, which can have influence on the performance of the system. Out of them, some must be critical in the sense that a disturbance in these parameters can lead to a significant change in the performance of the system, while others do not. Only a T-H expert can judge this behaviour through parametric calculations, and these parameters must be considered for the reliability analysis of the system.

For example, a buoyancy induced pump which drives natural circulation operates due to density difference between hot and cold legs. So far as the heat source and sinks are available, natural circulation always builds in. However, the flow rate may not be sufficient to fulfil the desired objectives of the system, which can be:

- Inadequate removal of heat causing rise in clad surface temperature;
- Occurrence of flow oscillations;
- Occurrence of critical heat flux (CHF).

The system designer may consider the system to fail if any of the above parameters exceeds the limit.

Step IV: Key parameters which may cause the failure

The studies in steps III and IV are complimentary to each other, in the sense that while the results of step III help in understanding the performance characteristics of the system due to variation of the critical parameters, step IV generates the results for those values of the critical parameters at which the system may fail for meeting any of the criteria given in step III.

Step V: Generation of failure surface and validation with test data

Once the key parameters are identified in step III (deviation of which can cause the failure of the system), the value of these parameters at which the system will fail, are calculated using a best estimate code. Hence there is another requirement for step V, i.e. the results should be generated using a best estimate code such as RELAP5 in order to reduce the uncertainty in the prediction of the failure conditions. The results of step IV generated using a simpler code is only useful in directing the inputs for step V in order to derive the failure conditions rather quickly.

As said before, applicability of the best estimate codes to passive systems are still not well understood. To reduce the uncertainty in prediction experiments for failure data for different passive systems are essential. The programme for benchmarking of the failure surface prediction is shown in Fig. 3.

Step VI: Root diagnosis to find deviation of key parameters for causing failure of system

After establishing the domain of failure, the next task is to find out the cause of deviation of key parameters which eventually result in the failure of the system. This is done through a root diagnosis method.

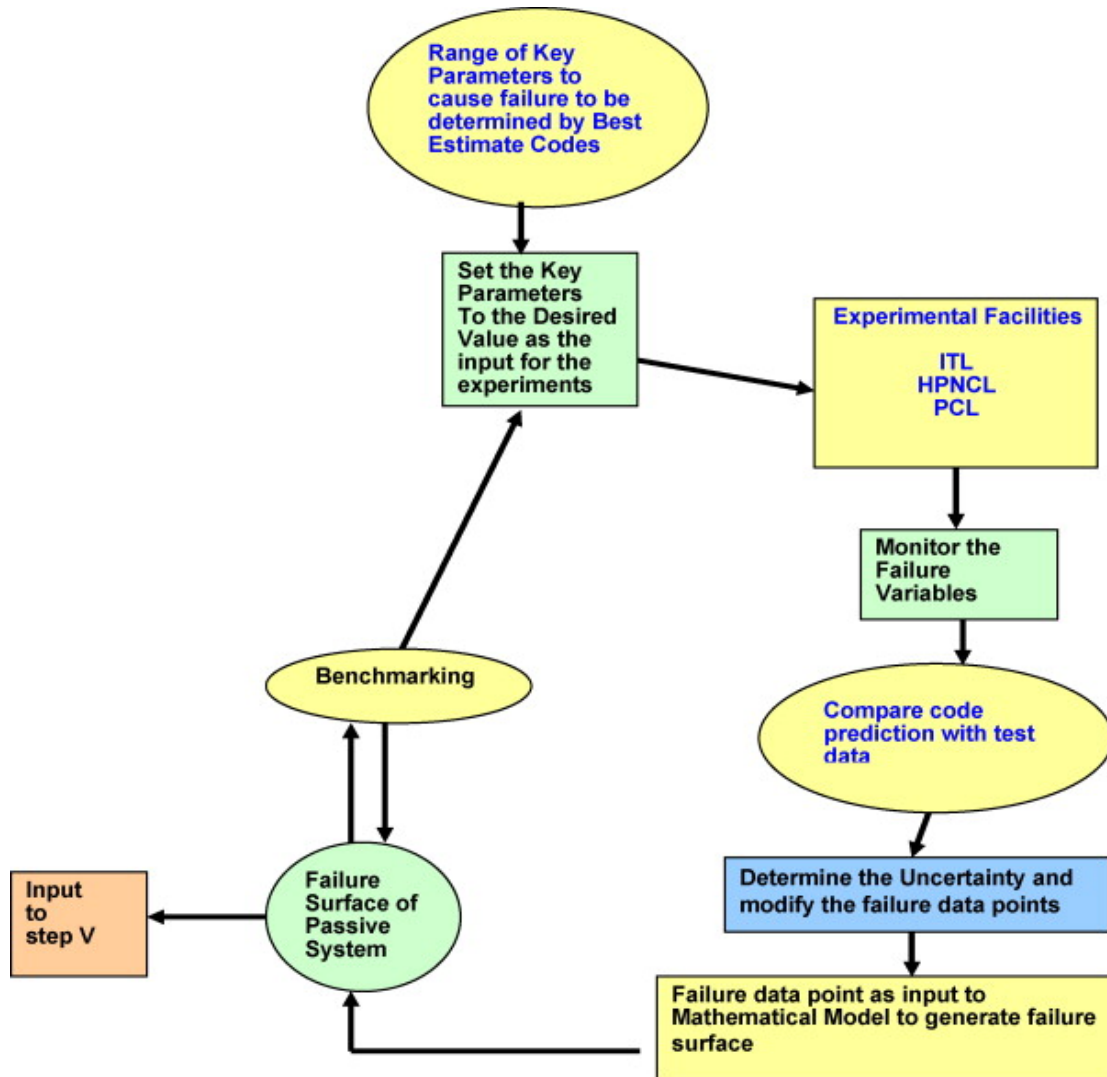


FIG. 3. The programme for benchmarking the failure surface.

For example, a reduction in core inlet sub-cooling in natural circulation reactor can be due to reduction of feed water flow rate. This can happen due to:

- Partial availability of the feed pumps;
- Malfunctioning of feed control valves or controller;
- Unavailability/failure of feed water heaters.

A passive system fails to carry out its function not due to failure of its mechanism, but definitely due to deviation of some of the parameters on which its performance depends. These so-called “key parameters” deviate from their nominal values due to failure of either some active components such as a control valve, or an external pump, or electric signal, etc. or due to failure of some passive components such a passive valve, or a relief valve, etc.

Step VII: Evaluation of failure probability of components causing the failure

This is the most critical step in evaluation of reliability of the system. Once the causes of deviation of key parameters are known in step VI, the failure probability of the components can be evaluated using the classical PSA treatment through a clean event/fault tree analysis.

Step VIII: Evaluation of system reliability

The component failure probability is integrated to evaluate the reliability of the system.

4. DESCRIPTION OF PROCESS USED TO COMPARE METHODOLOGIES

To perform the reliability analysis, the decay heat removal (DHR) system of the French 2400 MW(th) gas cooled fast reactor design was used as a benchmark problem. The detailed specifications of the benchmark are provided in Appendix I.

4.1. OVERVIEW OF 2400 MW(th) GFR FEATURES

The gas cooled fast reactor (GFR) is considered as a promising concept for future nuclear energy systems [20, 21]. The main specifications of the 2400 MW(th) GFR concept are driven by the internationally agreed Generation IV objectives which have been “translated” into the main features of the concept:

- A fast neutron core with a zero breeding gain (without fertile blankets) and characterized by an initial plutonium inventory allowing for the deployment of the GFR fleet near 2040 (sustainability and proliferation resistance concerns);
- A helium cooled primary circuit (7 MPa, around 900°C at core outlet) connected to a Brayton cycle secondary circuit allowing for a high thermodynamic efficiency (economics concern), and a steam–water ternary circuit;
- A decay heat removal system based on dedicated loops allowing forced or natural circulation (safety concern).

The main features of the GFR design are given in Table 1:

TABLE 1. 2400 MW(th) GFR FEATURES

Parameters	Reference values
Gas temperature at main vessel inlet/outlet (°C)	400 / 850
Core inlet mass flow (kg/s)	1020
Helium temperature at core outlet (°C)	900
Gas pressure at main vessel inlet/outlet (MPa)	7.12 / 6.98
Number of main loops	3
Main loop mass flow (kg/s)	340.8 * 3
Exchanged power in main loop IHX (MW)	803.3 * 3

Radially the core comprises two enrichment zones (see Fig. 4) represented by 6 core derivations i.e. from inner (Core0) to outer (Core5). The radial peaking factor is around 1.14. Among the 247 assemblies of the fissile zone, a proposition of arrangement is provided in Table 2 including the radial power factor attached to each zone.

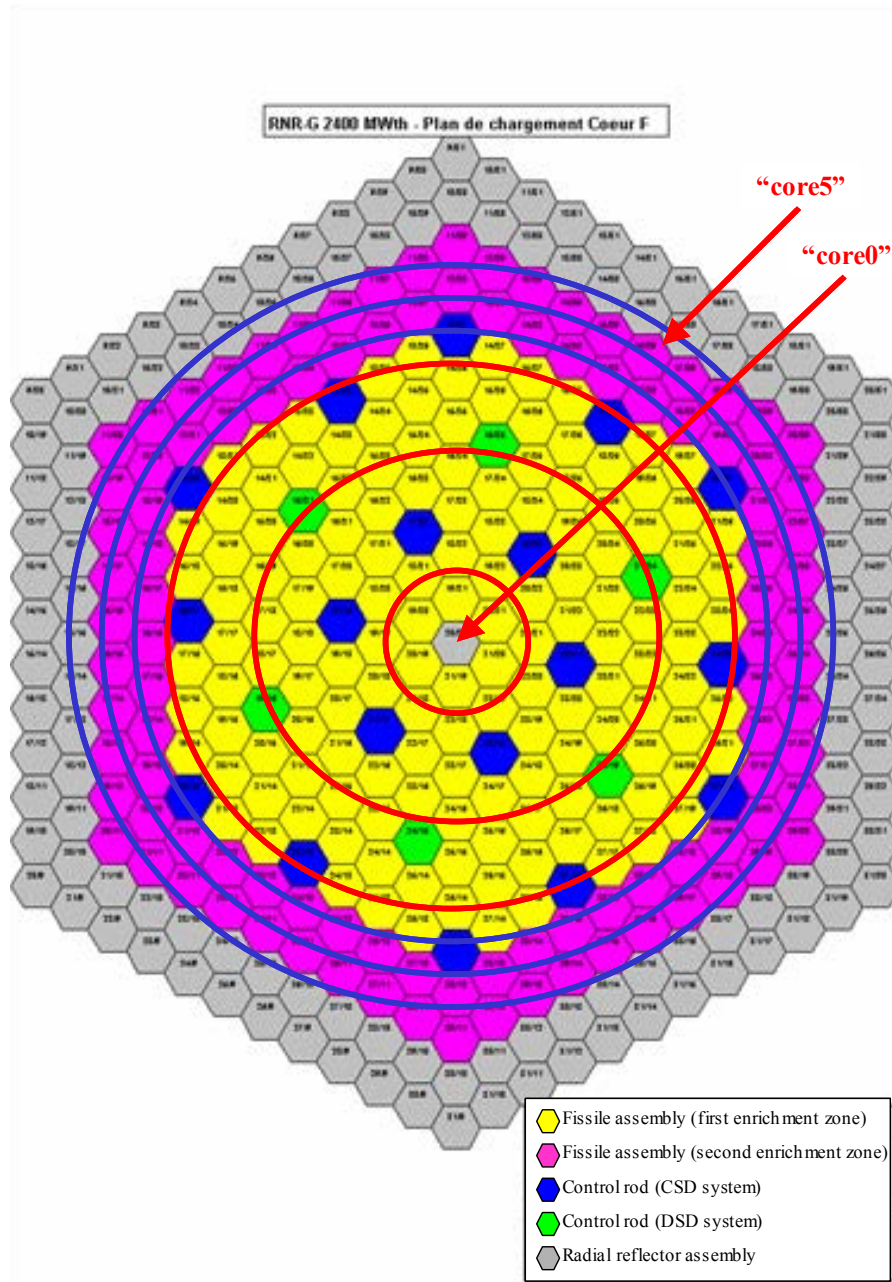


FIG. 4. GFR core loading and radial regions in the CATHARE nodalization.

TABLE 2: RADIAL POWER PROFILE FOR 6 RADIAL CORE ZONES

Core zone	Core0	Core1	Core2	Core3	Core4	Core5
Number of assemblies	18	36	54	36	42	60
Normalized power profile	1.105	1.0804	1.0353	0.9676	1.0629	0.8631

The axial peaking factor is equal to 1.29. The volumetric power distribution in the axial direction is given in Table 3.

TABLE 3. AXIAL POWER PROFILE

Elevation (cm)	P_{vol} (W/cm³)
100.30	57.9739
110.33	63.2259
120.36	71.8656
130.39	81.0065
140.42	89.8765
150.45	98.1295
160.48	105.5504
170.51	111.9855
180.54	117.3203
190.57	121.4695
200.60	124.3717
210.63	125.9859
220.66	126.2900
230.69	125.2799
240.72	122.9690
250.75	119.3890
260.78	114.5912
270.81	108.6487
280.84	101.6608
290.87	93.7599
300.90	85.1243
310.93	76.0137
320.96	66.9037
328.43	60.8672
335.90	57.6262

The decay power as a function of time was obtained with Darwin code¹ considering 11 groups of fission products (FPs) and is given in Table 4.

TABLE 4. DARWIN TABULATED LAW FOR DECAY HEAT (EXPRESSED IN TERMS OF PERCENTAGE OF THE NOMINAL POWER)

Time (s)	Darwin tabulated	Time (s)	Darwin tabulated	Time (s)	Darwin tabulated	Time (s)	Darwin tabulated	Time (s)	Darwin tabulated
0	0.0658	360	0.0284	1500	0.0210	2700	0.0178	8000	0.0133
0.1	0.0658	420	0.0277	1560	0.0208	2760	0.0177	9000	0.0129
0.15	0.0655	480	0.0270	1620	0.0206	2820	0.0176	10000	0.0126
0.2	0.0652	540	0.0265	1680	0.0204	2880	0.0175	36000	0.0098
0.5	0.0637	600	0.0259	1740	0.0202	2940	0.0174	54000	0.0091
1	0.0616	660	0.0255	1800	0.0200	3000	0.0173	72000	0.0085
5	0.0532	720	0.0250	1860	0.0198	3060	0.0172	86400	0.0082
11	0.0482	780	0.0246	1920	0.0197	3120	0.0171	-	-
15	0.0462	840	0.0242	1980	0.0195	3180	0.0170	-	-
20	0.0445	900	0.0238	2040	0.0193	3240	0.0169	-	-
30	0.0420	960	0.0235	2100	0.0192	3300	0.0168	-	-
40	0.0403	1000	0.0233	2160	0.0190	3360	0.0167	-	-
50	0.0389	1020	0.0232	2220	0.0189	3420	0.0166	-	-
60	0.0378	1080	0.0229	2280	0.0187	3480	0.0166	-	-
90	0.0355	1140	0.0226	2340	0.0186	3540	0.0165	-	-
100	0.0349	1200	0.0223	2400	0.0185	3600	0.0164	-	-
120	0.0339	1260	0.0220	2460	0.0183	4000	0.0159	-	-
180	0.0317	1320	0.0218	2520	0.0182	5000	0.0150	-	-
240	0.0303	1380	0.0215	2580	0.0181	6000	0.0142	-	-
300	0.0293	1440	0.0213	2640	0.0179	7000	0.0137	-	-

4.2. DHR SYSTEM DESCRIPTION AND FUNCTION

The DHR system shown in Fig. 5 consists of:

- The “external” DHR system which is made up of three loops (3 x 100% redundancy) in extensions of the pressure vessel. The choice of three loops is based on safety approach considerations, by assuming that one loop could fail due to an accident initiating event (i.e. break), while another is supposed to be unavailable (single failure criterion);
- A metallic guard containment enclosing the primary system (referred as close containment). It is not pressurized in normal operation and has a free volume such as the fast primary helium expansion gives an equilibrium pressure of 1.0 MPa in the first part of the transient (few hours).

Each dedicated DHR loop (Fig. 6) designed to work in forced circulation with blowers or in natural circulation (NC), and is composed of:

- A primary loop (cross duct connected to the core vessel), with a driving height of 10 meters between core and DHX mid-plan;

¹Darwin code is a tool developed by the CEA for computing physical quantities related to nuclear fuel cycle analysis, nuclear reactor dismantling, thermonuclear fusion, accelerator driven system etc.

- A secondary circuit filled with pressurized water at 1.0 MPa (driving height of 5 meters for natural circulation DHR);
- A ternary pool, initially at 50°C, whose volume is determined to handle one day heat extraction (after this time delay, additional measures are foreseen to fill up the pool).

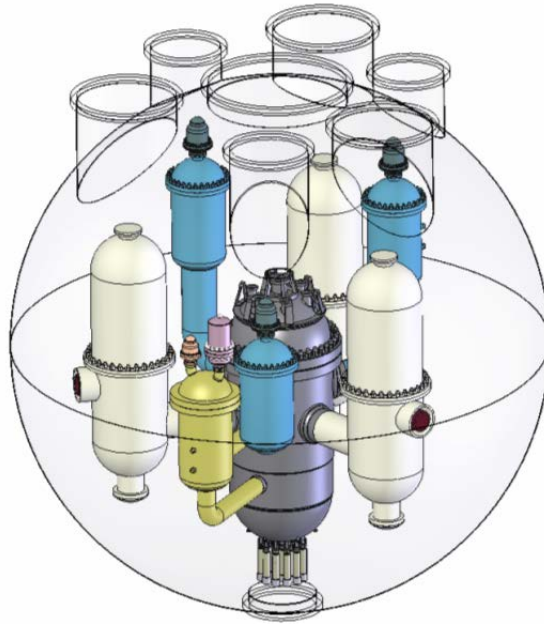


FIG. 5. View of the primary circuit (DHR loops in blue) and the close containment.

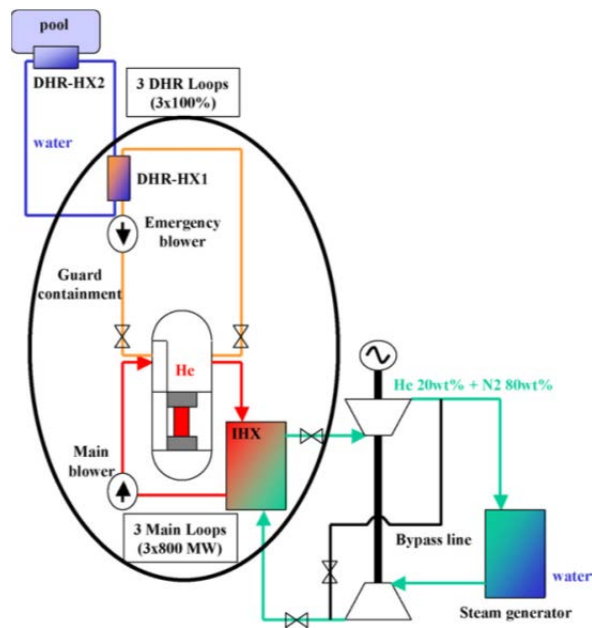


FIG. 6. Scheme of a DHR loop [21].

The design specifications of the DHR system have been proposed [21] according to a strategy presented in Fig. 7. According to this strategy, the natural circulation (NC) of gas through the DHR system is foreseen:

- (1) For pressurized situations (i.e. with intact helium pressure boundary);
- (2) For depressurized situations (i.e. with non-intact helium pressure boundary) with the supply of the dedicated nitrogen filled tanks discharge.

For the later, owing to the poor NC capability of gaseous coolant, a backup pressure level is provided by close-containment.

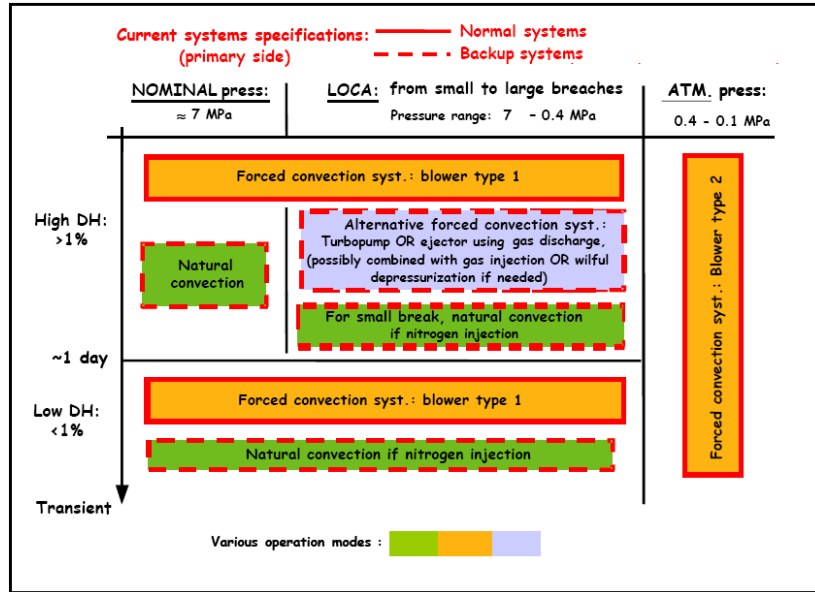


FIG. 7. Schematic of the first reference DHR strategy based on mixed natural and forced convection systems.

4.3. SCENARIOS SELECTED FOR NCDHR RELIABILITY EVALUATION

Two transient scenarios are selected to be representative of the situations of interest regarding the natural circulation DHR process for the GFR:

- (1) A station black out (SBO) initiating event, i.e. loss of station service power (LOSP) cumulated with all emergency diesel generators failure to start, and with only one DHR loop available. This “aggravated” LOFA transient is considered as an envelope case of the pressurized situations despite its very low frequency of occurrence.
- (2) A 3 inches diameter LOCA initiating event (maximum size of small break LOCA), located on the cold part of a main cross duct, representative of depressurized situations. The transient assumes a total loss of forced circulation DHR means (DHR blowers fail to start for example), with two DHR loops available and with nitrogen injection from the N2 filled tanks in order to ensure a sufficient backup pressure level (primary circuit linked to the close containment).

The sequences of events corresponding to the two scenarios are depicted in Appendix I.

5. SIMULATION RESULTS

This chapter provides the highlights of the results of all participants. The detailed results of both transients are presented in Appendix I & II.

5.1. CEA, FRANCE

5.1.1. Modelling

The calculations have been performed with the CATHARE2 code. In addition to the circuits shown in Fig. 8, a large free volume used to describe the spherical close containment and three nitrogen accumulators (540 m³, 7.5 MPa) have been modeled in the second scenario. The transient calculations have been performed over 7100s for transient I, and over 21600s (6 hours) in case of transient II.

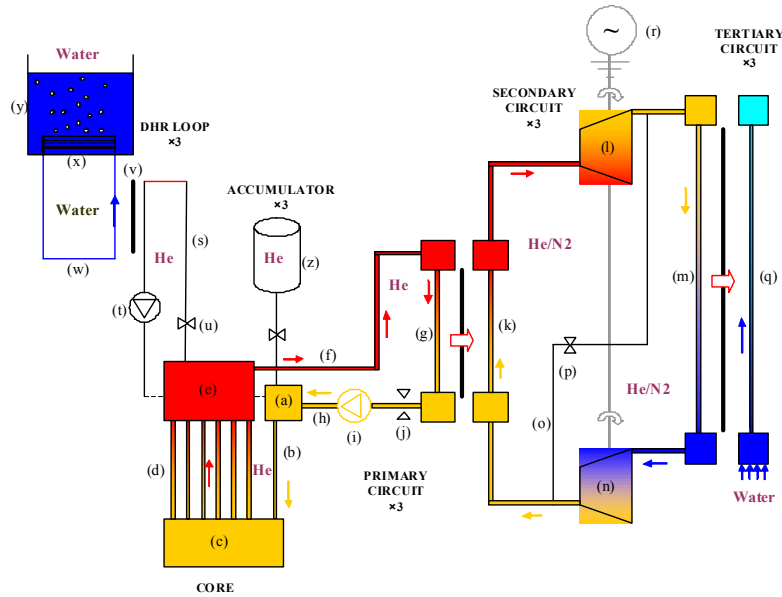


FIG. 8. Schematic drawing of the GFR CATHARE modelling. (a) Volcold, (b) Downcomer, (c) Lowerplenum, (d) Core, (e) Upperplenum, (f) Hotduct, (g) IHX primary side, (h) Coldduct, (i) primary blower, (j) primary isolating valve, (i) accumulators, (k) IHX secondary side, (l) Turbine, (m) GV gas side, (n) Compressor, (o) Bypass line, (p) Bypass valve, (q) GV water side, (r) generator, (s) DHR primary loop, (t) DHR blower, (u) DHR isolating valve, (v) DHR primary heat exchanger, (w) DHR secondary loop, (x) DHR secondary heat exchanger, (y) DHR water pool, (z) Helium accumulators.

5.1.2. Reference results of transient I (LOFA)

The reference calculation, with nominal values of the input parameters, shows that only one DHR loop working in natural circulation fulfills perfectly its mission. A stable flow rate of about 30 kg/s is quickly (in less than 100 s) established in the DHR loop and is maintained up to the end of the transient during the natural circulation phase. During two hours (time considered in the study) from the beginning of the transient, the heat removal is sufficient and all failure criteria are respected, with values staying well below the safety limits. A maximum clad temperature (criterion 2) equal to 1054°C is obtained at 195s, after the sequence

involving isolation of the main loops and connection of the DHR circuits (Fig. 9a). The maximum gas temperature (criterion 3) is equal to 1034°C.

5.1.3. Reference results of transient II (LOCA)

The reference calculation, with nominal values of the input parameters, shows that two DHR loops working in natural circulation fulfill their mission with the help of nitrogen injection from accumulators. After nitrogen injection, a flow rate of at least 50 kg/s is maintained up to the end of the transient during the natural circulation phase. During six hour from the beginning of the transient, the heat removal is sufficient and all failure criteria are respected, with values staying below the safety limits. Peak clad temperature (PCT) (criterion 2) equal to 1404°C at first peak is obtained at 624s and a second peak (criterion 4) equal to 840°C is observed at 6206s after nitrogen injection (Fig. 9b). The maximum gas temperature (criterion 3) is equal to 1241°C; however, the margin is only 9°C for this third criterion.

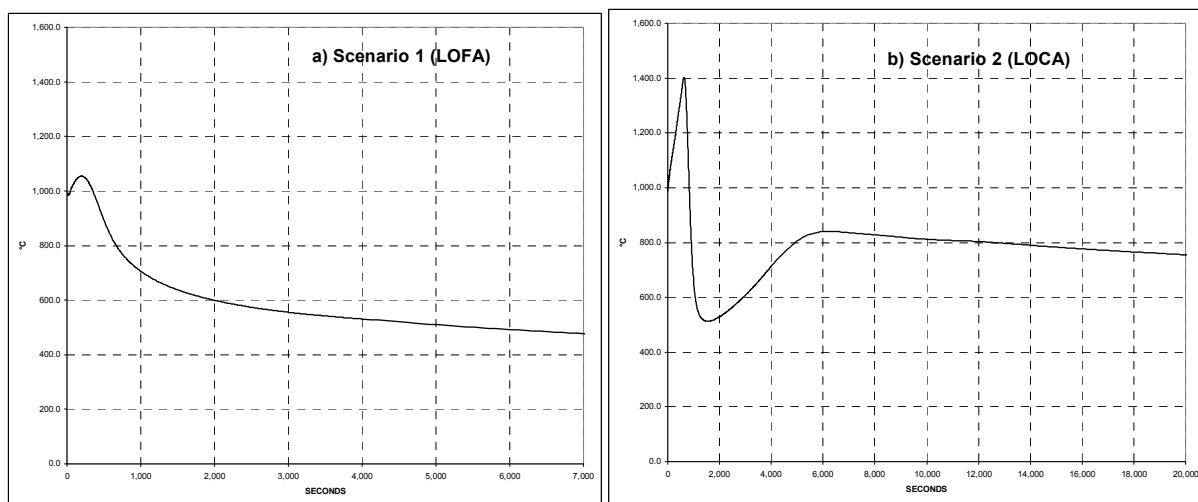


FIG. 9. Clad temperatures in the central channel of the core.

5.1.4. Identification and quantification of uncertainties

In order to identify the main sources of uncertainties in the estimation of the quantities associated with the failure criteria, sensitivity analyses have been performed for a number of input parameters in the CATHARE2 calculations. Classical OAT (one at a time) analysis, in which one factor is varied from the nominal condition, the others being kept at their nominal values, has been used for this sensitivity analysis.

5.1.4.1. Transient I (LOFA)

Among 24 parameters studied (see Table 5), very few have a significant influence on the transient, in the area investigated. The major effect is produced by the additional singular pressure drop coefficient (estimated by CFD analysis), which simulates the stopped DHR blower. In comparison with the reference case, the introduction of this pressure drop increases the peak clad temperature and the maximum temperature of helium at the core outlet by 600°C and the failure criteria are no more respected. The primary blower inertia has a noticeable effect on the transient sequence and on all system parameters. Initial power, delay between primary valves closure and DHR valves opening and wall inertia are others

parameters with significant influence on the transient sequence. All remaining parameters have a very limited impact on the transient. Especially uncertainties on materials properties play a very limited role. For reliability analysis, ten most relevant uncertain input parameters have been selected (shown as bold in Table 5). These selected parameters are supposed to follow uniform distributions. The singular pressure drop due to the stopped blower has not been taken into account, considering that a bypass will be installed and that, in this case, the uncertainty on this parameter will not have a significant effect. In the PSA analysis, however, the reliability of this bypass will have to be considered.

5.1.4.2. Transient II (LOCA)

The effects of 27 input parameters on the four responses of interest (1st PCT, 2nd PCT, maximum temperature of gas at core outlet and maximum pressure in the close containment) have been studied independently. Table 6 gives the list of these 27 parameters with their range of variation. In all the OAT cases, the clad temperature criterion is satisfied, but the criterion on the gas maximal temperature exceeded several times, and the criterion on the close containment maximum pressure exceeded one time. Table 7 presents the OAT cases of the parameters exceeding the failure criteria. These parameters have been chosen for the reliability analysis and they have been modeled by normal distributions. Note that the effects of some parameters (i.e. pressure for accumulator discharge, helium–clad heat transfer coefficient etc.) on the first and the second peak of clad temperature are contradictory. This is due to an early nitrogen injection which limits the first peak but is unfavorable for the second peak due to the nitrogen accumulators being emptied earlier. This gives a glimpse of the difficulties in the design of the reactor in finding an optimum for these parameters.

TABLE 5. PARAMETERS STUDIED FOR SCENARIO 1 (LOFA)

No.	Parameter	Selected No.	Reference	Min. value	Max. value
1	Secondary DHR loop pressure (MPa)		1	0.7	1.3
2	Plate type core laminar pressure drop coefficient	1	1	0.85	1.15
3	Singular pressure drop coefficient for DHR stopped blower		1	-	674
4	Natural leakage from primary circuits to containment (kg/s)		0	-	0.02
5	Singular pressure drop coefficients for core channels		K	K*0.9	-
6	Singular pressure drop coefficient at DHR IHX inlet	2	1	-	10
7	Singular pressure drop coefficient at DHR IHX outlet	3	1	-	10
8	DHR pool temperature (°C)		50	42.5	57.5
9	Helium–clad heat transfer multiplicative factor	4	1	0.95	1.05

No.	Parameter	Selected No.	Reference	Min. value	Max. value
10	Multiplicative factor for all wall thermal inertia	5	1	0.85	1.15
11	Corrective factor for HT in DHR IHX	6	1	0.9	1.1
12	Corrective factor for HT in DHR pool		1	0.5	1.5
13	Delay between main loop closure and DHR loop opening		6	-	26
14	Core flow rate threshold for primary valve closure		3% Q_{nom}	2.5% Q_{nom}	3.5% Q_{nom}
15	Core nominal power	7	P_{nom}	0.98 P_{nom}	1.02 P_{nom}
16	Core residual power	8	Pres	0.9 Pres	1.1 Pres
17	Primary blowers inertia	9	I_{ref}	0.75 I_{ref}	1.25 I_{ref}
18	Main circuit pressure (MPa)	10	P_{main}	0.8 P_{main}	1.2 P_{main}
19	Heat exchange coef. for DHR cross duct insulation (W/m/K)		0.6	0.1	10
20	Homogenized fuel specific heat capacity		$\rho.Cp_{FUEL} = f(T)$	-10%	+10%
21	Homogenized fuel thermal conductivity		$\lambda_{FUEL} = f(T)$	-10%	+10%
22	Helium specific heat (J/kg/K)		5193	-10%	+10%
23	Helium thermal conductivity		$\lambda_{HE} = f(T)$	-10%	+10%
24	Helium dynamic viscosity		$\mu_{HE} = f(T)$	-10%	+10%

TABLE 6. PARAMETERS STUDIED FOR SCENARIO 2 (LOCA)

No.	Parameter	Selected No.	Reference	Min. value	Max. value
1	Core total pressure drop		1	-15 %	+15%
2	Inlet k-factor in DHR primary loop		1	0	2
3	Outlet k-factor in DHR primary loop		1	0	2
4	Helium clad heat transfer coefficient	1	K	-25%	+25%
5	Multiplication factor for thermal inertia for all walls		1	-15 %	+15%

No.	Parameter	Selected No.	Reference	Min. value	Max. value
6	Corrective factor for heat transfer in DHR IHX	2		-25%	+25%
7	Core nominal power	3	P _{nom}	-2%	+2%
8	Core residual power	4	P _{res}	-10%	+10%
9	Primary blower inertia	5		-25%	+25%
10	Main circuit pressure (MPa)			-0.2	0.2
11	SCRAM actuation (P_{containment} in bar)	6	1.3	1	2
12	Accumulators discharge (Primary pressure in bar)	7	10	8	12
13	Delay between main loop isolation and DHR conection (s)		6	4	10
14	Gas mixture viscosity		Wilke law	-5%	+ 5%
15	Gas mixture conductivity	8	Mason & Saxena law	- 10%	+ 10%
16	Gas mixture heat capacity	9		-5%	+5%
17	Close containment leakages (kg/s)		2 10 ⁻⁴	-	+10%
18	Close containment free volume (m³)	10	11620	-10%	+10%
19	Close cont. heat exchange with the outside (w/m ² /K)		15	-10%	+10%
20	Close containment outside temperature (°C)		20	10	30
21	Close containment initial temperature		50	30	70
22	Volume of heat structures in close containment (m ³)		1574	-10%	+10%
23	Closed containment initial pressure (bar)		1	-10%	+10%
24	Accumulators initial pressure (bar)		75	70	80
25	Accumulators initial temperature (°C)		50	30	70
26	Discharge line singular pressure drop		15	-50%	+50%
27	Break size (inches)		3	-10%	+10%

5.1.5. Failure probabilities evaluations

For each scenario, Latin Hypercube Sampling (LHS) has been performed using the 10 respective input parameters with their corresponding distributions. 1000 samples of the input parameters were simulated for the first transient and 100 samples for the second and for each sample a T-H calculation was performed with the CATHARE2 code. For the transient I, response surfaces were calculated. The process carried out by the T-H code was approximated by a simple mathematical function in the region of interest. First order linear response surfaces were constructed for all the three quantities of interest and are given by:

$$Y = \beta_0 + \sum_{i=1}^p \beta_i X_i \quad (3)$$

with Y the response and X_i the input parameters. The quality of fitness of the assumed model, in comparison with the actual code response, is given by the coefficient of determination R^2 .

5.1.5.1. Transient I (LOFA)

None of the cases among the 1000 simulations met the failure criteria. Maximum clad temperature never exceeded 1600°C and maximum gas temperature at core outlet never exceeded 1250°C. The estimate of the probability of failure is defined as $p_f = m/N$, where m is the number of code runs which met the failure criterion and N = total number of code runs but in this case, p_f takes the value equal to zero since no code run provides an output observable within the failure domain. This result illustrates a limitation of Monte Carlo simulation. The complexity of the physical problem to solve involves large computational time on each run and enables only a limited number of simulations, which are not enough for achieving a proper estimation of failure probability. Wilks' formula for one sided tolerance interval can be used for calculating a conservative upper bound γ of the actual probability of failure p_f : $1 - (1-\gamma)^N \geq \beta$, where β expresses the "confidence" that p_f will be lower or equal than γ . Considering $\beta = 0.95$ and $N = 1000$, γ is equal to 0.003. This constitutes, however, a very high upper bound for the failure probability, according to the margins that we obtain on the two failure criteria.

Reliability analysis using the regression model

This reliability analysis has been performed on the failure criterion related to the maximum helium temperature at core outlet for which we have lesser margin. Considering the linear relation between the maximum helium temperature and the input parameters ($R^2 = 0.994$), we used this linear model instead of the CATHARE2 code to study the effect of changing the range of the input parameters uncertainties on the failure probability. The regression model is given by the following:

$$\text{Max Helium T} = 1022.6 + V_1 * 3.0972 + V_2 * 0.5621 + V_4 * 58.772 + V_5 * -203.18 + V_6 * -40.26 + V_7 * 738.8 + V_8 * 259 + V_9 * -287.14 + V_{10} * -21.541 \quad (4)$$

(V_i the input parameters with the subscript $i=1$ to 10 corresponding to column Selected No. in Table 7).

TABLE 7. PARAMETERS OF SCENARIO 2 (LOCA) EXCEEDING (IN BOLD) FAILURE CRITERIA

No.	Parameter	Modification	1st PCT (°C)	2nd PCT (°C)	He max. T (°C) at core outlet	Close containment max. P (bars)
	Failure criteria		1600	1000	1250	14.000
	Reference case		1404.4	842.2	1243.3	13.332
1	Helium clad heat transfer coefficient	- 25 %	1377.9	851.2	1219.6	13.330
		+ 25 %	1417.7	836.9	1253.0	13.331
2	Corrective factor for heat transfer in DHR IHX	- 25 %	1428.3	926.9	1263.8	13.514
		+ 25 %	1385.3	792.8	1226.1	13.215
3	Core nominal power	- 2 %	1378.7	825.9	1222.7	13.325
		+ 2 %	1426.5	858.8	1260.8	13.338
4	Core residual power	- 10 %	1327.7	761.0	1184.1	13.287
		+ 10 %	1472.3	921.8	1292.4	13.371
5	Primary blower inertia	- 25 %	1457.6	844.1	1284.9	13.312
		+ 25 %	1359.3	840.6	1206.4	13.351
6	SCRAM actuation (P_{containment})	- 0.03 MPa	1386.1	842.2	1227.0	13.320
		+ 0.07 MPa	1452.7	842.6	1282.8	13.350
7	Accumulators discharge (Primary pressure)	- 0.2 MPa	1460.7	839.9	1292.5	13.337
		+ 0.2 MPa	1356.1	844.3	1195.7	13.328
8	Gas mixture conductivity	- 10 %	1416.6	859.1	1253.0	13.418
		+ 10 %	1392.7	828.2	1232.8	13.261
9	Gas mixture heat capacity	- 5 %	1429.4	871.0	1269.4	13.396
		+ 5 %	1377.4	816.1	1215.7	13.281
10	Close containment free volume	- 10 %	1400.5	799.4	1239.5	14.367
		+ 10 %	1406.1	885.2	1244.5	12.450

Performing various numbers of simulations (up to 10^7) with this linear model and keeping the initial probabilistic model, the maximum value of He temperature is 67°C below the failure criterion. We have performed several modifications of the initial probabilistic model in order to test the influence of these changes on the failure probability. Table 8 shows the various modifications in the probabilistic model and the corresponding failure probabilities and maximum helium temperatures. We obtained in this way rough estimation of the failure probability of the DHR system in case of transient I. Even by doubling the range of variation of most important variables (blower inertia or wall thermal inertia), the failure probability obtained is very small. The same is observed by increasing the ranges of variation of all the input parameters by 50%. In order to obtain a relatively significant failure probability ($\sim 10^{-4}$), it is necessary to double the range of variation of the two most important variables simultaneously or to increase the ranges of all the parameters by 70%. However, studies should be sustained to evaluate the pressure drop caused by the stopped blower and to assess the need to bypass it in situations of natural circulation.

TABLE 8. EFFECT OF MODIFICATIONS OF THE PROBABILISTIC MODEL ON THE FAILURE PROBABILITY

Modification in the initial probabilistic model	Failure probability P_f	COV of P_f	Max. Helium T ($^\circ\text{C}$)
V9 (blower inertia) : [-50% , 50%]	7.2×10^{-7}	0.12	1256
V5 (wall thermal inertia) : [-30% , 30%]	No failure case	-	1209
V9 (blower inertia) : [-50% , 50%] and V5 (wall thermal inertia) : [-30% , 30%]	2.71×10^{-4}	0.06	1277
Uncertainty range of all variables * 1.1	No failure case	-	1197
Uncertainty range of all variables * 1.2	No failure case	-	1212
Uncertainty range of all variables * 1.3	No failure case	-	1229
Uncertainty range of all variables * 1.4	No failure case	-	1247
Uncertainty range of all variables * 1.5	3.5×10^{-6}	0.17	1263
Uncertainty range of all variables * 1.6	5.7×10^{-5}	0.13	1276
Uncertainty range of all variables * 1.7	3.2×10^{-4}	0.06	1292

Modification of the value of failure criteria

Due to extremely low probability of system failure obtained in this transient, a meaningful comparison between the two methodologies (RMPS and APSRA) may not be possible. It was

agreed to artificially lower one of the failure criterion (He maximum temperature) to 1050 °C to allow for a better comparison of the two methodologies.

With this new value, out of 1000 simulations, 316 cases exceeded the failure criteria. The failure probability (\overline{P}_f) of 0.316 was obtained with good accuracy (variation coefficient $cov(\overline{P}_f) = 0.04$). On the other hand, by using the regression model (Eq. 4), the same result was obtained (i.e. $\overline{P}_f = 0.316$) with 10^7 simulations.

5.1.5.2. *Transient II (LOCA)*

For each simulation performed, natural circulation DHR system was considered failed if at least one of the four failure criteria given in Table 21 (Appendix I) were exceeded.

With the 100 simulations, we obtained an estimate of the failure probability $\overline{P}_f = 0.49$ with an acceptable accuracy (variation coefficient $cov(\overline{P}_f) = 0.10$). To date, this estimation should be retained for this scenario in the PSA. However, this result also shows the necessity to improve the reliability of the natural circulation DHR. The improvements can be made by increasing the nitrogen volume, draining successively the three accumulators or reviewing the design of the close containment.

Failure probability with regard to each criterion considered independently

In this estimation, the four responses of interest have been modeled by normal distributions (hypothesis not rejected by goodness of fit tests), with averages and standard deviations obtained on 100 simulations. The failure probabilities (see Table 9) were then estimated by $P_f = P(Y \geq S) = 1 - P(Y < S) = 1 - F_Y(S)$, where Y is one of the responses, S is the associated failure criterion and F_Y is the cumulative function of Y (normal distribution). Note that here the failure probability for each response is evaluated independent of others and the sum of these four probabilities exceeds slightly the total failure probability of the system calculated previously ($\overline{P}_f = 0.49$). In some simulations, two failure criteria may have been exceeded at the same time. These results enable us to conclude that the most often exceeded failure criterion is the gas temperature at core outlet (1250 °C). Figure 10 shows the scatter in the 100 curves of evolution of this gas temperature and on the peak of temperature (zoomed view shown in Fig. 11). The distribution of gas peak temperature can be seen in Fig. 12. The second failure criterion, for which attention should be paid, is the pressure in the close containment. The criteria on the clad temperatures have very low probabilities compared to the two mentioned above.

TABLE 9. FAILURE PROBABILITIES WITH REGARDS TO EACH CRITERION

Responses of interest	P_f
Maximum clad temperature (1st peak)	2.46×10^{-4}
Maximum clad temperature (2nd peak)	3.61×10^{-4}
Maximum temperature of gas at core outlet	0.456
Maximum pressure in the close containment	0.092

5.1.6. Global sensitivity analysis

The objective of this analysis is to evaluate the importance of each input uncertain parameter in contributing to the overall uncertainty of each response of interest. A global sensitivity analysis has been carried out by the way of standard regression coefficients. Considering that the response Y is a linear function of the random input variables X_i , the standardized regression coefficients (SRC) are obtained from the regression model (Eq. 3). The SRC quantify the effect of varying each input variable away from its average by a fixed fraction of its variance and is given by:

$$SRC(Y, X_i) = \beta_i \sqrt{\frac{Var(X_i)}{Var(Y)}}$$

The sign of the SR coefficients indicates if the response increases (+) or decreases (-) when the variable increases. The sum of the SRC^2 is equal to the coefficient of determination R^2 .

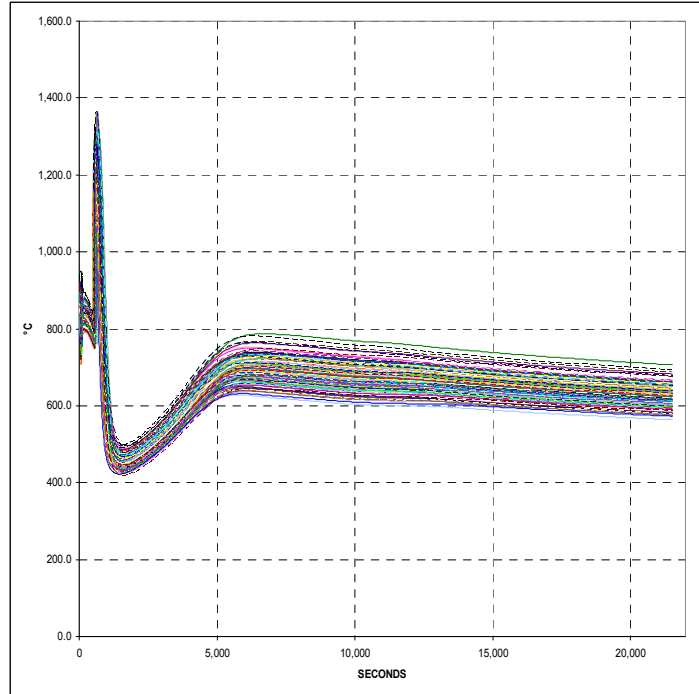


FIG. 10. LOCA scenario — 100 curves of evolution of gas temperature at core outlet.

5.1.6.1. Transient I (LOFA)

For the three responses of interest (maximum fuel, clad and helium temperatures), the hypothesis of a linear relation between the output and the input parameters is valid, because the values of R^2 are close to 1 in each case and so we can use SR coefficients as sensitivity indices. The results obtained on SR coefficients for the three temperatures are logically very close as the three temperatures are correlated. Table 10 gives for example SR coefficients obtained for the maximum clad temperature. The most influential parameters on this temperature are the primary blower inertia, wall thermal inertia and the core residual power. They describe together about 90% of the uncertainty on the clad temperature. The most

important parameter is the primary blower inertia, which describes about 69% of the uncertainty on the clad temperature.

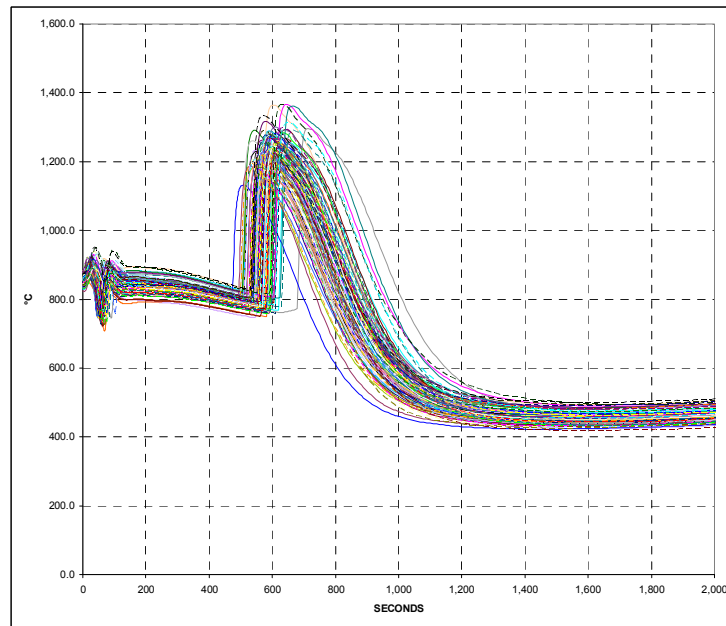


FIG. 11. LOCA scenario — Zoom on peak of temperature.

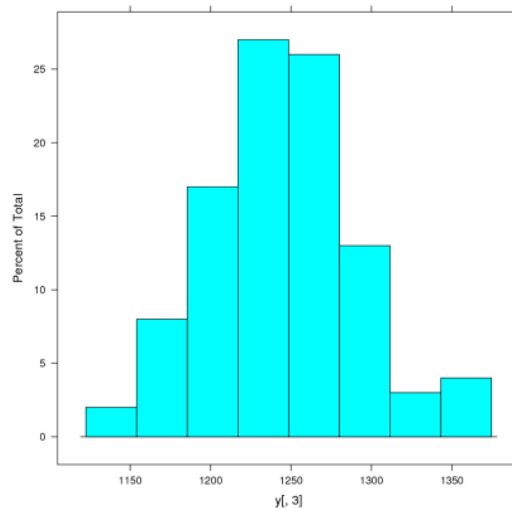


FIG. 12. LOCA scenario — Histogram of distribution of the peak.

5.1.6.2. Transient II (LOCA)

For the four responses of interest (maximum clad and gas temperatures at first and second peak, maximum helium temperature and close containment pressure), the hypothesis of a linear relation between the output and the input parameters is valid and *SR* coefficients are used as sensitivity indices. *SR* coefficients for the two temperatures (clad and helium) at first peak are very close because these two temperatures are correlated. The most influential parameters (see Table 11) are the core residual power, the lower plenum pressure for accumulator discharge and the primary blower inertia. For the maximum clad temperature at

second peak (see Table 12), the most influential parameters are the residual power and the close containment free volume.

TABLE 10. STANDARDIZED REGRESSION COEFFICIENT FOR MAXIMUM CLAD TEMPERATURE (LOFA)

Rank	Input parameter	SRC	SRC ²
1	Primary blower inertia	-0.829	0.687
2	Wall thermal inertia	-0.328	0.107
3	Core residual power	0.300	0.090
4	Core nominal power	0.193	0.037
5	Heat transfer in DHR IHX	-0.116	0.014
6	Helium clad heat transfer	0.114	0.013
7	Main circuit pressure	-0.054	0.003
8	Inlet k-factor in DHR primary loop	0.013	1.7×10^{-4}
9	Core total pressure drop	0.008	6.8×10^{-5}
10	Outlet k-factor in DHR primary loop	-0.008	5.9×10^{-5}

TABLE 11. STANDARDIZED REGRESSION COEFFICIENTS FOR MAXIMUM CLAD TEMPERATURE AT FIRST PEAK (LOCA)

Rank	Input parameter	SRC	SRC ²
1	Residual power	0.658	0.433
2	Lower plenum pressure for accumulator discharge	-0.495	0.245
3	Primary blower inertia	-0.480	0.230
4	Gas mixture heat capacity	-0.255	0.065
5	Nominal power	0.226	0.051

TABLE 12. STANDARDIZED REGRESSION COEFFICIENTS FOR MAXIMUM CLAD TEMPERATURE AT SECOND PEAK (LOCA)

Rank	Input parameter	SRC	SRC ²
1	Residual power	0.864	0.747
2	Close containment free volume	0.454	0.207
3	Gas mixture heat capacity	- 0.301	0.091

5.2. BARC, INDIA

A RELAP5 model of GFR was built for the performance assessment and sensitivity analysis of the reactor. A transient related to station Black Out under pressurized conditions was simulated for one hour with only one passive decay heat removal system available out of three. Sensitivity analysis, based on the parameters suggested to vary, has been carried out and failure criteria have been checked.

5.2.1. GFR RELAP5 modelling

The whole reactor system is divided into five parts:

- Main heat transport system;
- Secondary system for heat removal during normal operation (boundary condition given);
- DHR System:
 - DHR primary system;
 - DHR secondary system (water side);
 - DHR tertiary system (water pool side).

The reactor pressure vessel along with the primary circuit path has been considered as main heat transport system. Lower plenum, core, bypass and upper plenum are the components of reactor pressure vessel. Radial power distribution has been considered in the core by dividing it radially in six power channels and one bypass channel. During normal operation of the reactor the energy is transferred to the turbine secondary system which is simulated as the heat exchanger boundary condition. Secondary side of the GFR main circuit is simulated as the boundary condition. Flow rate along with secondary pressure and temperature is given and that is applied as the secondary boundary condition. The DHR circuit is divided into three parts: DHR primary circuit (He gas side), DHR secondary circuit (water loop), DHR tertiary Circuit (water Pool).

5.2.2. Performance analysis

Performance analysis of the passive decay heat removal system of 2400 MW(th) gas cooled fast reactor has been carried out for 3600 s. The analysis shows that the DHR primary side mass flow rate initially reduces quite fast and becomes zero because of non-availability of blower for some period and then rises to stable flow rate of almost 50 kg/s at the end of transient.

The peak clad temperature is around 1025 °C, the maximum gas outlet temperature is above 1000 °C and DHR structural temperature is around 450 °C at the end of 3600s. A stable natural circulation flow rate of around 300 kg/s is established in the DHR (water side). The DHR secondary side water temperature rises from initial 50 °C to nearly 120 °C at the end of transient and the pressure increases from initial 1 MPa to 1.15 MPa, which is controlled by the pressurizer. Moreover, it is found that all the parameters remain well below the failure limits.

5.2.3. Sensitivity analysis

Effects of various process parameters and model uncertainties on the system performance were investigated. As a result of this exercise, it is found that the key process parameters to affect system performance and may cause the failure of the system due to their variation from their nominal conditions are:

- High fission heat generation rate;
- Low pressure in the system;
- High decay power.

Important model parameters which can cause significant effect on system performance and failure of the system are:

- Frictional resistance in fuel assembly;
- Heat transfer coefficient (primary side);
- Primary blower inertia.

Effects of variation of other model parameters on system performance are found to be negligibly small.

5.2.4. Prediction of failure surface

The process parameters were varied from their nominal states and their effects on system failure were investigated. It is found that the most conservative variation of these parameters does not yield any system failure. The model uncertainties were propagated along with variation of system parameters. As a result for the worst combination of the parameters, it is found that the system is having sufficient margin to failure.

In order to understand the applicability of the methodology for the reliability of the DHR system, the failure criterion for the gas temperature at core outlet was reduced from 1250 °C to 1050 °C. With the new failure criterion (which was made as an academic exercise), failure points were generated for different combination of process parameters, which were allowed to vary from their nominal states in the range considered. With propagation of model uncertainties, the failure surface was modified.

5.2.5. Evaluation of reliability

The root causes for the variation of the process parameters are not known for GFR. Hence, the causes for failure are assumed in this exercise as an example of demonstration of application of APSRA methodology and not to accurately predict its reliability. The failure probability of the passive system depends on the variation of the three process parameters of the main heat transport system as discussed before. Hence, the metric considered is the failure frequency of

the components of the primary heat transport system to cause deviation of the parameters from their nominal values, while assessing the process parameters variation. The fault tree for deviation of process parameters was generated. Variation of main circuit pressure is attributed to failure of pressure controller or mismatch of heat removal in IHX circuit or leakage due to failure of the valves in the circuit since actual cause for GFR is not known. Variation of nominal power and residual power is attributed to malfunction of neutron flux monitoring system or reactor regulation system. However, it may be noted that variation of nominal power and residual power is also attributable to composition of fuel and burn up at the time of SBO, which is not considered here due to lack of information.

The failure frequency of the system was calculated based on the generic data available for components governing variation of these process parameters. The failure frequency of the system for variation of different process parameters without considering model uncertainty is found to be $7.052 \times 10^{-6}/\text{hr}$.

Treatment of model uncertainty in APSRA methodology is through comparison of model predictions with test data instead of a PDF treatment as assumed here; hence, APSRA does not consider different failure frequency of the system with model uncertainty. Since test data are not available, the model uncertainties have been treated in this analysis based on the assumption of uniform distribution as discussed earlier. Considering model uncertainties the fault trees were redeveloped and failure frequencies were recalculated. The failure frequency of the passive system is found to be $7.3 \times 10^{-6}/\text{h}$ by considering the model uncertainty. The result shows that contribution of model uncertainty is negligible (around 4%).

5.3. SCK-CEN, BELGIUM

5.3.1. Highlights of transient I results

The deterministic calculations were performed with the thermohydraulic code RELAP5 mod 3.2. The results of the deterministic calculations show that all the failure criteria are respected with the values staying well below the safety limits.

The reliability analysis was performed with SUSA software and input uncertainties were propagated through the T-H code RELAP5. 100 samples of the input parameters were simulated and for each, a thermohydraulic calculation was performed using RELAP5 code. The DHR system has demonstrated very high degree of reliability in both cases i.e. steady state and transient. The output parameters evaluated with a quantile of $X_{95\%}$ satisfy the LOFA failure criteria.

Helium temperature limit (for the core structures integrity), though respected, is very close to the maximum value obtained by the statistical analysis (the margin is only 15 °C). However, refining the statistical analysis by using different quantiles ($X_{99\%}$ or $X_{99.9\%}$) could result into higher margin. The other two failure criteria (maximum clad temperature and maximum temperature of DHR structural material) are satisfied with a much higher margin (> 200 °C).

The distributions of the output parameters are globally normal, with some deviations due to the relatively small number of runs considered (100). From the results of statistical analysis, a difference of about 30 °C between the reference values and the average values is seen. In addition, all the three failure criteria are satisfied during the entire duration of the transient.

The results of global sensitivity analysis results show the impact of the different distributions of input parameters considered (sensitivity coefficients) over the main output parameters

(directly connected with the failure criteria). It is observed that there are several parameters which have a strong impact on all the safety related temperatures, while other parameters show a relatively weak influence on the variations.

One of the most influential parameter is the inlet pressure drop factor in the DHR loop that represents the DHR stopped blower. This parameter has a direct impact on the natural circulation mass flow rate and also has a big influence on DHR structures.

Another important parameter is the heat transfer coefficient in the primary–secondary DHR heat exchanger. After 1000s, it influences all the considered output parameters.

The variation of fuel decay heat power curve also plays a very important role, especially for the DHR structural material temperatures, where its impact is most prominent.

The primary blower inertia is important in the early phase of transient (before reaching the pressure/temperature peak), but it has no effect in the later phase.

Other input parameters analyzed through the statistical evaluation proved to have relatively little impact on the transient evolution.

The DHR system working in natural circulation is a very reliable system for loss of flow accident (LOFA) as it satisfies all the failure criteria in its current design status.

5.3.2. Highlights of transient II results

The purpose of this benchmark calculation is to explore the capabilities of the GFR to withstand 21600 seconds (6 hours) from the beginning of the transient event in the accidental conditions specified, reaching a safe long term cooling phase and respecting the specified failure criteria.

A steady state was achieved after 200s, with all T-H parameters being close to their nominal value.

The LOCA transient evolution of main primary system, primary DHR and secondary DHR system T-H parameters (pressures, temperatures, mass flow rates, power exchanged in HXs) were analyzed. Below is the summary of timeline of events during transient evolution:

- (1) 0.0 s: start of transient (break in the cold part of main cross duct);
- (2) 22.0 s: containment pressure > 1.3 bars → reactor scram;
- (3) 80.0 s: start of DHR sequence (core mass flow rate below 3% of nominal value);
- (4) 83.0 s: valves in main loops start to close;
- (5) 91.0 s: valves in DHR loop start to open;
- (6) 96.0 s: DHR sequence is completed;
- (7) 468.0 s: pressure in primary system falls below 1 MPa → N₂ accumulators open.

At this point, the natural circulation (NC) is started and the system is entered into a safe long term cooling phase.

During this long term cooling phase, a low temperature peak is reached after ~8500s. This is important because of the second N₂ pressure peak maximum safety limits, though low in value compared to what the system experiences in the earliest phase of the transient.

Once the long term cooling phase has started, the power removed from the core, the heat exchanged in He–water DHR HX and heat transmitted to the final pool are identical. This clearly shows how the system has actually entered a long term safe cooling phase, where all residual decay power generated in the core can be safely removed by only natural circulation means, without the help of any active system, in the case of a LOCA.

Table 13 summarizes the LOCA transient failure criteria and the maximum pressures and temperatures obtained during the transient. It can be seen that maximum containment pressure exceeds the failure criterion.

TABLE 13. COMPARISON WITH FAILURE CRITERIA

Parameter	Unit	Failure limit	Value obtained from calculation
Maximum DHR structures T	°C	850	530.2
Maximum clad T (1st peak)	°C	1600	1073.0
Maximum clad T (2nd peak)	°C	1000	710.0
Maximum He T	°C	1250	1204.7
Maximum containment Pressure	MPa	1.4	1.78

6. DISCUSSION AND CONCLUSIONS

6.1. COMPARISON OF RESULTS FOR TRANSIENT I

6.1.1. Deterministic results

After the comparison of transient results and the following discussion among all participants, a series of differences in input data used for models has been noticed and identified as the main cause of the differences noted in the different transient evaluations. Thus, a second iteration of calculations for LOFA transient was decided, in order to resolve the differences in input data before starting the "sensitivity" phase. Table 14 and Table 15 summarize the comparison of results.

TABLE 14. RESULTS FOR NOMINAL CONDITIONS

Parameters	CEA (CATHARE)	BARC (RELAP5/Mod 3.2)	SCK-CEN (RELAP5)
Max. vessel pressure (MPa)	7.18	7.05	6.92
Max. fuel centreline Temp. (°C)	1060	1050	1076
Max. clad Temp. (C°)	1054	1013	1070
Max. gas outlet Temp (°C)	1034	1008	1021
Max. DHR structural Temp (°C)	-	386	433
DHR primary side flow rate (kg/s) at 3500 s	30	50	26
DHR secondary side flow rate (kg/s) at 3500 s	180	280	337
DHR secondary side max. fluid Temp. (°C) at 3500 s	150	120	140

TABLE 15. EFFECT OF SENSITIVITY STUDIES

Sensitive Parameters	Variation	Peak Clad Temperature ($\Delta T = T - T_{ref}$) (°C)			DHR Structural Temperature ($\Delta T = T - T_{ref}$) (°C)			Gas Maximum Temperature at core outlet ($\Delta T = T - T_{ref}$) (°C)		
		CEA	BARC	SCK-CEN	CEA	BARC	SCK-CEN	CE A	BARC	SCK-CEN
Core power	- 2 %	-16	-15.0	-	-	-6.0		-16	-16.0	-
	+ 2 %	15	30.78	-	-	8.18		15	31.0	-
Residual power	- 10 %	-26	-13.0	-	-	-24.0		-24	-13.0	-
	+ 10 %	29	10.0	-	-	30.67		28	22.0	-

Sensitive Parameters	Variation	Peak Clad Temperature ($\Delta T = T - T_{ref}$) (°C)			DHR Structural Temperature ($\Delta T = T - T_{ref}$) (°C)			Gas Maximum Temperature at core outlet ($\Delta T = T - T_{ref}$) (°C)		
Main Circuit pressure	- 2 bar	4	19.0	-	-	0.5		4	20.0	-
	+ 2 bar	-5	-16.0	-	-	-0.7		-4	-10	-
Fuel heat transfer coeff.	- 25 %	-12	29.0	-	-	-3.0		-19	33.0	-
	+ 25 %	8	-10.0	-	-	14.0		12	-19.0	-
Heat transfer coeff. in DHR secondary side	- 25 %	13	0.30	8.3	-	4.5	11	13	0.79	-30
	+ 25 %	-9	0.89	-	-	-3.0	-	-8	0.84	-
DHR primary side inlet loss coeff.	- 200 %		0.54	-	-	16.02	-	-	0.83	-
	+ 200 %		0.5	14.3	-	-3.0	18	1	0.4	-30
DHR primary side outlet loss coeff.	-200 %		0.5	-	-	-3.0	-	-	0.79	-
	+ 200 %		0.44	14.3	-	16.35	18	0.5	0.75	-30
Pressure drop in fuel channels	- 15 %		-17.0	-	-	-4.0	-	-0.5	-28.0	-
	+ 15 %		27.0	-	-	4.5	-	0.5	17.0	-
Thermal inertia of primary system comp	- 15 %	33	0.3	-	-	10.5	-	34	0.8	-
	+ 15 %	-30	0.33	-	-	10.7	-	-31	0.83	-
Primary blower inertia	- 25 %	76	43.56	32.3	-	2.5	0	76	45.0	-13
	+ 25 %	-70	-20.0	-	-	-3.0	-	-70	-44.0	-

Table 15 shows the effect of variation of sensitive parameters on failure criteria. BARC results show that the key parameters, which may cause system failure, are pressure, nominal power, residual power, blower inertia, core pressure drop and primary side heat transfer coefficient. The first three parameters are process parameters followed by three model parameters.

In the case of CEA, primary blower inertia, thermal inertia of primary components and the core residual power are the key parameters, which affect the performance of DHRS.

According to SCK-CEN findings, the key parameters which affect the performance of DHRS are primary blower inertia (-25%) and DHR primary side outlet loss coefficient. The other enlisted parameters are not studied by SCK-CEN in the sensitivity analysis.

6.1.2. Reliability results

CEA

After performing 1000 Monte Carlo simulations no failure is obtained, and upper bound of the failure probability was obtained by the Wilks formula and is equal to 0.003. By changing the failure criterion on the He maximum temperature from 1250 °C to 1050 °C, the conditional failure probability is found to be 0.316.

BARC

For the assessment of reliability of the DHRS only three parameters were considered as key parameters causing failure of the system. They are power, blower inertia and heat transfer coefficient. 27 numbers of combinations, by varying the process parameters and model parameters, have been simulated and no failure is obtained. Then by changing the failure criterion of He maximum temperature from 1250 °C to 1050 °C, the failure frequency of the passive decay heat removal system is found to be 7.052×10^{-6} /hour considering the variation of process parameters only. By considering the model uncertainty, the failure frequency is found to be 7.3×10^{-6} /hour.

SCK-CEN

After performing 100 Monte Carlo simulations no failure is obtained. By lowering the maximum coolant temperature criterion from 1250 °C to 1050 °C, the failure probability is found to be 0.413.

6.2. COMPARISON OF RESULTS FOR TRANSIENT II

BARC did not participate in this exercise because of the non-availability of computation tools. SCK-CEN performed the reference calculations and some sensitivity studies. CEA performed the whole exercise.

6.2.1. Deterministic results

The summary of the deterministic results for transient II are given in Table 16 and Table 17.

TABLE 16. RESULTS OF NOMINAL CONDITIONS

Parameters	CEA (CATHARE)	SCK-CEN (RELAP5)
Max. vessel pressure (MPa)	4.5 (Peak)	5.1
Max. fuel centreline temp (°C)	1408	1210
Max. clad temp 1st peak (°C)	1404	1206
Max. clad temp 2nd peak (°C)	840	714
Max. gas outlet temp (°C)	1241	1203
Max. DHR structural temp (°C)	-	530
DHR primary side flow rate (kg/s)) at 3500 s	41 (for each loop)	36
DHR secondary side flow rate (kg/s)) at 3500 s	124 (for each loop)	219
DHR secondary side max. fluid temp (°C) at 3500 s	115	105
Close containment max. pressure (MPa)	1.33	1.78

TABLE 17. EFFECT OF SENSITIVITY STUDIES

Parameters	Variation	Peak Clad Temperature (°C) 1st peak		Peak Clad Temperature (°C) 2nd peak		He Max. T at core outlet (°C)		Close containment Max. P (bars)	
		CEA	SCK-CEN	CEA	SCK-CEN	CEA	SCK-CEN	CEA	SCK-CEN
Helium clad heat transfer coefficient	- 25 %	1377.9	-	851.2	-	1219.6	-	13.330	-
	+ 25 %	1417.7	-	836.9	-	1253.0	-	13.331	-
Corrective factor for heat transfer in DHR IHX	- 25 %	1428.3	1206	926.9	722	1263.8	1203	13.514	18.024
	+ 25 %	1385.3	-	792.8	-	1226.1	-	13.215	
Core nominal power	- 2 %	1378.7	-	825.9	-	1222.7	-	13.325	-
	+ 2 %	1426.5	-	858.8	-	1260.8	-	13.338	-
Core residual	- 10 %	1327.7	-	761.0	-	1184.1	-	13.287	-

Parameters	Variation	Peak Clad Temperature (°C) 1st peak		Peak Clad Temperature (°C) 2nd peak		He Max. T at core outlet (°C)		Close containment Max. P (bars)	
Power	+ 10 %	1472.3	-	921.8	-	1292.4	-	13.371	-
Primary blower inertia	- 25 %	1457.6	-	844.1	-	1284.9	-	13.312	-
	+ 25 %	1359.3	-	840.6	-	1206.4	-	13.351	-
SCRAM actuation (P _{containment})	- 0.03 MPa	1386.1	-	842.2	-	1227.0	-	13.320	-
	+ 0.07 MPa	1452.7	-	842.6	-	1282.8	-	13.350	-
Accumulators discharge (Primary pressure)	- 0.2 MPa	1460.7	-	839.9	-	1292.5	-	13.337	-
	+ 0.2 MPa	1356.1	-	844.3	-	1195.7	-	13.328	-
Gas mixture conductivity	- 10 %	1416.6	-	859.1	-	1253.0	-	13.418	-
	+ 10 %	1392.7	-	828.2	-	1232.8	-	13.261	-
Gas mixture heat capacity	- 5 %	1429.4	-	871.0	-	1269.4	-	13.396	-
	+ 5 %	1377.4	-	816.1	-	1215.7	-	13.281	-
Close containment free volume	- 10 %	1400.5	-	799.4	-	1239.5	-	14.367	-
	+ 10 %	1406.1	-	885.2	-	1244.5	-	12.450	-
DHR pressure loss	200%	-	1206	-	716	-	1203	-	17.834

From Table 17, it can be seen that in the case of CEA, the key parameters which affect the first peak clad temperature and He gas maximum temperature at core outlet are: residual power, accumulator discharge pressure and primary blower inertia. The parameters which affect the second peak clad temperature are: residual power, close containment free volume and gas mixture heat capacity. Close containment free volume is the key parameter, which affects the close containment maximum pressure.

SCK-CEN studied only two parameters, which include DHR pressure loss and corrective factor for heat transfer in DHR IHX.

6.2.2. Reliability results

CEA

After performing 100 Monte Carlo simulations, the failure probability is estimated to be 0.49. The most often exceeded failure criterion is the He maximum temperature at core outlet (failure probability = 0.456). The second failure criterion, for which attention should be paid, is the pressure in the close containment. The criteria on the clad temperatures have very low probabilities compared to the other two criteria.

The most important parameters, which affect the DHR performance, are residual power, accumulator discharge pressure and primary blower inertia

6.3. INSIGHTS FROM THE APPLICATION OF TWO METHODOLOGIES

- (1) CEA and SCK-CEN have used quite similar methodologies to propagate uncertainties through the T-H system code, to assess the reliability and to perform sensitivity analysis. But they have used different system code: CATHARE for CEA and RELAP for SCK-CEN. The results obtained on transient I on the uncertainty boundaries for the response of interest are very close. But the conclusions of the sensitivity analysis are slightly different.
- (2) The methodology used by CEA (RMPS) and SCK-CEN (SUSA) in one side and BARC (APSRA) in the other side are different:
 - RMPS and SUSA consider uncertainties in the form of probability density functions (PDF), then performs random sampling on these PDF and propagate these uncertainties through the system code to evaluate the failure probability and to perform sensitivity analysis.
 - APSRA distinguishes between process and model parameters, does not consider uncertainties in the process (operating) parameters, and consider that if there are deviations of the parameters from their nominal values, this is due to failure of components or system. APSRA calculates a failure surface in the space of the process variables; this failure surface can necessitate many calculations (it depends on the number of process parameters to be considered). APSRA searches for the root causes for deviation of process parameters.

Since RMPS and SUSA evaluate the failure probability from the probability density functions (PDFs) of the process parameters as well as the model uncertainties, the reliability of the system is expressed as probability number. On the other hand, APSRA treats the failure of the process parameters by the failure of the components or systems which affect the process parameters; hence, the probability number is expressed as a failure rate and not probability number. The model uncertainty in APSRA is treated in the same way as that in RMPS by PDFs. However, it gets multiplied with the failure probability of the process parameters, which is obtained as failure rate.

6.3.1. Similarities

- Both of the methodologies use best estimate codes to find the T-H operating behaviour of the passive system and influence of sensitive parameters (which include process parameters and model uncertainties) on the system performance.
- Both the methodologies define T-H failure criteria of the system.
- Both the methodologies use probabilistic and deterministic tools to assess the reliability of the system.

6.3.2. Differences

Treatment of process parameters variation

- RMPS: Variation of process parameters are considered through a PDFs treatment. For example, variation of the nominal power: in normal operation of the reactor, there is an acceptable range of variation of the power, depending for instance on the electricity

demand in the network, so there is an uncertainty (equal to + or -2%) on the nominal power of the reactor at the time the accidental transient occurs. This variation can be treated by a PDF for example through a uniform distribution.

- APSRA: Variation of process parameters are considered through root diagnosis for example, the variation of the nominal operating power could be due to malfunction of the reactor control systems, position of control rods etc. These malfunctions can be treated through a failure probability of the active components or systems.

Treatment of model uncertainties

- RMPS: Model uncertainties are treated through a PDF. They are propagated along with the PDF of the process parameters together in the same way.
- APSRA: Model uncertainties are evaluated from experiments. In the absence of experimental data they are treated through PDF like in RMPS. They are propagated separately after evaluating the failure probability of the system through failure of process parameters.

Way of calculating the reliability of the passive system

- RMPS: Propagation of the input uncertainties through the T-H system code:
 - Monte-Carlo sampling on the PDF of the input parameters (for instance 100 samples);
 - Calculation by the code for each sample;
 - For each sample, comparison of the responses of interest (i.e. max. clad T) with fixed failure criteria (i.e. 1600°C).

This method may require a great number of simulations if the expected failure probability is very low. In this case variance reduction techniques or meta-models may be necessary. This uncertainty propagation approach also enables global sensitivity analysis.

- APSRA:
 - Simple code which can generate the passive system performance:
 - Understand behaviour of the system;
 - Identify the key parameters: critical in the sense that a disturbance in these parameters can lead to a significant change in the performance of the system;
 - System code (best estimate) for generating the failure surface.

Root diagnosis/fault tree

- RMPS: It does not attribute functional failures to mechanical failure of components or systems. Instead, hardware failure is considered at the level of PSA in combination with functional failure. The functional failures are attributed to the uncertainties in the models and variations of process parameters.
- APSRA: It attributes functional failures to the variation of process parameters which are correlated to the failure of mechanical components or systems through root diagnosis. The model uncertainties are treated through comparison with experiments.

Failure probability evaluation

- RMPS: Monte-Carlo evaluation or FORM/SORM methods;
- APSRA: failure surface + fault tree.

6.4. PROPOSAL FOR UNIFIED DEFINITION OF RELIABILITY

The probability that a system will perform its intended function in a satisfactory manner for a given period of time $[0, t]$, when used under specified operating conditions. This definition has been used by both the methodologies.

6.5. MERGING OF TWO METHODOLOGIES

The major difference between the two methodologies is the treatment of the variability of the process parameters. Further investigations need to be conducted to ascertain the failure modes of hardware or components that control certain classes of process parameters such as pressure, sub cooling, non-condensable gases etc. For those process parameters which cannot be controlled (e.g. ambient temperature etc.) may be treated by using appropriate models. For certain new reactor designs having innovative fuel, materials and components for which no design data available, conservative assumptions may be considered for modelling the uncertainties of the relevant parameters (e.g. heat transfer coefficient, pressure drop, blower characteristics etc.).

6.6. FUTURE R&D

It was proposed that there is a need for the development of a R&D framework to facilitate the development of a generic methodology that combines features from both APSRA and RMPS. For example:

- Treatment of certain process parameters variations because of failure mode of hardware or components;
- Experiments to ascertain the failure surface or the effects of the model parameters on system performance and failures;
- Treatment of the residual uncertainties (e.g. scaling uncertainties) when code validation data are available;
- In complex systems involving many passive systems which interact with each other with time delay, treatment of the dynamic behaviour of uncertain parameters need to be considered.

Some aspects of the above recommendations are being addressed under IAEA CRP I31018.

6.7. CONCLUSIONS

INPRO initiated an international collaborative project to evaluate the performance and reliability of the passive decay heat removal system of French GFR using the reliability methodologies available in Member States. Under this framework RMPS and APSRA methodologies were used to assess the performance and reliability of passive decay heat removal system of the French GFR design for station blackout (SBO) condition and loss of coolant accident (LOCA) combined with loss of forced circulation with two DHR loops available.

The Benchmark was comprised of two phases:

- Deterministic calculations were performed for simulation of above two transients taking into account nominal values of design and operation parameters. Two different computer codes (CATHARE and RELAP5) were used for the deterministic analysis to evaluate the performance and failure of the DHR for the above condition. Sensitivity analyses were performed to identify the critical process parameters and model uncertainties which have strong influence on the performance of the DHR. The analyses showed that both the codes could predict the system performance and failure states satisfactorily. The results were consistent with each other so far the effects of sensitive parameters on system performance are concerned. However, some differences were observed with regard to values of the output parameters associated with the failure criteria.
- Reliability calculations were performed using the above two methodologies. RMPS was used to calculate the reliability of DHR for SBO and LOCA combined with loss off-site power. APSRA was used to calculate the reliability of DHR for SBO condition only. Both the methodologies showed that DHR is capable enough to remove the decay heat in case of SBO without any failure. However, to understand the applicability of the methodologies the failure criteria was made stringent artificially (gas outlet temperature was reduced to 1050 °C instead of 1200 °C). With these criteria, it was found that DHR has a high probability of failure as predicted by both the methodologies. RMPS predicted the probability of failure of the DHR as 0.316 and APSRA predicted a failure frequency of 7.3×10^{-6} / hour for the SBO condition. Since APSRA treats the process parameters variations to the failure of the components or the systems which control them, the failure probability of the system is predicted to be a failure frequency unlike RMPS method. For second transient, the failure probability estimated by RMPS was relatively high and equal to 0.49. This result shows that the design of DHR system must be improved so as to have high reliable natural circulation system with regard to LOCA combined with loss of forced circulation. The improvement in the design can be made by increasing the nitrogen volume, valve-in the nitrogen accumulator one by one or by reviewing the design of the close containment.
- The exercise helped in the discussion of the features of the two methodologies. This facilitated to elaborate the similarities and differences of the two methodologies. Possibility of unifying the features of the two methodologies in order to develop a generic methodology was also discussed.
- The participants also agreed on a common definition of reliability of T-H passive systems.

APPENDIX I. BENCHMARK SPECIFICATIONS AND TRANSIENT DEFINITIONS

I.1. SITUATION OF INTEREST AND TRANSIENT CONSTRAINTS

The representative scenarios for this exercise were determined without giving consideration to their frequencies of occurrence and to the number of subsystems failing (e.g. number of DHR loops available):

- *TRANSIENT I*: The station blackout (SBO) is selected as the representative transient for pressurized situation (i.e. loss of station service power (LOSP) cumulated with all emergency diesel generators failure to start); with only one DHR loop available.
- *TRANSIENT II*: 3 inches LOCA initiating event (located on the cold part of a main cross duct) with a total loss of forced circulation DHR means (DHR circulator fail to start for example), with two DHR loops available. The transient ends after 6 hours.

Sequence of events

The schematic of the sequence of events for both transients is shown in Fig 13.

- For transient I, scram is performed at initiating event (the LOSP initiating event leads to the de-energization of concomitant control rods magnets).
- For transient II, scram is performed when the close containment pressure becomes higher than 1.3 bars. The injection from 3 nitrogen accumulators is performed when the lower plenum pressure becomes less than 10 bars.

Then, for both situations:

- The starting of the main blowers rundown is performed at scram.
- The decrease of the mass flow rate in the secondary circuit of the main loops (represented as boundary condition) is performed at scram.
- The starting of main loops isolating valves closure is done with a time lag of 3s after the mass flow at core inlet becomes less than 3% of nominal one [$Q_{nom} \approx 1020 \text{ kg/s}$] (the full closure of the main loops isolating valves is obtained in 2s).
- The opening of DHR loops isolating valves (in 5s for the full opening) is performed when the main loops isolating valves are fully closed. A time lag of 6s is foreseen in the reference CATHARE model for DHR blower startup. This point is not relevant for this exercise, except the time lag for NCDHR performance assessment.

I.1.1. Main circulator rundown (Boundary condition for benchmark)

To avoid the whole description of the main circulators features and performance maps, it was decided to provide a list of blower rotational speed evolution with time for both transients. The blower rotational speed evolution with time is shown in Fig. 14 and Fig. 15. This “discrete” data list is based on reference calculations performed with the CATHARE 2 code.

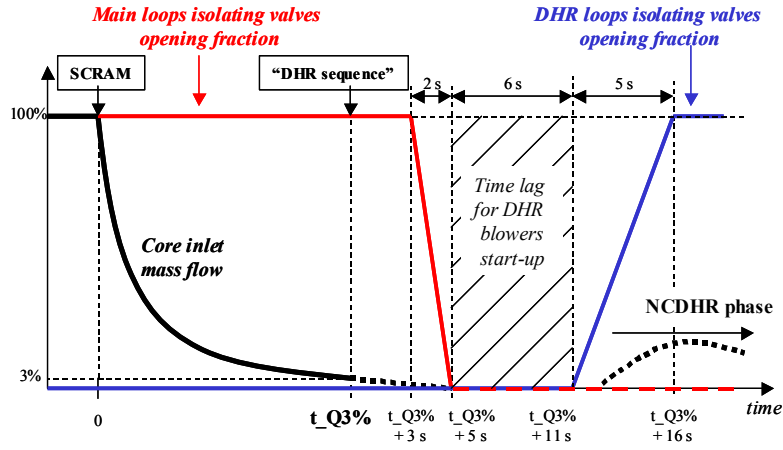


FIG. 13. Schematic of the sequence of events for both transients.

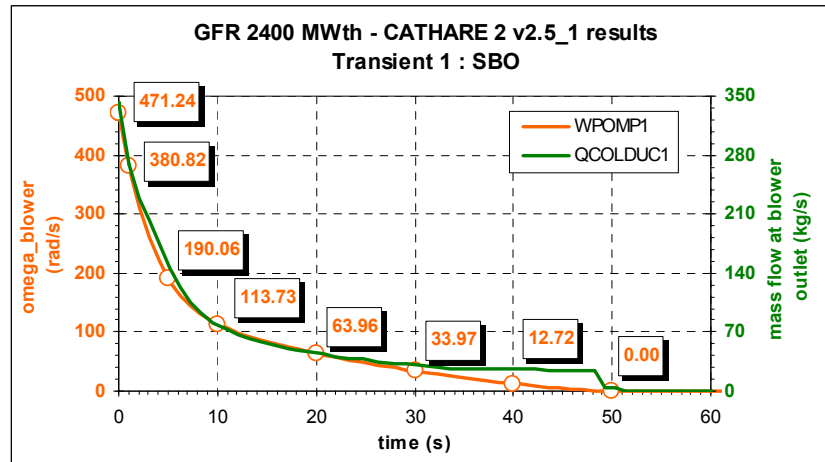


FIG. 14. Blower speed and related outlet mass flow for transient I.

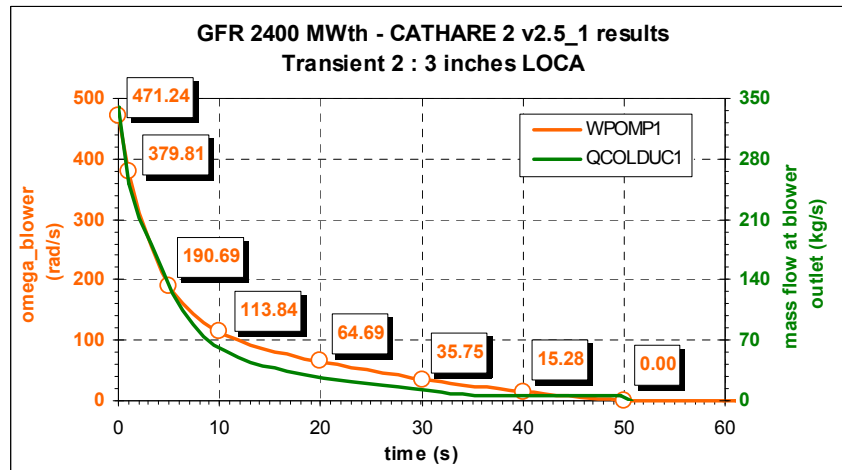


FIG. 15. Blower speed and related outlet mass flow for transient II.

Table 18 shows the boundary conditions that are employed for both transients.

TABLE 18. MAIN BLOWERS SPEED VERSUS TIME FOR BOTH TRANSIENTS

Time (s)	Main blower rotational speed (rad/s)
0	471.24
1	380
5	190
10	114
20	64
30	35
40	15
50	0

I.1.2. Secondary circuit boundary condition (BC)

The secondary circuit is simulated as boundary conditions (in the framework of this benchmark, it seems difficult and superfluous to model the turbo machinery and the associated systems). This BC set is defined with the CATHARE 2 code (for both transients). The successive events relative to the secondary circuit “management” are (in each loop):

- At scram, the generator linked to the turbo machinery, is disconnected from the grid. As the resisting torque due to generator is set to zero, the turbo machinery rotating speed starts to increase.
- To protect turbo machinery from over speed, the bypass valve(s) (at least two bypass lines and associated isolating valves for redundancy concern) quickly open, leading to the rapid rundown of the turbo machinery (TM).

For both transients, at scram initiation, a set of simulated BC for secondary side of IHX is given in Table 19.

TABLE 19. SECONDARY CIRCUIT BOUNDARY CONDITIONS (AT IHX INLET / OUTLET) FOR BOTH TRANSIENTS

Time (s)	Q_{inlet} (kg/s)	T_{inlet} (°C)	P_{outlet} (Pa)
0	895	366	6.5×10^6
1	392	297	4.6×10^6
2	317	265	3.9×10^6
5.2	209	235	3.2×10^6
10.5	113	208	2.8×10^6
20.1	41	187	2.6×10^6
30	0	178	2.5×10^6
1200	0	37	2.0×10^6

The evolution of the secondary circuit main variables with time (at IHX boundaries) is shown in Fig. 16 to Fig. 19. It is obtained with the CATHARE 2 code (including the turbo machinery rundown kinetics) and fixed as a set of BC for this benchmark.

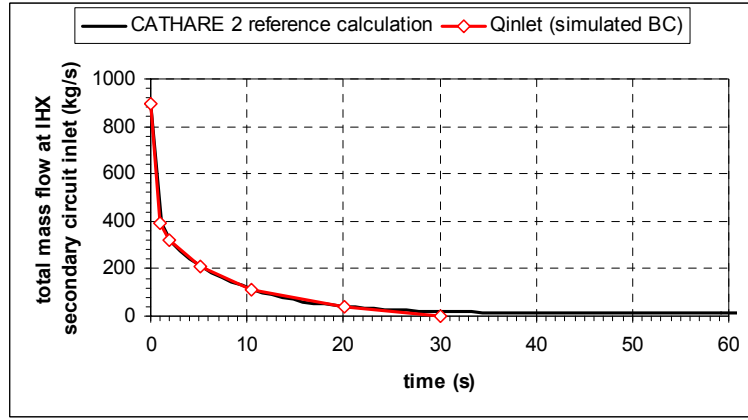


FIG. 16. Reference calculation (mass flow at secondary circuit inlet) and boundary condition set for both transients (in red).

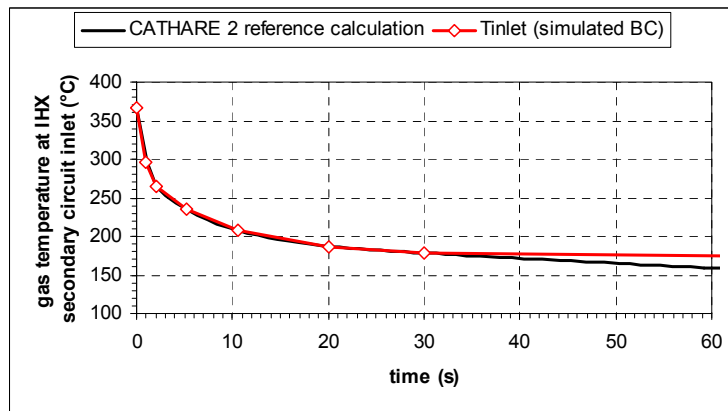


FIG. 17. Reference calculation (gas temperature at secondary circuit inlet) and a set of boundary condition for both transients (in red).

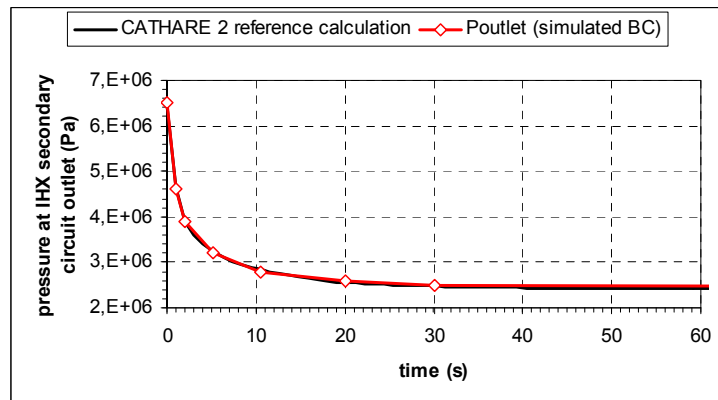


FIG. 18. Reference calculation (pressure at secondary circuit outlet) and a set of boundary condition for both transients (in red).

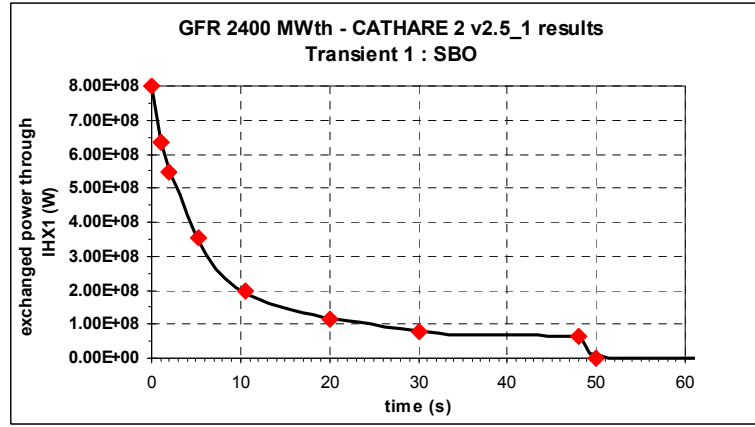


FIG. 19. Power Exchanged through main IHX versus time.

Figure 19 shows the power exchanged through main IHX with time and the representative values of the exchanged power through main IHX with time are provided in Table 20.

TABLE 20. POWER EXCHANGED IN IHX AS BOUNDARY CONDITIONS FOR BOTH TRANSIENTS

Time (s)	Power Exchanged (W)
0	8×10^8
1	6.36×10^8
2	5.45×10^8
5.2	3.55×10^8
10.5	2×10^8
20.1	1.15×10^8
30	8×10^7
48	6.60×10^7
50	0

I.2. FAILURE CRITERIA

The DHR system failure criteria is defined as the failure to maintain a decay heat removal rate that is required to limit the temperatures of vital components (vessel boundary, core plates) to the values of “4th category” design safety limits defined, to date, for GFR safety studies:

- 1600°C for fissile core (cladding);
- 1250°C for He temperature in upper plenum (vessel structures).

Several failure criteria are then selected for each representative transient, as given in Table 21.

In addition, it was proposed to add two more failure criteria:

- the imposed limit on the DHR pipe wall is set to be 850°C;
- the maximum allowable pressure in the close containment is fixed at 1.4 MPa (1.4 times the design pressure).

TABLE 21. FAILURE CRITERIA FOR EACH SITUATION

Criteria	Transient I	Transient II
(DHR loop structural integrity) Maximum temperature of DHR structural material (stainless steel)	850°C	850°C
(Cool ability + core integrity) Maximum SiC coating temperature	1600°C	1600°C
(Core upper structures integrity) Maximum temperature for gas at core outlet	1250°C	1250°C
(Nitriding + exothermic reactions) Maximum SiC coating temperature	(not concerned)	1000°C
Close containment integrity Maximum pressure in the close containment	(not concerned)	1.4 MPa (design = 1.0 MPa)

I.3. IDENTIFIED SET OF CRITICAL PARAMETERS AND ASSOCIATED DISTRIBUTION

A list of critical parameters (and their associated distribution) is selected. These parameters are selected on the basis of engineering judgment and are shown in Fig. 20.

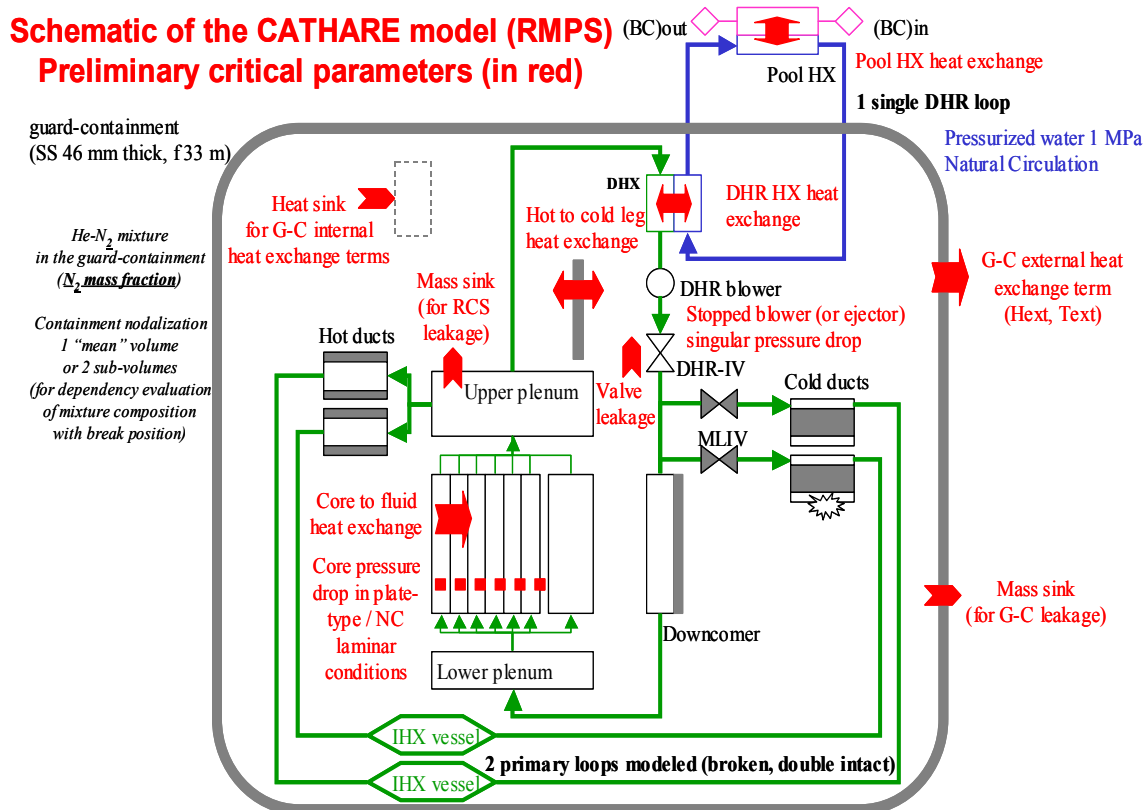


FIG. 20. Schematic of GFR and critical parameters for NCDHR performance assessment.

Transient I (SBO, pressurized situation)

For transient I, ten critical parameters are identified which are given in Table 22:

TABLE 22. CRITICAL PARAMETERS AND DISTRIBUTIONS FOR TRANSIENT I (SBO)²

No	Parameter	Minimal value	Maximal value	Distribution
1	Core total pressure drop	-0.15	0.15	Uniform
2	Inlet k-factor in DHR primary loop	0	2	Uniform
3	Outlet k-factor in DHR primary loop	0	2	Uniform
4	Helium clad heat transfer coefficient	-0.25	0.25	Uniform
5	Multiplication factor for thermal inertia for all walls	-0.15	0.15	Uniform
6	Corrective factor for heat transfer in DHR IHX	-0.25	0.25	Uniform
7	Core nominal power	-0.02	0.02	Uniform
8	Core residual power	-0.10	0.10	Uniform
9	Primary blower inertia	-0.25	0.25	Uniform
10	Main circuit pressure (MPa)	-0.2	0.2	Uniform

Transient II (LOCA, depressurized situation)

For transient II, there are some additional critical parameters along with already identified critical parameters for transient I. They are presented in Fig. 20. The critical parameters specific to the transient II can be subdivided into different categories: threshold measurement uncertainties (see Table 23), gas mixture properties uncertainties (see Table 24), closed containment data uncertainties (see Table 25) and accumulator data uncertainties (see Table 26).

² All minimal and maximal variations are given in percentages with respect to the nominal value, except for the main circuit pressure (parameter 10), where an absolute variation of 0.2 MPa has been considered.

TABLE 23. THRESHOLD MEASUREMENT UNCERTAINTIES

Parameter	Mean value	Range of uncertainty
Scram actuation	$P_{\text{containment}} > 1.3 \text{ bar}$	[1 – 2] bar
Accumulators discharge	$P_{\text{lower}} < 10 \text{ bar}$	[8 – 12] bar

TABLE 24. GAS MIXTURE PROPERTIES UNCERTAINTIES

Parameter	Mean value	Range of uncertainty
Gas mixture viscosity	Wilke law	+/- 5%
Gas mixture conductivity	Mason & Saxena law	+/- 10%
Gas mixture heat capacity	-	+/- 5%

TABLE 25. CLOSED CONTAINMENT DATA UNCERTAINTIES

Parameter	Mean value	Possible range of uncertainty
Closed containment leakages	0 kg.s-1	+10%
Closed containment free volume	11620 m ³	+/-10%
Closed containment heat exchange with the outside	15 W/m ² /K	+/-10%
Close containment outside temperature	20°C	[10 – 30] °C
Closed containment initial temperature	50°C	[30 – 70] °C
Volume of heat structures	3421m ² * 0.046m = 1574m ³	+/-10%
Initial pressure	1 bar	+/-10%

TABLE 26. ACCUMULATOR DATA UNCERTAINTIES

Parameter	Mean value	Possible range of uncertainty
Accumulators initial pressure	75 bar	+/- 5 bars
Accumulators initial temperature	50°C	[30 – 70] °C
Discharge line singular pressure drop	K=15	+/- 50%

In addition, according to the work performed by the MIT [22], the isolation valves leakage seems to be a critical parameter for the performance assessment of the natural circulation.

APPENDIX II. TRANSIENT I RESULTS

II.1. CEA

II.1.1. Deterministic evaluation

The calculations were performed with the CATHARE 2 code V2.5_2 mod 2.1. The CATHARE 2 model for 2400 MW(th) GFR is composed of (see Fig. 21) the following:

- The primary circuit with helium as coolant, including the main reactor vessel comprising the core, three principal independent loops (one “single” plus one “double” in the CATHARE model) each containing a finned plate intermediate heat exchanger (IHX) and a blower, three tanks for helium supply (for guard containment pressure) and three dedicated decay heat removal (DHR) loops, each with its own water filled secondary and pool type tertiary circuits.
- Each main loop has its own secondary circuit for power conversion including the second part of IHX, a single shaft mounted turbo machinery, a steam generator. The working fluid in the secondary circuit is a mixture of helium and nitrogen with mass fractions equal to 20% and 80% respectively.
- A ternary steam–water circuit (second part of the once through counter current steam generator). At present, the steam–water circuit is restricted to boundary conditions fixed at SG inlet and outlet.

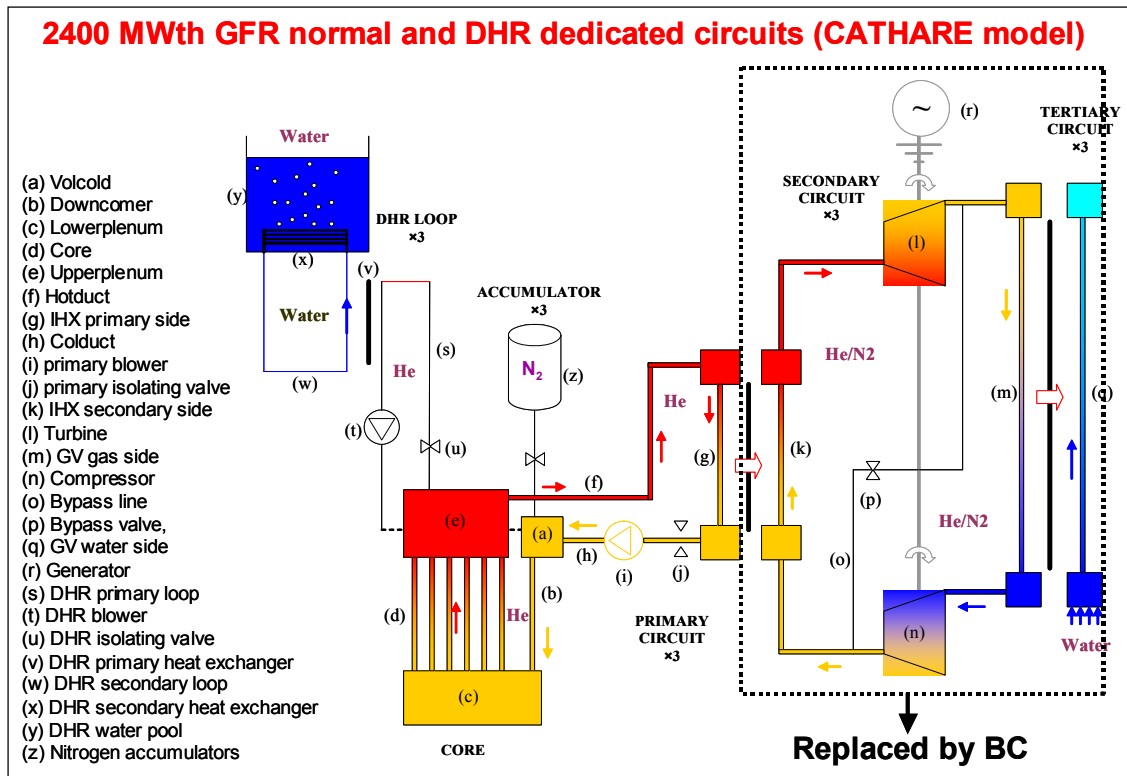


FIG. 21. CATHARE 2 model for 2400 MW(th) GFR.

The transient calculations were performed for 7100s.

II.1.1.1. Steady state results

A well stabilized steady state was achieved, with all T-H parameters being close to their nominal value. The main steady state results are summarized in Table 27. All values are in good agreement with nominal steady state parameters.

TABLE 27. CODE RESULTS COMPARED WITH THE FORESEEN GFR FEATURES

Parameters	Design	CATHARE
Gas temperature at main vessel inlet/outlet (°C)	400 / 850	399.9 / 849.5
Gas temperature at core outlet (°C)	900	900.5
Gas pressure at main vessel inlet/outlet (MPa)	7.12 / 6.98	7.11 / 6.98
ΔP vessel (upper plenum – lower plenum) (MPa)	0.14	0.121
Temperature at main blower inlet/outlet (°C)	396 / 400	396.1 / 399.9
Gas pressure at main blower inlet/outlet (MPa)	6.95 / 7.13	69.5 / 71.2
ΔP blower (MPa)	0.18	0.17
Main loop mass flow (kg/s)	340.8 * 3	342.2 * 3
Exchanged power in main loop IHX	803.3 * 3	806.4 * 3
ΔP IHX (MPa)	0.02	0.02

A detailed description of all core channels, with values of inlet/outlet temperatures, pressures, mass flows and velocities is presented in Table 28.

In Fig. 22, temperature profiles of gas, fuel assemblies and SiC cladding are shown at the center of the core (core 0 zone). The fissile zone is at 1.75 m from the base of the assembly. It can be seen that the highest value of fuel temperature is at 1.6 m (in the fissile zone). The value is close to 1400°C. The maximum clad temperature and maximum gas temperature are observed at the exit of the core. The value of maximum clad temperature is close to 990°C and that of maximum gas temperature is close to 900°C.

TABLE 28. CODE STEADY STATE RESULTS FOR THE MAIN VESSEL PARTS

Channels	P (MPa)	T _{gas} (°C)	Q _{channel} (kg/s)	v (m/s)
COLDUC1	7.109	399.9	342.2	43.9
DOWNCOMER inlet	7.106	399.7	1027.0	34.1
outlet	7.106	399.6	1027.0	34.1
LOWERPLE	7.106	399.6	-	-
Core0 (w=972) inlet	7.096	399.3	0.0769	61.5
outlet	6.985	899.5	(total 74.7 kg/s)	53.3
Core1 (w=1944) inlet	7.092	399.3	0.0753	60.2
outlet	6.985	898.7	(total 146.4 kg/s)	52.1
Core2 (w=2916) inlet	7.084	399.3	0.0722	57.8
outlet	6.985	898.5	(total 210.5 kg/s)	50.0
Core3 (w=1944) inlet	7.073	399.3	0.0673	54.0
outlet	6.985	899.6	(total 130.9 kg/s)	46.6
Core4 (w=2268) inlet	7.089	399.3	0.0741	59.3
outlet	6.985	898.7	(total 168.0 kg/s)	51.3
Core5 (w=3240) inlet	7.056	399.3	0.0600	48.2
outlet	6.985	900.5	(total 194.2 kg/s)	41.6
BYPASCO inlet	6.991	399.6	102.0	10.7
outlet	6.985	399.6	(~ 10% total)	
UPPERPLE	6.985	849.8	-	-
HOTDUCT	6.980	849.5	342.2	60.5

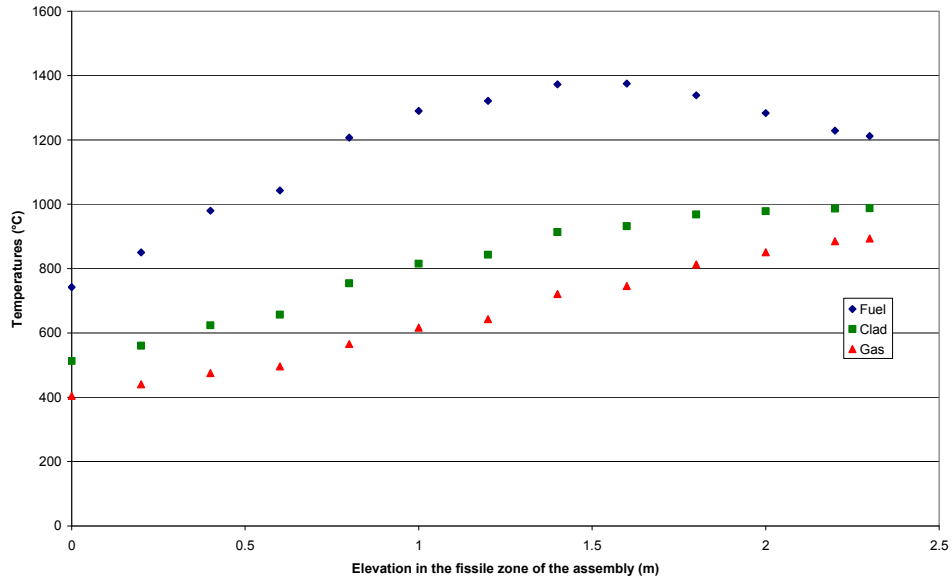


FIG. 22. Initial temperatures in the core 0 zone.

II.1.1.2. Transient results

Transient event sequence

The evolution of transient sequence as obtained with CATHARE 2 code is:

- Start of transient : 0 s;
- Start of DHR sequence (core mass flow rate below 3% of nominal value) : 40.9 s;
- Valves in main loops start closing : 43.9 s;
- Valves in main loop closed : 45.9 s;
- Valves in DHR loop start opening : 51.9 s;
- Valves in DHR loop opened : 56.9 s.

Core mass flow rate

The evolution of the mass flow rate at the inlet of the core is shown in Fig. 23. The mass flow rate decreases after the scram due to the decrease of velocity of the main blower. The flow rate is reduced to 3% of the nominal flow rate at 44s when the closure of the main loop isolating valves starts. There is a time interval of 6s with no flow. Then the DHR loop isolating valves open and, in less than 100s, a stable flow rate of about 30 kg/s is established, which is maintained up to the end of the transient during the natural circulation phase.

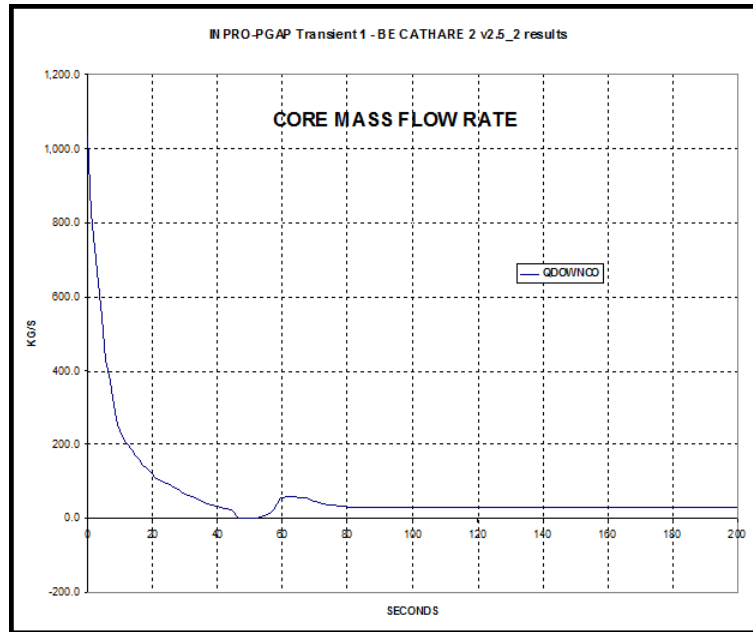


FIG. 23. Core mass flow rate at the inlet of the core.

The detailed flow rates in the different zones of the core for short term duration are shown in Fig. 24. We observe a relatively homogeneous flow due to the gaggings at the inlet of the assemblies, which introduce singular pressure drop.

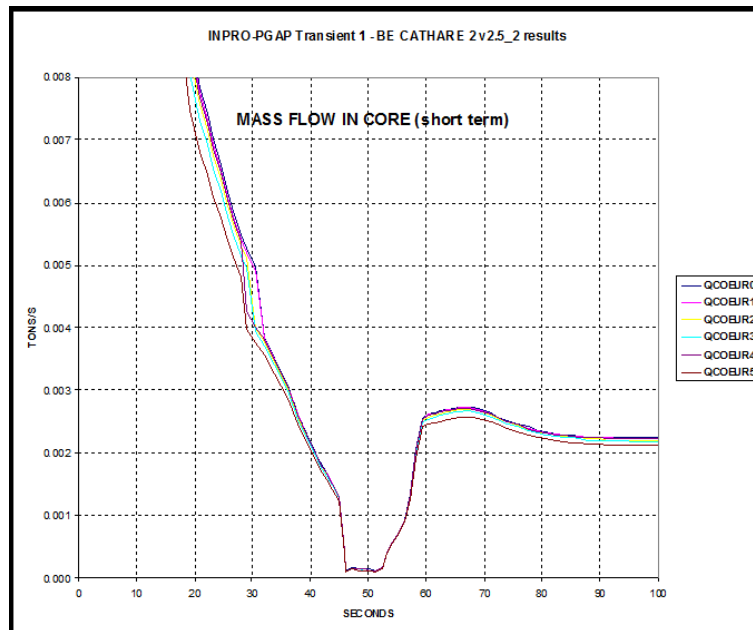


FIG. 24. Mass flow rates in the core at short term.

Fuel temperatures in central channel

The evolutions of the temperatures in the « Core 0 » zone for different elevation in the assembly are shown in Fig. 25. The maximum fuel temperature is obtained at core exit (at

maximum elevation). The fuel temperature decreases from 1200°C at the beginning of the transient due to the power reduction (after scram) and increases again after the transient sequence of event up to 1060 °C.

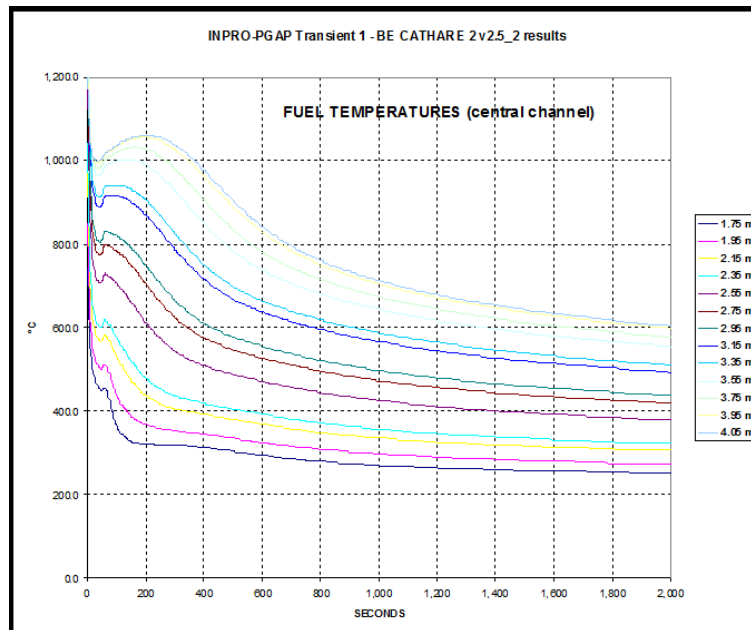


FIG. 25. Fuel temperatures in the central channel of the core.

Clad and gas temperature in the central channel

For the clad temperature (Fig. 26), a decrease in temperature at the beginning of the transient (except at the exit of the assembly) can be seen followed by an increase up to a maximum of 1054 °C at 195 s. Concerning the gas temperature at core 0 (Fig. 27), a first peak at 52 s (1006°C) can be observed, when all circuits were closed. Then the temperature decreases followed by an increase up to a maximum of 1034°C at 175 s.

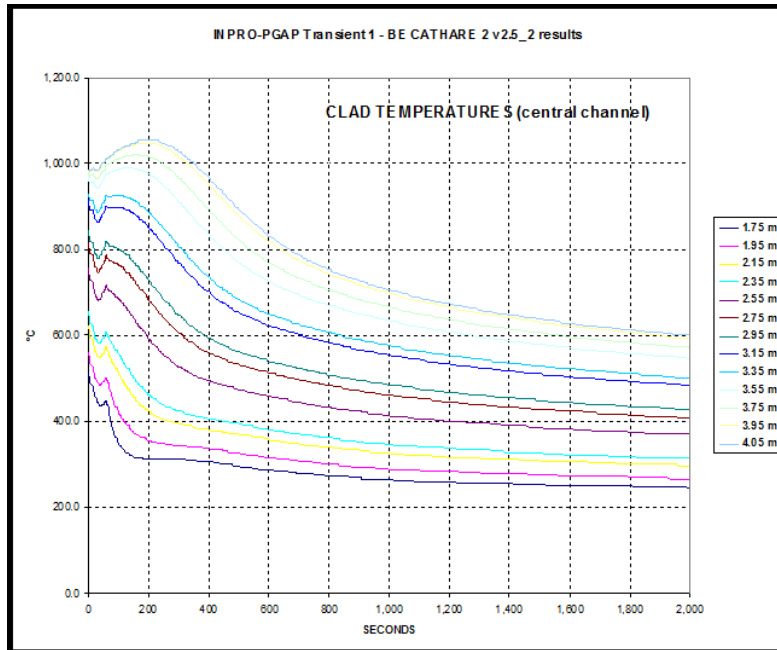


FIG. 26. Clad temperatures in the central channel of the core.

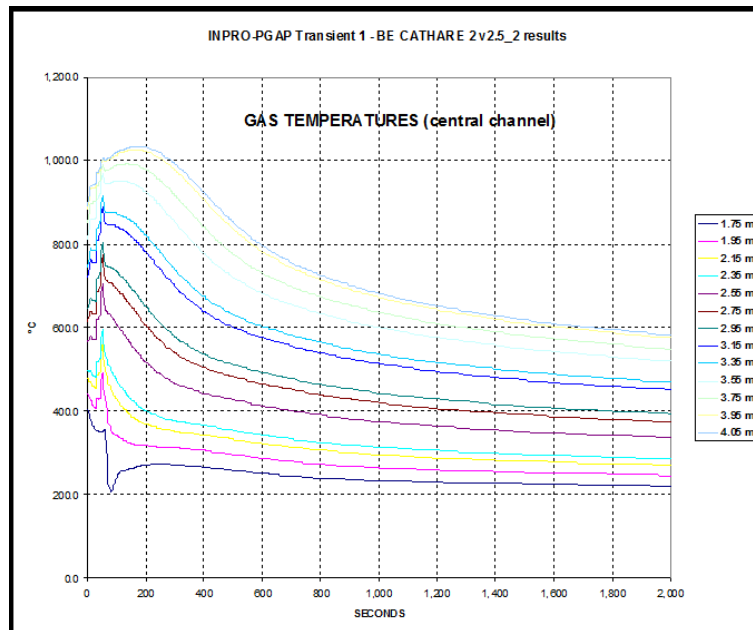


FIG. 27. Gas temperatures in the central channel of the core.

Primary pressure

The evolution of the primary pressure is shown in Fig. 28. The initial pressure is 7.12 MPa at core inlet and 7.00 MPa at core outlet. At the beginning of the transient the pressure decreases (due to blower velocity rundown) and then increases. The maximum pressure is equal to 7.18 MPa at 183 s.

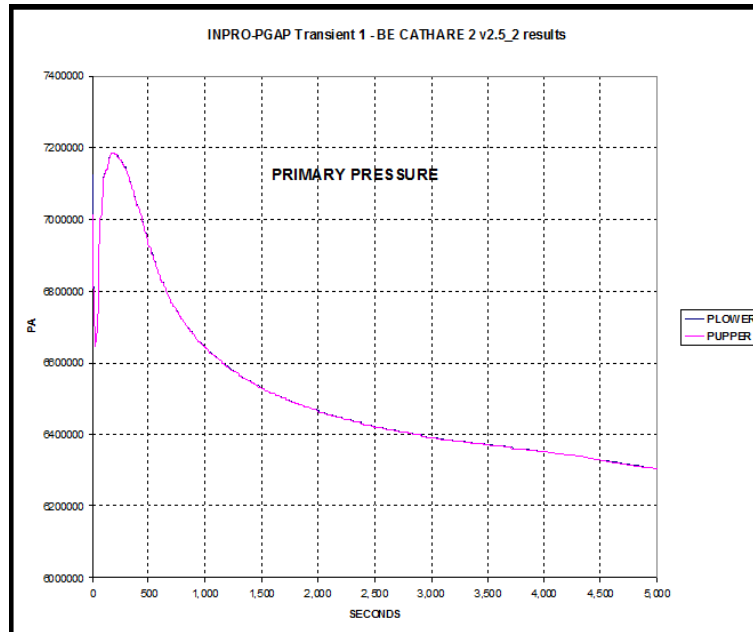


FIG. 28. Primary pressure in lower and upper plenum.

Power

The residual power curve and the power exchanged through the DHR exchangers (DHR HX1: exchanger between DHR helium loop and DHR water loop and DHR HX2: exchanger between DHR water loop and the cooling pool) are shown in Fig. 29. After a long time, the exchanged power is identical and equal to the power exchanged in the core (not shown in the figure).

DHR pressure

Figure 30 shows the pressure in the DHR loops. The pressure of He in the loop (at the top) is initially at 7 MPa and 6.2 MPa after one hour. Water pressure at the bottom is initially at 1 MPa and 1.8 MPa at end.

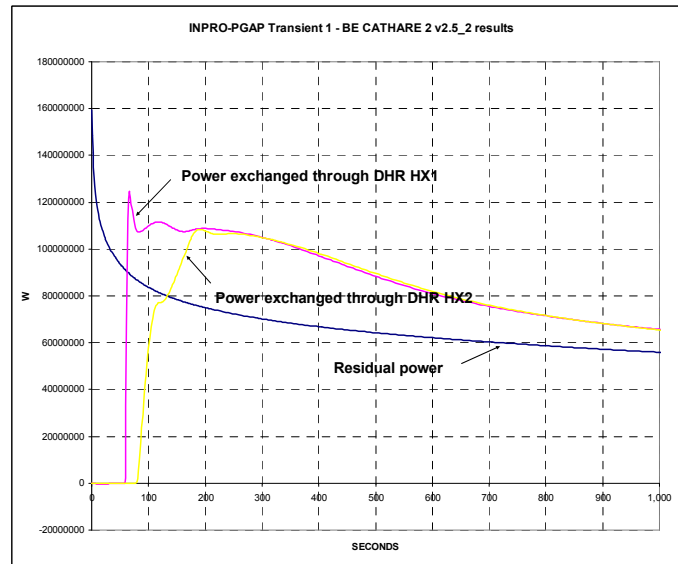


FIG. 29. Residual power and power exchanged through the DHR HXs.

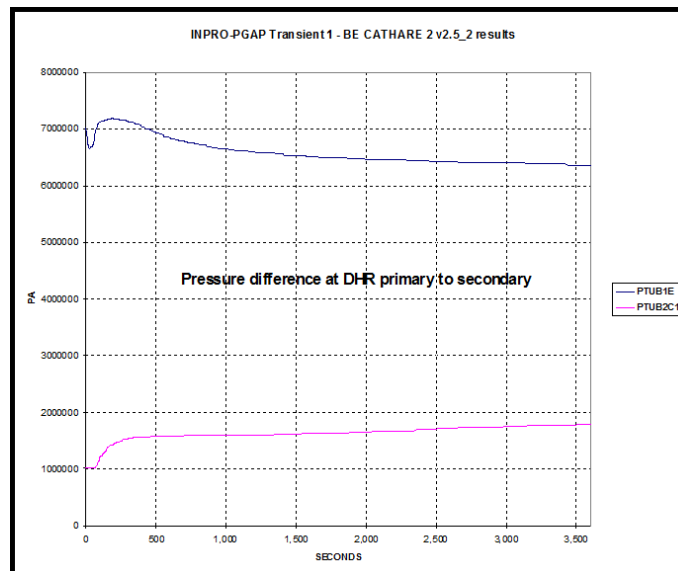


FIG. 30. DHR pressures.

DHR temperatures

The temperatures in the DHR system are shown in Fig. 31:

- The DHR He side hot leg temperature (in dark blue) at the beginning of transient is equal to 235°C. The two peaks can be seen in the figure. The temperature corresponding to first peak is 925 °C at 86 s and to second peak is 926 °C at 180 s. The decrease in temperature shows cooling phase by natural circulation.
- The temperature of the pressurized water is initially at 50°C and increases rapidly at the beginning of the natural circulation phase and then stabilizes at around 150°C.
- The cooling pool is initially at 50°C. The temperature of the pool increases rapidly when natural circulation gets started and then it increases slowly.

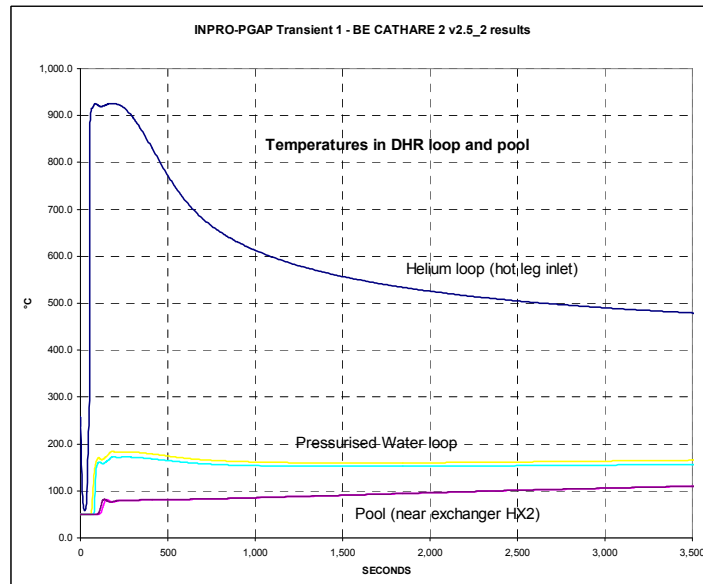


FIG. 31. Temperatures in DHR loops and pool

Mass flow rates in DHR

In the case of mass flow rates in DHR, a quasi-stabilization flow rate on helium side (at 30 kg/s) and, a decrease of water flow rate (177 kg/s at one hour) are obtained.

Summary of main T-H parameters and conclusion on the deterministic calculation

Here is a summary of the main results:

- Maximum vessel pressure: 7.18 MPa (184 s);
- Maximum clad temperature: 1054 °C (195 s) (Failure limit: 1600 °C);
- Maximum coolant temperature: 1034.0 °C (175 s) (Failure limit: 1250 °C);
- He DHR mass flow : ~ 30 kg/s;
- Water DHR mass flow: ~180 kg/s (at 3600s).

For this reference case, with nominal values of the input parameters, it can be seen that only one DHR loop working in natural circulation fulfills perfectly its mission. A stable flow rate of about 30 kg/s is quickly (in less than 100 s) established in the DHR loop and is maintained up to the end of the transient during the natural circulation phase. During one hour (time considered in the specification) from the beginning of the transient, the heat removal is sufficient and all failure criteria are respected, with values staying well below the safety limits.

II.1.2. Sensitivity analysis

The objective of this sensitivity analysis is to evaluate the influence of the input parameters on the main T-H characteristics of the system. The sensitivity analysis has been performed for a number of input parameters in the CATHARE 2 calculations. Classical OAT (one at a time) analysis, which varies one factor from the nominal condition, the others being kept at their nominal values, has been used for this sensitivity analysis.

Studied parameters

The input parameters for sensitivity analysis have been subdivided into four categories (pressure, thermal, general and material properties) and are given in Table 29 to Table 32.

TABLE 29. SENSITIVITY STUDY PARAMETERS: PRESSURE ASPECTS

Parameter	Description	Reference	Min. value	Max. value
P2DHR	Secondary DHR loop pressure	1.0 MPa	0.70 MPa	1.3 MPa
FRPLAQ	Plate type core laminar pressure drop coefficient	1	-15%	+15%
XDPSOUF	Singular pressure drop coefficient for DHR stopped blower	1	-	674
LEAKAGE	Natural leakage from primary circuit to containment	0 kg/s	-	2×10^{-2} kg/s
GAGGIN	Singular pressure drop coefficient for core channels	PLECOE0	PLECOEi * 0.9 PLECOED: unchanged	
			PIECOE0 = PLECOE1 = 0.58 PLECOEi: unchanged	
SINGULARi	Singular pressure drop coefficient at DHR IHX inlet	1	-	10
SINGULARo	Singular pressure drop coefficient at DHR IHX outlet	1	-	10

TABLE 30. SENSITIVITY STUDY PARAMETERS: THERMAL ASPECTS

Parameter	Description	Reference	Min. value	Max. value
T2DHR	DHR pool temperature	50 °C	42.5 °C	57.5 °C
ECPLAQ	Helium-clad heat transfer multiplication factor	1	-5%	+5%
ROCP	Multiplication factor for all walls thermal inertia (including fuel) during transient	1	0.85	1.15
ECHDHX1	Corrective factor for HT in DHR IHX	1	-10%	+10%
ECHDHX2	Corrective factor for HT in DHR pool	1	-50%	+50%

TABLE 31. SENSITIVITY STUDY PARAMETERS: GENERAL PARAMETERS

Parameter	Description	Reference	Min. value	Max. value
DELAY	Delay between main loops closure and DHR loop opening	6s	-	26s
FLOW	Core flow rate threshold for primary valve closure	3% Q_N	2.5% Q_N	3.5% Q_N
DELAY and FLOW	Delay and flow threshold	6s and 3% Q_N	-	26s and 2.5% Q_N (conservative)
POWER	Core nominal power	2400	-5%	+5%
ROTV	Primary blower inertia	Reference velocity decrease law	-50%	+50%

TABLE 32. SENSITIVITY STUDY PARAMETERS: MATERIAL PROPERTIES

Parameter	Description	Reference	Min. value	Max. value
HISOLDHR	Heat exchange coefficient for DHR cross duct internal insulation material	0.6 W/m/K	0.1 W/m/K	10 W/m/K
RHOC_Pu	Homogenized fuel product (specific mass * Specific heat)	$RHOC_Pu=f(T)$	-10%	+10%
LAMBDA_Pu	Homogenized fuel thermal conductivity	$LAMBDA_Pu=f(T)$	-10%	+10%
CP_He	Helium specific heat	5193 J/kg/K	-10%	+10%
LAMBDA_He	Helium thermal conductivity	$LAMBDA_He=f(T)$	-10%	+10%
MU_He	Helium dynamic viscosity	$MU_He=f(T)$	-10%	+10%

The first failure criterion has been checked in the cases related to material properties only, while the other two failure criteria have been checked in all cases.

First failure criterion: Maximum temperature of DHR structural material

The first criterion is based on the DHR structural material temperature limit. Figure 32 shows the DHR cross duct section with the central structure between the internal hot flow and the external cold flow of helium. In the CATHARE 2 input data deck, this structure is cut into eight meshes (three for the insulating material, five for stainless steel). The failure criterion concerns the 4th mesh i.e. stainless steel internal side. In Fig. 33, eight meshes temperature evolutions are shown. It can be observed that there is strong thermal gradient across the insulating material. On the contrary, stainless steel has a flat profile due to its high conductivity. The stainless steel temperature stabilizes around 210°C, far below the failure limit of 850°C.

All the cases concerning material properties parameters are shown in Fig. 34 and especially the four cases where a different value of the insulating material conductivity (from 0.1 W/m/K to 10 W/m/K) has been imposed. It can be seen that the evolutions are very close for all the cases (with a stabilized temperature around 200°C) except when the insulating conductivity is set to a very high value of 10 W/m/K (17 times more than the reference case value), where the stainless steel temperature reaches a maximum of 325°C during the transient.

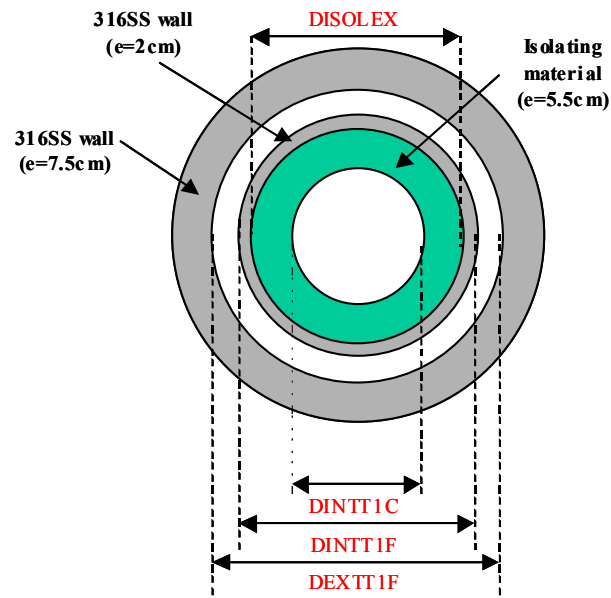


FIG. 32. DHR cross-duct geometrical features.

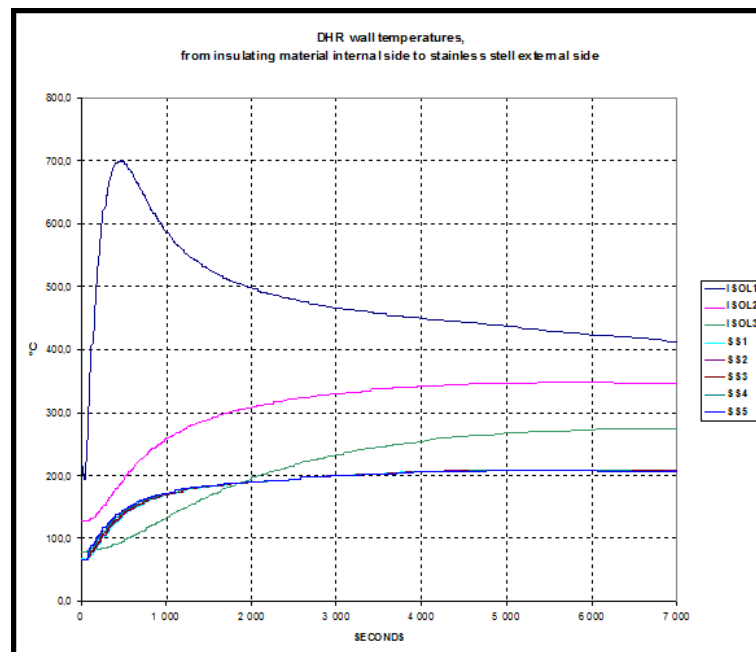


FIG. 33. DHR wall temperatures (from insulating material internal side to stainless steel external side).

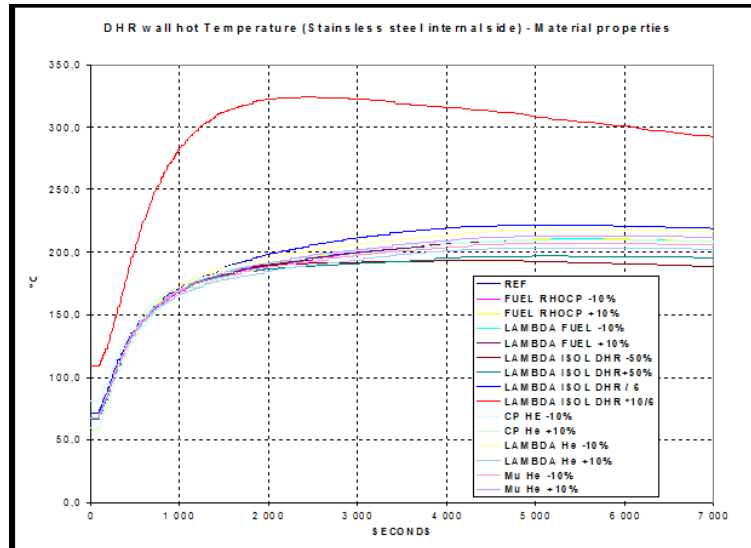


FIG. 34. DHR wall temperatures (stainless steel internal side).

Second failure criterion: Maximum clad temperature

For the second failure criterion, the effects of different types of parameters have been checked which include pressure parameters (Fig. 35), thermal parameters (Fig. 36), general parameters (Fig. 37 and Fig. 38) and material parameters (Fig. 39). All cases respect the failure criterion (1600°C) except in one case where the DHR stopped blower pressure drop coefficient has been put to a very high value of 674³ (instead of 1 in reference case). In this case, the failure criterion is slightly exceeded (the maximum clad temperature is close to 1660°C).

Third failure criterion: Hot channel outlet temperature

In the same way, for the third failure criterion, the effects of different types of parameters have been checked which include pressure parameters (Fig. 40), thermal parameters (Fig. 41), general parameters (Fig. 42 and Fig. 43) and material parameters (Fig. 44). All cases respect the failure criterion (1250°C) except in one case where the DHR stopped blower pressure drop coefficient has been put to a very high value of 674 (instead of 1 in the reference case). In this last case, the failure criterion is highly exceeded (hot channel outlet temperature is close to 1640°C).

³ This high value of the singular pressure drop due to the DHR stopped blower has been obtained by a CFD calculation. But in the final design of the GFR, we can imagine a bypass of the blower when the DHR will work in natural circulation. It is this situation which is considered in the reference case, with a value of the singular pressure drop equal to one.

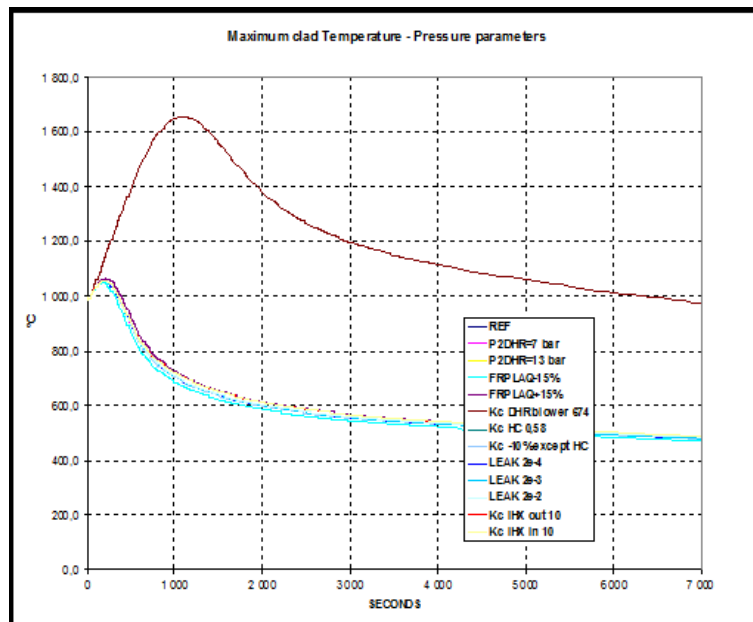


FIG. 35. Influence of pressure parameters maximum clad temperature.

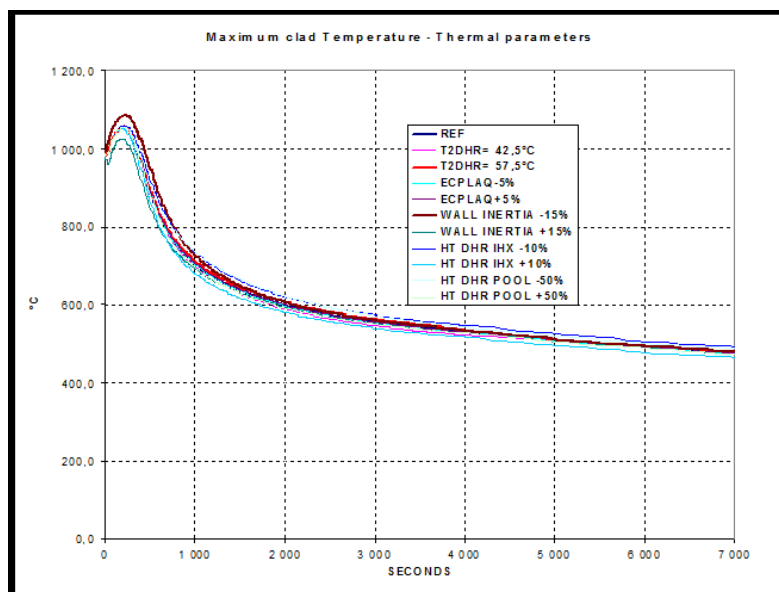


FIG. 36. Influence of thermal parameters on maximum clad temperature.

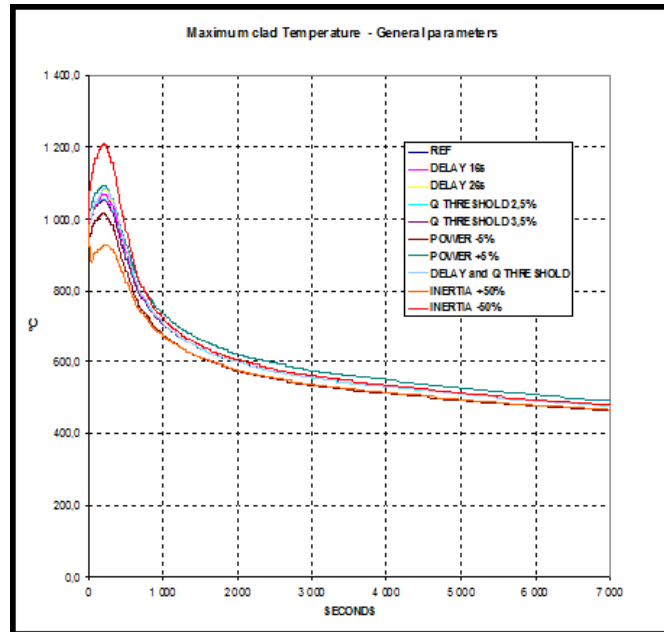


FIG. 37. Influence of general parameters on maximum clad temperature.

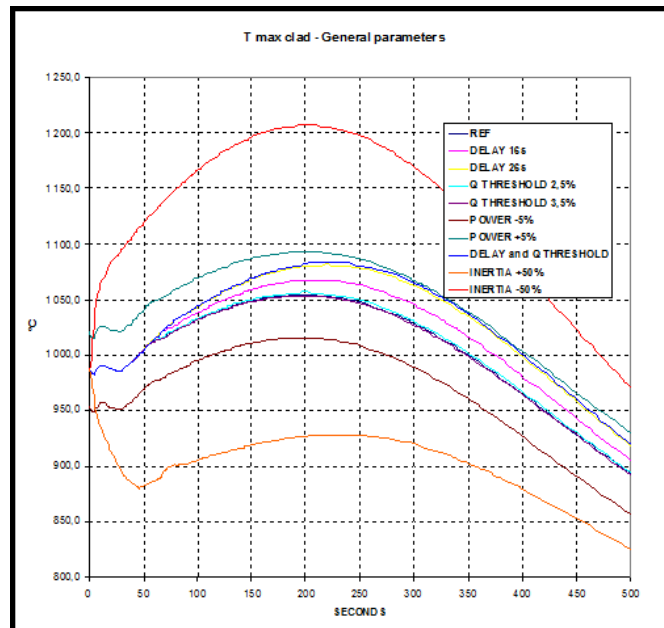


FIG. 38. Influence of general parameters on maximum clad temperature (zoomed view).

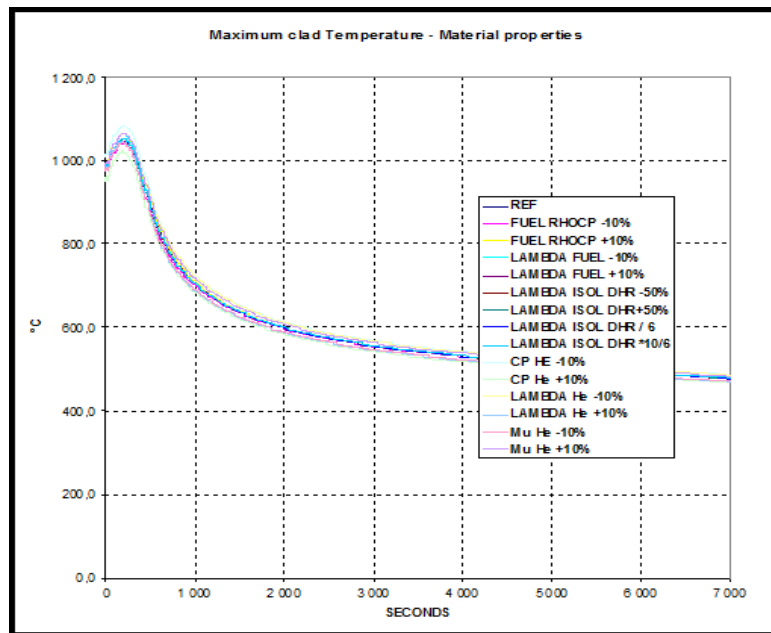


FIG. 39. Influence of material properties on maximum clad temperature.

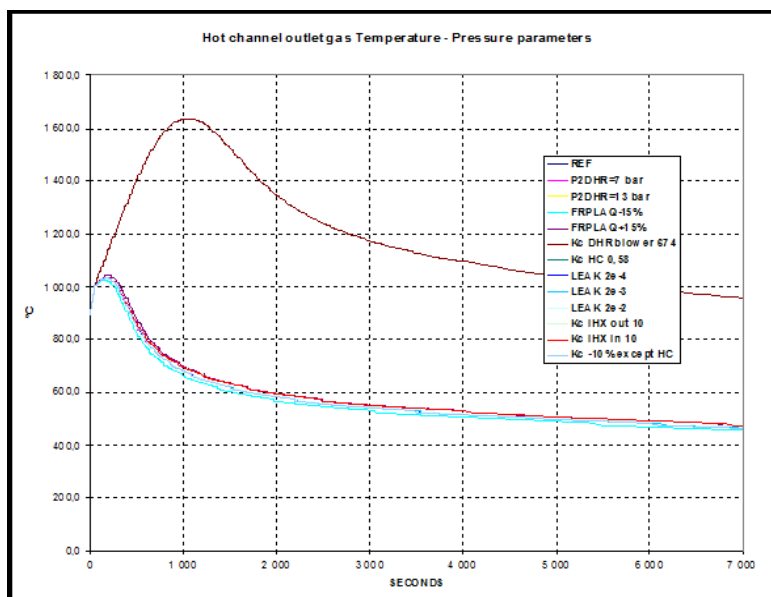


FIG. 40. Influence of pressure parameters on hot channel outlet temperature.

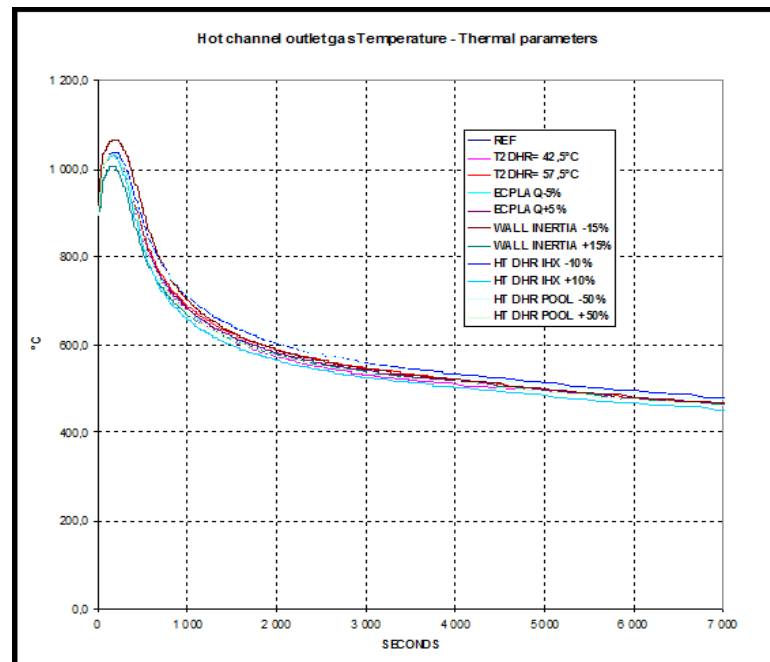


FIG. 41. Influence of « thermal » parameters on hot channel outlet temperature.

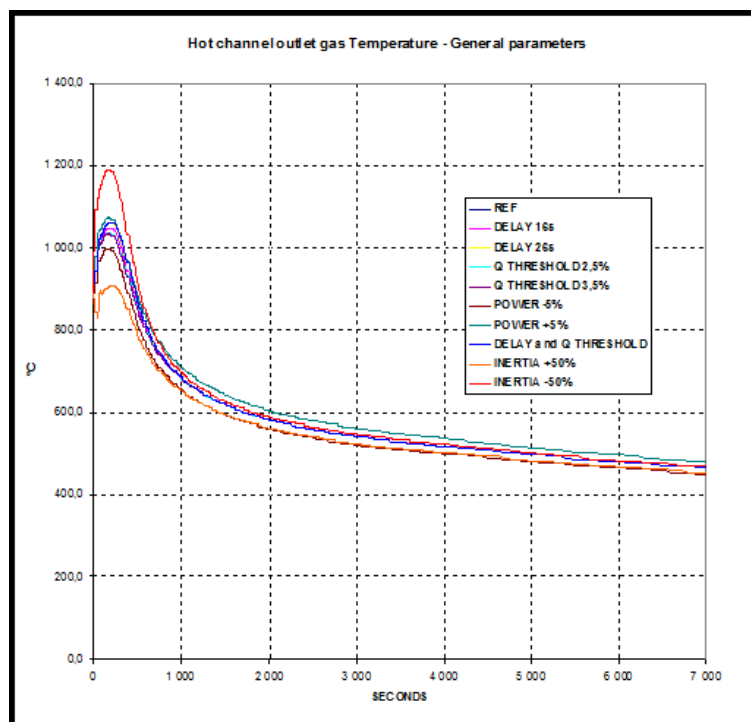


FIG. 42. Influence of general parameters on hot channel outlet temperature.

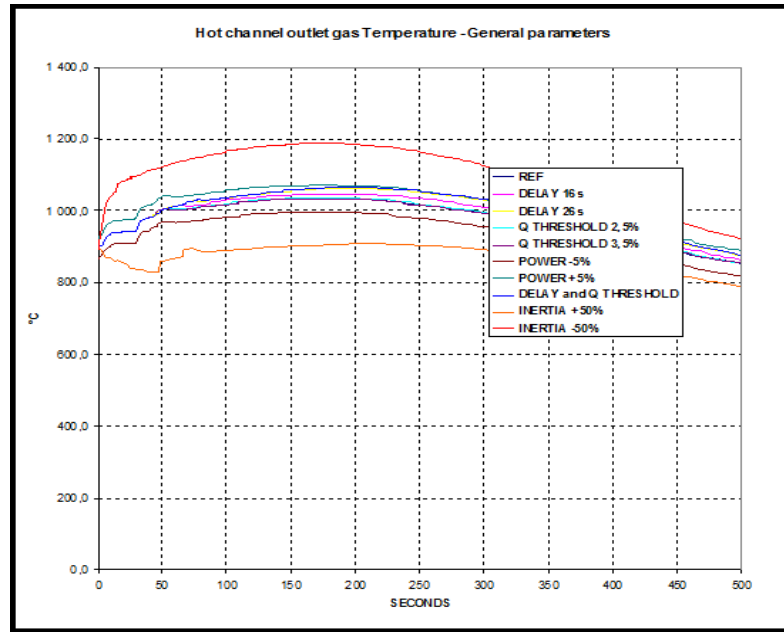


FIG. 43. Influence of general parameters on hot channel outlet temperature (zoomed view).

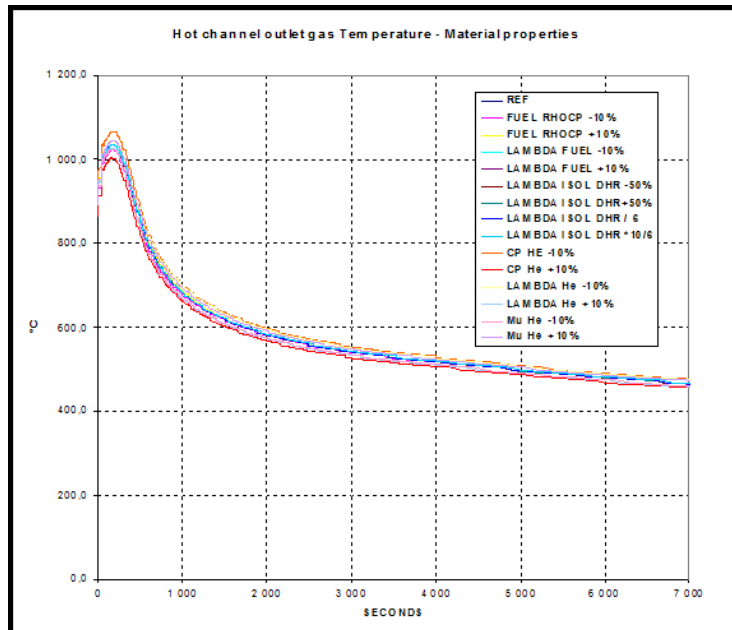


FIG. 44. Influence of material properties on hot channel outlet temperature.

Influence of DHR stopped blower pressure drop

Considering that there is no bypass of the stopped blower in the DHR and that the singular pressure drop coefficient is equal to 674 (value obtained by CFD code), the impact is important on the transient. The higher temperatures obtained in the core are the consequence of the lower natural convection flow that takes place through the stopped blower (10 kg/s instead of 30 kg/s) and can be seen in Fig. 45 and Fig. 46.

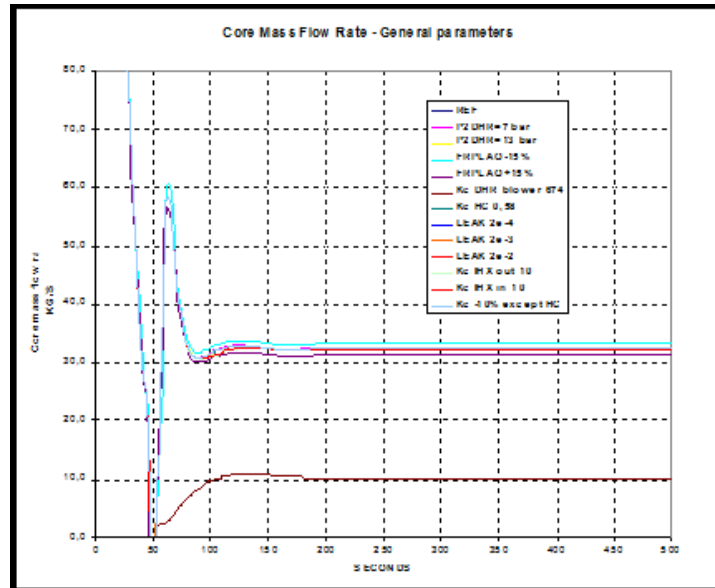


FIG. 45. Effect of the parameters on the core mass flow rate.

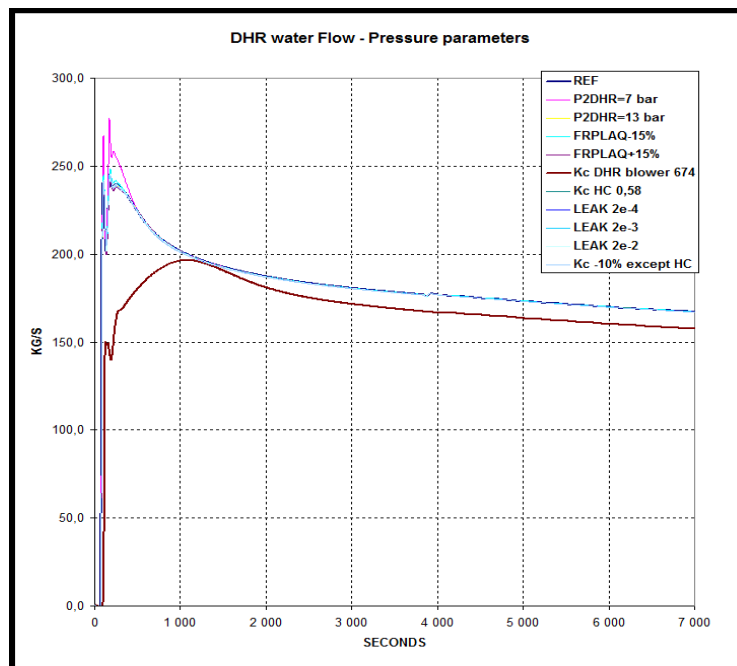


FIG. 46. Effect of the parameters on the DHR water flow rate.

Additional singular pressure drop in the DHR water loop

A singular pressure drop coefficient of 10 added in the DHR water loop (hot or cold leg) does not compromise the system cooling by natural convection. The flow and the temperature in the water loop are influenced but the consequences in the helium loop are very limited (Fig. 47 and Fig. 48).

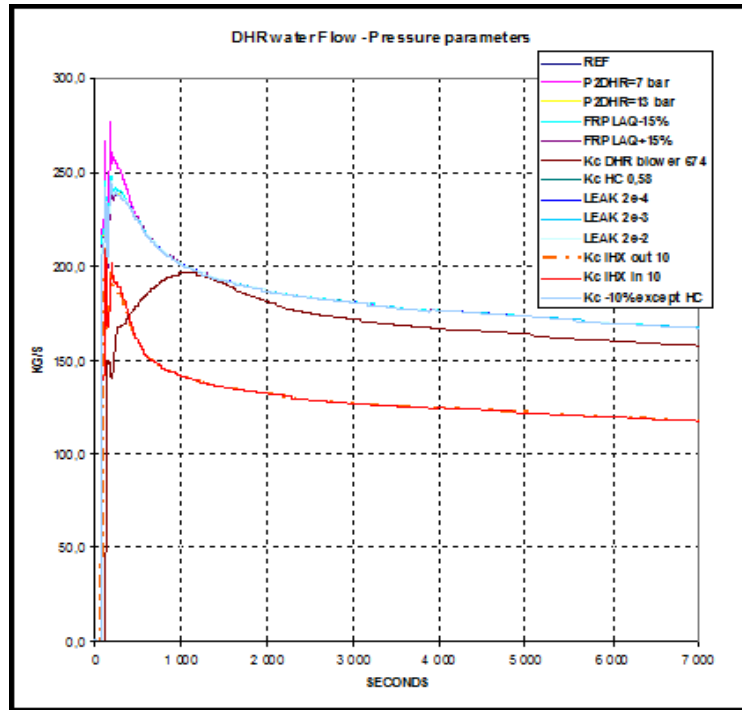


FIG. 47. Effect of the parameters on the DHR water flow rate.

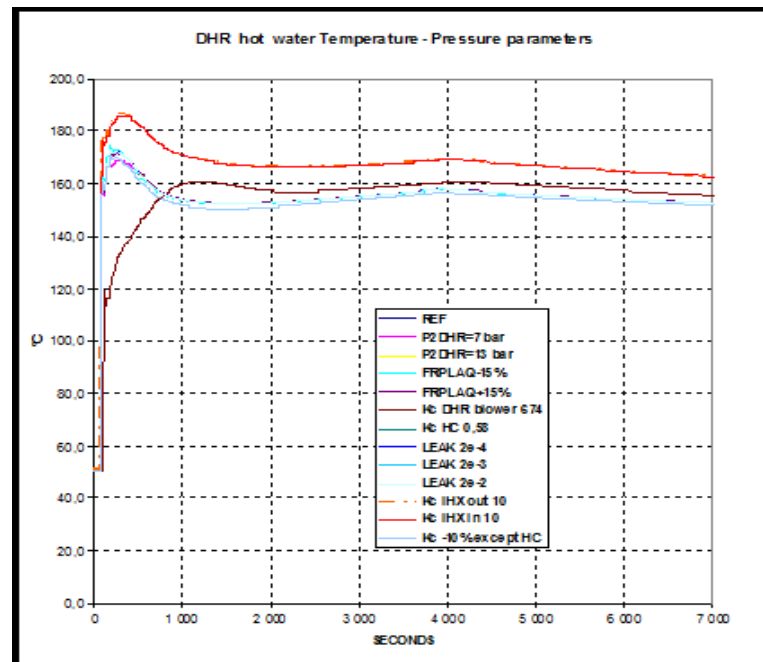


FIG. 48. Effect of the parameters on the DHR water temperature.

Primary circuit natural leakage

A variation of the natural leakage from 2×10^{-4} to 2×10^{-2} kg/s (0.2 to 20 g/s) has a very low impact on the transient (Fig. 49). For these values, the leakage has a little impact on pressure in the loop i.e. with a leakage flow rate of 20 g/s, the pressure is still 61 bar after 7000s (instead of 62 bar in the reference case). The natural convection is not compromised.

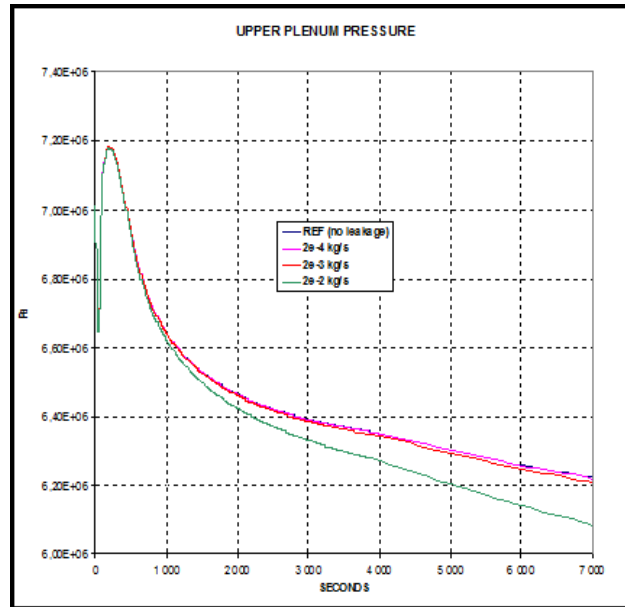


FIG. 49. Effect of a natural leakage in the primary circuit on the pressure.

DHR sequence: Influence of delay and flow rate threshold

In the reference case, the DHR sequence is initiated when the primary flow rate falls below 3% of the nominal value and a delay of 6s is assumed for the DHR valve opening after the primary valves closure (time lag for DHR blower startup). A combination of an increase in flow threshold (Q/Q_N) of 2.5% and a delay value of 26s have been implemented in the data set (these are conservative values for both parameters). This effect of an increase in delay and flow rate threshold core mass flow rate can be seen in Fig. 50. The effect of the flow threshold parameter is negligible in comparison with the delay parameter effect as can be seen in Fig. 51. The system cooling is still satisfactory (maximum clad temperature increases by 30 °C), despite the sequence chronology modified.

Primary blower inertia

By decreasing the velocity during the blower rundown, the primary blower inertia is modified. By doing so, the transient sequence is modified i.e. DHR sequence, which is triggered on the Q/Q_N threshold, is shifted in time (start of DHR sequence at 20.6s instead of 40.9s when inertia decreases to 50%). The influence is observed on both primary circuit and DHR loops. All variables evolutions are affected (Fig. 52 to Fig. 55).

When the blower inertia is divided by 2, the maximum clad and helium temperatures at hot channel outlet are increased by 150 °C. This effect is much more noticeable than the combination of delay and flow rate threshold shown previously.

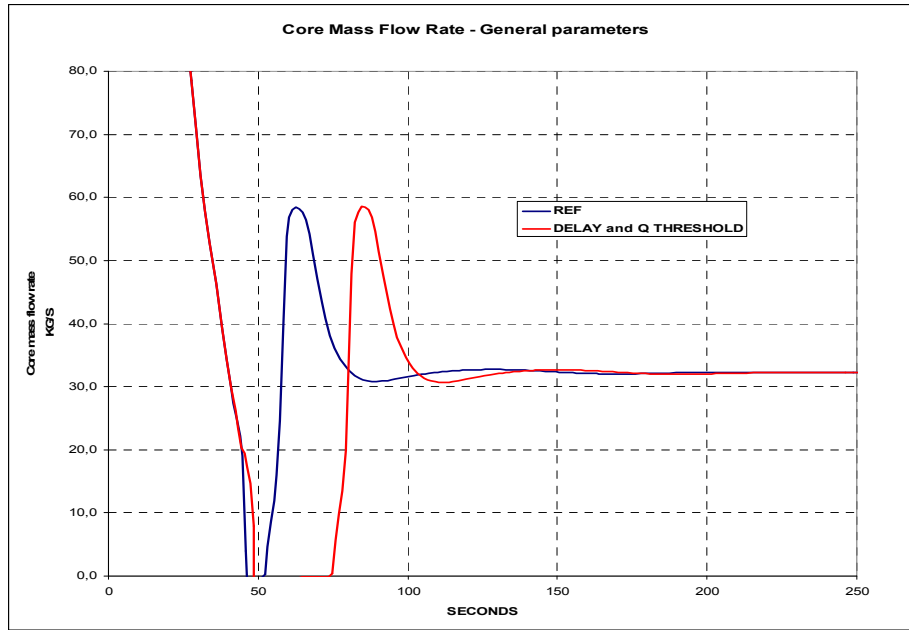


FIG. 50. Effect of an increase in delay and flow rate threshold on core mass flow rate.

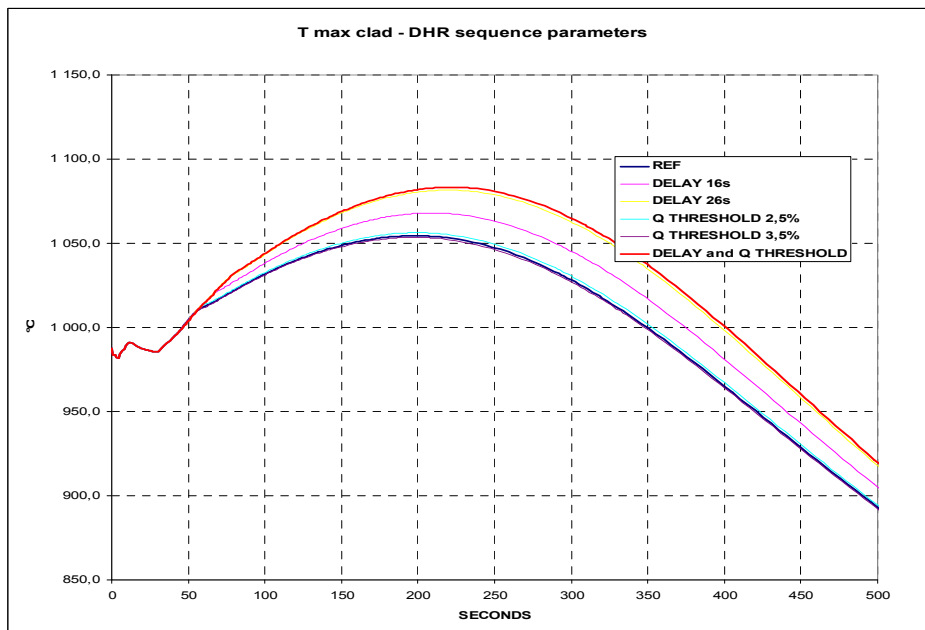


FIG. 51. Effect of delay and flow rate threshold on core mass flow rate.

Core nominal power and wall inertia

The effect of an increase or a decrease of 5% of the nominal power on the maximum clad temperature has been studied. It has an effect of $\pm 40^{\circ}\text{C}$ on the maximum clad temperature. The effect of wall inertia parameter has been studied by varying $\pm 15\%$ of the reference value. These cases have shown a limited effect of this parameter in this uncertainty range. The maximum clad temperature is affected by $\pm 30^{\circ}\text{C}$.

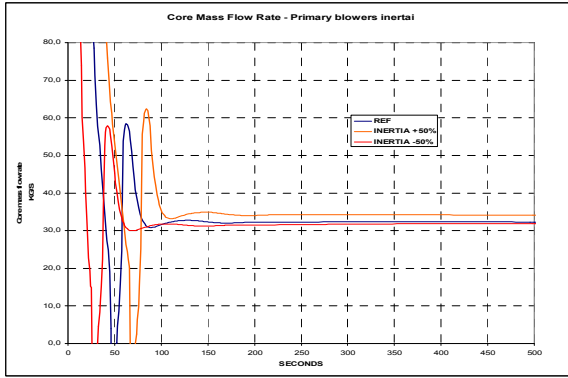


FIG. 52. Effect of primary blower inertia on core mass flow rate.

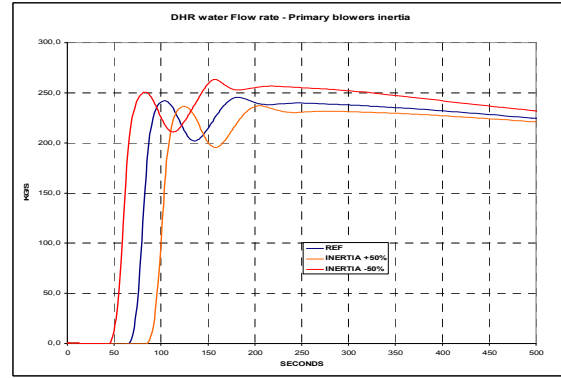


FIG. 53. Effect of primary blower inertia on DHR water flow rate.

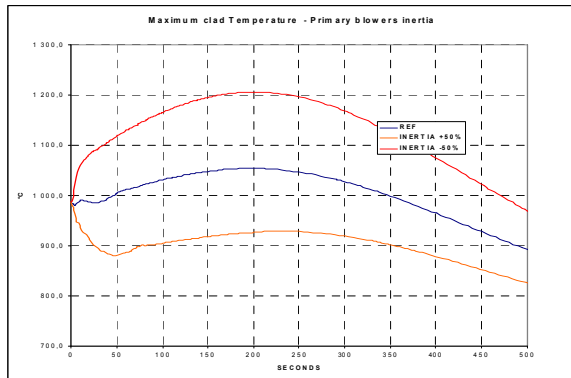


FIG. 54. Effect of primary blower inertia on maximal clad temperature.

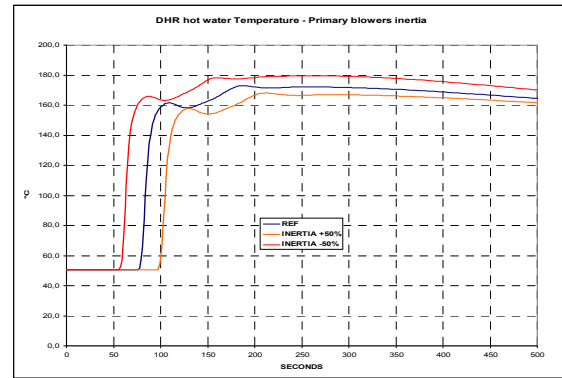


FIG. 55. Effect of primary blower inertia on DHR hot water temperature.

II.1.3. Reliability evaluation

For the reliability evaluation, RMPS methodology is used. The input uncertainties are propagated through the T-H code CATHARE2 in order to evaluate the uncertainty on the response of interest and assess the reliability of the DHR system.

Input uncertainties

Ten uncertain input parameters (see Appendix I) follow uniform distributions between the defined bounds. Table 33 summarizes the probabilistic model.

Input sampling and propagation of uncertainties

A Latin Hypercube Sampling (LHS) has been performed using the 10 uniform distributions given in Table 33.

1000 samples of the input parameters have been simulated and for each, a T-H calculation has been performed with the CATHARE2 code.

TABLE 33. PROBABILISTIC MODEL OF THE RANDOM VARIABLES

No	Parameter	Min. value	Max. value	Distribution
1	Core total pressure drop	-0.15	0.15	Uniform
2	Inlet k-factor in DHR primary loop	0	2	Uniform
3	Outlet k-factor in DHR primary loop	0	2	Uniform
4	Helium clad heat transfer coefficient	-0.25	0.25	Uniform
5	Multiplication factor for thermal inertia for all walls	-0.15	0.15	Uniform
6	Corrective factor for heat transfer in DHR IHX	-0.25	0.25	Uniform
7	Core nominal power	-0.02	0.02	Uniform
8	Core residual power	-0.10	0.10	Uniform
9	Primary blower inertia	-0.25	0.25	Uniform
10	Main circuit pressure (MPa)	-0.2	0.2	Uniform

Response of interest

The following responses given by the CATHARE2 code have been studied:

- The maximum fuel temperature obtained during the transient (after 40s) at core exit for the central channel.
- The maximum clad temperature obtained during the transient at core exit for the central channel.
- The maximum helium temperature obtained during the transient at core exit for the central channel.
- The maximum primary pressure during the transient.

Statistical analysis of the response of interest

Table 34 gives the main statistical results obtained on the four responses of interest and Fig. 56 shows the histograms of distribution for these four responses.

It can be seen that the distributions are globally normal. The average values are slightly less than the reference values. The coefficients of variation (standard deviation on average) are close to 5% for the different temperatures and less than 2% for the primary pressure. It means that for given input uncertainties, the uncertainties on the responses of interest are small.

All the quantiles considered (even $X_{99.9\%}$) are below the failure criteria.

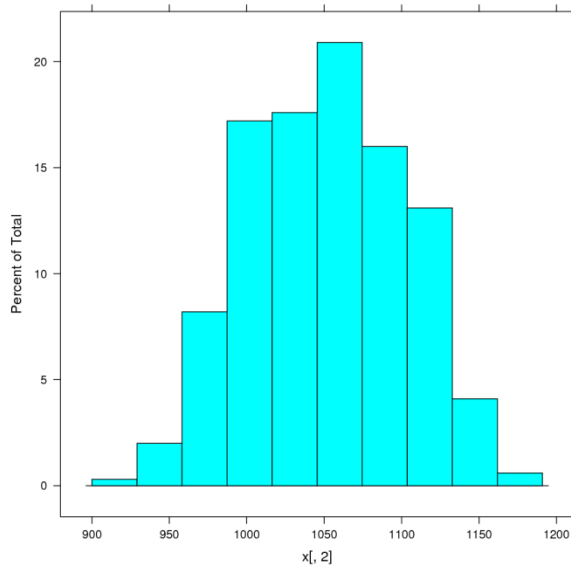
Table 35 shows the linear correlation coefficients between the various responses of interest. It can be seen that the three maximum temperatures are highly correlated, while the maximum primary pressure is not correlated with these temperatures.

TABLE 34. STATISTICAL CHARACTERISTIC OF THE RESPONSES

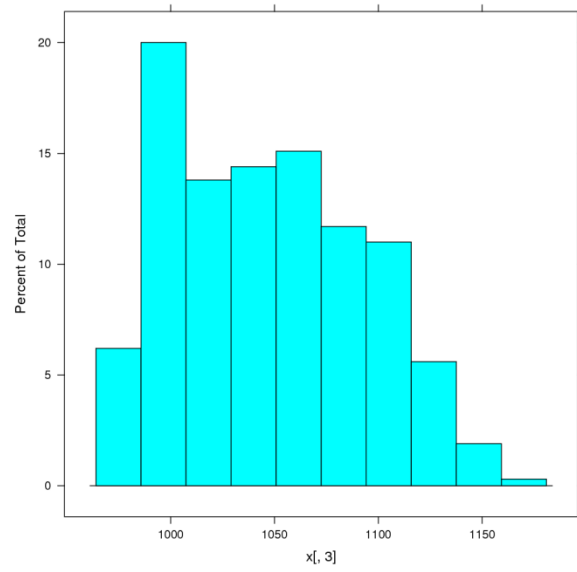
Statistical Characteristics	Fuel Max. T (°C)	Clad Max. T (°C)	Helium max. T (°C)	Max. primary pressure (MPa)
Average (μ)	1051	1047	1023	7.19
Standard deviation (σ)	50.2	45.4	50.1	0.112
Variation coefficient (σ/μ) in %	4.8	4.3	4.9	1.6
Minimal value	911	972	894	6.94
Maximal value	1180	1173	1154	7.53
X _{90%}	1116	1109	1090	7.34
X _{95%}	1132	1125	1105	7.38
X _{99%}	1152	1145	1125	7.46
X _{99,9%}	1171	1163	1145	7.52

TABLE 35. MATRIX OF LINEAR CORRELATION COEFFICIENTS

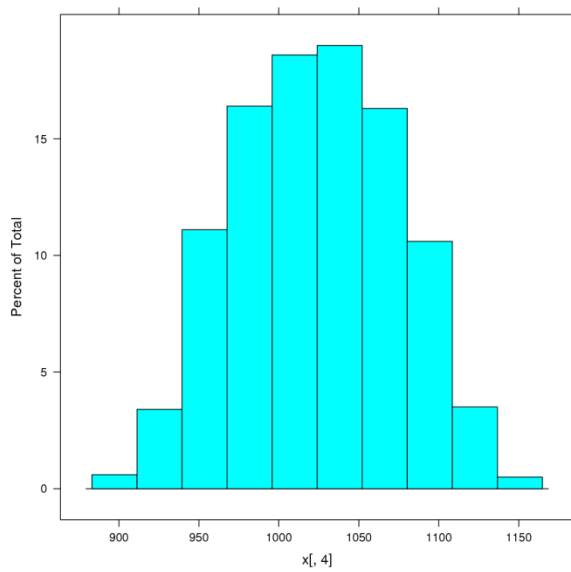
Parameter	Fuel Max. T	Clad Max. T	Gas Max. T	Primary Pressure
Fuel Max. T	1	0.984	0.997	-0.249
Clad Max. T	0.984	1	0.985	-0.261
Gas Max. T	0.997	0.985	1	-0.255
Primary Pressure	-0.249	-0.261	-0.255	1



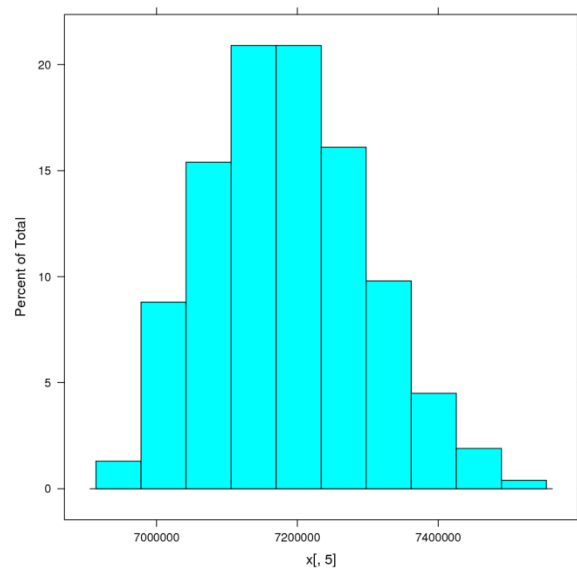
Maximum temperature of the fuel (°C)



Maximum temperature of the clad (°C)



Maximum temperature of the helium (°C)



Maximum pressure in the primary circuit (Pa)

FIG. 56. Histogram of the 4 responses of interest.

Global sensitivity analysis

In complement to the OAT sensitivity analysis performed previously, a global sensitivity analysis has been carried out using standard regression coefficients.

Considering that the response Y is a linear function of the random input variables X_i ,

$$Y = \beta_0 + \sum_{i=1}^p \beta_i X_i$$

the standardized regression coefficients (*SRC*) can be obtained from the regression model which allows us to determine the importance of each input. They quantify the effect of varying each input variable away from its average by a fixed fraction of its variance. If the input variables are independent, the sum is one. They are used to identify and quantify linear relations between the inputs and the outputs, and are given by:

$$SRC(Y, X_i) = \beta_i \sqrt{\frac{Var(X_i)}{Var(Y)}}$$

The validity of the indices obtained relies on the quality of the linear approach adopted. If such hypothesis is not valid, other more suitable techniques should be used. To validate this hypothesis, it is important to calculate the determination coefficient of the regression model, i.e. R^2 :

$$R^2 = \frac{\sum_{i=1}^N (\hat{y}_i - \bar{y})^2}{\sum_{i=1}^N (y_i - \bar{y})^2}$$

where \hat{y}_i denotes the estimate of y_i obtained from the regression model. The coefficient represents the fraction of variation compared to the average explained by the regression model, i.e. the variance percentage of output variables Y explained by the regression model \hat{y} . Thus, R^2 provides a measurement of how well the linear regression model can reproduce the actual output y , so it is a global measure of the goodness of fit. The closer R^2 is to unity, the better is the model performance, and so we can use the standardized regression coefficients as sensitivity indices.

The sign of the *SRCs* shows how the input parameter affects the output i.e. a positive sign means that an increase of the input parameter will increase the output, and in case of negative sign opposite is true. The sum of SRC^2 is equal to R^2 .

The scatterplots are also drawn (Fig. 57 to Fig. 60), which give the evolution of the response of interest against each input parameter and enable us to see the effect of these input parameters.

Results obtained on the four response of interest

- *Maximum fuel temperature*

The standardized regression coefficients for maximum fuel temperature when $R^2 = 0.996$ are given in Table 36.

TABLE 36. STANDARDIZED REGRESSION COEFFICIENT FOR MAXIMUM FUEL TEMPERATURE

Rank	Parameter No	Input parameter	SRC	SRC ²
1	9	Primary blower inertia	-0.829	0.687
2	5	Wall thermal inertia	-0.345	0.119
3	8	Core residual power	0.329	0.108
4	7	Core nominal power	0.177	0.032
5	6	Heat transfer in DHR IHX	-0.128	0.016
6	4	Helium clad heat transfer	0.113	0.013
7	10	Main circuit pressure	-0.050	0.003
8	2	Inlet k-factor in DHR primary loop	0.005	3.6×10^{-5}
9	1	Core total pressure drop	0.004	1.6×10^{-5}
10	3	Outlet k-factor in DHR primary loop	0.002	5.3×10^{-6}

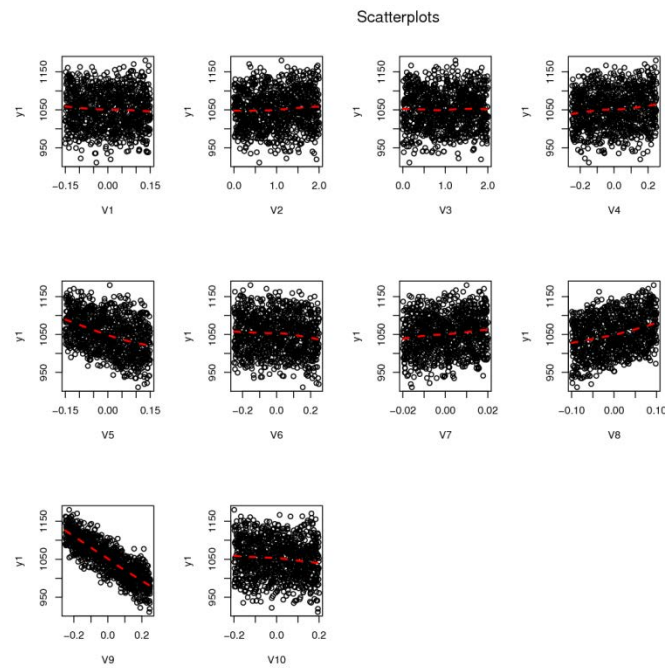


FIG. 57. Scatterplots for maximum fuel temperature.

- *Maximum clad temperature*

The standardized regression coefficients for maximum clad temperature when $R^2 = 0.968$ are given in Table 37.

TABLE 37. STANDARDIZED REGRESSION COEFFICIENT FOR MAXIMUM CLAD TEMPERATURE

Rank	Parameter No	Input parameter	SRC	SRC ²
1	9	Primary blower inertia	-0.829	0.687
2	5	Wall thermal inertia	-0.328	0.107
3	8	Core residual power	0.300	0.090
4	7	Core nominal power	0.193	0.037
5	6	Heat transfer in DHR IHX	-0.116	0.014
6	4	Helium clad heat transfer	0.114	0.013
7	10	Main circuit pressure	-0.054	0.003
8	2	Inlet k-factor in DHR primary loop	0.013	1.7×10^{-4}
9	1	Core total pressure drop	0.008	6.8×10^{-5}
10	3	Outlet k-factor in DHR primary loop	-0.008	5.9×10^{-5}

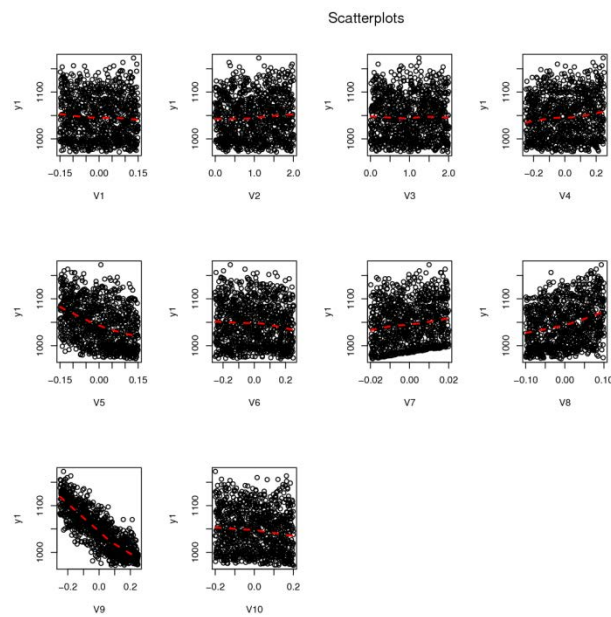


FIG. 58. Scatterplots for maximum clad temperature.

- *Maximum helium temperature*

The standardized regression coefficients for maximum helium temperature when $R^2 = 0.994$ are given in Table 38.

TABLE 38. STANDARDIZED REGRESSION COEFFICIENT FOR MAXIMUM HELIUM TEMPERATURE

Rank	Parameter No	Input parameter	SRC	SRC ²
1	9	Primary blower inertia	-0.828	0.686
2	5	Wall thermal inertia	-0.352	0.124
3	8	Core residual power	0.299	0.089
4	7	Core nominal power	0.170	0.029
5	4	Main circuit pressure	0.169	0.029
6	6	Helium clad heat transfer	-0.116	0.013
7	10	Heat transfer in DHR IHX	-0.050	0.002
8	2	Inlet k-factor in DHR primary loop	0.006	4.2×10^{-5}
9	1	Core total pressure drop	0.005	2.9×10^{-5}
10	3	Outlet k-factor in DHR primary loop	0.0004	1.9×10^{-7}

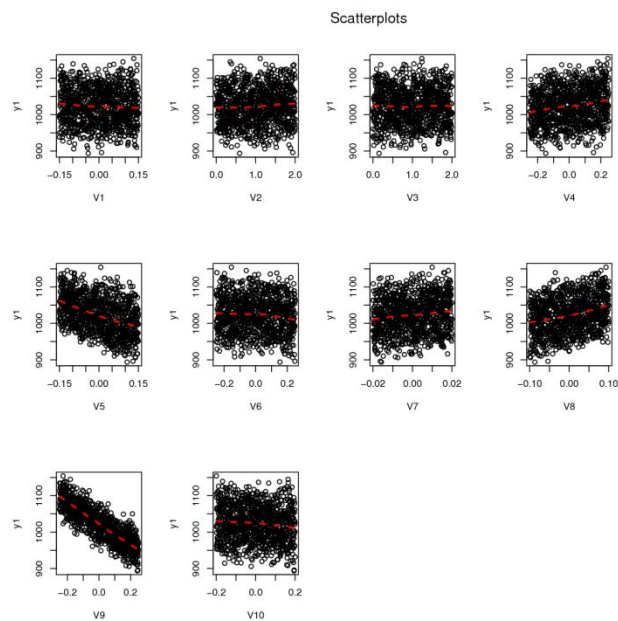


FIG. 59. Scatterplots for maximum helium temperature.

- *Maximum primary pressure*

The standardized regression coefficients for maximum primary pressure when $R^2 = 0.977$ are given in Table 39.

TABLE 39. STANDARDIZED REGRESSION COEFFICIENT FOR MAXIMUM PRIMARY PRESSURE

Rank	Parameter No	Input parameter	SRC	SRC ²
1	6	Heat transfer in DHR IHX	-0.692	0.479
2	9	Primary blower inertia	0.502	0.252
3	10	Main circuit pressure	0.418	0.175
4	5	Wall thermal inertia	-0.187	0.035
5	8	Core residual power	0.147	0.022
6	4	Helium clad heat transfer	0.099	0.010
7	7	Core nominal power	0.062	0.004
8	1	Core total pressure drop	-0.009	8.9×10^{-5}
9	2	Inlet k-factor in DHR primary loop	-0.007	5.1×10^{-5}
10	3	Outlet k-factor in DHR primary loop	-0.004	1.8×10^{-5}

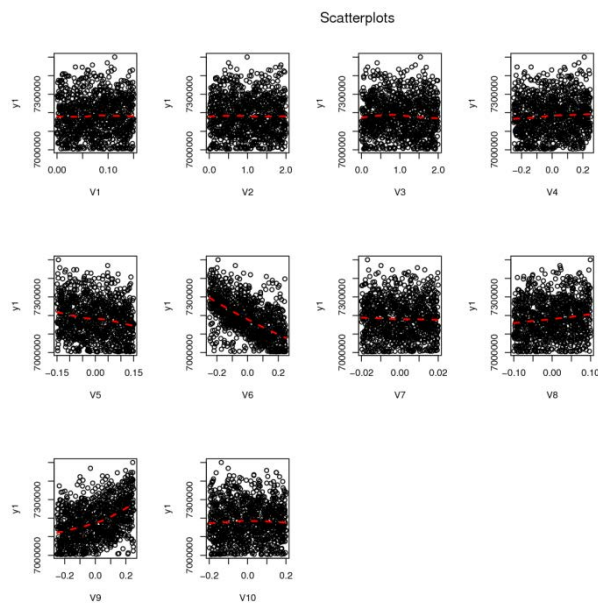


FIG. 60. Scatterplots for maximum primary pressure.

It can be seen that for the four responses of interest (see Table 36 to Table 39) , the hypothesis of a linear relation between the output and the input parameters is valid as the values of R^2 are close to 1 in each case. Therefore, the standardized regression coefficients can be used as sensitivity indices.

The results obtained on the *SRCs* for the three temperatures are very close because the three temperatures are correlated (as discussed previously). The most influential parameters on the maximum temperatures are the primary blower inertia, the wall thermal inertia and the core residual power. Ninety per cent of the uncertainty on the temperatures is associated with these parameters. The most important parameter is the primary blower inertia, which has major contribution to this uncertainty (69%).

For the maximum primary pressure (which is not a failure criterion for this benchmark), the results are different. The most influential parameters are the heat transfer coefficient in DHR exchanger, the primary blower inertia and the main circuit initial pressure.

Reliability analysis

None of the cases out of 1000 simulations met the failure criteria i.e. maximum clad temperature never exceeded 1600°C and maximum gas temperature at core outlet never exceeded 1250°C.

The probability of failure is estimated by: $p_f = \frac{N_f}{N}$

where N_f is the number of simulations leading to the failure of the system and N is the total number of simulations..

In this case, p_f takes the value of zero since no code run provides an output observable within the failure domain. This result shows a limitation of Monte Carlo simulation for estimating rare events probabilities since a large amount of calculations are needed. Moreover, Monte Carlo simulation involves large computational time on each run (given the complexity of the physical problem to solve) allowing only a limited number of output observables, which are not enough for achieving a proper upper bound of the probability of failure.

Wilks' formula for one sided tolerance interval can be used for calculating a conservative upper bound γ of the actual probability of failure p_f :

$$1 - (1 - \gamma)^N \geq \beta$$

where β expresses the “confidence” that p_f will be lower or equal than γ .

Considering $\beta = 0.95$ and $N = 1000$, we obtained $\gamma = 0.003$. This constitutes, however, a very high upper bound for the failure probability, according to the margins that we have obtained for the two failure criteria.

Rough estimation of the margins

Based on Table 33, the margins obtained for different choices of the quantile are given in Table 40. Considering the quantile of 99.9%, a positive margin of 437°C for the maximum clad temperature and of 100°C for the maximum helium temperature is obtained.

TABLE 40. SAFETY MARGINS (DEFINED AS SAFETY CRITERION – UPPER QUANTILE)

Quantile	Margin on Max. Clad T (°C)	Margin on Max. He T (°C)
SC – X _{90%}	491	160
SC – X _{95%}	475	145
SC – X _{99%}	455	125
SC – X _{99.9%}	437	105

Reliability analysis using the regression model

This reliability analysis concerns the failure criterion on maximum He temperature at core outlet for which we have less margin.

Considering the linear relation between the maximum helium temperature and the input parameters ($R^2 = 0.994$), this linear model has been used instead of the CATHARE2 code to study the effect of changing the range of uncertainty of input parameters on the failure probability.

For maximum helium temperature, the following is the regression model:

$$\begin{aligned} \text{Max. Helium } T = & 1.0226\text{e}+03 + V1 * 3.0972 + V2 * 5.6210\text{e}-01 + V4 * 5.8772\text{e}+01 + V5 * \\ & -2.0318\text{e}+02 + V6 * -4.0257\text{e}+01 + V7 * 7.3880\text{e}+02 + V8 * 2.5900\text{e}+02 + V9 * \\ & -2.8714\text{e}+02 + V10 * -2.1541\text{e}+01 \end{aligned}$$

Figure 61 shows a good agreement between maximum helium temperatures obtained by the CATHARE2 and linear model.

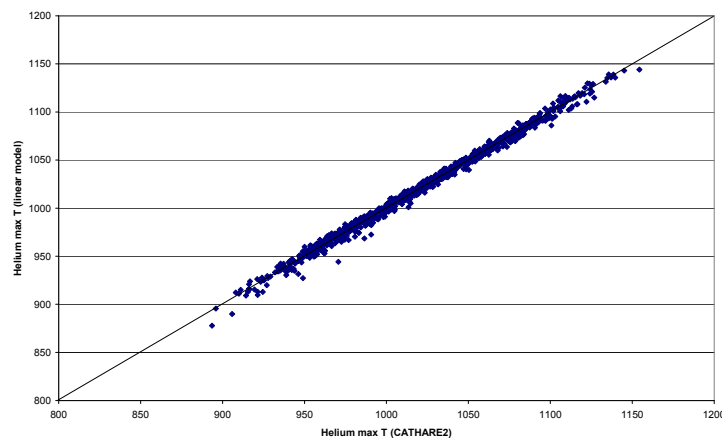


FIG. 61. Comparison of maximum helium temperature obtained by the CATHARE2 and by the linear model.

With the initial probabilistic model

By performing different numbers of simulations together with this linear model and initial probabilistic model (Table 33), the results obtained are given in Table 41.

TABLE 41. RESULTS OBTAINED WITH THE INITIAL PROBABILISTIC MODEL

Number of simulations	Failure probability P_f	Maximal value (°C) of Max. He T obtained
10^6	No failure case	1181
10^7	No failure case	1183

With 10^7 simulations, the maximum value obtained is 67°C below the failure criteria.

Pessimistic calculation

A “pessimistic” case is also studied by taking all the input parameters at their envelope value (with the values of the initial probabilistic model). That is:

$$V1 = + 0.15$$

$$V2 = + 2.$$

$$V3 = + 2.$$

$$V4 = + 0.25$$

$$V5 = - 0.15$$

$$V6 = - 0.25$$

$$V7 = + 0.02$$

$$V8 = + 0.10$$

$$V9 = - 0.25$$

$$V10 = - 0.2$$

In this case, no failure cases are observed and the maximum value of He temperature is equal to 1166°C with the CATHARE2 code and 1196°C with the linear regression model.

By using the linear regression model, which is slightly more conservative, and by modifying the envelope values of the parameters, the results obtained are shown in Table 42.

Only in one case, when the blower inertia is equal to -0.50, the failure criterion is exceeded.

TABLE 42. EFFECT OF MODIFICATIONS OF ENVELOPE VALUES ON THE MAXIMAL VALUE OF MAXIMUM HELIUM TEMPERATURE

Modification in the initial pessimistic case	Max. He Temperature (°C)
V9 (blower inertia) : - 0.40	1239
V9 (blower inertia) : - 0.50	1268
V5 (wall thermal inertia) : - 0.30	1227
V5 (wall thermal inertia) : - 0.40	1247
V8 (Core residual power) : + 0.20	1222
V8 (Core residual power) : + 0.30	1248
All envelope values * 1.1	1213
All envelope values * 1.1	1231
All envelope values * 1.1	1248

With a modified probabilistic model

Several modifications in the initial probabilistic model have been performed in order to test the influence of these modifications on the failure probability. Table 43 shows the various modifications in the probabilistic model and the corresponding failure probabilities and maximum helium temperature.

In this way, rough estimation of the failure probability of the DHR system for transient I is obtained. In addition, it is observed that by doubling the range of variation of the most important parameters (blower inertia or wall thermal inertia), the failure probabilities are very small. The same is true if the ranges of variation of all the input parameters are increased by 50%. In order to obtain a relatively significant failure probability ($\sim 10^{-4}$), it is necessary to double the range of variation of the two most important parameters simultaneously or to increase all the ranges by 70%.

Given that the frequency of occurrence of transient I is very small (loss of station service power + emergency diesel generators failure to start + only one of two DHR loop available for natural circulation), the global risk (product of the failure probability and frequency of occurrence of the transient) associated with this transient will be very low.

As we know that, the failure probability is estimated by:

$$\overline{P_f} = \frac{N_f}{N}$$

where N_f is the number of simulations leading to the failure of the system and N is the total number of simulations.

TABLE 43. EFFECT OF MODIFICATIONS OF THE PROBABILISTIC MODEL ON THE FAILURE PROBABILITY

Modification in the initial probabilistic model (Table 33)	Failure probability P_f	COV of P_f	Max. He T (°C)
V9 (blower inertia) : [-50% , 50%]	7.2×10^{-7}	0.12	1256
V5 (wall thermal inertia) : [-30% 30%]	No failure case	-	1209
V9 (blower inertia) : [-50% , 50%] and V5 (wall thermal inertia) : [-30% , 30%]	2.71×10^{-4}	0.06	1277
Uncertainty range of all variables * 1.1	No failure case	-	1197
Uncertainty range of all variables * 1.2	No failure case	-	1212
Uncertainty range of all variables * 1.3	No failure case	-	1229
Uncertainty range of all variables * 1.4	No failure case	-	1247
Uncertainty range of all variables * 1.5	3.5×10^{-6}	0.17	1263
Uncertainty range of all variables * 1.6	5.7×10^{-5}	0.13	1276
Uncertainty range of all variables * 1.7	3.2×10^{-4}	0.06	1292

When N tends to infinity, $\overline{P_f}$ tends to the actual value of the failure probability. The accuracy of the estimation can be evaluated by its variance calculated in an approximate way by:

$$Var(\overline{P_f}) \cong \frac{(1 - \overline{P_f})\overline{P_f}}{N}$$

A good estimation of the statistical accuracy is given by the coefficient of variation:

$$COV(\overline{P_f}) \cong \frac{\sqrt{\frac{(1 - \overline{P_f})\overline{P_f}}{N}}}{\overline{P_f}}$$

The lower the coefficient of variation (COV), the more accurate is the estimation of the failure probability. The coefficient of variation (COV) close to 10% indicates a good level of accuracy.

Conclusion

In the reference case, with nominal values of the input parameters, it can be seen that only one DHR loop working in natural circulation fulfills perfectly its mission. A stable flow rate of about 30 kg/s is quickly (in less than 100 s) established in the DHR loop and is maintained up to the end of the transient during the natural circulation phase. After one hour from the beginning of the transient, the heat removal is sufficient and all failure criteria are respected, with values staying well below the safety limits.

Among all the parameters studied in the sensitivity analysis, very few have a significant influence on the transient, in the area investigated. The major effect is produced by the additional singular pressure drop coefficient, which simulates the stopped DHR blower. During the analysis, we have considered that around the DHR blower there is a bypass, which is opened when the DHR blower is stopped. The reliability of this bypass system will have to be investigated in future studies.

The primary blower inertia has a noticeable effect on the transient sequence and on all system parameters. Nominal power, delay between primary valves closure and DHR valves opening, and wall inertia are others parameters of influence. All remaining parameters have a very limited impact on the transient. Especially uncertainties on materials properties play a very limited role and do not need to be taken into account.

The failure probability of the DHR system in case of transient I is very small.

The DHR system working in natural circulation is a very reliable system for loss of flow accident (LOFA).

II.2. BARC, INDIA

II.2.1. Modelling of primary heat transport system

The reactor pressure vessel along with the primary circuit path has been considered as primary heat transport system. Lower plenum, core, bypass and upper plenum are the components of reactor pressure vessel. Radial power distribution has been considered in the core by dividing it radially in six power channels and one bypass channel. During normal operation of the reactor the energy is transferred to the secondary system which is simulated as the heat exchanger boundary condition. The details of the primary heat transport system are given in Table 44. Figure 62 shows the RELAP 5 nodalization of the primary heat transport system of GFR.

TABLE 44. GEOMETRICAL DETAILS OF PRIMARY HEAT TRANSPORT SYSTEM AS CONSIDERED IN RELAP5

		Components	Area (m ²)	Length (m)	Volume (m ³)
Primary Heat Transport System	Reactor Pressure vessel	Lower plenum	-	3.2	68.63
		Core0	0.27 0.2505816 0.27	5.8	-
		Core1	0.54 0.5011632 0.54	5.8	-
		Core2	0.81 0.7517448 0.81	5.8	-
		Core3	0.54 0.5011632 0.54	5.8	-
		Core4	0.63 0.5846904 0.63	5.8	-
		Core5	0.9 0.835272 0.9	5.8	-
		Bypass	1.9068	5.8	-
		Upper plenum1	32.3713	3.3	-
		Upper plenum2	-	3.2	68.63
		Downcomer	5.5	7.0	-
	Primary Circuit	Primary hot leg	1.89	2.0	-
		Inlet main IHX	2.0126	7.95	-
		IHX primary side	10.73	0.821	-
		Outlet main IHX	2.0126	7.95	-
		Buffer volume	-	6.0	100.0
		Blower	-	3.0	9.42
		V Circol	20.0	2.5	-
		Primary cold leg	-	1.53	2.0

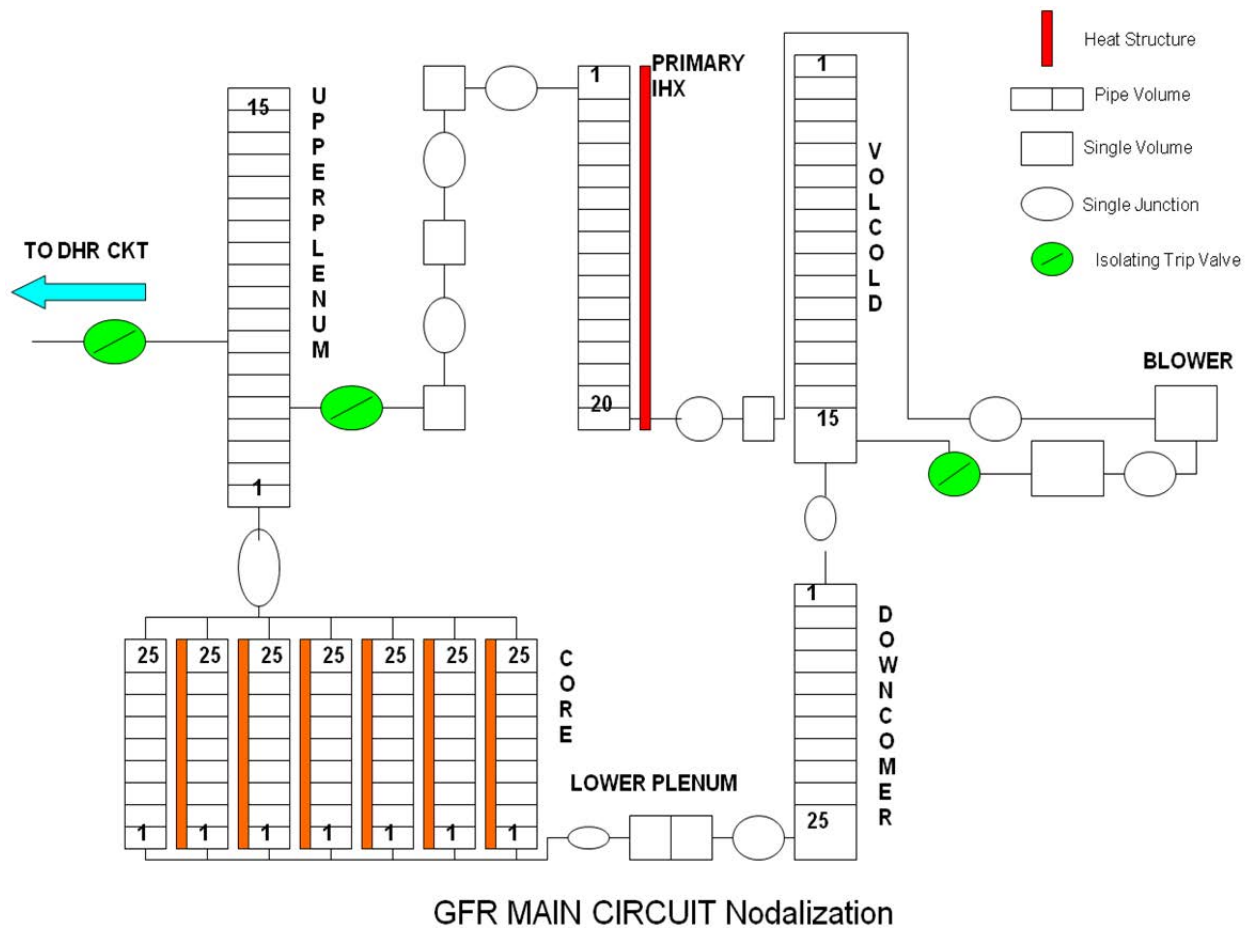


FIG. 62. RELAP5 Nodalization of Main circuit of GFR.

II.2.2. Modelling of secondary system for heat removal during normal operation

Secondary side flow, pressure and temperature of the GFR main circuit are simulated as the boundary condition for steady state simulation in the RELAP5.

II.2.3. Modelling of DHR circuit

DHR circuit is divided into three parts viz. DHR primary circuit (He side), DHR secondary circuit (water side), DHR tertiary circuit (water pool). The RELAP5 nodalization of DHR circuit is shown in Fig. 63. Details of the DHR circuit are given in Table 45.

During SBO, the heat is transferred from the primary loop of helium coolant to the secondary water loop and subsequently to the tertiary water pool of passive decay heat removal system by natural convection.

TABLE 45. VARIOUS COMPONENTS OF THE DHR SYSTEM

		Components	Area (m ²)	Length (m)	Volume (m ³)
DHR System	DHR Primary Circuit	Lower plenum	-	3.2	68.63
		Core0	0.27 0.2505816 0.27	5.8	-
		Core1	0.54 0.5011632 0.54	5.8	-
		Core2	0.81 0.7517448 0.81	5.8	-
		Core3	0.54 0.5011632 0.54	5.8	-
		Core4	0.63 0.5846904 0.63	5.8	-
		Core5	0.9 0.835272 0.9	5.8	-
		By-pass	1.9068	5.8	-
		Upper plenum1	32.3713	3.3	-
		Upper plenum2	-	3.2	68.63
		Downcomer	5.5	7.0	-
		DHR Primary Hot Leg	2.0106	9.901	-
		DHX1 Primary Side	7.93	4.5	-
		DHR Primary Cold Leg	2.5035	5.401	-
	DHR Secondary Circuit	DHX1 Secondary Side	1.51	4.5	-
		DHR Secondary Hot Leg	0.19635	3.22	-
		DHX2 Secondary Side	1.634864	4.5	-
		DHR Secondary Cold Leg	0.19635	16.25	-
		Pressuriser	To maintain pressure 10MPa		
	DHR Ternary Circuit	Tertiary Pool		10.0	900.0
		Pressuriser	To maintain pressure 1.01325 bar		

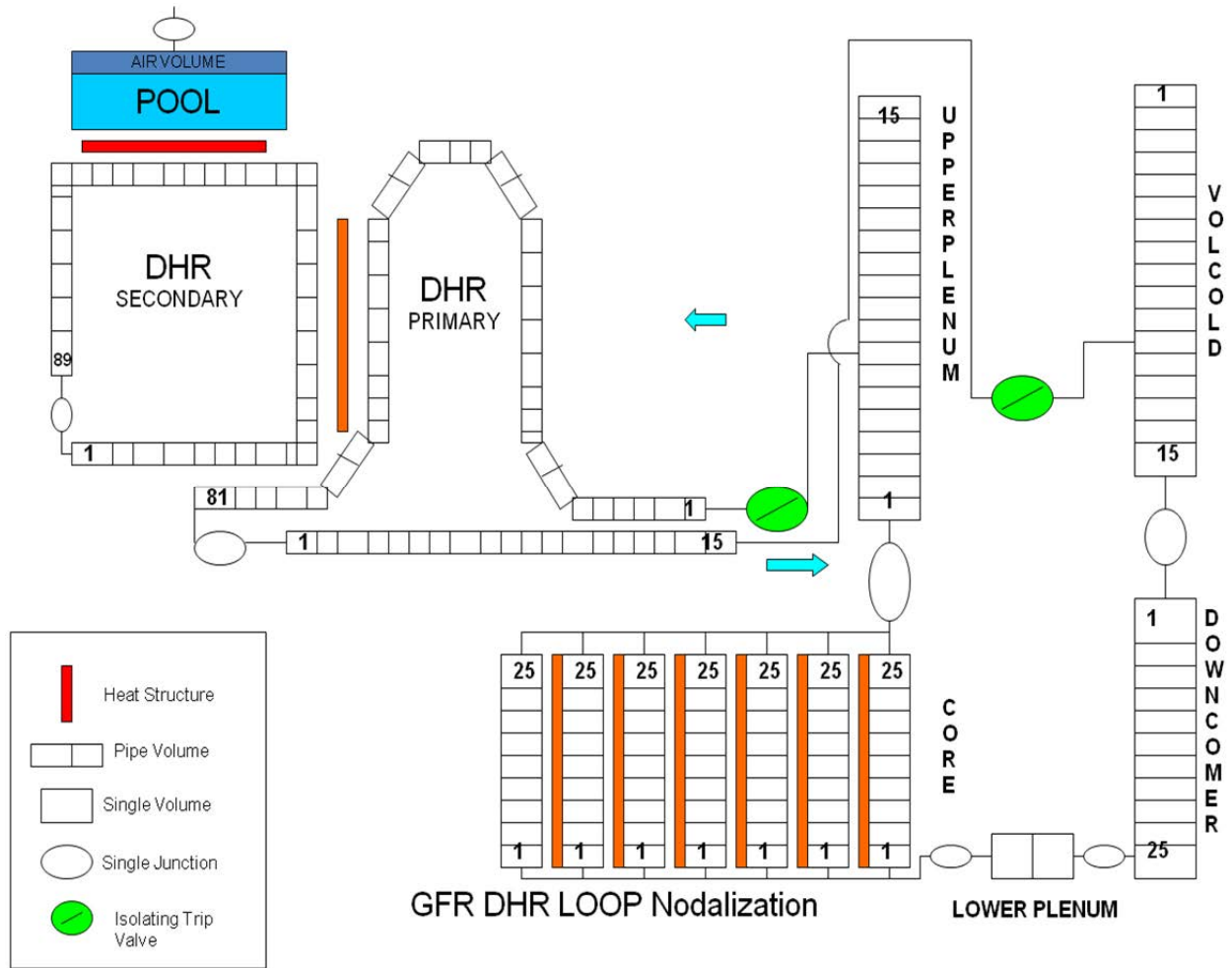


FIG. 63. RELAP5 nodalization of DHR circuit of GFR.

II.2.4. Validation of RELAP5 nodalization for steady state

The RELAP5 computations were started with assumed initial conditions till steady state is achieved. For this, code calculations were continued for 500s. Figures 64 to 67 show the system behaviour before initiation of transient. It is observed that the operating parameters like mass flow rate in individual channels, clad surface temperature, fuel centerline temperature, pressure and temperature in upper and lower plenums do not change after nearly 50s of computations indicating that steady state has been achieved. Figures 68 and 69 show the clad surface temperature and fuel centerline temperature, respectively, along the axis of the core at steady state. Table 46 and Table 47 show summary of steady state results and their differences from reference values. The results show that the RELAP5 nodalization is capable enough to simulate the GFR initial conditions.

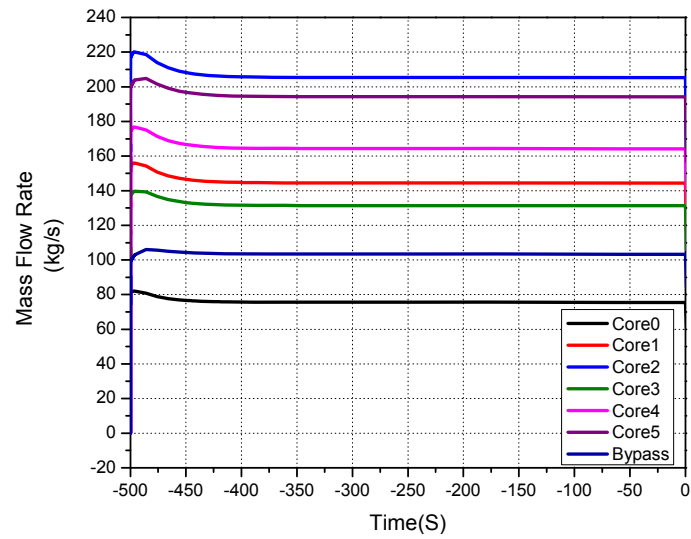


FIG. 64. Mass flow rate (various channels).

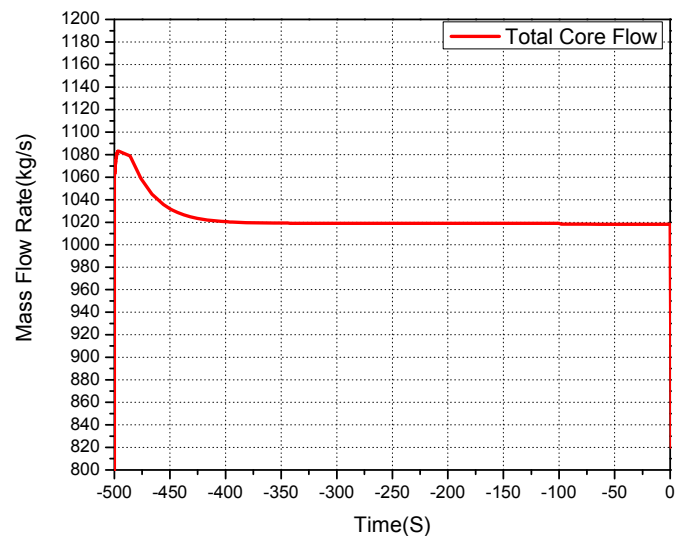


FIG. 65. Mass flow rate (total core).

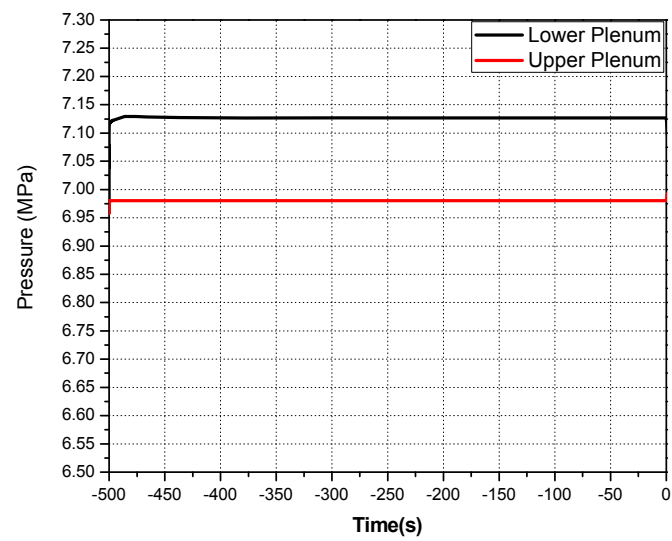


FIG. 66. Pressure across core.

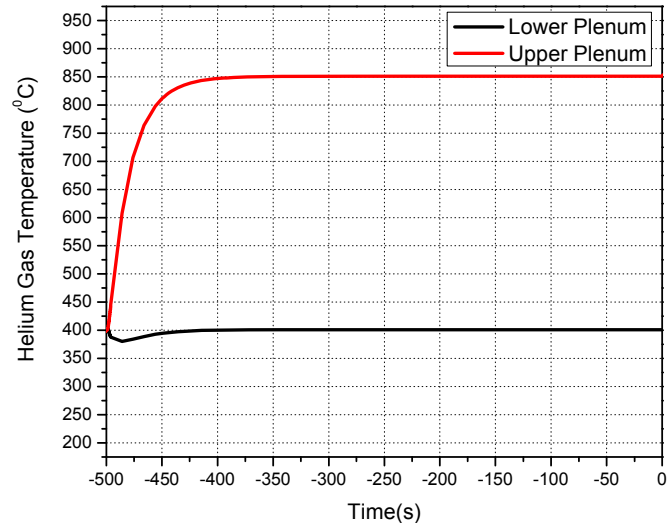


FIG. 67. Temperature main vessel inlet/outlet.

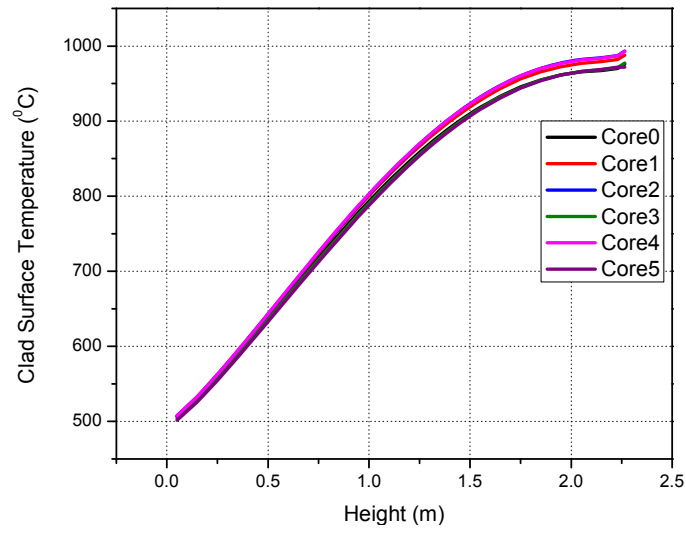


FIG. 68. Clad surface temperature (steady state).

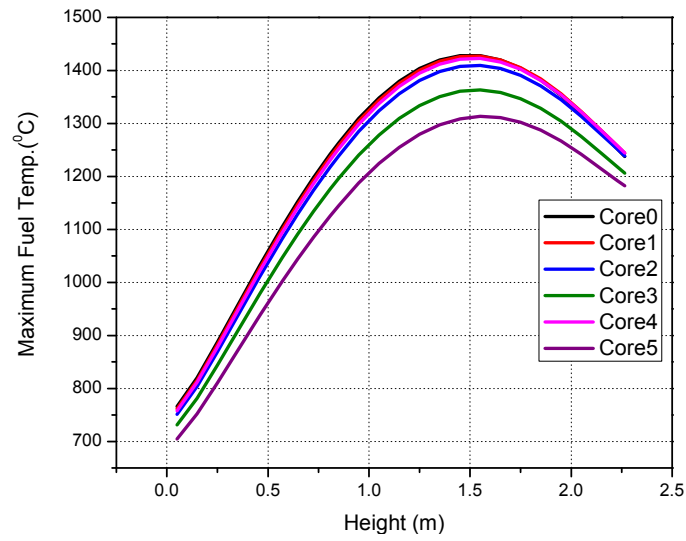


FIG. 69. Fuel centreline temperature (steady state).

TABLE 46. STEADY STATE PARAMETERS OF GFR-2400 MW(TH)

Parameter	Reference	RELAP5	Error (%)
Main vessel inlet/outlet gas temperatures (°C)	400/850	400/851	-
Core outlet gas temperature (°C)	900	902	0.22
Main vessel inlet/outlet gas pressure (MPa)	7.12/6.98	7.13/6.98	-
ΔP vessel (upper plenum/lower plenum) (MPa)	0.14	0.12	14.28
Main loop mass flow rate (kg/s)	340.8x3	1019	0.09
Core inlet mass flow	1020	1019	0.09
Main loop IHX exchanged power (MW)	803.3x3	2400	-

TABLE 47. STEADY STATE FLOW RATE OF GFR-2400 MW(TH)

Component	Q_{channel} (kg/s) (reference)	RELAP5	Error (%)
Downcomer	1020.2	1019	0.09
Core0	74.5	76.0	-2.01342
Core1	145.7	144.0	1.166781
Core2	208.4	206.0	1.151631
Core3	130.1	132.0	-1.46042
Core4	166.8	165.0	1.079137
Core5	193.3	194.0	-0.36213
Bypass	101.4	102.0	-0.5917

II.2.5. Application of APSRA for reliability assessment of PDHRS of GFR during SBO transient

Step I: Passive system considered — Passive Decay Heat Removal System (PDHRS) of the GFR under SBO condition.

Step II: After several discussions among the participants of this exercise, it was decided to study the following parameters, which may influence the natural circulation in PDHRS primary side:

- (1) Core power;
- (2) Residual power ;
- (3) Main circuit pressure;
- (4) Fuel heat transfer coefficient;
- (5) Heat transfer coefficient in DHR secondary side;
- (6) DHR primary side inlet loss coefficient;
- (7) DHR primary side outlet loss coefficient;
- (8) Pressure drop in fuel channels;
- (9) Thermal inertia of primary system components;
- (10) Primary blower inertia.

Out of these parameters listed above, parameters 1–3 are the operating process parameters of DHR primary circuit and 4–10 are the model parameters.

Step III: To understand the natural circulation characteristics of the GFR, the natural circulation flow rate as a function of different parameters has been predicted. The computer code RELAP5/MOD3.2 has been used for the purpose due to unavailability of simpler codes relevant to gas cooled systems, which can carry out the computations relatively at a faster speed.

The key parameters are varied over a range as given in Table 22 (Appendix I).

Apart from the operating parameters in DHR primary circuit, operating parameters in the DHR secondary circuit such as initial water temperature, pressure in the water loop and operating parameters in the DHR tertiary circuit such as pool level, pool initial temperature may affect the performance of the PDHRS of GFR. Earlier sensitivity analysis showed that these parameters have negligible effect on the performance of DHR, hence, they are not considered in the analysis here.

Effect of core nominal Power

The effect of initial operating power of the reactor on natural circulation characteristics of the system during SBO has been analysed. The results show that having higher initial power results in higher clad surface temperature, higher gas outlet temperature and higher structural temperature as shown in Figs 70 to 72.

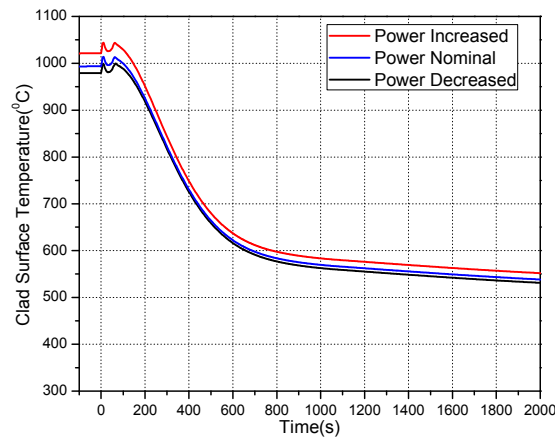


FIG. 70. Effect of nominal power on clad surface temperature.

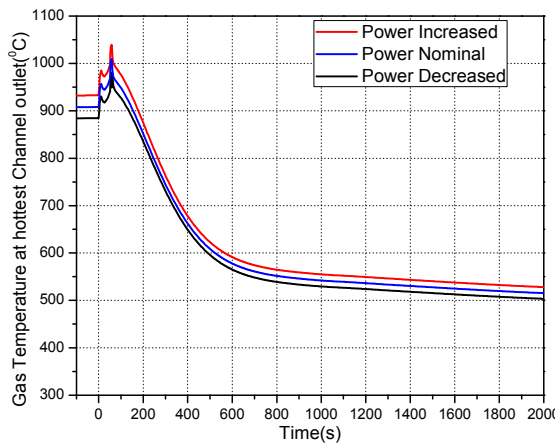


FIG. 71. Effect of nominal power on gas temperature at channel outlet.

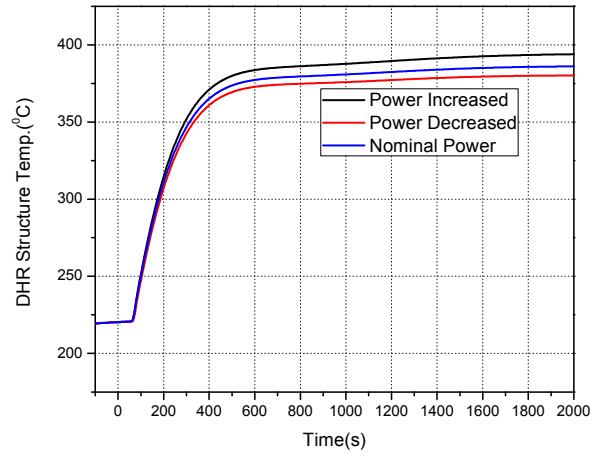


FIG. 72. Effect of nominal power on DHR structure temperature.

Effect of residual power

Similar effects are observed on clad surface temperature, gas outlet temperature and DHR structural temperature for higher residual power as shown in Fig. 73 to Fig. 75.

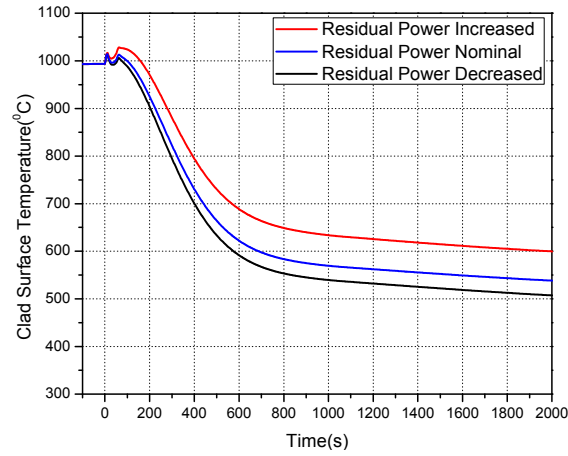


FIG. 73. Effect of residual power on clad surface temperature.

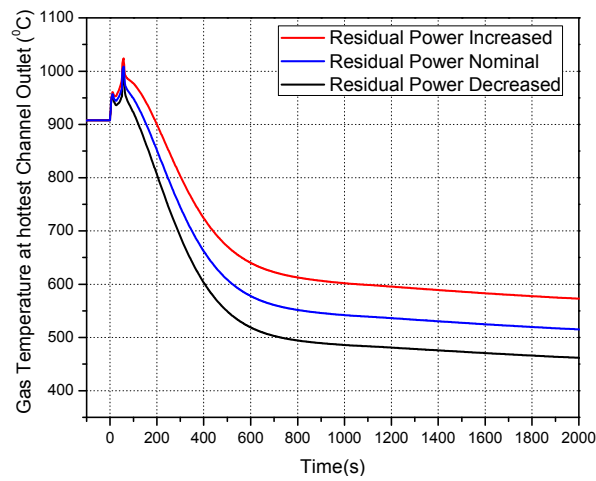


FIG. 74. Effect of residual power on gas temperature at channel outlet.

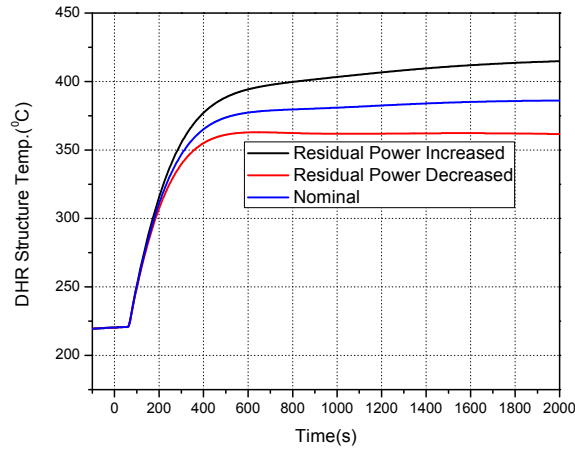


FIG. 75. Effect of residual power on DHR structure temperature.

Effect of main circuit pressure

An increase in system pressure gives a higher natural circulation flow rate, which causes reduction in clad surface temperature, gas outlet temperature and DHR structural temperature as shown in Fig. 76 to Fig. 78.

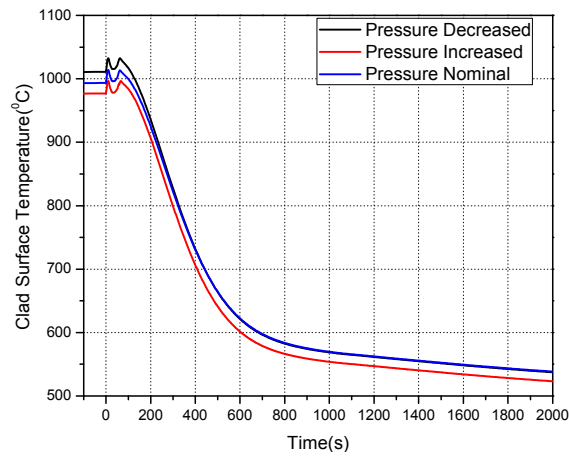


FIG. 76. Effect of primary pressure on clad surface temperature.

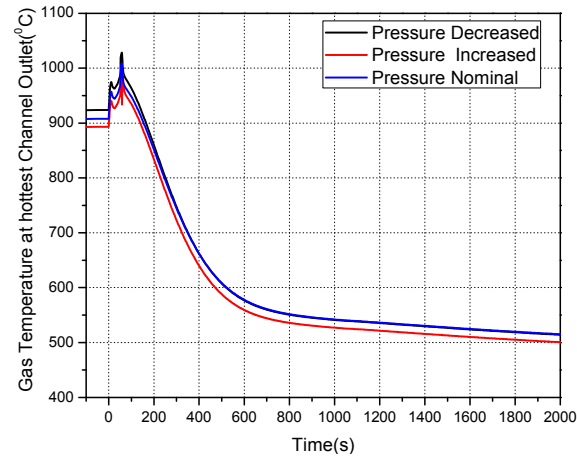


FIG. 77. Effect of primary pressure on gas temperature at channel outlet.

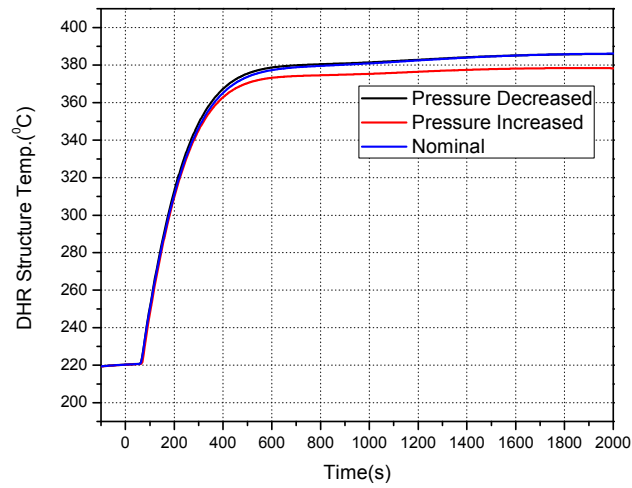


FIG. 78. Effect of primary pressure on DHR structure temperature.

Pressure drop in fuel assembly (Core ΔP)

As expected, increasing the pressure drop in the fuel assembly reduces the natural circulation flow rate, which results in increase in clad surface temperature, gas outlet temperature and DHR structural temperature as shown in Fig. 79 to Fig. 81.

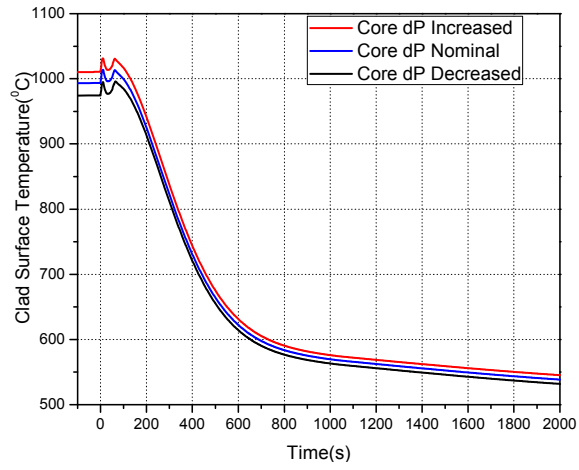


FIG. 79. Effect of core ΔP on clad surface temperature.

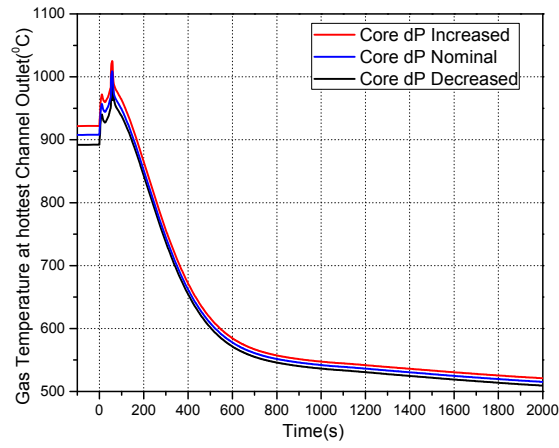


FIG. 80. Effect of core ΔP on gas temperature at channel outlet.

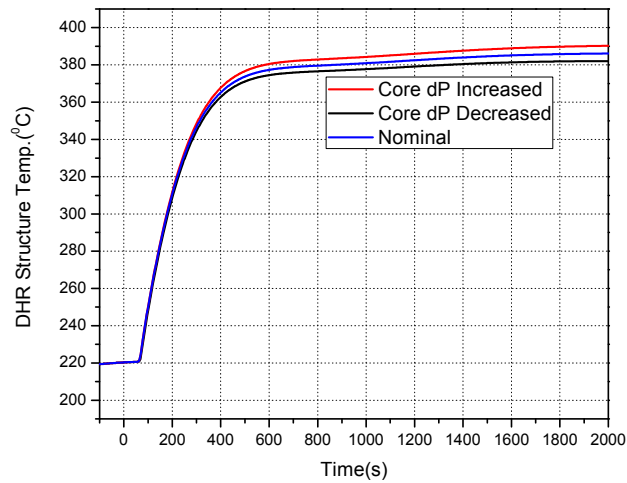


FIG. 81. Effect of core ΔP on DHR structure temperature.

Effect of heat transfer coefficient (primary side)

RELAP5 mod 3.2 does not have a provision for changing the heat transfer coefficient manually since it calculates the heat transfer coefficient based on operating and geometric conditions using suitable models. To account for variation in heat transfer coefficient in the analysis, the heat transfer area was proportionately varied. An increase in heat transfer coefficient reduces the clad surface temperature. However, this results in increase in gas outlet temperature and DHR structural temperature as shown in Fig. 82 to Fig. 84.

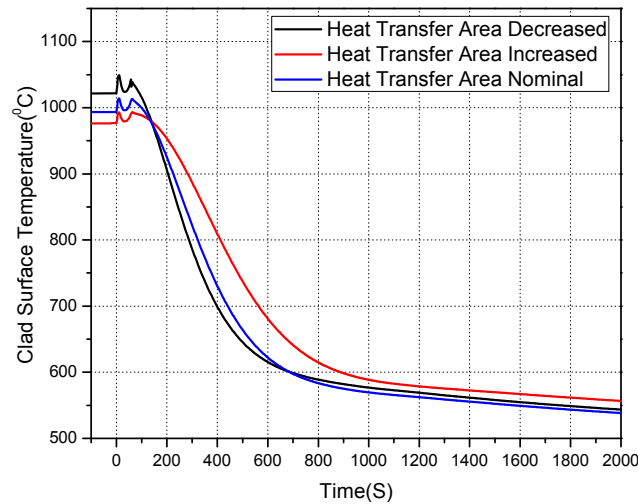


FIG. 82. Effect of heat transfer area on clad surface temperature.

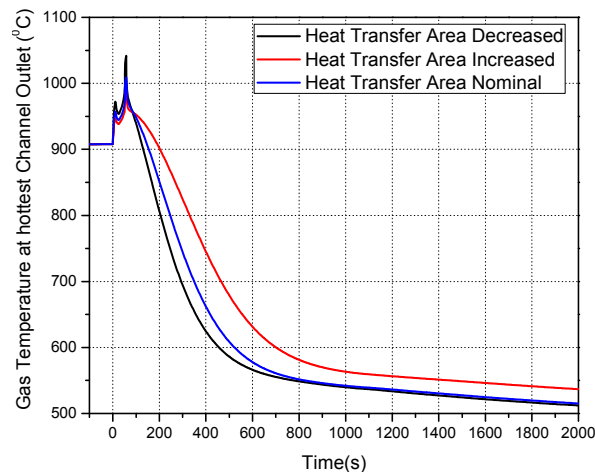


FIG. 83. Effect of primary heat transfer area on gas temperature at channel outlet.

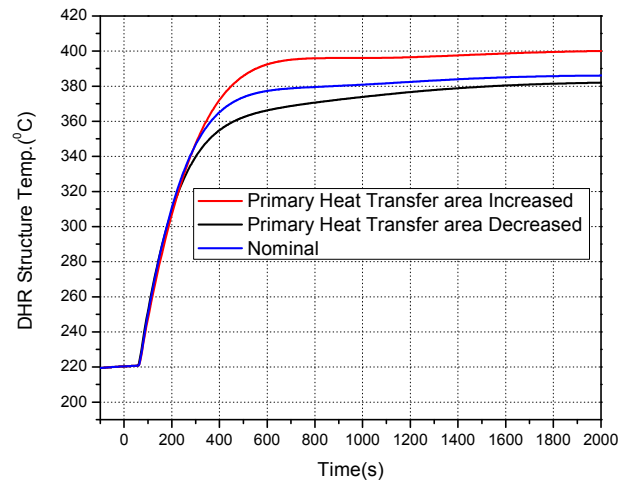


FIG. 84. Effect of primary heat transfer area on DHR structure temperature.

Effect of DHR heat transfer coefficient (water side)

Variation in heat transfer coefficient of DHR water side is found to have negligible effects on the primary side temperatures as shown in Fig. 85 to Fig. 87.

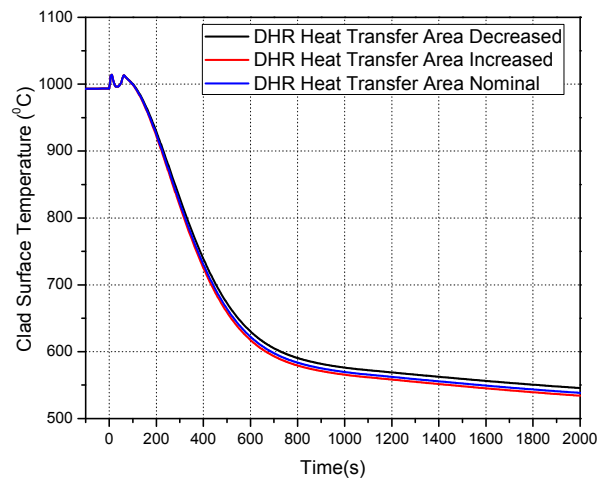


FIG. 85. Effect of DHR heat transfer area on clad surface temperature.

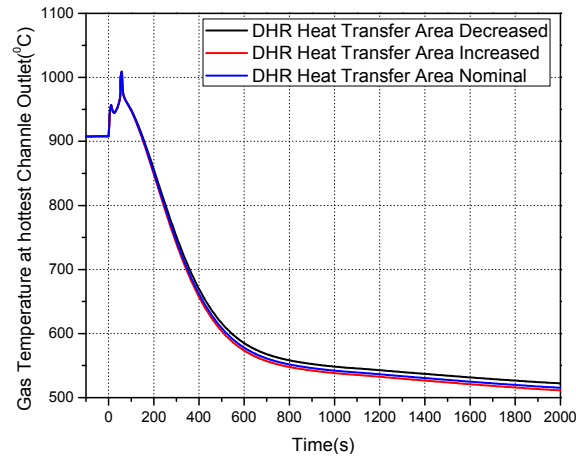


FIG. 86. Effect of DHR heat transfer area on gas temperature at channel outlet.

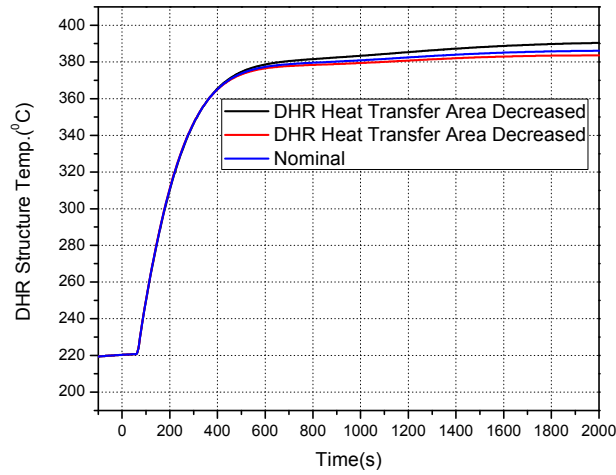


FIG. 87. Effect of DHR heat transfer area on DHR structure temperature.

Effect of DHR primary inlet/outlet loss coefficient

By increasing the loss coefficients at the DHR primary side inlet and outlet valves the natural circulation flow rate reduces, which results in increase in the clad surface temperature, gas outlet temperature and DHR structural temperature as shown in Fig. 88 to Fig. 90.

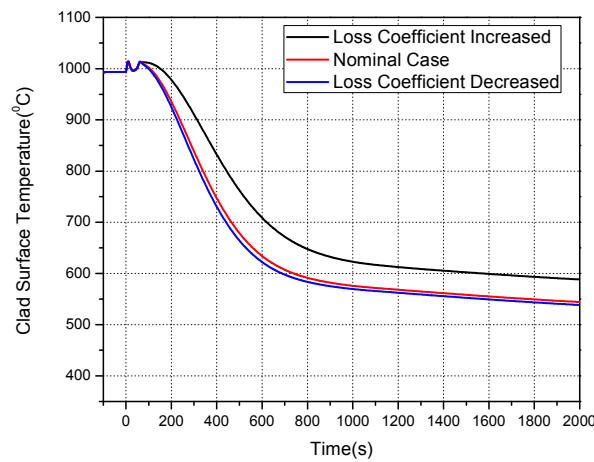


FIG. 88. Effect of loss coefficient (inlet/outlet) on clad surface temperature.

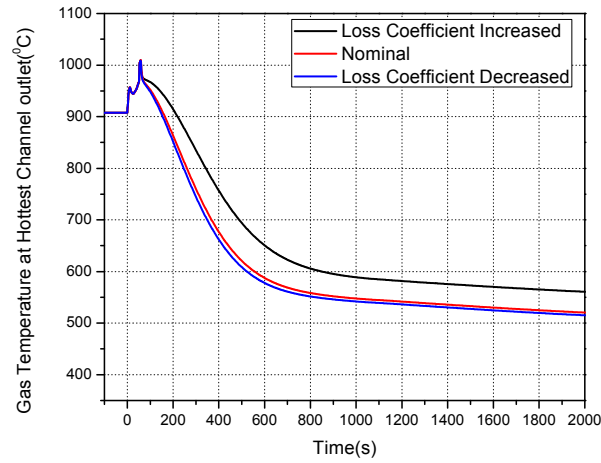


FIG. 89. Effect of loss coefficients (inlet/outlet) on gas temperature at channel outlet.

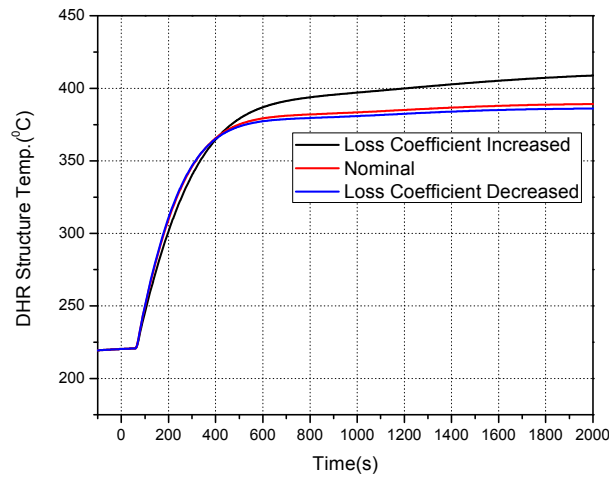


FIG. 90. Effect of loss coefficient (inlet/outlet) on DHR structure temperature.

Effect of thermal inertia of primary system

Increase in thermal inertia of primary system results in accumulation of the heat in the structures during normal operation. Effect of thermal inertia on clad surface temperature, gas outlet temperature and DHR structural temperature is shown in Fig. 91 to Fig. 93.

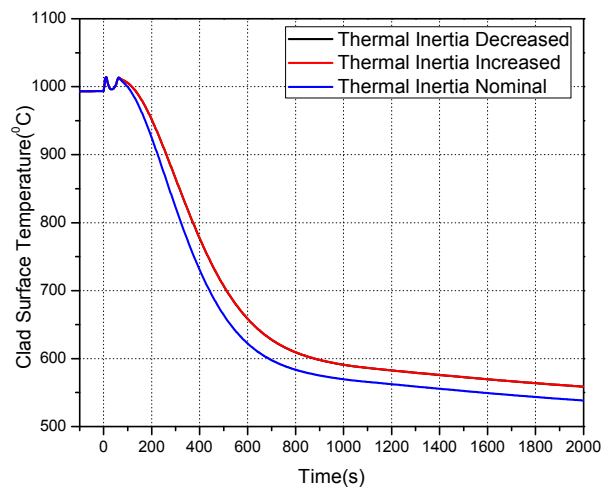


FIG. 91. Effect of thermal inertia on clad surface temperature.

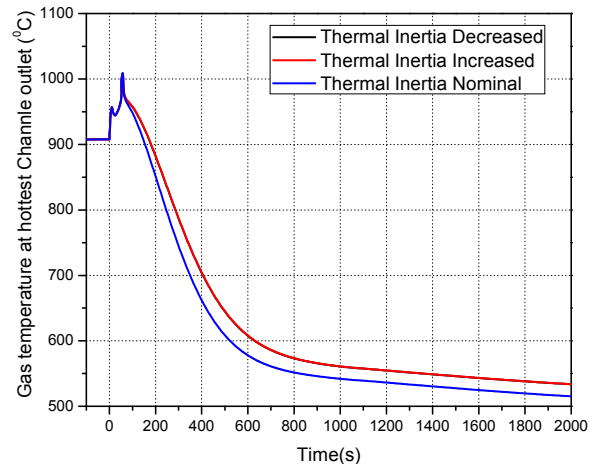


FIG. 92. Effect of thermal inertia on gas temperature at channel outlet.

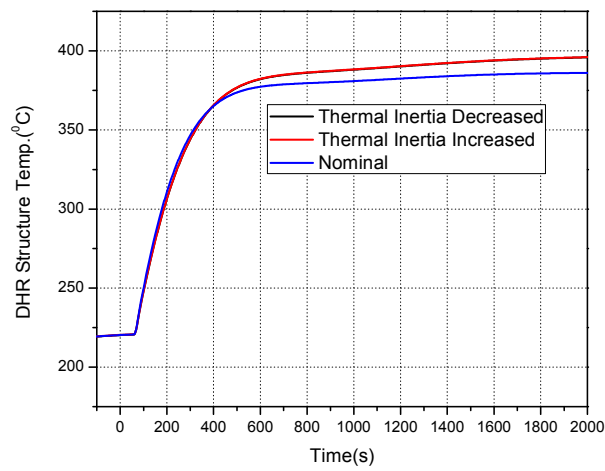


FIG. 93. Effect of thermal inertia on DHR structure temperature.

Effect of primary blower inertia

Increase in blower inertia results in decrease in clad surface temperature, gas outlet temperature and DHR structural temperature as shown in Fig. 94 to Fig. 96.

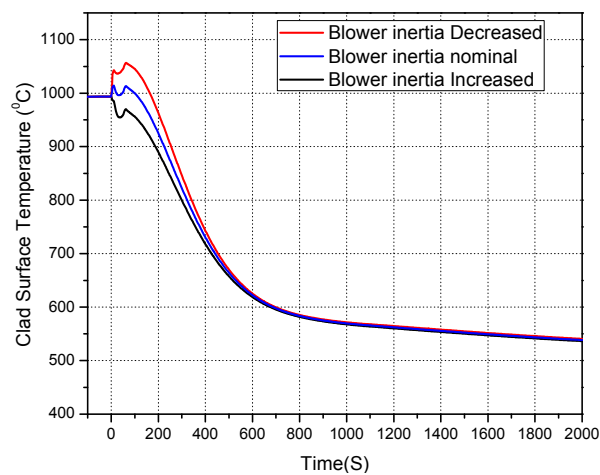


FIG. 94. Effect of blower inertia on clad surface temperature.

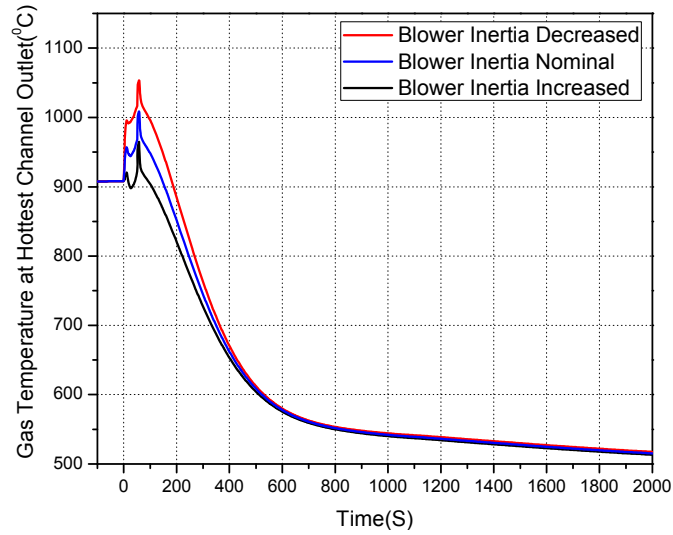


FIG. 95. Effect of blower inertia on gas temperature at channel outlet.

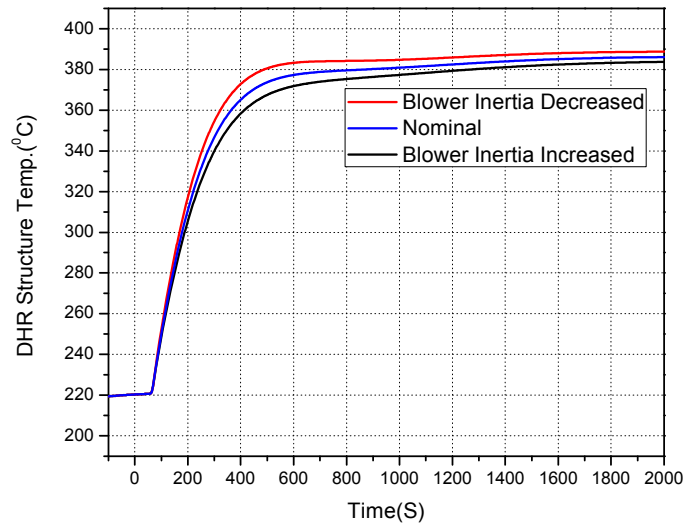


FIG. 96. Effect of blower inertia on DHR structural temperature.

Step IV: Key parameters causing the failure

Identification of natural circulation failure

For SBO, natural circulation failure in the GFR is considered to occur according to the conditions given in Table 21 (see Appendix I).

After doing the sensitivity analysis with variation of the various governing parameters, their effects on peak clad surface temperature, maximum gas temperature at core outlet and maximum DHR structural temperature have been calculated and the results are summarized in Table 48.

TABLE 48. EFFECT OF VARIATION OF PARAMETERS ON THE PEAK CLAD SURFACE TEMPERATURE, MAXIMUM GAS TEMPERATURE AT CORE OUTLET AND MAXIMUM DHR STRUCTURAL TEMPERATURE

Sensitive Parameter	Variation	$(\Delta T = T_{\text{failure clad}} - T)$ $T_{\text{failure}}=1600\text{ }^{\circ}\text{C}$	$(\Delta T = T_{\text{failure DHR}} - T)$ $T_{\text{failure}}=850\text{ }^{\circ}\text{C}$	$(\Delta T = T_{\text{failure gas outlet}} - T)$ $T_{\text{failure}}=1250\text{ }^{\circ}\text{C}$
Core power	- 2 %	602	470	258
	+ 2 %	556.22	455.82	211
Residual power	- 10 %	600	488	255
	+ 10 %	577	433.33	220
Main Circuit pressure	- 2 bar	568	463.5	222
	+ 2 bar	603	464.7	252
Fuel heat transfer coefficient	- 25 %	558	467	209
	+ 25 %	597	450	261
Heat transfer coefficient in DHR secondary side	- 25 %	586.7	459.5	241.21
	+ 25 %	586.11	467	241.16
DHR primary side inlet loss coefficient	- 200 %	586.46	447.98	241.17
	+ 200 %	586.5	467	241.6
DHR primary side outlet loss coefficient	-200 %	586.5	467	241.21
	+ 200 %	586.56	447.65	241.25
Pressure drop in fuel channels	- 15 %	604	468	270
	+ 15 %	560	459.5	225
Thermal inertia of primary system components	- 15 %	586.7	453.5	241.2
	+ 15 %	586.67	453.3	241.17
Primary blower inertia	- 25 %	543.44	461.5	197
	+ 25 %	607	467	286

From Table 48, it is clear that variation of these parameters have negligible effect and large margins on failure of the PDHRS, especially against clad surface temperature and DHR structural temperature. To find out the effects of the combinations of the parameters on the failure of the system, three most critical parameters are chosen based on their negative effect on gas outlet temperature. From Table 48, the key parameters which may cause the system failure are:

- (1) Blower inertia;
- (2) Nominal power;
- (3) Primary heat transfer area.

These parameters have relatively lesser margin against failure with respect to the gas outlet temperature.

Effect of variation of key parameters on system failure

Effect of variation of process parameters on system failure: The only process parameter which may have some effect on system failure is nominal power. Variation of nominal power alone does not lead to failure of the system as shown in Table 48.

Effect of variation of model parameters on system failure: The two most critical model parameters considered are blower inertia and primary heat transfer coefficient. Independent variations of model parameters do not lead to system failure as shown in Table 48.

Effect of variation of combinations of process and model parameters on system failure: 27 combinations of the above three most critical parameters are considered to find out their effect on system failure. Effect of combination of variation of these parameters on the system performance has been shown in Table 49.

TABLE 49. EFFECT OF VARIATION OF CRITICAL PARAMETERS ON PEAK CLAD SURFACE TEMPERATURE, MAXIMUM GAS TEMPERATURE AT CORE OUTLET AND MAXIMUM DHR STRUCTURAL TEMPERATURE

No	Cases	DHR Structure Temp. (°C)	($\Delta T = T_{\text{failure DHR}} - T$) $T_{\text{failure}}=850\text{ }^{\circ}\text{C}$	Gas Temp. at core outlet (°C)	($\Delta T = T_{\text{failure gas outlet}} - T$) $T_{\text{failure}}=1250\text{ }^{\circ}\text{C}$	Clad Surface Temp. (°C)	($\Delta T = T_{\text{failure clad}} - T$) $T_{\text{failure}}=1600\text{ }^{\circ}\text{C}$
	Reference Value	386.0	-	1008.0	-	1013.0	-
1	BI, Ap, P (Nom, Nom, Nom)	386.0	464.0	1008.0	242.0	1013.0	587.0
2	BI, Ap, P (Nom, Max., Max.)	408.5	441.5	1018.46	231.54	1022.34	577.66
3	BI, Ap, P (Nom, Min., Min.)	376.38	473.62	1010.38	239.62	1030.17	569.83
4	BI, Ap, P (Nom, Max., Min.)	393.0	457.0	961.40	288.6	978.35	621.65
5	BI, Ap, P (Nom, Min., Max.)	390.0	460.0	1075.0	175.0	1077.16	522.84
6	BI, Ap, P (Nom, Nom, Max.)	394.18	455.82	1039.0	211.0	1043.78	556.22
7	BI, Ap, P (Nom, Nom, Min.)	380.20	469.8	979.8	270.2	999.45	600.55
8	BI, Ap, P (Nom, Min., Nom)	382.0	468.0	1041.0	209.0	1049.0	551.0
9	BI, Ap, P (Nom, Max., Nom)	400.2	449.8	989.2	260.8	992.0	608.0
10	BI, Ap, P (Max., Max., Max.)	409.0	441.0	1055.48	194.52	1058.05	541.95
11	BI, Ap, P (Max., Min., Min.)	378.6	471.4	1065.06	184.94	1083.85	516.15
12	BI, Ap, P (Max., Nom, Nom)	388.7	461.3	1053.61	196.39	1056.56	543.44
13	BI, Ap, P (Max., Min., Nom)	384.6	465.4	1098.52	151.48	1097.35	502.65
14	BI, Ap, P (Max., Nom, Min.)	382.7	467.3	1021.83	228.17	1041.0	559.0
15	BI, Ap, P (Max., Max., Min.)	396.6	453.4	995.83	254.17	1012.24	587.76
16	BI, Ap, P (Max., Max., Nom)	392.2	457.8	1024.94	225.06	1027.66	572.34

No	Cases	DHR Structure Temp. (°C)	($\Delta T = T_{\text{failure}}$ DHR- T) $T_{\text{failure}}=850\text{ }^{\circ}\text{C}$	Gas Temp. at core outlet (°C)	($\Delta T = T_{\text{failure}}$ gas outlet- T) $T_{\text{failure}}=1250\text{ }^{\circ}\text{C}$	Clad Surface Temp. (°C)	($\Delta T = T_{\text{failure}}$ clad- T) $T_{\text{failure}}=1600\text{ }^{\circ}\text{C}$
17	BI, Ap, P (Max.,Nom, Max.)	374.0	476.0	1085.82	164.18	1088.59	511.41
18	BI, Ap, P (Max.,Min., Max.)	383.87	466.13	1134.0	116.0	1134.22	465.78
19	BI, Ap, P (Min.,Min., Min.)	406.5	443.5	901.18	348.82	1006.86	593.14
20	BI, Ap, P (Min.,Nom, Nom)	383.87	466.13	964.75	285.25	969.99	630.01
21	BI, Ap, P (Min.,Max., Max.)	406.5	443.5	978.3	271.7	1003.83	596.17
22	BI, Ap, P (Min.,Max., Nom)	397.94	452.06	952.54	297.46	976.56	623.44
23	BI, Ap, P (Min.,Nom, Max.)	391.87	458.13	993.64	256.36	1021.67	578.33
24	BI, Ap, P (Min.,Min., Max.)	388.68	461.32	1018.44	231.56	1051.32	548.68
25	BI, Ap, P (Min.,Min., Nom)	380.57	469.43	987.47	262.53	1022.03	577.97
26	BI, Ap, P (Min.,Nom, Min.)	377.91	472.09	937.45	312.55	979.27	620.73
27	BI, Ap, P (Min.,Max., Min.)	391.28	458.72	926.15	323.85	962.61	637.39

All the combinations of these three parameters (blower inertia: BI, primary heat transfer area: Ap and nominal power: P) with their Nominal (Nom), Minimum (Min.) and Maximum (Max.) values are simulated and a distribution is obtained for peak clad surface temperature, maximum gas temperature at core outlet and maximum DHR structural temperature. The distribution of these parameters is shown in Fig. 97 to Fig. 99.

It is clear from Fig. 97 that 45% cases of the total combinations for clad surface fall in the range of 1000–1050 °C while nearly 25% cases falls in the range of 950–1000 °C and 1050–1100 °C respectively and the rest 5% cases fall in the range of 1100–1150 °C.

Figure 98 depicts that 30% of the total cases fall in the range of 950–1000 °C and 1000–1050 °C respectively, while less than 5% cases fall in the upper range i.e. 1100–1150 °C for the gas temperature at core outlet.

For the DHR structural temperature, as shown in Fig. 99, nearly 40 % of the total cases lie between 380–390 °C. Nearly 30 % of the total cases fall in the range of 390 to 400 °C. About 18 % of total cases fall in the range of 370–380 °C and nearly 15 % of the total cases fall in the range 400 to 410 °C.

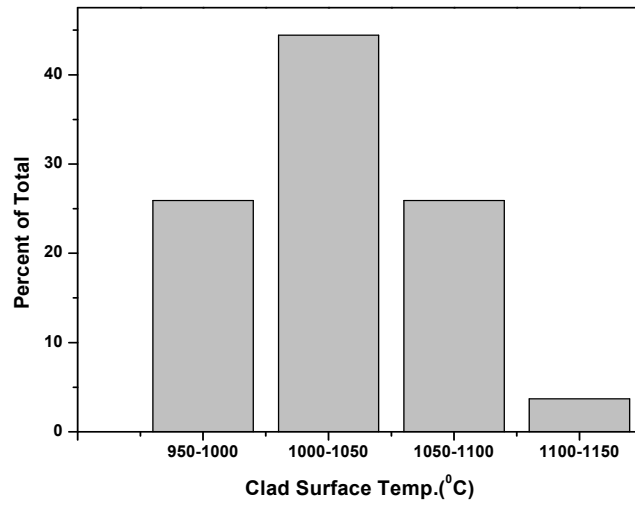


FIG. 97. Distribution of clad surface temperature.

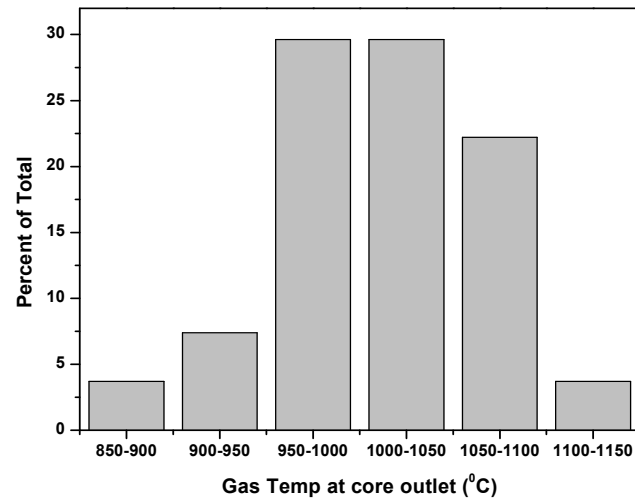


FIG. 98. Distribution of gas temperature at channel outlet.

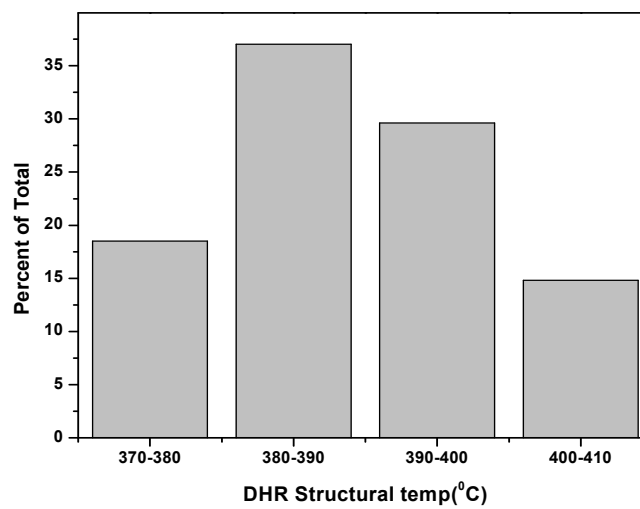


FIG. 99. Distribution of DHR structural temperature.

Table 50 shows the statistical parameters of the peak clad surface temperature, maximum gas temperature at core outlet and maximum DHR structural temperature.

TABLE 50. STATISTICS OF FAILURE PARAMETERS

Statistical Parameters	Clad Surface Temp. (°C)	Gas Temp. at Channel Outlet (°C)	DHR Structural Temp. (°C)
Average(μ)	1029.59	1011.75	389.8463
Standard Deviation(σ)	42.6107	54.62799	10.0725
Variation Coefficient (σ/μ) in %	4.138609	5.4	2.58
Minimum	962.61	901.18	374.00
Maximum	1134.22	1134.00	409.00
X _{90%}	1084.131	1081.674	402.7391
X _{95%}	1099.897	1101.886	406.4659
X _{99%}	1128.871	1139.033	413.3152
X _{99.99%}	1191.508	1219.336	428.1218

From the above analysis, it is concluded that even though the operating parameters of the reactors are varied to a maximum range, no failure is found. Clad surface temperature and DHR structural temperature are far below their failure limit. There is least margin in gas temperature at channel outlet but it is still below the failure limit. The probability of the failure of the reactor in such case is zero. Hence, the system reliability is 100%.

Re-identification of natural circulation failure

Since the failure probability of the system is found to be zero, for the sake of application of the APSRA methodology to the PDHRS of the GFR, the failure criteria for SBO conditions is redefined according to the conditions given in Table 51.

TABLE 51. FAILURE CRITERIA

Criterion	Failure limit
(DHR loop structural integrity) Maximum temperature of DHR structural material	850 °C
Maximum clad temperature	1600 °C
(Core upper structures integrity) Maximum temperature of gas at hot channel outlet	1050 °C

The step V to step VIII of APSRA has been continued to evaluate the failure probability of the system.

From the sensitivity analysis as seen from Table 49, the key process parameters that affect system performance and may cause the failure of the system due to their variation from their nominal conditions are segregated in two categories i.e. process and model parameters. The important process parameters are:

- Fission heat generation rate;
- Pressure in the system;
- Decay power.

Important model parameters which can cause significant effect on system performance and failure of the system are:

- Frictional resistance in fuel assembly, i.e. core pressure drop;
- Heat transfer coefficient (primary side);
- Primary blower inertia.

Effects of variation of other model parameters on system performance are negligibly small, hence, they are not considered in further analysis.

Effect of process parameters on failure without consideration of modelling uncertainty

Effect of combinations of some of the above parameters on the failure of natural circulation is discussed below.

Figure 100 shows an example of the effects of increase of residual power and initial operating power from their nominal values on system behaviour while the system operates at nominal pressure of 6.98 MPa. It can be observed that the gas temperature exceeds the failure criteria limits even though the clad surface temperature and DHR structural temperatures have large margins to failure.

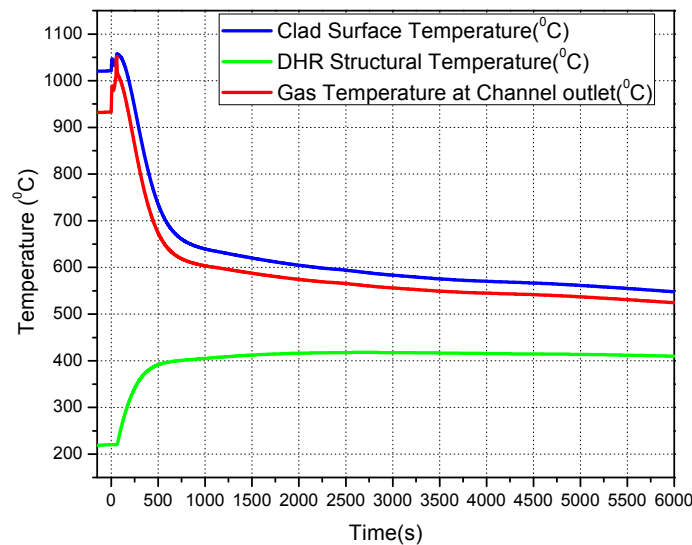


FIG. 100. Performance behaviour of DHR — at varied residual power and initial power (without model uncertainty).

Figure 101 shows an example of the effect of decrease of main circuit pressure together with increase of nominal operating power on system behaviour. In this case, the gas temperature at hot channel outlet also exceeds the failure limit. Such failure cases are summarized in Table 52.

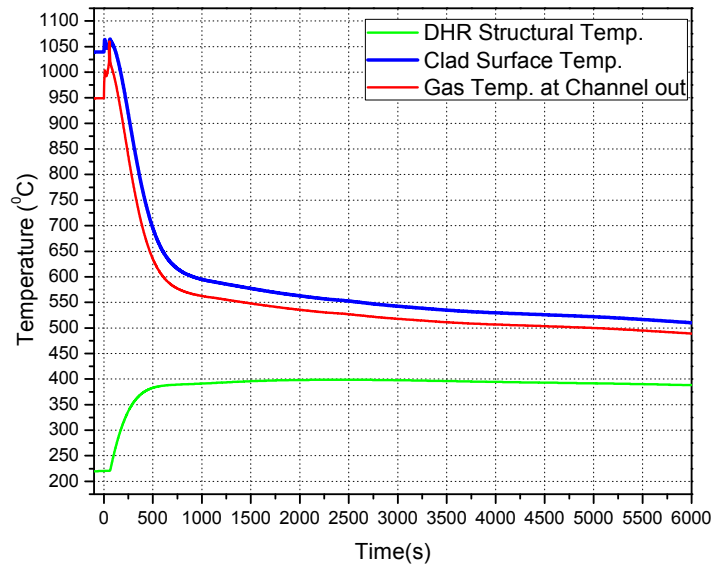


FIG. 101. Performance behaviour of DH — pressure decreased, nominal residual power and initial power increased (Without model uncertainty).

TABLE 52. FAILURE THRESHOLD POINTS WITH VARIATION OF PROCESS PARAMETERS ALONE

Parameters/Cases	Normalized Pressure	Normalized Residual Power	Normalized Power
1	0.98	1.1	1.0
2	0.98	1.0	1.01
6	0.98	0.9	1.02
4	0.99	1.1	1.012
9	0.99	0.99	1.02
5	1.0	1.1	1.015
3	1.01433	1.1	1.01
8	1.01433	1.05	1.02
7	1.02	1.1	1.02

Effect of model uncertainty on failure

Figure 102 shows an example of the effect of the variation of operating power which is decreased by 2% and residual power which is decreased by 10% keeping the system pressure at nominal value. The system in this case is found to be safe. However, when model uncertainty is applied to this case, the system is found to fail as shown in Fig. 103. The model uncertainty is treated by considering the worst combination of all model parameters in this case (i.e. core pressure drop increased by 15 %, DHR primary side heat transfer coefficient reduced by 15 % and Blower inertia reduced by 25 %). This exercise further implies that the PDHRS is likely to fail even at nominal conditions with considerations of the worst combination of model uncertainty.

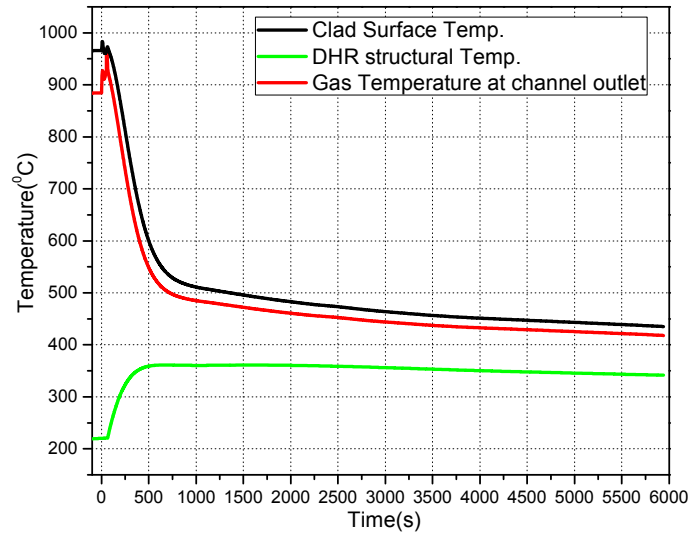


FIG. 102. Performance behaviour of DHR — nominal pressure, residual power and initial power decreased (without model uncertainty).

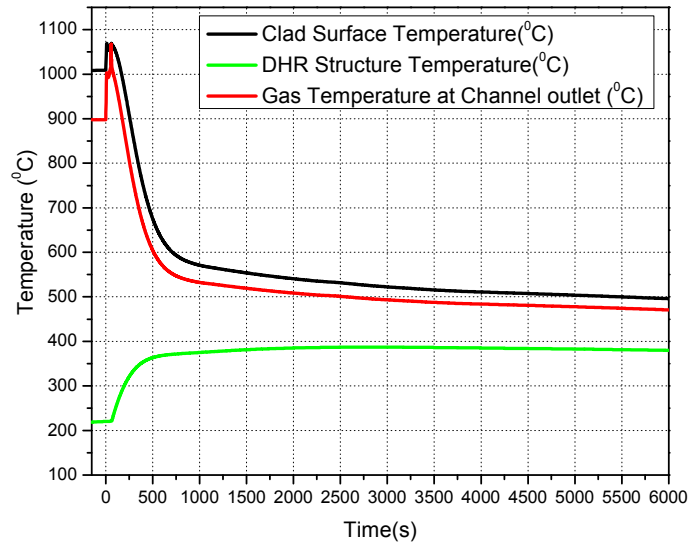


FIG. 103. Performance behaviour of DHR — nominal pressure, residual power and initial power decreased (with model uncertainty).

Step V: Failure surface generation

The loci of all failure points, shown in Table 52, can be joined to generate the failure surface as shown in Fig. 104.

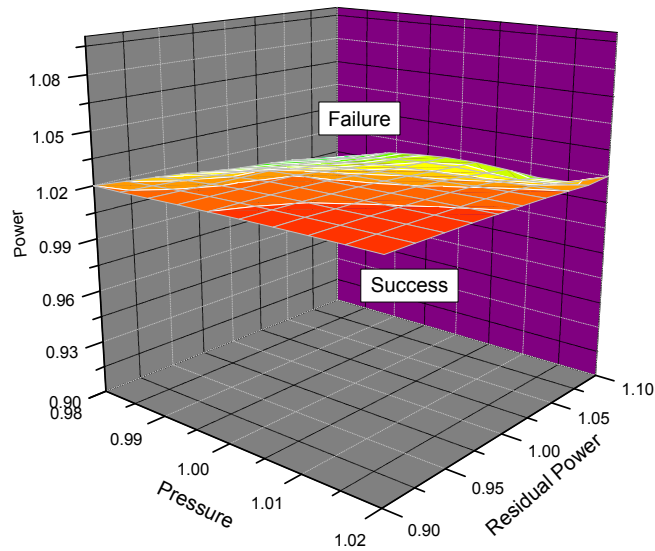


FIG. 104. Failure Surface without model uncertainty.

The failure points shown in Fig. 104 are strongly affected by treating variation of model parameters over the process parameter variations. The model parameters were varied over their ranges with a uniform distribution assumption as shown in Table 53. The failure surface with consideration of model parameter variation is shown in Fig. 105.

TABLE 53. VARIATION OF MODEL PARAMETERS AND THEIR DISTRIBUTION

Parameter number	Parameter	Minimal value	Maximal value	Distribution
1	Core total pressure drop	-0.15	0.15	Uniform
2	Helium clad heat transfer coefficient	-0.25	0.25	Uniform
3	Primary blower inertia	-0.25	0.25	Uniform

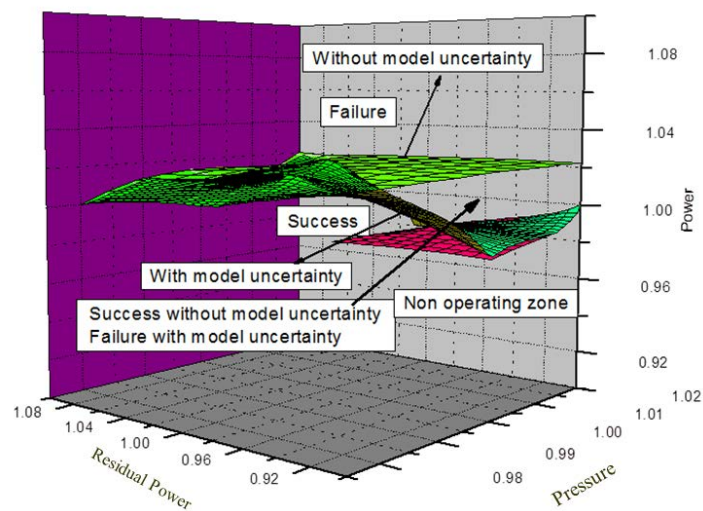


FIG. 105. Failure surface with and without model uncertainty.

Step VI: Root Diagnosis

The root causes for the variation of the process parameters are not known for the GFR. Hence, the causes for failure are assumed in this exercise as an example of demonstration of application of APSRA methodology and not to accurately predict its reliability. The failure probability of the PDHRS depends on the variation of the three process parameters of the main heat transport system as discussed before. Hence, the metric considered is the failure frequency of the components of the primary heat transport system to cause deviation of the parameters from their nominal values, while assessing the process parameters variation. The fault tree for deviation of process parameters is as shown in Fig. 106.

Variation of main circuit pressure is attributed to failure of pressure controller or mismatch of heat removal in IHX circuit or leakage due to failure of the valves in the circuit since actual cause for the GFR is not known.

Variation of nominal power and residual power is attributed to malfunction of neutron flux monitoring system or reactor regulation system. However, it may be noted that variation of nominal power and residual power is also attributable to composition of fuel and burn up at the time of SBO, which is not considered here due to lack of information.

Step VII: Evaluation of failure probability of components causing the failure

The failure frequency of the system is calculated based on the generic data [23, 24] available for components governing variation of these process parameters. The failure frequency of the system for variation of different process parameters without considering model uncertainty is shown in Fig. 107. The results show that the limiting failure frequency of the system is $7.052 \times 10^{-6}/\text{hr}$.

Treatment of model uncertainty in APSRA methodology is through comparison of model predictions with test data instead of a PDF treatment as assumed here; hence, APSRA does not consider different failure frequency of the system with model uncertainty. Since test data are not available, the model uncertainties have been treated in this analysis based on the assumption of uniform distribution as discussed earlier. Considering model uncertainties the fault trees have been redeveloped and failure frequencies have been recalculated as described below.

A typical fault tree considering the model uncertainty (DHR primary side heat transfer coefficient, pressure drop and blower inertia in primary circuit) along with variation of process parameters is shown in Fig. 108. As observed in the Fig. 108, the system can fail if the model parameters vary from their nominal values either with variation of process parameters or in absence of that. Figure 109 shows the failure frequencies with consideration of variation of model parameters. The limiting failure frequency is found to be $7.3 \times 10^{-6}/\text{hr}$.

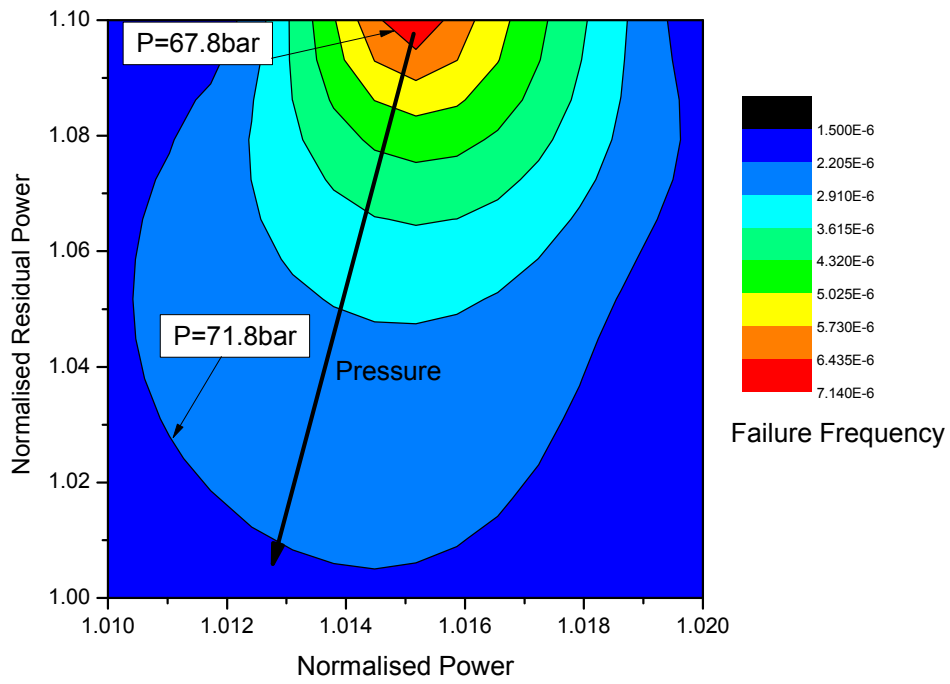


FIG. 107. Failure frequency without model uncertainty.

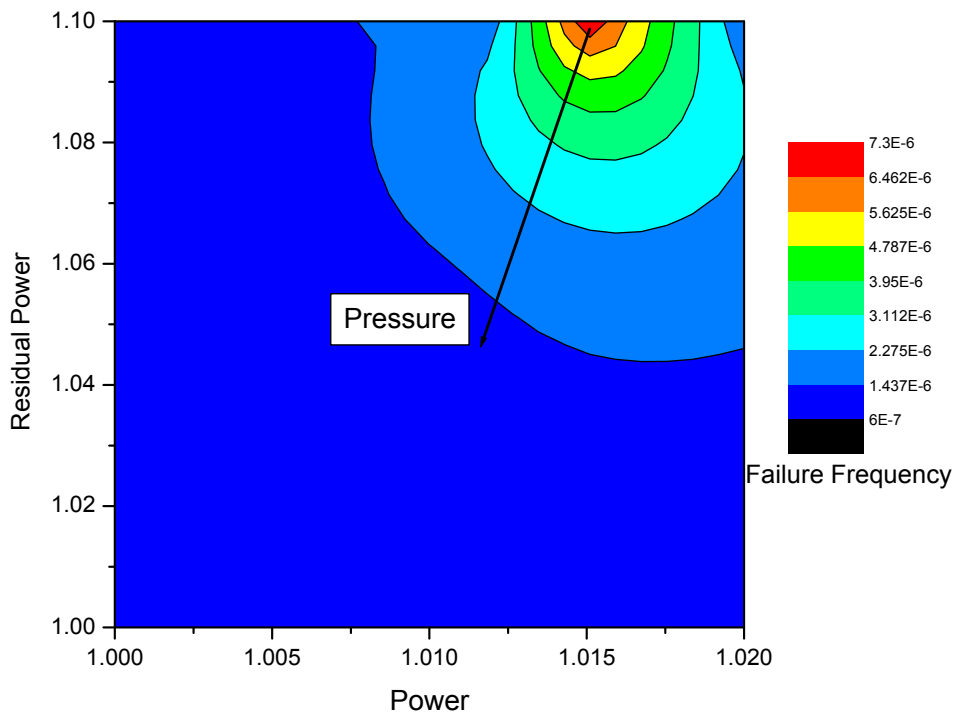


FIG. 108. Failure frequency with consideration of model uncertainty.

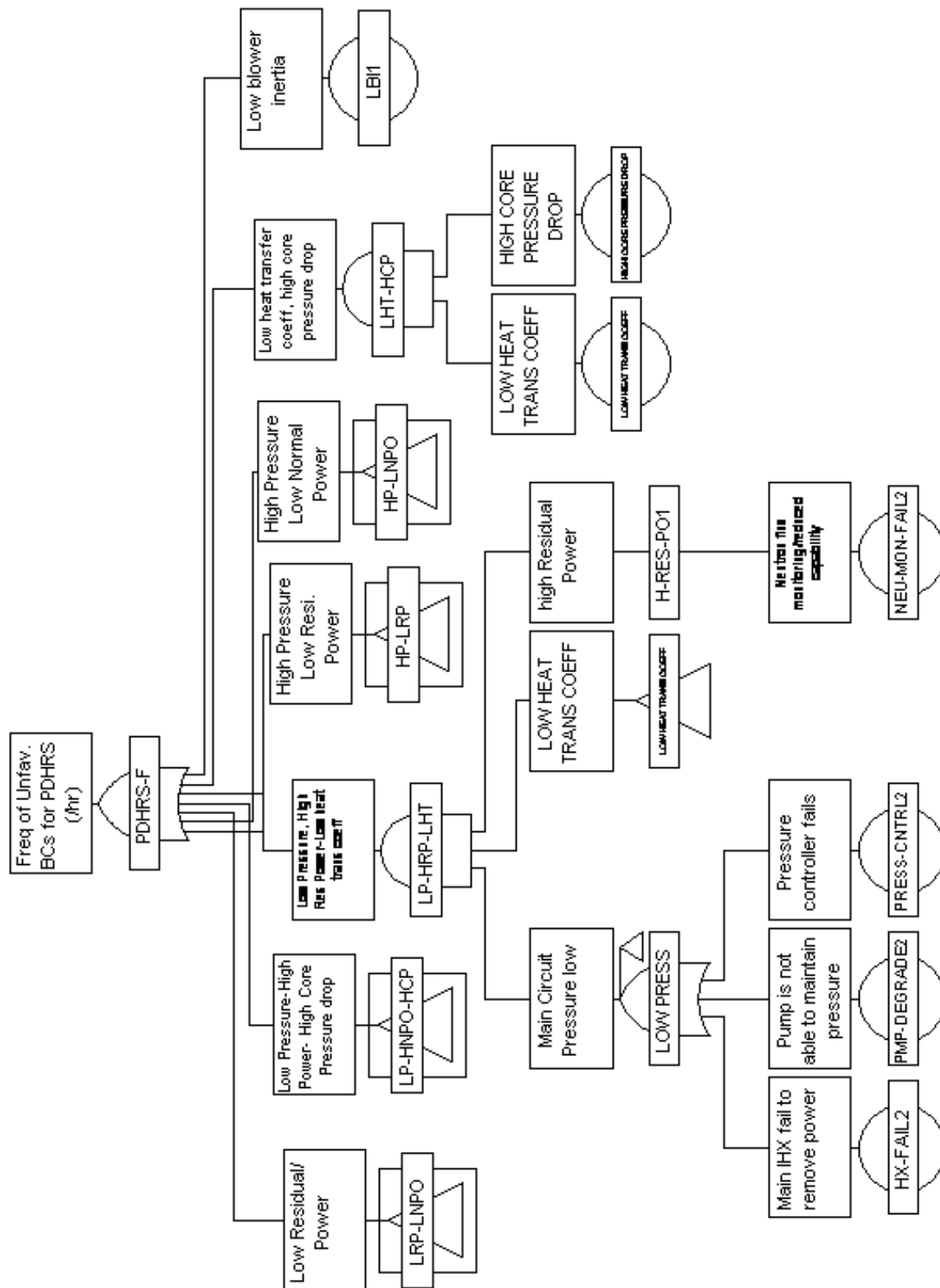


FIG. 109. Typical fault tree considering deviation of process parameters along with model uncertainty.

Conclusion

Evaluation of passive system reliability is a challenging task. It involves a clear understanding of the operation and failure mechanism of the system, which the designer must identify prior to prediction of its reliability. Besides, applicability of the so called 'best estimate codes' to the reliability of passive systems are neither proven nor understood enough due to lack of sufficient plant/experimental data. That also creates another problem in assessing the uncertainties of the best estimate codes when applied to passive system safety analysis.

The failure frequency of PDHR system in the GFR has been calculated and found to be $7.052 \times 10^{-6}/\text{h}$ by considering variation of process parameters only. With considerations of model uncertainty (all model parameters varied to their worst combination) the system is found to fail at nominal operating conditions.

The failure frequency of the PDHRS system is found to be $7.3 \times 10^{-6}/\text{h}$ by considering the model uncertainty. The result shows that contribution of model uncertainty is negligible (around 4%).

II.3. SCK-CEN, BELGIUM.

II.3.1. Reliability calculation

The input uncertainties are propagated through the T-H code RELAP5 mod3.2 in order to evaluate the uncertainty on the response of interest and assess the reliability of the DHR system. 100 samples of the input parameters have been simulated and for each, a T-H calculation has been performed using RELAP5 code.

The parameters used in reliability analysis, together with their variations and distributions, are summarized in Table 22 (see Appendix I).

Considering the failure criteria specified in Table 21 (Appendix I), the following five output parameters have been analyzed in the reliability analysis after the complete run of 100 samples of input parameters:

- (1) Upper plenum pressure;
- (2) He core outlet temperature;
- (3) Maximum fuel temperature;
- (4) Maximum clad temperature;
- (5) Maximum temperature of DHR structural material.

The procedure used for the reliability analysis is based on the SUSANA software.

II.3.1.1. SUSANA software

The SUSANA (Software for uncertainty and sensitivity analysis) program has been developed by the Gesellschaft fuer Anlagen- und Reaktorsicherheit mbH (GRS) [25]. This tool can be used to evaluate the influence of parameter variations on selected output parameters, following the input error propagation approach by means of probabilistic methods. Different output will be resulted by changing the input parameters each time. By varying only one input parameter, the effect on the output can easily be determined. However, in case of several parameters, statistical methods need to be applied in order to identify their effect on the output parameters. Such measures are implemented inside SUSANA tool.

Once the user has defined the statistical fidelity in terms of probability content (α) and confidence level (β), Wilks formula is used to evaluate the number of runs (n). Wilks formula is independent of the number of uncertain parameters, as given by the following equations for the one-sided and the two-sided tolerance limit respectively:

$$1 - \alpha^n = \beta$$

$$1 - \alpha^n - n \cdot (1 - \alpha) \cdot \alpha^{n-1} \geq \beta$$

SUSA has different measures to evaluate the sensitivity of input parameters changes on the selected output parameter. These measures are: Pearson's product-momentum coefficient, Blomquist's medial correlation coefficient, Kendall's rank correlation coefficient and Spearman's rank correlation coefficient. These four coefficients can be expressed in their ordinary form as well as partial correlation coefficient (PCC) and standard regression coefficient (SRC). Only Pearson's product-momentum coefficient is described here.

The ordinary Pearson product-momentum coefficient gives a linear relation between an input (x) and an output (y) variable and it is one of the most widely used sensitivity measure in science and engineering. The coefficient is calculated by the covariance of two variables (x and y) divided by the product of the standard deviation of the two variables. The equation to determine the coefficient is given by:

$$c_i = \frac{\sum_{n=1}^n (x_{in} - m_i) \cdot (y_n - m_j)}{\left[\sum_{n=1}^n (x_{in} - m_i)^2 \cdot \sum_{n=1}^n (y_n - m_j)^2 \right]^{1/2}}$$

Besides the ordinary coefficient, a PCC can also be calculated. The PCC between two variables (x and y) is the correlation between the two least square residuals of the two variables. These residuals have been calculated via linear regression. Since the output variable (y) is determined by more than one input parameters, the partial correlation evaluates the dependence between variables, which are not accounted for.

$$c_{ij} = \frac{c_i}{[c_{ii} \cdot c_{jj}]^{1/2}}$$

where

$$c_{ii} = \frac{\sum_{n=1}^n (x_{in} - m_i) \cdot (x_{in} - m_i)}{\left[\sum_{n=1}^n (x_{in} - m_i)^2 \cdot \sum_{n=1}^n (x_{in} - m_i)^2 \right]^{1/2}}, \quad c_{jj} = \frac{\sum_{n=1}^n (y_n - m_j) \cdot (y_n - m_j)}{\left[\sum_{n=1}^n (y_n - m_j)^2 \cdot \sum_{n=1}^n (y_n - m_j)^2 \right]^{1/2}}$$

A third measure is the standardized regression coefficient (SRC). For details on SRC, see section II.1.1.3.

II.3.1.2. Response of interest analysis

Uncertainty analysis

After the complete run of 100 samples of input parameters, the five output parameters have been analyzed in the reliability analysis.

In order to evaluate the uncertainty on the response of interest, the input uncertainties are propagated through T-H code RELAP5. 100 samples of input parameters have been simulated and for each, a T-H calculation has been performed. Figures 110 to 114 show the maximum, minimum, median, mean and the reference value of each response of interest with time.

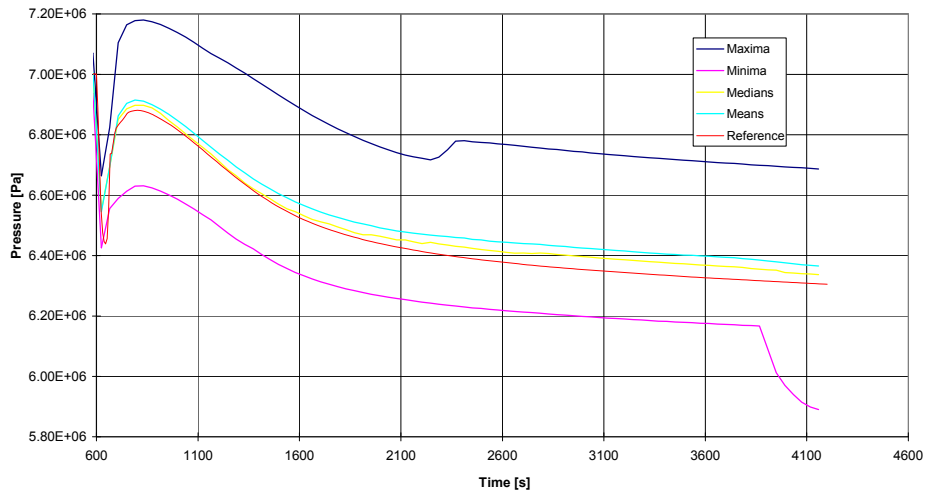


FIG. 110. Upper plenum pressure.

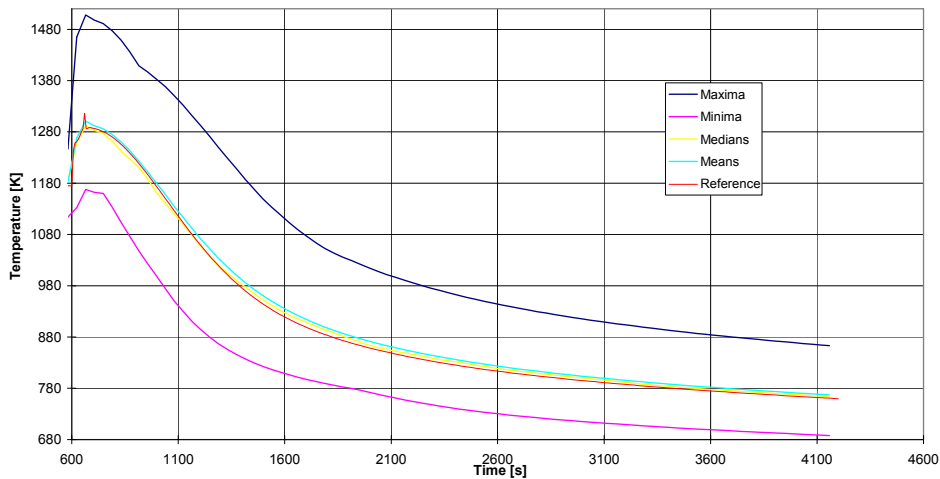


FIG. 111. Helium core exit temperature.

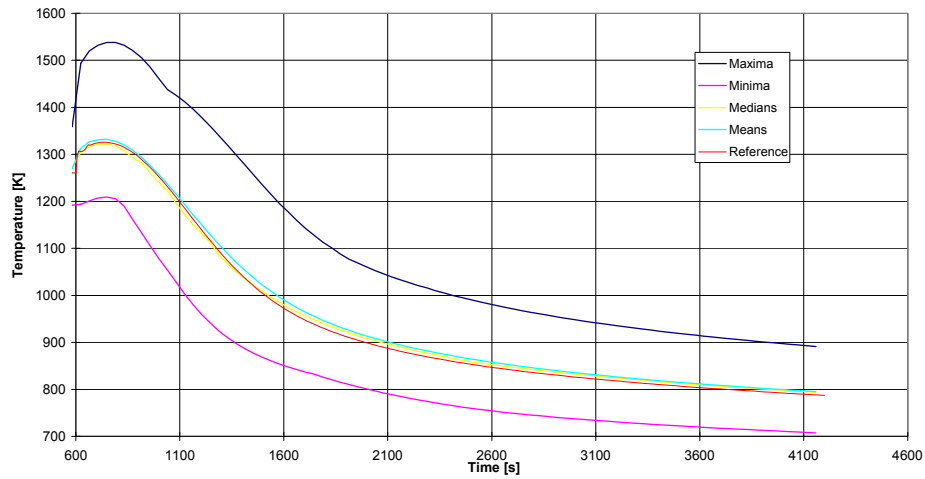


FIG. 112. Maximum clad temperature.

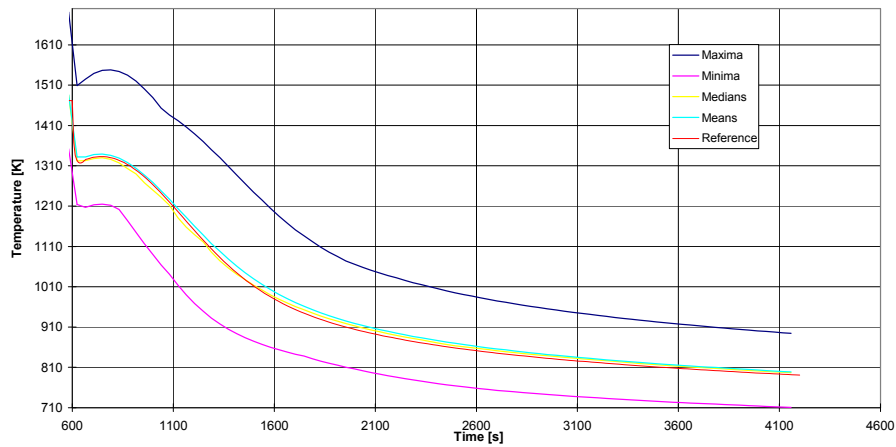


FIG. 113. Maximum fuel temperature.

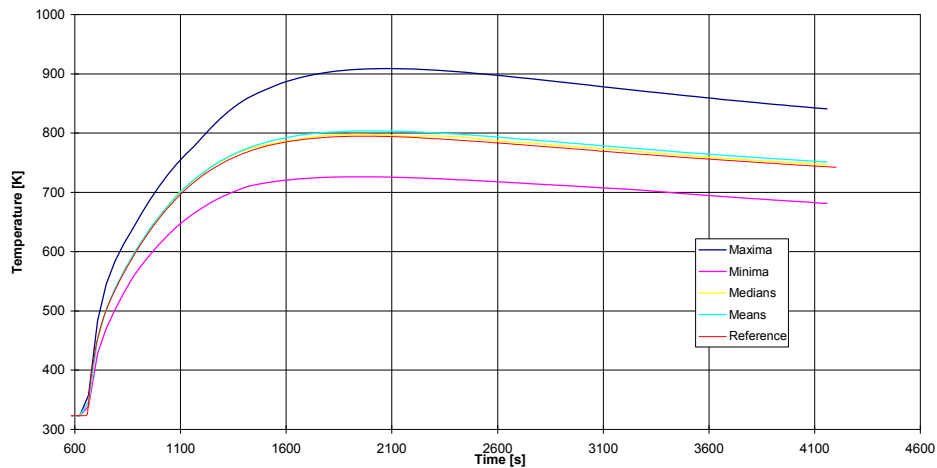


FIG. 114. Maximum temperature of DHR structural material.

For both steady state and transient conditions, the maximum, minimum and the reference value of each parameter is summarized in Table 54 and Table 55 respectively. All results have been evaluated with a quantile of $X_{95\%}$:

TABLE 54. UNCERTAINTY BOUNDARY VALUES IN STEADY STATE

Parameter	Unit	Maximum value	Minimum value	Reference value
Upper plenum pressure	MPa	7.07	6.94	6.98
He core exit temperature	K	1247	1114	1173
Fuel maximum temperature	K	1691	1352	1472
Cladding maximum temperature	K	1359	1192	1260
DHR wall maximum temperature	K	323	323	323

TABLE 55. UNCERTAINTY BOUNDARY VALUES IN TRANSIENT

Parameter	Unit	Maximum value	Minimum value	Reference value
Upper plenum pressure	MPa	7.18	6.63	6.88
He core exit temperature	K	1508	1168	1316
Fuel maximum temperature	K	1551	1215	1332
Cladding maximum temperature	K	1539	1214	1325
DHR wall maximum temperature	K	909	726	795

The results of the response of interest analysis for the five parameters considered are given (for transient condition only) in Fig. 115 to Fig. 119.

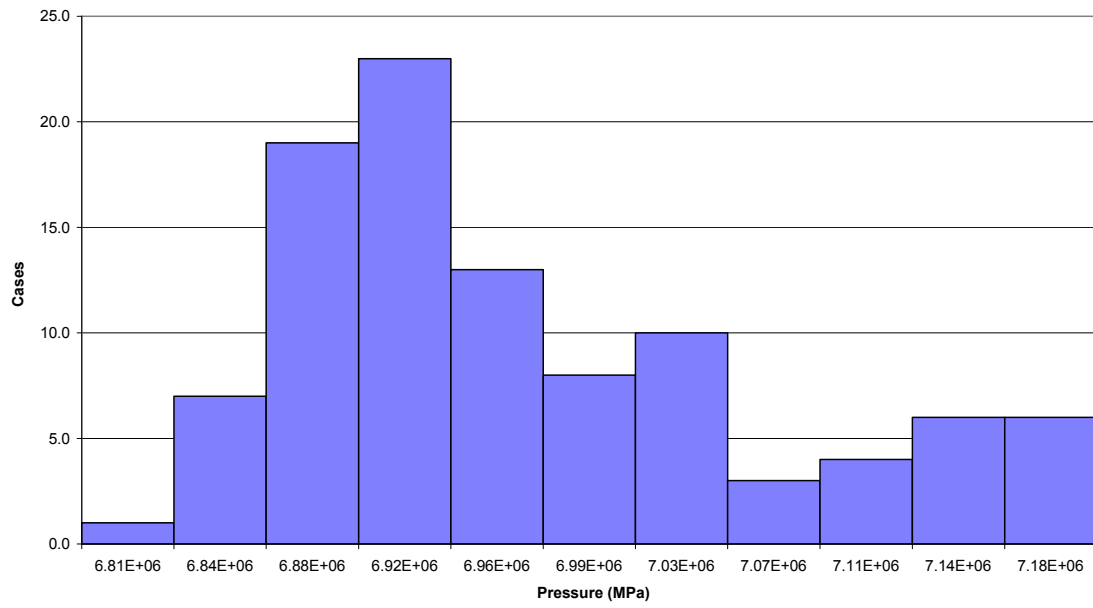


FIG. 115. Upper plenum pressure distribution.

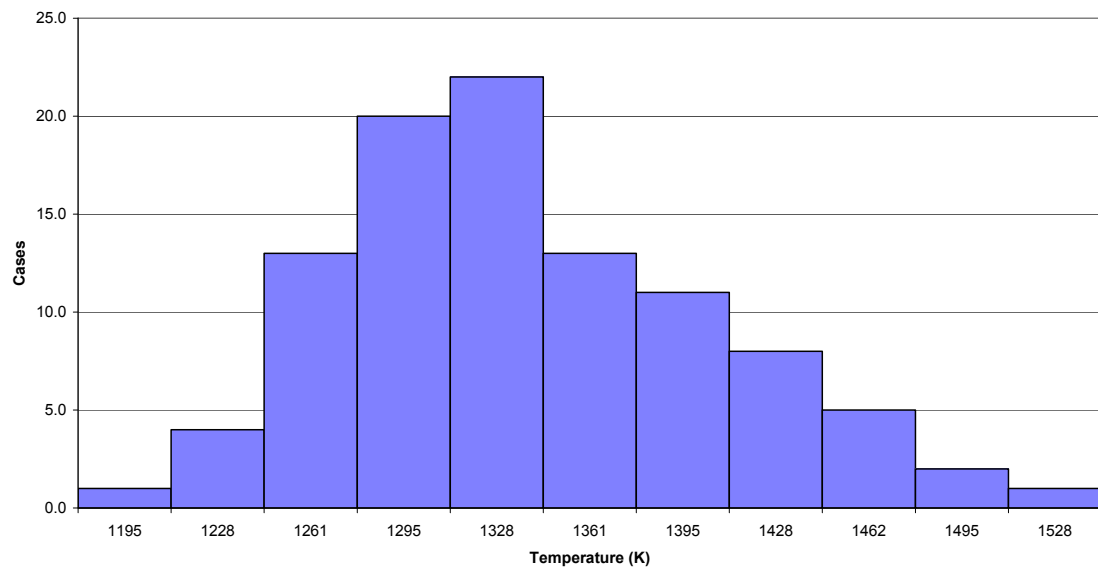


FIG. 116. Helium core exit temperature distribution.

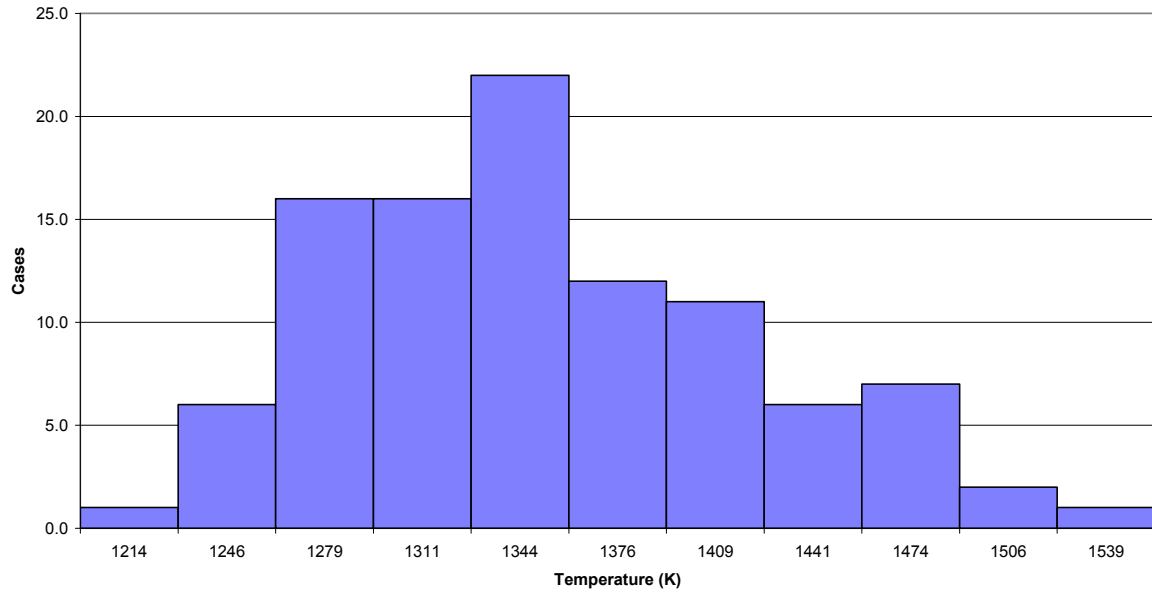


FIG. 117. Maximum clad temperature distribution.

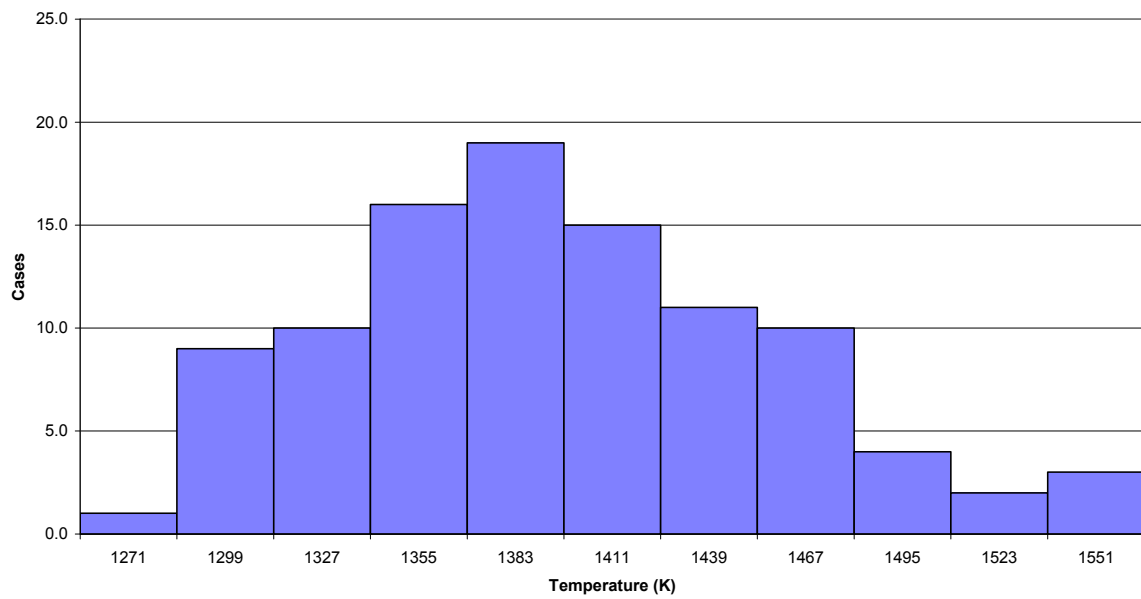


FIG. 118. Maximum fuel temperature distribution.

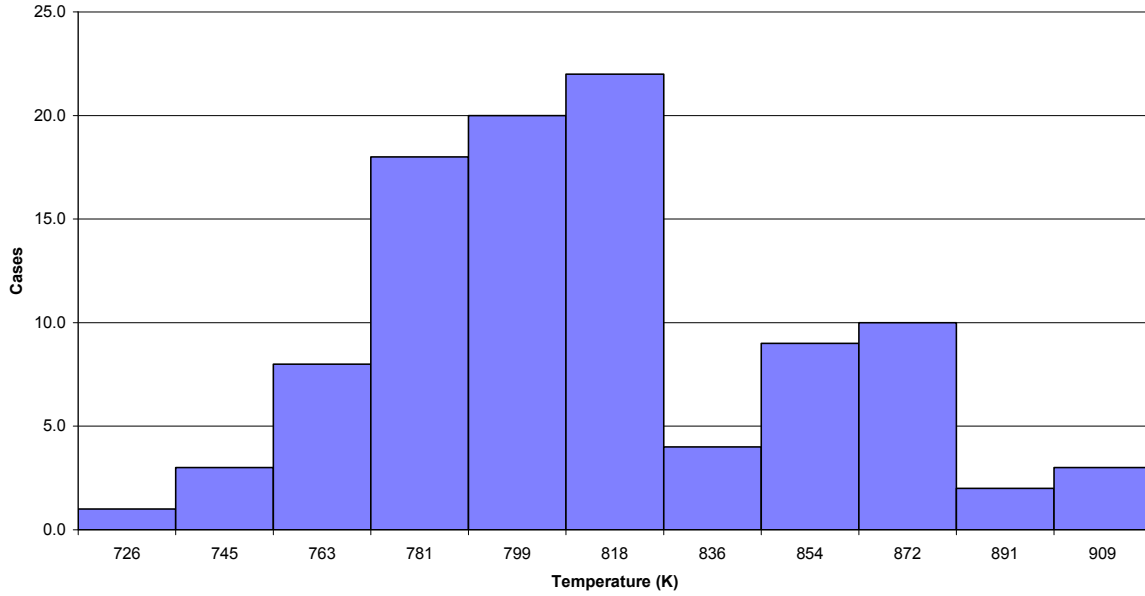


FIG. 119. Maximum DHR structural material temperature distribution.

The distributions of the output parameters are globally normal, with some deviations due to the relatively small number of runs considered (100). From the results of statistical analysis, a difference of about 30 °C between the reference values and the average values can be seen. In addition, all the three failure criteria are satisfied during the entire duration of the transient.

Helium temperature limit (for the core structures integrity), though respected, is very close to the maximum value obtained by the statistical analysis (the margin is only 15 °C). However, refining the statistical analysis by using different quantiles ($X_{99\%}$ or $X_{99.9\%}$) could result into higher margin.

The other two failure criteria (maximum clad temperature and maximum temperature of DHR structural material) are satisfied with a much higher margin (> 200 °C).

II.3.1.3. Global sensitivity analysis

A global sensitivity analysis has been performed in order to evaluate the impact of the different distributions input parameters considered (sensitivity coefficients) over the main output parameters directly connected with the failure criteria.

The approach is based on the use of the SRC (standardized regression coefficients) that can be obtained from the regression model, which is used to determine the coefficients of relative importance of each of the ten input parameters considered. These coefficients quantify the effect of varying each input parameter away from its nominal value by a fixed fraction of its variance. If the input parameters are independent, the sum is one, and hence, they obey variance decomposition of the response.

The influence of input parameters on the output parameters considered during the entire transient evolution (including steady state) can be seen in Fig. 120 to Fig. 124.

Uncertainty and Sensitivity Analysis
S.R.C. with respect to Ordinary Correlation
10 Parameters admitted

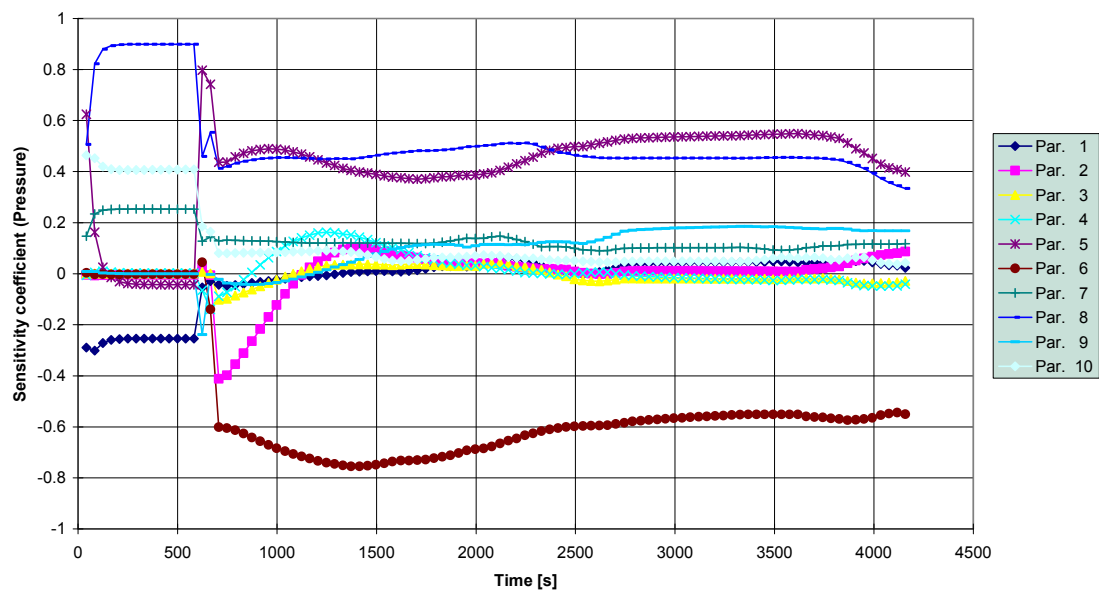


FIG. 120. Sensitivity coefficients for upper plenum pressure.

Uncertainty and Sensitivity Analysis
S.R.C. with respect to Ordinary Correlation
10 Parameters admitted

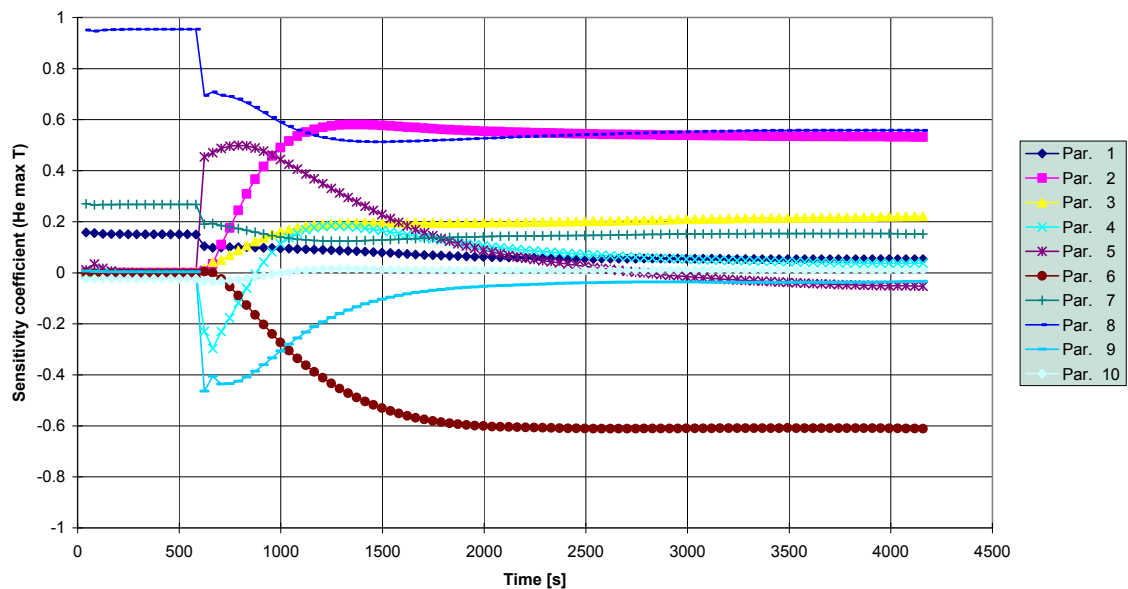


FIG. 121. Sensitivity coefficients for maximum He temperature.

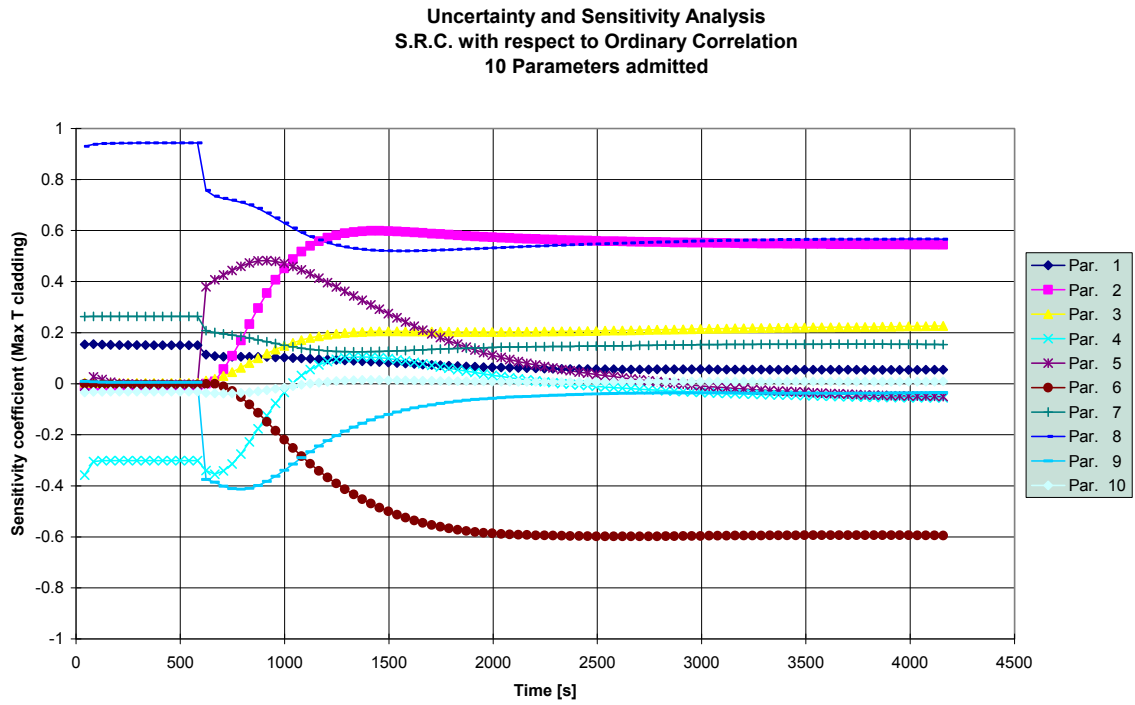


FIG. 122. Sensitivity coefficients for maximum clad temperature.

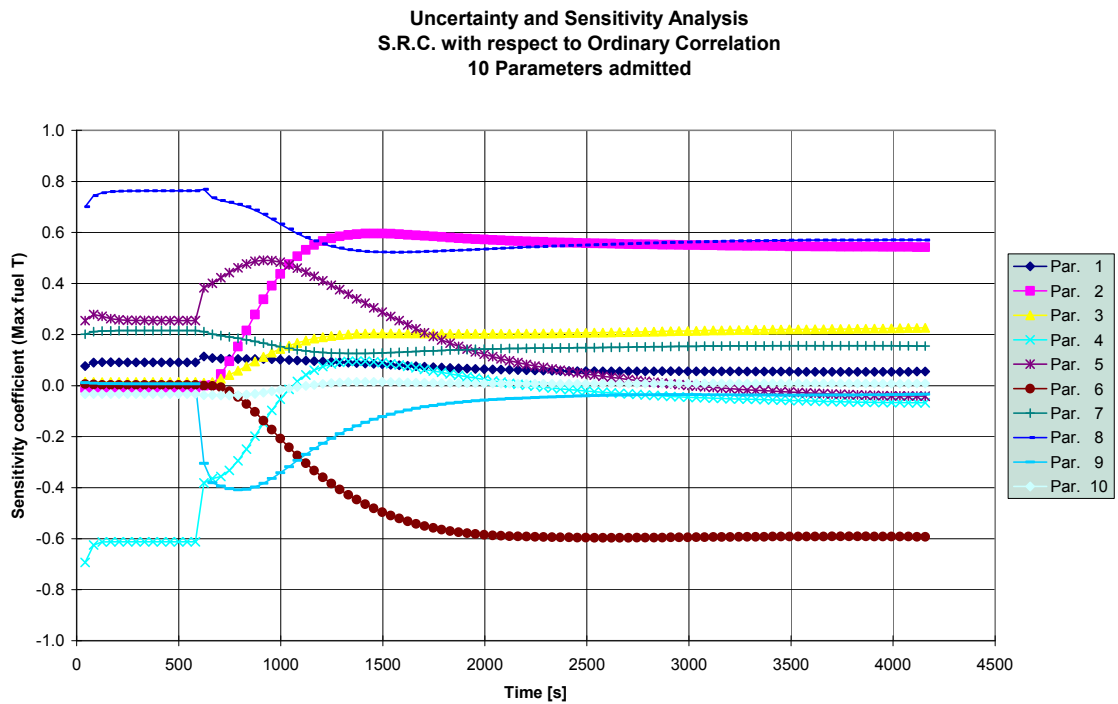


FIG. 123. Sensitivity coefficients for maximum fuel temperature.

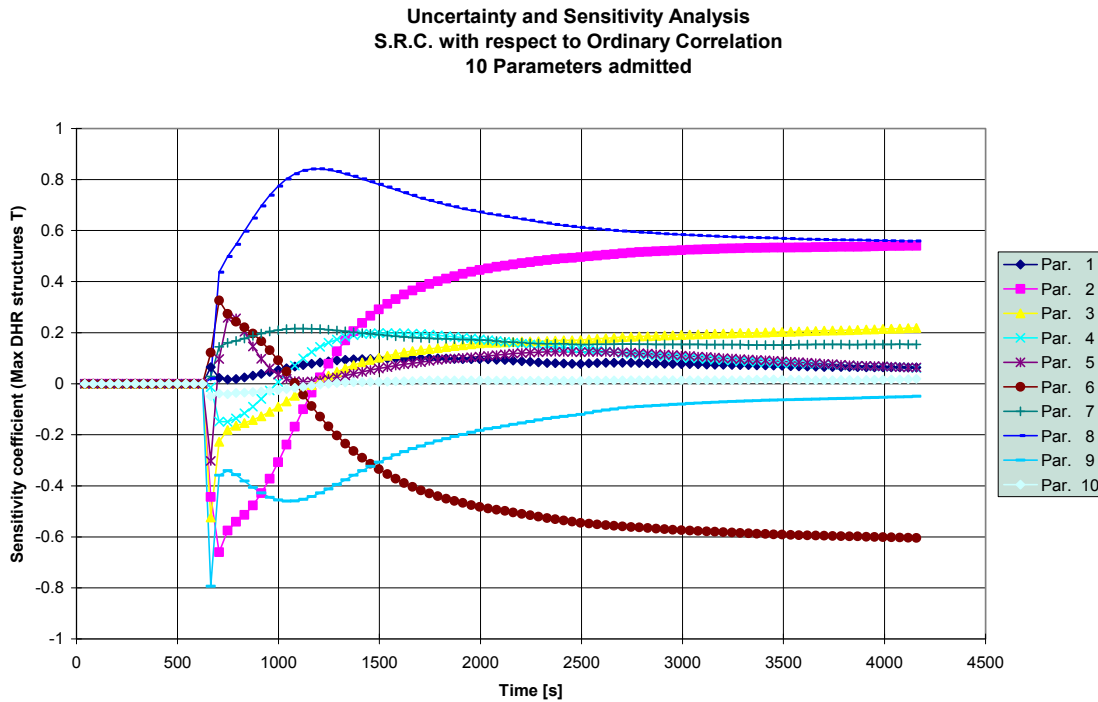


FIG. 124. Sensitivity coefficients for maximum temperature of DHR structural material

For the upper plenum pressure, it appears that the most influencing parameters are:

- Variation of HTC (heat transfer coefficient) in primary DHR HX;
- Increase of thermal inertia in all system structures;
- Variation of fuel decay heat curve;
- Inlet pressure drop K-factor in DHR primary loop.

It appears that the system pressure is influenced by the input variations that have a long term impact on heat deposition in the primary He. The worsening of the HTC in primary DHR HX causes the primary heat to be removed more slowly and the increased thermal inertia causes the heat to be released more slowly from the structures, hence, keeping the system pressure higher for longer time. Having a higher decay heat rate contributes in storing more power into the primary coolant, thus increasing system pressure. The DHR inlet pressure drop coefficient is important in the very beginning of the transient only.

For the He temperature at the core exit, the most influencing parameters are:

- Inlet K-factor in DHR primary loop;
- Variation of HTC in primary DHR HX;
- Variation of fuel decay heat curve;
- Primary blower inertia;
- Increase of thermal inertia in all system structures.

The increase of pressure loss K factor at the inlet of DHR primary loop causes the primary mass flow rate to decrease and the He temperature to increase accordingly. The worsening of HTC in the primary DHR HX slows down the power transfer between the two DHR loops, hence, raises the He temperature. The increase of fuel decay power also raises the He temperature at the core exit. The decrease of primary blower inertia, with the consequent

decrease of the blower run down time, has a strong influence in the first part of the transient. However, after about 1000 seconds, its effect has disappeared. Increase of thermal inertia of all system structures raises the He temperature in the primary system in the first part of the transient evolution.

For maximum clad and fuel temperature, the most influencing parameters are the same as for the He temperature at the core exit. Since He temperature is maximum at the exit of the hot channel, this area is also expected to have highest transient clad and fuel temperatures. The phenomenon behind the evolution of these three temperature values are the same, hence, the same influencing parameters.

The maximum temperature of DHR structural material is mostly influenced by:

- Variation of fuel decay heat curve;
- Variation of HTC in primary DHR HX;
- Inlet K-factor in DHR primary loop;
- Primary blower inertia;
- Outlet K-factor in DHR primary loop.

The decay heat curve has a major impact on the maximum temperature of DHR structural material. The reduction of primary DHR HTC (which means more power in the primary system) and the increase of DHR inlet pressure loss K-factor lead to increase in DHR walls temperatures. The first three parameters have a major influence over the entire transient duration. The primary blower inertia and the DHR outlet pressure loss K-factor mainly influence in the first 100 seconds of the transient evolution, when the blower is still not completely stopped and the DHR valves are just opened.

Conclusion

The deterministic calculations are performed with the T-H code RELAP5 mod 3.2. The results of the deterministic calculations show that all the failure criteria are respected with the values staying well below the safety limits.

The reliability analysis is performed with SUSA software and input uncertainties are propagated through the T-H code RELAP5. 100 samples of the input parameters have been simulated and for each, a T-H calculation has been performed using RELAP5 code. The DHR system has demonstrated very high degree of reliability in both cases i.e. steady state and transient. The output parameters evaluated with a quantile of $X_{95\%}$ satisfy the LOFA failure criteria.

The helium temperature limit (for the core structures integrity), though respected, is very close to the maximum value obtained by the statistical analysis (the margin is only 15 °C). However, refining the statistical analysis by using different quantiles ($X_{99\%}$ or $X_{99.9\%}$) could result into higher margin. The other two failure criteria (maximum clad temperature and maximum temperature of DHR structural material) are satisfied with a much higher margin (> 200 °C).

The distributions of the output parameters are globally normal, with some deviations due to the relatively small number of runs considered (100). From the results of statistical analysis, a difference of about 30 °C between the reference values and the average values can be seen. In addition, all the three failure criteria are satisfied during the entire duration of the transient.

The results of global sensitivity analysis results show the impact of the different distributions of input parameter considered (sensitivity coefficients) over the main output parameters (directly connected with the failure criteria). It is observed that there are several parameters which have a strong impact on all the safety related temperatures, while other parameters show a relatively weak influence on the variations.

One of the most influencing parameter is the inlet pressure drop factor in the DHR loop that represents the DHR stopped blower. This parameter has a direct impact on the natural circulation mass flow rate and also has a big influence on DHR structures.

Another important parameter is the heat transfer coefficient in the primary–secondary DHR heat exchanger. After 1000s, it influences all the considered output parameters.

The variation of fuel decay heat power curve also plays a very important role, especially for the DHR structural material temperatures where its impact is most prominent.

The primary blower inertia is important in the early phase of transient (before reaching the pressure/temperature peak), but it has no effect in the later phase.

Other input parameters analyzed through the statistical evaluation proved to have relatively little impact on the transient evolution.

The DHR system working in natural circulation is a very reliable system for loss of flow accident (LOFA) as it satisfies all the failure criteria in its current design status.

APPENDIX III. TRANSIENT II RESULTS

III.1. CEA, FRANCE

The calculations have been performed with the CATHARE 2 code V2.5_2 mod 2.1.

For this transient analysis, it was necessary to model (Fig. 125):

- The 3 DHR loops even if only two are used because of the helium inventory;
- The 3 nitrogen accumulators;
- The mixing of helium and nitrogen;
- The close containment.

The **close containment** has the following characteristics:

- Geometry : 33 m diameter sphere;
- Free volume : 11620 m³;
- Wall thickness : 46mm;
- Wall exchange area : 3421 m²;
- Heat exchange with the outside:
 - $H = 15 \text{ W/m}^2/\text{K}$;
 - $T_{ext} = 20^\circ\text{C}$.
- Wall material:
 - $\lambda = 42.5 \text{ W/m/K}$;
 - $\rho = 7850 \text{ kg/m}^3$;
 - $C_p = 500 \text{ J/kg/K}$.

The close containment has been modeled in the CATHARE2 code with 2 axial modules representing a toroid square (Fig. 126).

The **accumulators** have the following characteristics:

- for each of the three accumulators:
 - ✓ Initial pressure : 75bar;
 - ✓ Initial temperature : 50°C;
 - ✓ Free volume : 540 m³;
 - ✓ Filled with Nitrogen.
- For the connecting lines:
 - ✓ Section : $\pi / 400 \text{ m}^2$;
 - ✓ Singular pressure loss : $k = 15$;
 - ✓ Length : 1m.

The nitrogen properties in the CATHARE code are:

- ✓ $C_p = 1158.46 - 0.86297.T + 0.0020562.T^2 - 1.8584.10^{-6}.T^3 + 8.5387.10^{-10}.T^4 - 1.98709.10^{-13}.T^5 + 1.86132.10^{-17}.T^6 \text{ J/kg/K}$
- ✓ $\lambda = 5.04526.10^{-3} + 0.07222.10^{-3}.T - 14.2466165.10^{-3}.T^2 \text{ W/m/K}$
- ✓ $\mu = 4.8705124.10^{-6} + 0.044382518.10^{-6}.T - 9.058270677.10^{-12}.T^2 \text{ Pa.s}$
- ✓ $M = 28 \text{ g/mol}$

The mixture (He + N2) properties are:

$$Cp_{mix} = X_{m_{He}} \times Cp_{He} + X_{m_{N2}} \times Cp_{N2}$$

Viscosity (Wilke law):

$$\mu = \sum_{i=1}^{ns} \frac{X_{m_i} \mu_i}{\sum_{j=1}^{ns} X_{m_j} \phi_{ij}}$$

Conductivity (Mason and Saxena law):

$$\lambda = \sum_{i=1}^{ns} \frac{X_{m_i} \lambda_i}{\sum_{j=1}^{ns} X_{m_j} \phi_{ij}}$$

with

$$\phi_{ij} = \frac{1}{\sqrt{8}} \left(1 + \frac{M_i}{M_j} \right)^{-1/2} \left[1 + \left(\frac{\mu_i}{\mu_j} \right)^{1/2} \left(\frac{M_j}{M_i} \right)^{1/4} \right]^2$$

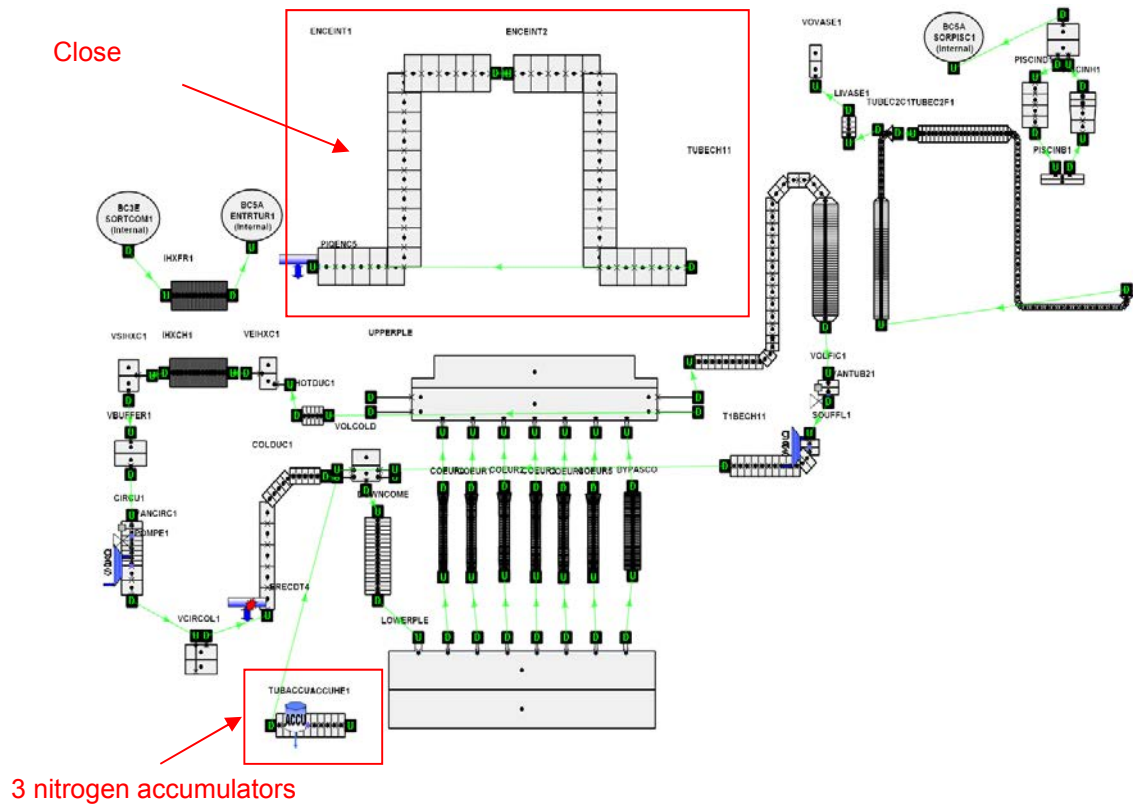


FIG. 125. Details of the CATHARE 2 model of 2400 MW(th) GFR.

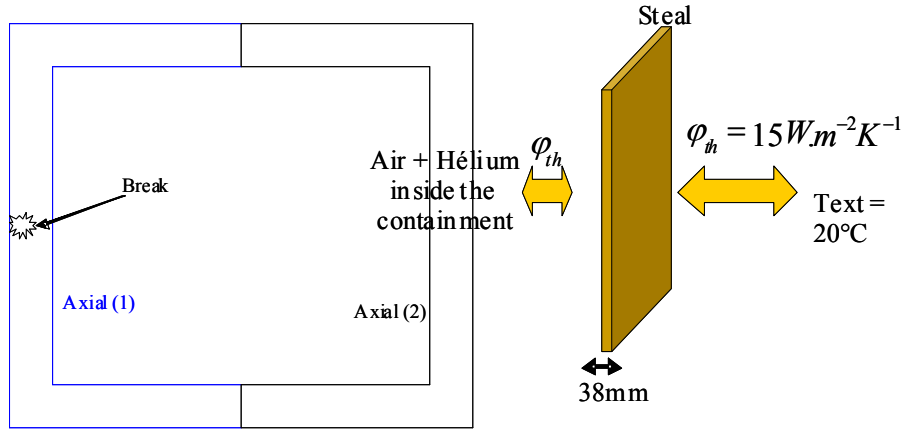


FIG. 126. Close containment modelling in CATHARE2 code.

Steady state part of this transient is common with the first transient (see Appendix I).

III.1.1. Transient results

Transient event sequence

The sequence of events for the transient and their timings with CATHARE 2 code are:

- Start of transient : 0s;
- SCRAM (containment pressure > 1.3 bars) : 9.4s;
- Start of DHR sequence (core mass flow rate below 3% of nominal value) : 45.3s;
- Valves in main loops start closing : 48.3s;
- Valves in main loop closed : 50.3s;
- Valves in DHR loop start opening : 56.3s;
- Valves in DHR loop opened : 61.3s ;
- Sequence duration for closure of valves in main loop and opening of valves in DHR : 16s;
- Accumulators injection (lower plenum pressure < 10 bars) : 554s;
- End of transient : 21600s (6 h).

Core mass flow rate

The evolution of the mass flow rate at the inlet of the core is shown in Fig. 127 (short term i.e. 0–1000s) and Fig. 128 (long term i.e. 0–20,000s). The mass flow rate decreases after the scram due to the decrease of velocity of the main blower. Three per cent of the nominal flow rate is reached at around 45s and then the closure of the main loop isolating valves starts. There is a time interval of 6s with a reverse flow rate. Then the DHR loop isolating valves open and the flow rate increases quickly up to 74 kg/s at 66s and then due to the leak at the breach, it starts to decrease slowly and is less than 5 kg/s at 400s. At 554s, the nitrogen accumulators injection start and the flow rate increases quickly up to 204 kg/s at 880s and then decreases slowly. A quasi stable flow rate is reached and practically maintained up to the end of the transient i.e. 59 kg/s at 5000s and 50kg/s at 21600s.

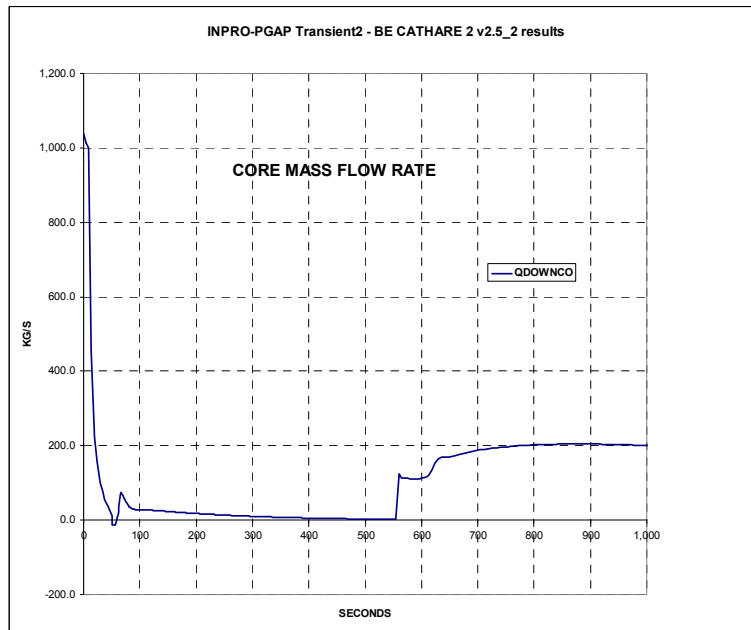


FIG. 127. Core mass flow rate at the inlet of the core (0–1000s).

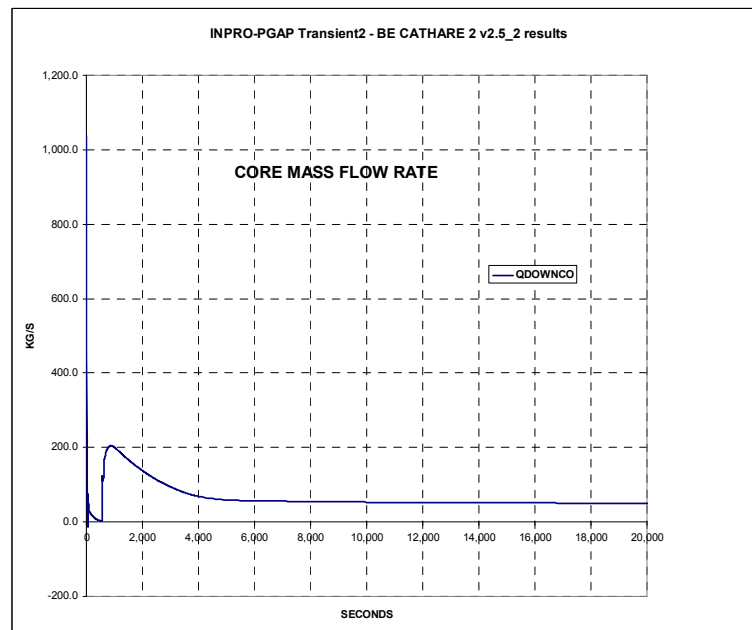


FIG. 128. Core mass flow rate at the inlet of the core (0–20 000s).

The detailed flow rates in the different zones of the core are shown for short term duration in Fig. 129 and for long term duration in Fig. 130. During the stable phases, a relatively homogeneous flow rate due to the gaggings at the inlet of the assemblies is observed which introduces singular pressure drop.

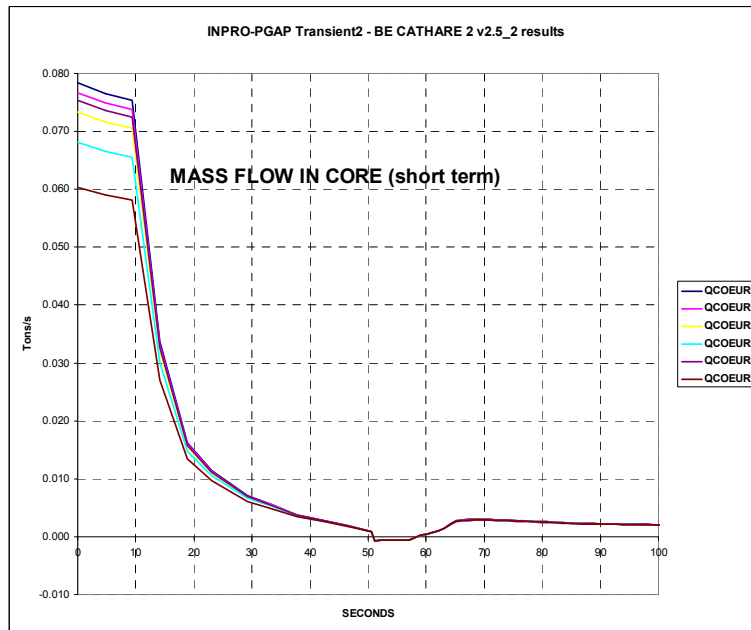


FIG. 129. 1 Mass flow rates in the various channels of the core (0–100s).

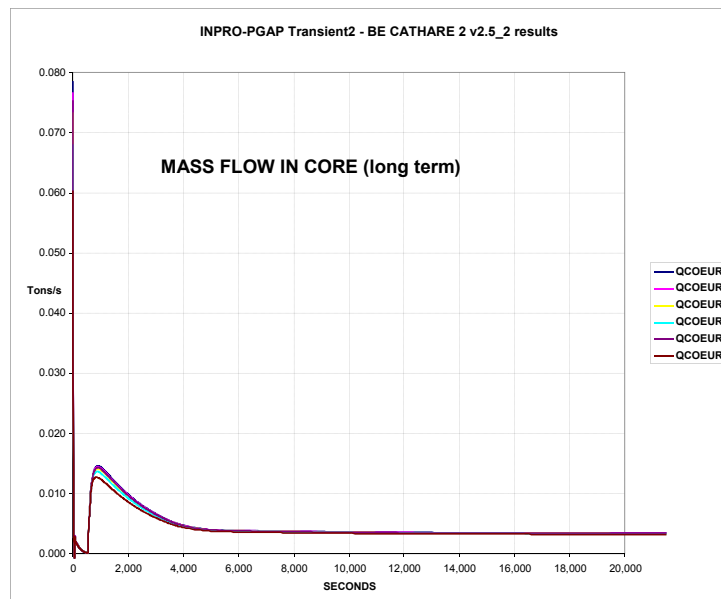


FIG. 130. Mass flow rates in the various channels of the core (0–20000s).

Fuel temperatures in central channel

The evolutions of the temperatures in the « Core 0 » at different points along the height of the assembly are shown in Fig. 131 to Fig. 132. The maximum fuel temperature (1408°C) is obtained at core exit at 636s. The fuel temperature decreases after nitrogen injection down to 517°C at 1556s and then increases again (empty nitrogen accumulators and the residual power

is still high) up to a maximum of 843°C at 6206s and decreases again slowly until the end of the transient (751°C).

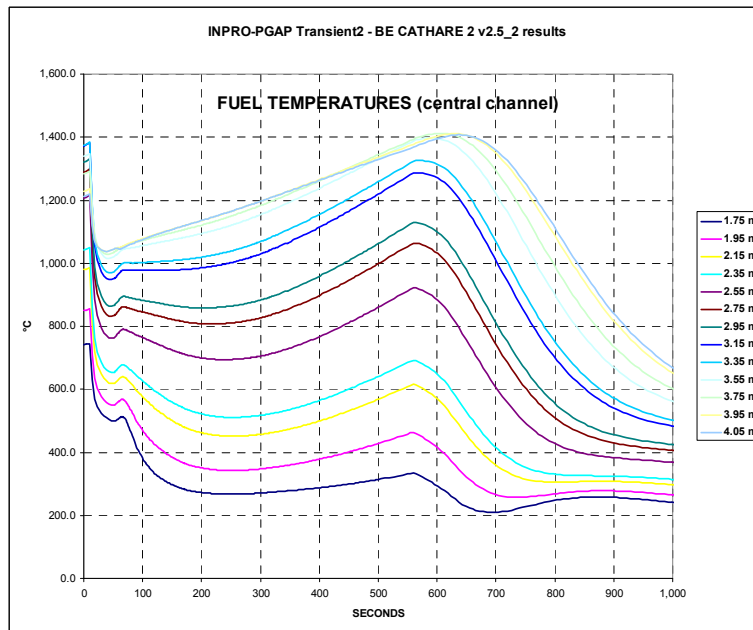


FIG. 131. Fuel temperatures in the central channel of the core (0–1000s).

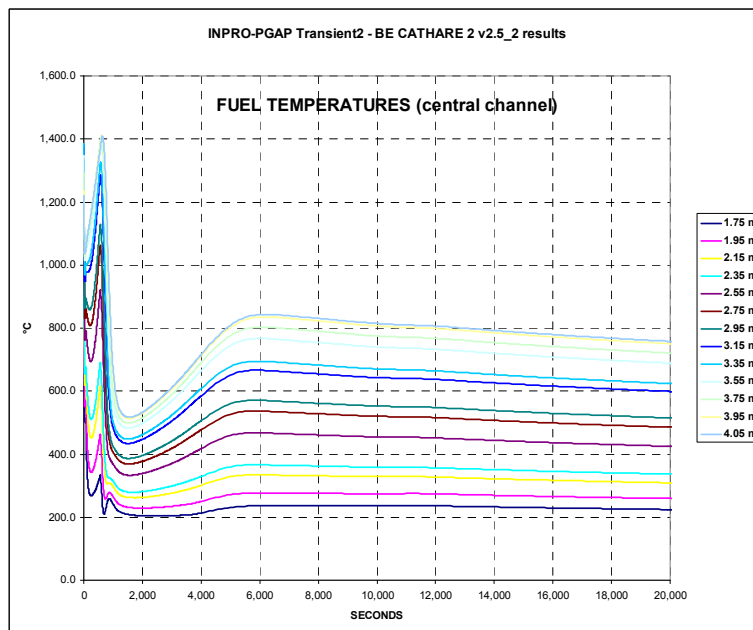


FIG. 132. Fuel temperatures in the central channel of the core (0–20000s).

Clad and gas temperatures in the central channel

We observe the same evolution for the clad temperature (Fig. 133) and for the gas temperature (Fig. 134). The first peak of clad maximum temperature is corresponding to

1404°C at 624s and the second peak after nitrogen injection is corresponding to 840°C at 6206s. They are, respectively, 196°C and 160°C below the failure criteria.

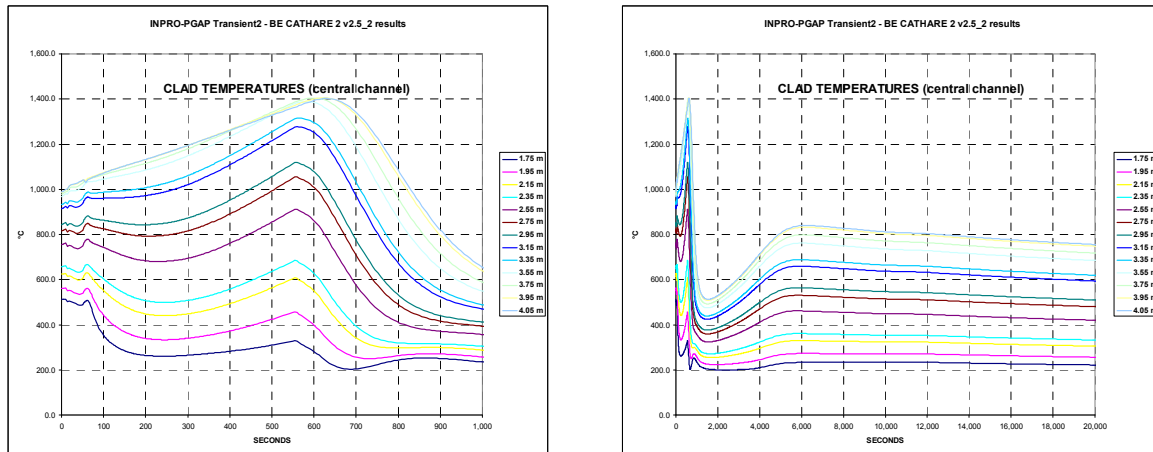


FIG. 133. Clad temperatures in the central channel of the core (Left: 0–1000 s, Right: 0–20,000s).

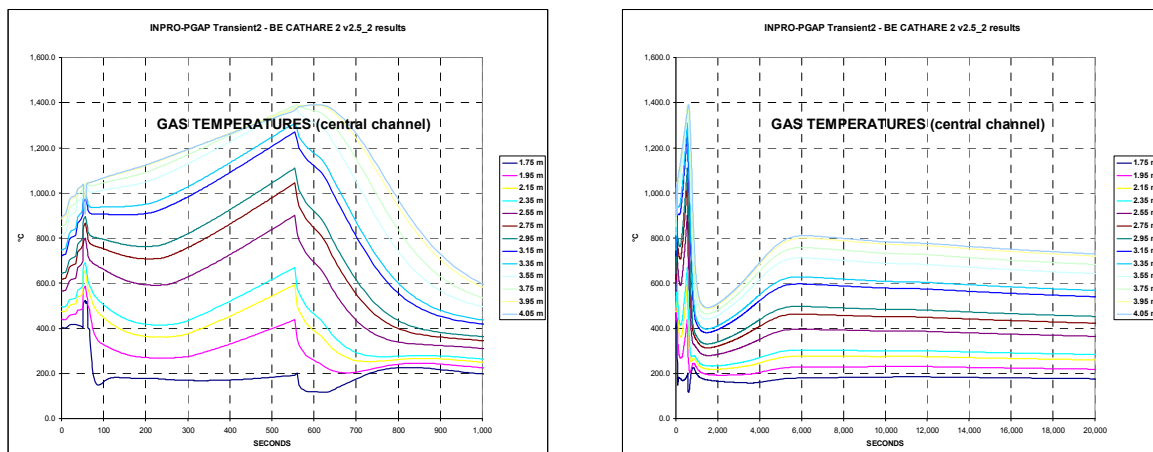


FIG. 134. Gas temperatures in the central channel of the core (Left: 0–1000 s, Right: 0–20,000s).

Gas temperatures in the upper plenum

The evolution of the gas temperature in the upper plenum is given in Fig. 135. The peak temperature is equal to 1241°C at 590s. It is only 9°C below the failure criterion.

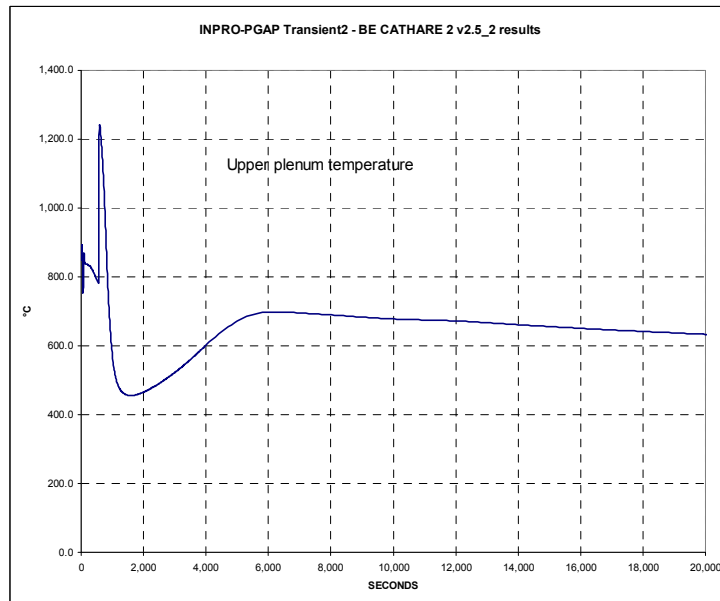


FIG. 135. Gas temperatures in the upper plenum.

Primary pressure

The evolution of the primary pressure is shown in Fig. 136. The initial pressure is 7.12 MPa at core inlet and 7 MPa at core outlet. The pressure decreases to 1 MPa (at 554s) at which point the nitrogen injection by accumulators takes place. Then the pressure increases up to 4.57 MPa at 831s and decreases again to about 1.2 MPa.

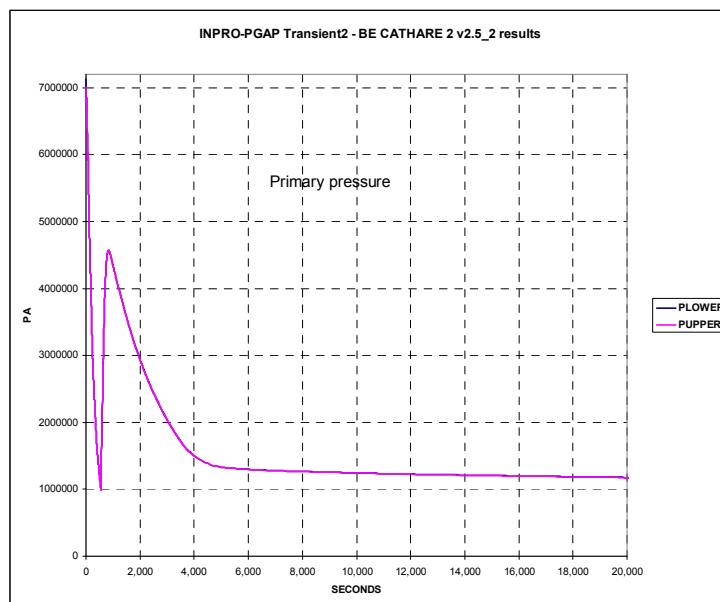


FIG. 136. Primary pressure in lower and upper plenum.

Power

The residual power curve and the power exchanged through the DHR exchangers (DHR HX1 i.e. exchanger between DHR helium loop and DHR water loop and DHR HX2 i.e. exchanger between DHR water loop and the cooling pool) are shown in Fig. 137. In the long term, the exchanged powers are identical and equal to the power exchanged in the core (not represented in the figure).

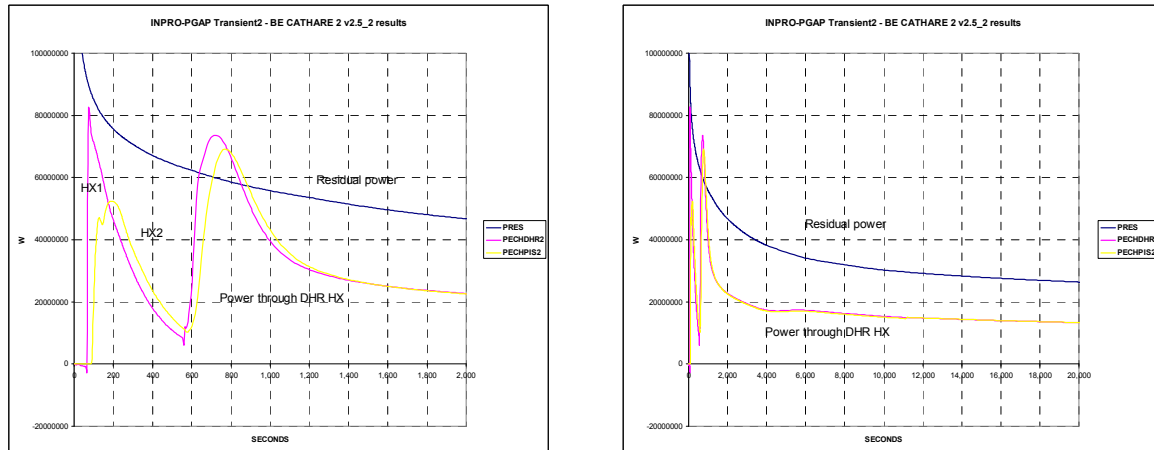


FIG. 137. Residual power and power exchanged through the DHR HXs.

DHR pressures

Figure 138 shows the pressures in the DHR loops:

- Helium loop is initially at 7 MPa and 1.2 MPa at the end of transient.
- Water pressure initially at 1 MPa and 1.6 MPa at end of transient.

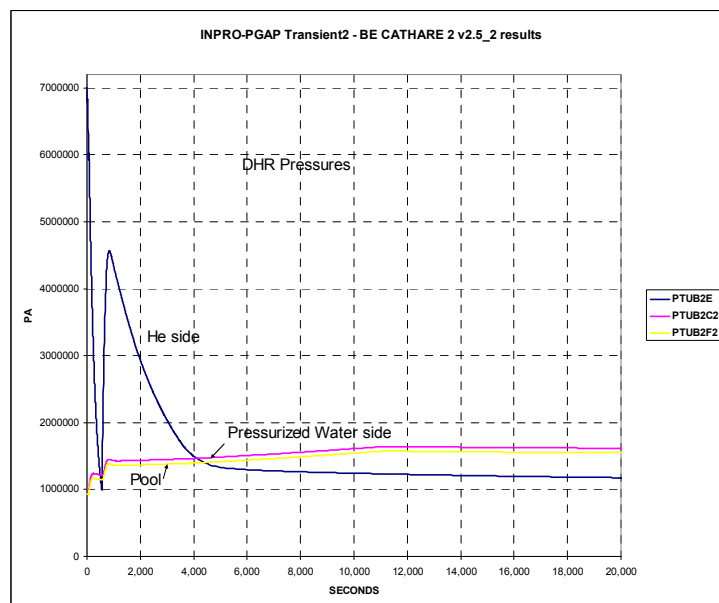


FIG. 138. DHR pressures.

DHR temperatures

The temperatures in the DHR system are shown in Fig. 139. It can be seen that:

- DHR HE side hot leg temperature is initially equal to 238°C at the beginning of the transient. A decrease in temperature due to power reductions is observed. Then a first peak corresponding to 870 °C at 85s, a second peak corresponding to 1240 °C at 595s and finally a third peak corresponding to 698 °C at 6000s can be seen.
- Temperature of the pressurized water is initially at 50°C and increases quickly. Then it goes through to two peaks, the first peak corresponding to 138°C at 110s and the second corresponding to 155° at 760s. The temperature of the pressurized water finally stabilizes at around 135°C.
- The cooling pool is also initially at 50°C. Vaporization appears around the exchanger after 8300 s.

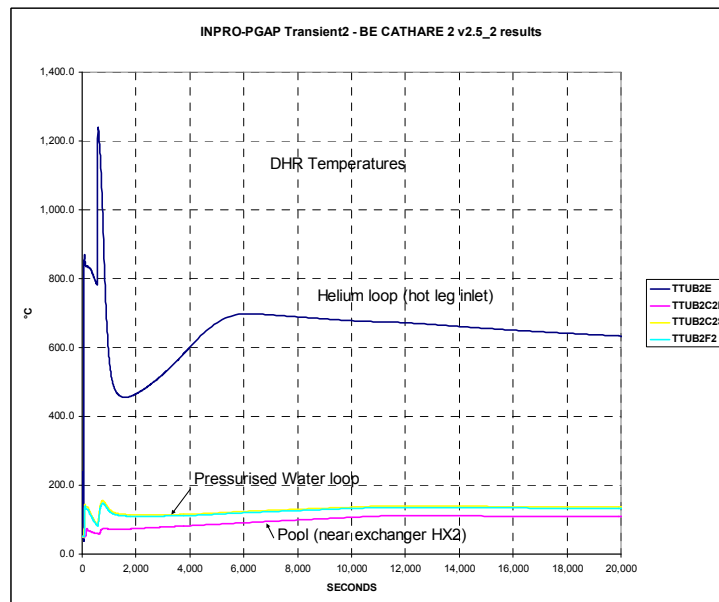


FIG. 139. Temperatures in DHR loops and pool.

Mass flow rates in DHR

The mass flow rates in DHR (for one of the two loops) are presented in Fig. 140. After nitrogen injection, the gas mass flow rate increases quickly up to 100 kg/s and then decreases slowly. This decrease is due to the decrease in pressure, which in turn is due to the decrease in temperature in the closed containment. A quasi-Stabilization of the helium flow rate at about 25 kg/s (after 5000s) and of the water flow rate at about 120 kg/s can be observed.

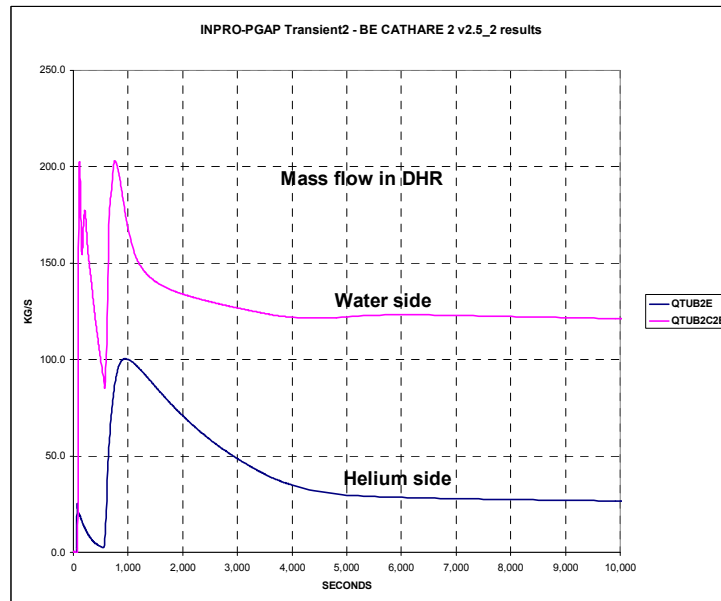


FIG. 140. Mass flow rates in DHR.

Accumulator

Pressure and flow rate of accumulator are shown in Fig. 141. Nitrogen accumulators mass flow rates are initially equal to 63.4 kg/s and decrease to less than 0.1 kg/s at 7100s.

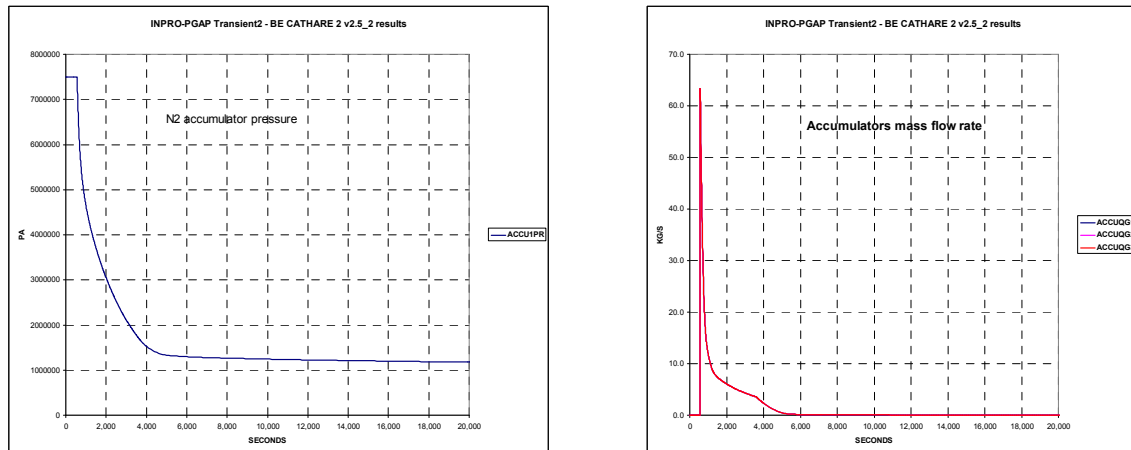


FIG. 141. Nitrogen accumulator pressure (left) and mass flow rate (right).

Break flow

Gas flow rate at the break is shown in Fig. 142.

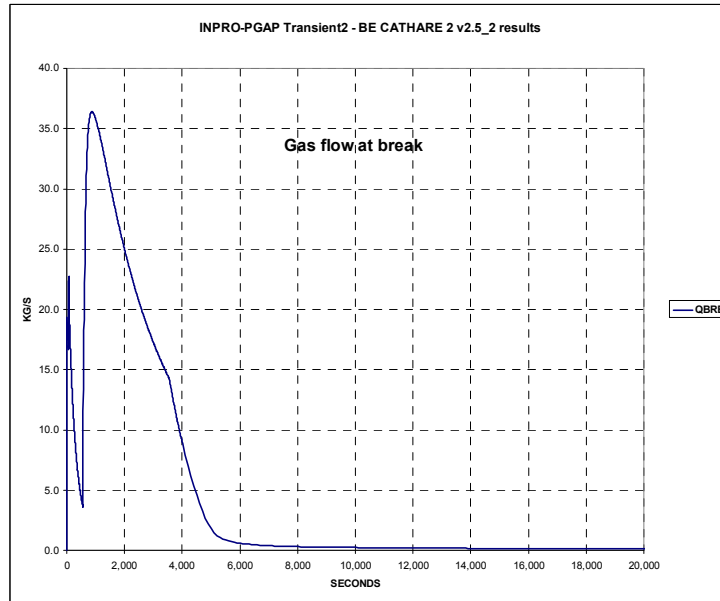


FIG. 142. Gas flow rate at the break.

Close containment

The evolutions of pressures and temperatures in the close containment are shown in Fig. 143. The pressure in the close containment increases initially due to the leak of helium at the break and after 600s due to the leak of nitrogen at the break. It reaches a maximum of 1.33 MPa at 4400s and then decreases because of the decrease in temperatures. This decrease in the temperature in the close containment is due to the heat exchange with the outside.

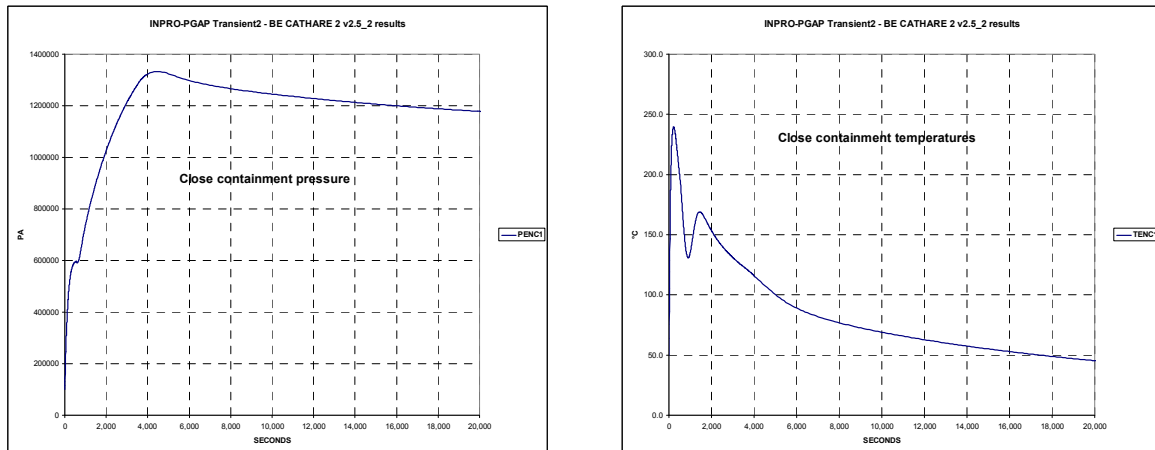


FIG. 143. Close containment pressures (left) and temperatures (right).

Summary of main T-H parameters

Here is a summary of main results:

- Maximum clad temperature: 1404 °C at 624s (Failure limit: 1600 °C);
- Maximum clad temperature after nitrogen injection: 840 °C at 6206s (Failure limit: 1000 °C);

- Maximum coolant temperature at core outlet: 1241 °C (590s) (Failure limit: 1250 °C);
- Maximum of close containment pressure: 1.33 MPa (failure limit 1.4 MPa);
- He DHR mass flow : ~ 25 kg/s (for each loop);
- Water DHR mass flow : ~120 kg/s (for each loop).

In this reference case, with nominal values of the input parameters, we can see that two DHR loops working in natural circulation fulfill their mission with the help of nitrogen injection from accumulators. After nitrogen injection, a flow rate of at least 50 kg/s is maintained up to the end of the transient during the natural circulation phase. During six hour (time considered in the specification) from the beginning of the transient, the heat removal is sufficient and all failure criteria are respected, with values staying below the safety limits (but the margin is only 9°C for the third criterion).

III.1.2. Sensitivity analysis

The objective of this sensitivity analysis is to evaluate the influence of the input parameters on the main T-H characteristics of the system. The sensitivity analysis has been performed for a number of input parameters in the CATHARE 2 calculations. Classical OAT (one at a time) analysis, which varies one factor from the nominal condition, the others being kept at their nominal values, has been used for this sensitivity analysis. The sensitivity parameters used in the sensitivity analysis for the transient II are described in Appendix I. Table 53 summarizes the results of the sensitivity analysis.

TABLE 56. PARAMETERS STUDIED, WITH MAXIMUM TEMPERATURES AND CLOSED CONTAINMENT PRESSURE OBTAINED (**BOLD VALUES INDICATE THAT THE CRITERION IS EXCEEDED**)

Modified Parameter number	Modified Parameter	Variations	Clad Maximum Temperature 1st peak (°C)	Clad Maximum Temperature 2nd peak (°C) (after N2 injection)	Gas Maximum Temperature at core outlet (°C)	Close containment max. pressure (bars)
Reference case			1404.4	842.2	1243.3	13.3317
1	Core total pressure drop	+ 15 %	1402.6	842.7	1241.6	13.3306
2	Inlet k-factor in DHR primary loop	+ 2	1405.0	843.8	1241.6	13.3303
3	Outlet k-factor in DHR primary loop	+ 2	1403.5	842.9	1242.5	13.3309
4	Helium clad heat transfer coefficient	- 25 %	1377.9	851.2	1219.6	13.3298
		+ 25 %	1417.7	836.9	1253.0	13.3308

Modified Parameter number	Modified Parameter	Variations	Clad Maximum Temperature 1st peak (°C)	Clad Maximum Temperature 2nd peak (°C) (after N2 injection)	Gas Maximum Temperature at core outlet (°C)	Close containment max. pressure (bars)
5	Multiplication factor for thermal inertia for all walls	- 15 %	1390.2	846.0	1238.2	13.2668
		+ 15 %	1417.5	838.6	1246.3	13.3892
6	Corrective factor for heat transfer in DHR IHX	- 25 %	1428.3	926.9	1263.8	13.5141
		+ 25 %	1385.3	792.8	1226.1	13.2148
7	Core nominal power	- 2 %	1378.7	825.9	1222.7	13.3247
		+ 2 %	1426.5	858.8	1260.8	13.3375
8	Core residual power	- 10 %	1327.7	761.0	1184.1	13.2871
		+ 10 %	1472.3	921.8	1292.4	13.3712
9	Primary blower inertia	- 25 %	1457.6	844.1	1284.9	13.3123
		+ 25 %	1359.3	840.6	1206.4	13.3507
10	Main circuit pressure	- 0.2 MPa	1406.2	843.7	1244.5	13.2927
		+ 0.2 MPa	1396.5	840.9	1236.2	13.3717
11	Containment Pressure for SCRAM release	- 0.03 MPa	1386.1	842.2	1227.0	13.32
		+ 0.07 MPa	1452.7	842.6	1282.8	13.35
12	Lower plenum Pressure for Accumulator discharge	- 0.2 MPa	1460.7	839.9	1292.5	13.3365
		+ 0.2 MPa	1356.1	844.3	1195.7	13.3280
13	Time between main circuit valves closure and DHR valves opening	- 2 s	1399.2	842.3	1238.7	13.3304
		+ 4 s	1413.2	842.1	1250.5	13.3341

Modified Parameter number	Modified Parameter	Variations	Clad Maximum Temperature 1st peak (°C)	Clad Maximum Temperature 2nd peak (°C) (after N2 injection)	Gas Maximum Temperature at core outlet (°C)	Close containment max. pressure (bars)
14	Break size	- 10 %	1408.2	831.9	1243.3	13.2346
		+ 10 %	1397.2	852.0	1238.6	13.4187
15	Close containment leakage	+ 10 %	1404.4	851.7	1243.3	13.1470
16	Close containment free volume	- 10 %	1400.5	799.4	1239.5	14.3666
		+ 10 %	1406.1	885.2	1244.5	12.4498
17	Close containment heat exchange with the outside	- 10 %	1404.4	840.4	1243.3	13.3640
		+ 10 %	1404.4	843.9	1243.3	13.3002
18	Close containment outside temperature	- 10 °C	1404.4	845.9	1243.3	13.2635
		+ 10 °C	1404.4	838.6	1243.3	13.3996
19	Close containment initial pressure	- 0.01 MPa	1400.5	846.5	1239.5	13.2380
		+ 0.01 MPa	1406.1	838.1	1244.5	13.4253
20	Close containment initial temperature	- 20 °C	1404.4	856.5	1243.3	13.0169
		+ 20 °C	1404.4	828.6	1243.3	13.6461
21	Volume of heat structures in close containment	- 10 %	1404.4	835.5	1243.3	13.4912
		+ 10 %	1404.4	847.9	1243.3	13.1971
22	Accumulator initial pressure	- 0.5 MPa	1406.4	879.4	1239.4	12.7114
		+ 0.5 MPa	1402.1	808.8	1246.5	13.9557
23	Accumulator initial temperature	- 20 °C	1403.1	814.6	1239.4	13.7742
		+ 20 °C	1405.7	869.0	1247.0	12.9367

Modified Parameter number	Modified Parameter	Variations	Clad Maximum Temperature 1st peak (°C)	Clad Maximum Temperature 2nd peak (°C) (after N2 injection)	Gas Maximum Temperature at core outlet (°C)	Close containment max. pressure (bars)
24	Discharge line singular pressure drop	- 50 %	1393.9	844.5	1254.6	13.3458
		+ 50 %	1410.7	840.2	1234.5	13.3144
25	Gas mixture viscosity	- 5 %	1390.8	835.4	1232.9	13.3143
		+ 5 %	1415.9	848.9	1251.0	13.3478
26	Gas mixture conductivity	- 10 %	1416.6	859.1	1253.0	13.4176
		+ 10 %	1392.7	828.2	1232.8	13.2612
27	Gas mixture heat capacity	- 5 %	1429.4	871.0	1269.4	13.3957
		+ 5 %	1377.4	816.1	1215.7	13.2810

III.1.2.1. Effect of changing parameters on the four failure criteria

Effect on clad maximum temperature (1st peak): $T_{max_clad_P1}$

The reference value obtained considering nominal values of the parameters is 1404.4 °C

It can be seen that all the values of $T_{max_clad_P1}$ obtained (see Table 56) are far below the failure criterion of 1600°C. The maximum value of $T_{max_clad_P1}$, obtained for the upper value (+ 10%) of the core residual power, is equal to 1472.3 °C, which is 128°C below the failure criterion.

In order to evaluate the effect of the parameter, the following ratio has been calculated:

$$\Delta_i = \frac{abs(T_{low} - T_{upp})}{T_{ref}}$$

where

T_{low} : value of $T_{max_clad_P1}$ for minimum value of the parameter

T_{upp} : value of $T_{max_clad_P1}$ for maximum value of the parameter

T_{ref} : value of $T_{max_clad_P1}$ for nominal value of the parameter (=1404.4°C)

Thirteen parameters out of 27 have a significant impact (with $\Delta_I > 1\%$). They have been listed in descending order of Δ_I in Table 57.

TABLE 57. INFLUENCING PARAMETERS ON CLAD MAXIMUM TEMPERATURE (1ST PEAK) IN DESCENDING ORDER

Order	Parameter	Ratio Δ_I in %
1	Core residual power	10.3
2	Lower plenum pressure for accumulator discharge	7.4
3	Primary blower inertia	7.0
4	Containment pressure for SCRAM release	4.7
5	Gas mixture heat capacity	3.7
6	Core nominal power	3.4
7	Corrective factor for heat transfer in DHR IHX	3.1
8	Helium clad heat transfer coefficient	2.8
9	Multiplicative factor for thermal inertia for all walls	1.9
10	Gas mixture viscosity	1.8
11	Gas mixture conductivity	1.7
12	Discharge line singular pressure drop	1.2
13	Time between main circuit valves closure and DHR valves opening	1.0

Effect on clad maximum temperature (2nd peak): $T_{max_clad_P2}$

The reference value obtained considering nominal values of the parameters is 842.2 °C

It can be seen that the values of $T_{max_clad_P2}$ obtained (see Table 56) are all below the failure criterion of 1000°C. The maximum value of $T_{max_clad_P2}$, obtained for the lower value (-25 %) of the heat transfer in DHR IHX, is equal to 926.9 °C, which is 73°C below the failure criterion.

We have also calculated the ratio Δ_2 corresponding to $T_{max_clad_P2}$.

Fifteen parameters out of 27 have a significant impact (with $\Delta_2 > 1\%$). They have been listed in descending order of Δ_2 in Table 58.

TABLE 58. INFLUENCING PARAMETERS ON CLAD MAXIMUM TEMPERATURE (2nd PEAK) IN DESCENDING ORDER

Order	Parameter	Ratio Δ_2 in %
1	Core residual power	19.1
2	Corrective factor for heat transfer in DHR IHX	15.9
3	Close containment free volume	10.2
4	Accumulator initial pressure	8.3
5	Gas mixture heat capacity	6.5
6	Accumulator initial temperature	6.4
7	Core nominal power	3.9
8	Gas mixture conductivity	3.7
9	Close containment initial temperature	3.3
10	Break size	2.4
11	Helium clad heat transfer coefficient	1.7
12	Gas mixture viscosity	1.6
13	Volume of heat structures in close containment	1.5
14	Close containment leakage	1.1
15	Close containment initial pressure	1.0

Effect on gas maximal temperature at core outlet: T_{max_gas}

The reference value obtained considering nominal values of the parameters is 1243.3 °C.

It can be seen that the criterion on T_{max_gas} (1250°C) is exceeded several times for:

- High value of helium clad heat transfer coefficient;
- Low value of corrective factor for heat transfer in DHR IHX;
- High value of core nominal power;
- High value of core residual power;
- Low value of primary blower inertia;
- High value of containment pressure for scram release;
- Low value of lower plenum pressure for accumulator discharge;
- High value of Time between main circuit valves closure and DHR valves opening;
- Low value for discharge line singular pressure drop.
- High value of gas mixture viscosity;

- Low value of gas mixture conductivity;
- Low value of gas mixture heat capacity.

The maximum value of T_{max_gas} , obtained for the lower value (-25 %) of lower plenum pressure for accumulator discharge is equal to 1292.5 °C, which is 42.5°C above the failure criterion. Hence, with a lower pressure, the nitrogen injection is delayed and T_{max_gas} is higher.

We have also calculated the ratio Δ_3 corresponding to T_{max_gas} .

Ten parameters out of 27 have a significant impact (with $\Delta_3 > 1\%$). They have been listed in descending order of Δ_3 in Table 59. This order is almost the same as for clad maximum temperature (first peak).

TABLE 59. INFLUENCING PARAMETERS ON GAS MAXIMUM TEMPERATURE IN DESCENDING ORDER

Order	Parameter	Ratio Δ_3 in %
1	Core residual power	8.7
2	Lower plenum pressure for accumulator discharge	7.7
3	Primary blower inertia	6.3
4	Containment pressure for SCRAM release	4.4
5	Gas mixture heat capacity	4.3
6	Core nominal power	3.1
7	Corrective factor for heat transfer in DHR IHX	3.0
8	Gas mixture conductivity	1.6
9	Discharge line singular pressure drop	1.6
10	Gas mixture viscosity	1.5

Effect on close containment maximum pressure: P_{MAX_CONT}

The reference value obtained considering nominal values of the parameters is 1.33 MPa.

It can be seen that the criterion on P_{MAX_CONT} (1.4 MPa) is exceeded only one time for a low value of the close containment free volume. In this case $P_{MAX_CONT} = 1.44$ MPa, which is 0.04 MPa above the failure criterion.

We have also calculated the ratio Δ_4 corresponding to P_{MAX_CONT} .

11 parameters out of 27 have a significant impact (with $\Delta_4 > 1\%$). They have been listed in descending order of Δ_4 in Table 60.

TABLE 60. INFLUENCING PARAMETERS ON CLOSE CONTAINMENT MAXIMUM PRESSURE

Order	Parameter	Ratio Δ_i in %
1	Close containment free volume	14.4
2	Accumulator initial pressure	9.3
3	Accumulator initial temperature	6.3
4	Close containment initial temperature	4.7
5	Corrective factor for heat transfer in DHR IHX	2.2
6	Volume of heat structures in close containment	2.2
7	Close containment initial pressure	1.4
8	Close containment leakage	1.4
9	Break size	1.4
10	Gas mixture conductivity	1.2
11	Close containment outside temperature	1.0

III.1.2.2. Effects of the most important parameters on the four responses of interest

Core residual power

An increase in core residual power results into an increase in four responses.

Lower plenum pressure for accumulator discharge

This parameter has conflicting effect. Indeed, when we reduce the pressure for accumulator discharge, there is a delay in nitrogen discharge. As a result of this delay, there is an increase in the maximum temperatures of gas and clad (first peak). Also, the flow rate of nitrogen is higher at the time of the second peak and, as a result, low temperature of the second peak is obtained. Therefore, a decrease in this parameter is favourable for the second peak of clad temperature but unfavourable for the first peak.

Primary blower inertia

When the blower inertia is reduced to 25%, $T_{max_clad_P1}$ is increased by 54°C and T_{max_gas} by 42°C. The effect is lower on $T_{max_clad_P2}$.

Containment pressure for SCRAM release

When we decrease the containment pressure, it triggers the SCRAM earlier. The rods are dropped earlier and, as a result, low residual power is obtained. As a consequence, the maximum gas and clad (first peak) temperatures decrease. There is no effect on $T_{max_clad_P2}$.

Gas mixture heat capacity

An increase of gas mixture heat capacity results into a decrease in the four responses. Indeed, when the heat capacity C_p of the gas is increased, the amount of heat stored in the gas, for a given temperature, rises. Inversely, for a given quantity of heat transferred from the clad to the gas, the gas temperature will increase less, when increasing C_p . Therefore, an increase in C_p of gas is favourable.

Core nominal power

An increase in the core nominal power results into an increase in the four responses.

Heat transfer in DHR IHX

An increase in this parameter results into a decrease in the four responses. Indeed, when this parameter increases, the efficiency of the DHR heat exchanger increases resulting into a better cooling.

Helium–clad heat transfer coefficient

This parameter H has conflicting effects as can be seen in Fig. 144. An increase of H results into an increase of gas and clad temperatures (first peak). Indeed, an increase in heat transfer coefficient favours the increase in heat exchanged between the clad and gas resulting into an increase of gas temperature. At core exit, the clad temperature also increases, while it decreases down the core. At the second peak, increase of H has no effect on the gas temperature but causes a decrease in clad temperature (the clad is better cooled by the gas). Therefore, an increase in this parameter is favourable for the second peak and unfavourable for the first peak.

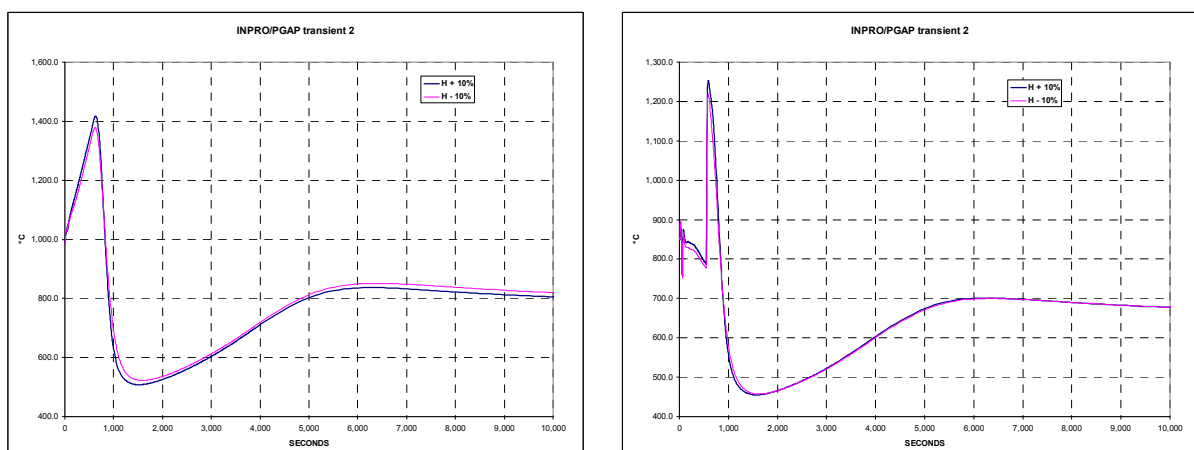


FIG. 144. Influence of helium–clad heat transfer coefficient H on clad (left) and gas (right) temperatures.

Close containment free volume

An increase in this parameter results into a decrease of P_{max_cont} , but results into an increase of $T_{max_clad_P1}$, $T_{max_clad_P2}$ and T_{max_gas} . The increase in the temperatures is especially significant at the second peak. Indeed, the increase in free volume results into a decrease in the pressure in the close containment resulting into a decrease in primary pressure, which is unfavorable to enhance natural circulation.

Accumulator initial pressure

An increase in this parameter results into a decrease in the temperature at the first peak but an increase in temperature at the second peak. Indeed, an increase in pressure results into a quicker discharge of the accumulators resulting into an increase of the gas flow rate at the first peak, which is favourable to enhance natural circulation. But at the second peak, the gas flow rate is lower because the accumulators were emptied earlier.

Accumulator initial temperature

A decrease in this parameter results into a decrease in $T_{max_clad_P1}$, $T_{max_clad_P2}$ and T_{max_gas} but results into an increase of P_{max_cont} . A decrease in the temperatures is especially sensitive to $T_{max_clad_P2}$. Indeed, injection of colder nitrogen is favourable to enhance natural convection and the heat exchange between clad and gas.

Close containment initial temperatures

This parameter has no effects on the temperatures at the first peak. However, an increase in this parameter results into a decrease in $T_{max_clad_P2}$ and an increase in P_{max_cont} . Indeed, an increase in this parameter results into an increase in the pressure in the close containment and then to an increase of equilibrium pressure between the containment and the primary circuit, which is favourable to enhance natural circulation.

Break size

An increase in the break size results into a decrease in $T_{max_clad_P1}$ and T_{max_gas} and an increase in $T_{max_clad_P2}$ and P_{max_cont} . Indeed, when the break size increases, the primary circuit is depressurized faster and, as a result, the SCRAM occurs earlier and the nitrogen is injected earlier from the accumulators than in the reference case. The first peak of clad and helium temperature is less than the reference break size. But the nitrogen accumulators are emptied more quickly and as there is more leakage in the break, the natural circulation flow is lower than in the reference case, hence; the second peak of clad temperature is higher than in the reference case.

Gas mixture conductivity

An increase in gas mixture conductivity results into a decrease in $T_{max_clad_P1}$, $T_{max_clad_P2}$, T_{max_gas} and P_{max_cont} . Indeed, in this case, the cooling of gas is better in the DHR exchanger and, as a result, the clad is also better cooled.

Conclusion on sensitivity analysis

We have identified the most important parameters influencing the four responses linked to the failure criteria.

The effects of these parameters on the first and second peak of clad and gas temperatures are often contradictory. This gives a glimpse of the difficulties in the design of the reactor to find an optimum for these parameters.

The clad temperature criterion is satisfied in all the sensitivity cases, but the criterion on the gas maximum temperature is exceeded several times and the criterion on the close containment maximum pressure is exceeded only one time.

III.1.3. Reliability evaluation

Based on the previous sensitivity analysis, 10 parameters out of 25 uncertain parameters have been selected, for which one of the failure criteria is exceeded, with the exception of two parameters i.e. the discharge line singular pressure drop, because it is necessary to decrease it by 50 % in order to exceed the failure criterion on the gas maximum temperature by only 4°C, and the gas mixture viscosity for which the failure criteria is only exceeded by 0.9 °C. Following is the list of selected parameters:

- Helium clad heat transfer coefficient;
- Corrective factor for heat transfer in DHR IHX;
- Core nominal power;
- Core residual power;
- Primary blower inertia;
- Containment pressure for scram release;
- Lower plenum pressure for accumulator discharge;
- Close containment free volume;
- Gas mixture conductivity;
- Gas mixture heat capacity.

For the reliability evaluation, we used the RMPS methodology. The input uncertainties are propagated through the T-H code CATHARE in order to evaluate the uncertainty on the response of interest and assess the reliability of the DHR system.

III.1.3.1. Input uncertainties

We have considered that the ten uncertain input parameters follow normal distributions and that there is a probability of 0.95 for the value of each parameter to lie between the minimum and maximum values defined above. Table 61 summarizes the probabilistic model.

III.1.3.2. Input sampling and propagation of uncertainties

A Latin Hypercube Sampling (LHS) has been performed using the 10 above normal distributions.

100 samples of the input parameters were simulated and for each, a thermohydraulic calculation was performed with the CATHARE2 code. The number of simulations is limited to 100 because of time duration for each CATHARE2 calculations (30 minutes).

TABLE 61. PROBABILISTIC MODEL OF THE RANDOM VARIABLES

Parameter number	Parameter	Mean value	Standard deviation
1	Primary blower inertia (% vs ref. value)	0	0.1275
2	Lower plenum pressure for accumulator discharge (bar)	10	1.0204
3	Containment pressure for SCRAM release (bar)	1.3	0.3571
4	Helium clad heat transfer coefficient (% vs reference value)	0	0.1276
5	Core nominal power (% vs. reference value)	0	0.0102
6	Corrective factor for heat transfer in DHR IHX (% vs. reference value)	0	0.1276
7	Core residual power (% vs. reference value)	1	0.051
8	Close containment free volume (% vs. reference value)	0	0.051
9	Gas mixture conductivity (% vs. reference value)	0	0.051
10	Gas mixture heat capacity (% vs. reference value)	0	0.0255

III.1.3.3. Response of interest

The following responses given by the CATHARE2 code have been studied:

- Maximum clad temperature (1st peak);
- Maximum clad temperature (2nd peak);
- Maximum temperature of gas at core outlet;
- Maximum pressure in the close containment.

Statistical analysis of the responses of interest

Table 62 gives the main statistical results (average, standard deviation, 95% quantile, safety margin and histogram) obtained on the four responses of interest. The safety margin is defined as the gap between the 95% quantile and the safety criterion.

Goodness of fit tests has been performed for various probability distributions. It can be concluded from these tests that the probability distributions of the response of interest can be modeled by a normal law with good accuracy. As an example, Fig. 145 shows the comparison of the quantiles obtained on the results of Maximum clad T (2nd peak) and the quantile given by the normal law. It can be observed that all the points are close to the straight line $y = x$ (in red) indicating the goodness of fit by the normal law.

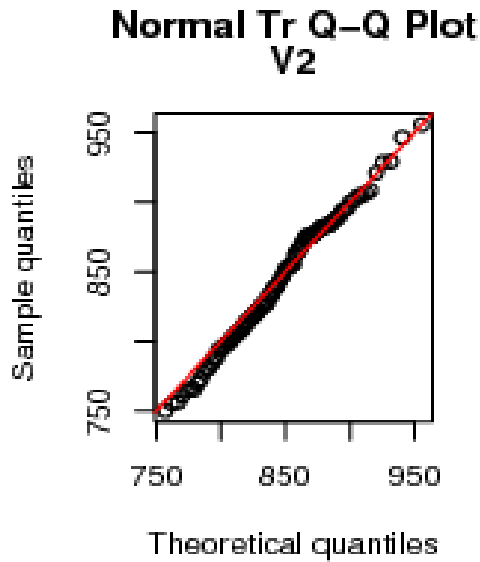


FIG. 145. Quantiles of maximum clad T.

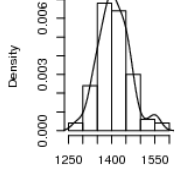
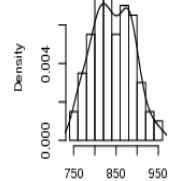
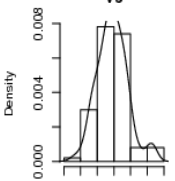
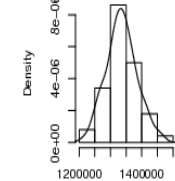
Global sensitivity analysis

A global sensitivity analysis has been carried out by the way of standard regression coefficients (SRC). For details on SRC, see section II.1.1.3.

Results obtained on the four response of interest

Input parameters with a SRC^2 greater than 5% are only considered here. The results are given in Tables 63 to Table 66.

TABLE 62. STATISTICAL CHARACTERISTICS OF THE RESPONSE OF INTEREST

Response of interest	Average	Standard deviation	95% Quantile	Safety margin	Histogram
Maximum clad T (1st peak) (°C)	1408	55.1	1499	101	<p>Histogram & density V1</p> 
Maximum clad T (2nd peak) (°C)	842	46.9	919	81	<p>Histogram & density V2</p> 
Maximum T of gas at core outlet (°C)	1245	45.3	1320	-70	<p>Histogram & density V3</p> 
Maximum pressure in the close containment (bar)	13.35	0.489	14.15	- 0.15	<p>Histogram & density V5</p> 

- *Maximum clad temperature (1st peak)*

The standardized regression coefficients for maximum clad temperature (1st peak), when $R^2 = 0.998$, are given in Table 63.

TABLE 63. STANDARDIZED REGRESSION COEFFICIENTS FOR MAXIMUM CLAD TEMPERATURE AT FIRST PEAK

Rank	Parameter No	Input parameter	SRC	SRC ²
1	7	Residual power	0.658	0.433
2	2	Lower plenum pressure for accumulator discharge	-0.495	0.245
3	1	Primary blower inertia	-0.480	0.230
4	10	Gas mixture heat capacity	-0.255	0.065
5	5	Nominal power	0.226	0.051

- *Maximum clad temperature (2nd peak)*

The standardized regression coefficients for maximum clad temperature (2nd peak), when $R^2 = 0.999$, are given in Table 64.

TABLE 64. STANDARDIZED REGRESSION COEFFICIENTS FOR MAXIMUM CLAD TEMPERATURE AT SECOND PEAK

Rank	Parameter No	Input parameter	SRC	SRC ²
1	7	Residual power	0.864	0.747
2	8	Close containment free volume	0.454	0.207
3	10	Gas mixture heat capacity	- 0.301	0.091

- *Maximum temperature of gas at core outlet*

The standardized regression coefficients for maximum temperature of gas at core outlet, when $R^2 = 0.992$, are given in Table 65.

TABLE 65. STANDARDIZED REGRESSION COEFFICIENTS FOR MAXIMUM GAS TEMPERATURE AT CORE OUTLET

Rank	Parameter No	Input parameter	SRC	SRC ²
1	7	Residual power	0.598	0.358
2	2	Lower plenum pressure for accumulator discharge	-0.556	0.310
3	1	Primary blower inertia	-0.464	0.215
4	10	Gas mixture heat capacity	-0.314	0.099
5	5	Nominal power	0.225	0.051

- *Maximum pressure in the close containment*

The standardized regression coefficients for maximum pressure in the close containment, when $R^2 = 0.997$, are given in Table 66.

TABLE 66. STANDARDIZED REGRESSION COEFFICIENTS FOR CLOSE CONTAINMENT PRESSURE

Rank	Parameter No	Input parameter	SRC	SRC ²
1	8	Close containment free volume	-0.995	0.99

It can be seen that for the four responses of interest, the hypothesis of a linear relation between the output and the input parameters is valid, because the values of the R^2 are close to 1 in each case and so we can use the standardized regression coefficients as sensitivity indices.

The results obtained on the SRCs for the two temperatures (maximum clad and gas temperatures at first peak) are very close and this is logical because these two temperatures are correlated. The most influencing parameters are the core residual power, lower plenum pressure for accumulator discharge, primary blower inertia, gas mixture heat capacity and the nominal power.

For the maximum clad temperature at second peak, the most influencing parameters are the residual power, close containment free volume and the gas mixture heat capacity.

Finally, the close containment free volume demonstrates 99% of the uncertainty of maximum pressure in the close containment

The ranking based on a global sensitivity analysis is slightly different than the one obtained by OAT sensitivity analysis.

III.1.3.4. Reliability analysis

For each simulation performed, the natural circulation DHR system is considered failed if at least one of the four failure criteria is exceeded: $T_{\max_clad_1st_peak} > 1600^{\circ}\text{C}$ or $T_{\max_clad_2nd_peak} > 1000^{\circ}\text{C}$ or $T_{\max_gas} > 1250^{\circ}\text{C}$ or $P_{close_containment} > 1.4 \text{ MPa}$.

The failure probability is estimated by:

$$\overline{P_f} = \frac{N_f}{N}$$

where N_f is the number of simulations leading to the failure of the system and N is the total number of simulations.

When N tends to infinity, $\overline{P_f}$ tends to the actual value of the failure probability. The accuracy of the estimation can be evaluated by its variance calculated in an approximate way by:

$$Var(\overline{P_f}) \cong \frac{(1 - \overline{P_f})\overline{P_f}}{N}$$

A good estimation of the statistical accuracy is given by the coefficient of variation:

$$COV(\overline{P_f}) \cong \frac{\sqrt{\frac{(1 - \overline{P_f})\overline{P_f}}{N}}}{\overline{P_f}}$$

The lower the coefficient of variation (COV), the more accurate is the estimation of the failure probability. The coefficient of variation (COV) close to 10% indicates a good level of accuracy.

Result: with the 100 simulations, we obtain $\overline{P_f} = 0.49$ and $COV(\overline{P_f}) = 0.10$. The accuracy is acceptable.

Failure probability with regards to each criterion considered independently

For this evaluation, we have considered that the four responses followed normal distributions, with averages and standard deviations obtained on the 100 simulations (Table 67).

The failure probabilities are then estimated by:

$$P_f = P(Y \geq S) = 1 - P(Y < S) = 1 - F_Y(S)$$

Where

Y = one of the responses,

S = the associated failure criterion and

F_Y = the cumulative function of Y (Normal distribution).

TABLE 67. FAILURE PROBABILITIES WITH REGARDS TO EACH CRITERION

Responses of interest	P_f
Maximum clad temperature (1st peak)	2.46×10^{-4}
Maximum clad temperature (2nd peak)	3.61×10^{-4}
Maximum temperature of gas at core outlet	0.456
Maximum pressure in the close containment	0.092

Note that here we have evaluated the failure probability for each response independent of the others. The total failure probability of the system calculated previously ($P_f = 0.49$) is not equal to the sum of failure probabilities for each parameter, because in some simulations, two failure criteria may have been exceeded at the same time.

These results enable us to conclude that the most often exceeded failure criterion is the gas temperature at core outlet (1250 °C). The second failure criterion, for which attention should be paid, is the pressure in the close containment. The criteria on the clad temperatures have very low probabilities as compared to other two failure criteria.

Conclusion

In the reference case, with nominal values of the input parameters, it is observed that two DHR loops working in natural circulation fulfill their mission with the help of nitrogen injection from accumulators. After nitrogen injection, a flow rate of at least 50 kg/s is maintained up to the end of the transient during the natural circulation phase. During six hour (time considered in the specification) from the beginning of the transient, the heat removal is sufficient and all failure criteria are respected, with values staying below the safety limits (for third criterion, the margin is only 9°C).

By sensitivity analysis, the most important parameters influencing the four responses linked to the failure criteria have been identified. The effect of these parameters on the first and second clad and gas peak of temperature are often contradictory. This gives a glimpse of the difficulties in the design of the reactor to find an optimum for these parameters. The clad temperature criterion is satisfied in all the sensitivity cases, but the criterion on the gas maximum temperature is exceeded several times and the criterion on the close containment maximum pressure is exceeded only one time.

Finally the reliability analysis of the DHR system for this transient shows a high conditional probability of failure essentially due to the risk of exceeding the failure criterion associated to the gas temperature at core outlet. This risk can be limited by increasing the reference value and by limiting the uncertainty on the lower plenum pressure for accumulator discharge.

III.2. SCK-CEN, BELGIUM

The calculations have been performed using the RELAP5 mod 3.3 patch 3 system code⁴.

III.2.1. Steady state evaluation

A steady state is reached after about 200 seconds, with all T-H parameters being close to their nominal value. All steady state parameters are summarized in Table 68.

TABLE 68. STEADY STATE RESULTS

No	Parameter	Unit	Design value	RELAP5	Error (%) ⁵
1	Thermal power	MW	2400	2400	0.000
2	Pressure at core inlet	MPa	7.12	7.1215	-0.021
3	Pressure at core outlet	MPa	6.98	6.9932	-0.189
4	Pressure at blower inlet	MPa	6.95	6.9646	-0.210
5	Pressure at blower outlet	MPa	7.13	7.1327	-0.038
6	Core inlet temperature	°C	400	401.158	-0.289
7	Core outlet temperature	°C	900	899.35	0.072
8	Vessel outlet temperature	°C	850	849.977	0.003
9	MHX inlet temperature	°C	850	848.246	0.206
10	Main blower inlet temperature	°C	396	397.53	-0.386
11	Main blower outlet temperature	°C	400	401.55	-0.387
12	MCP speed	rad/s	471.24	471.24	0.000
13	Pressure drop on the MHX	MPa	0.02	0.020793	-3.965
14	Pressure drop in the core		0.14	0.128509	8.208

⁴ The previous transient (LOFA) benchmark has been analyzed with RELAP5 mod 3.2 version. For the LOCA, the use of mod 3.2 is not a suitable option because of some limitations concerning the presence of two different non-condensable gases (He and N₂) in the same system.

⁵ Error defined as $\frac{(\text{Design value}) - (\text{RELAP5 value})}{\text{Design value}} * 100$

No	Parameter	Unit	Design value	RELAP5	Error (%) ⁵
15	MCP head	MPa	0.18	0.168405	6.442
16	Total loop coolant flow rate	kg/s	1020	1018.93	0.105
17	Exchanged power in MHX	MW	803.3	808.4	-0.635
18	Helium mass in primary circuit (DHR included)	kg	-	5810.2	-

III.2.2. LOCA transient evolution description

The transient evolution of main primary system, primary DHR and secondary DHR system T-H parameters (pressures, temperatures, mass flow rates, power exchanged in HXs) are shown in Fig. 146 to Fig. 150.

The LOCA transient starts with the break in the cold part of the main cross duct (0s). As a result, the primary system pressure starts dropping while helium coolant is released into the close containment. Once the close containment pressure drops to 1.3 bars after 22s, the reactor scram is activated and the full DHR sequence follows, as described in Appendix I.

After ~96s since the start of transient, the DHR sequence is completed i.e. the main blowers are fully stopped, the primary valves are closed and the two DHR loops are fully opened. The system continues towards depressurization.

Once system pressure reaches 1 MPa (~ 468s), the 3 N₂ accumulators valves are opened, starting to release nitrogen gas into the primary system. The primary system then experiences an increase in pressure (reaching a peak value of 5.11 MPa after 690s) generating a second pressure peak (the "N₂ pressure peak"). The maximum pressure in this phase is, however, well below the system nominal pressure.

After the accumulators opening and the second pressure peak, the pressure starts decreasing. This can be seen as a starting of long term cooling phase. During this long term cooling phase, a low temperature peak is reached after ~8500 s. This is important because of the second N₂ pressure peak maximum safety limits, though low in value compared to what the system experiences in the earliest phase of the transient.

Figure 151 shows N₂ concentration in the core during the LOCA transient. This is an important parameter, together with the maximum cladding temperature (LOCA failure criteria).

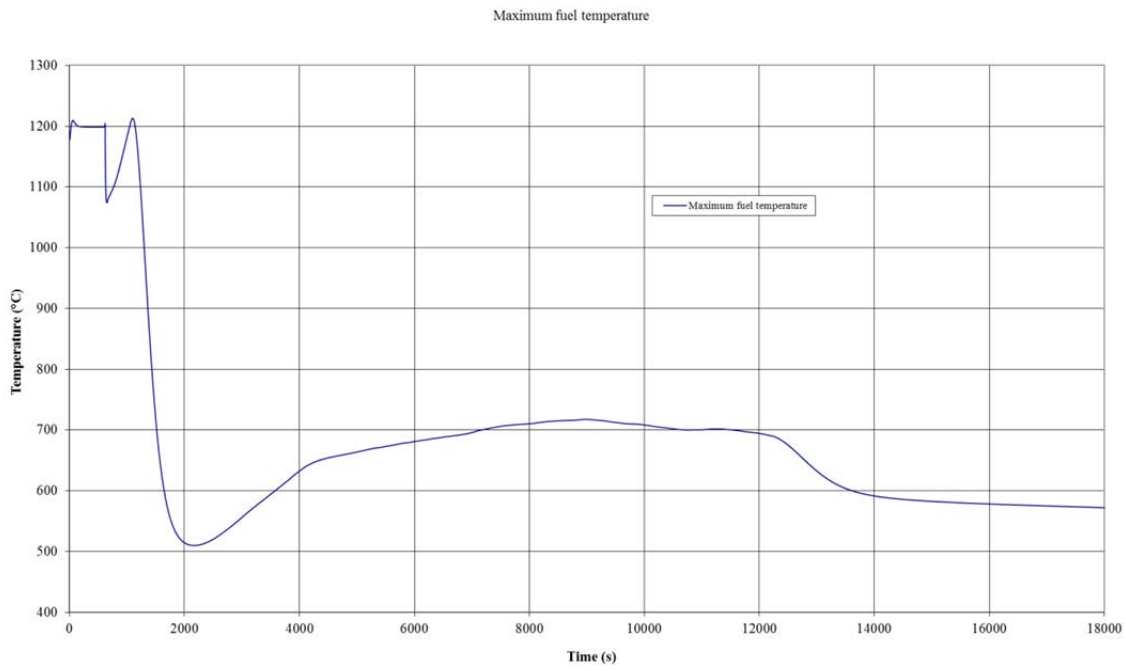


FIG. 146. Fuel temperature⁶.

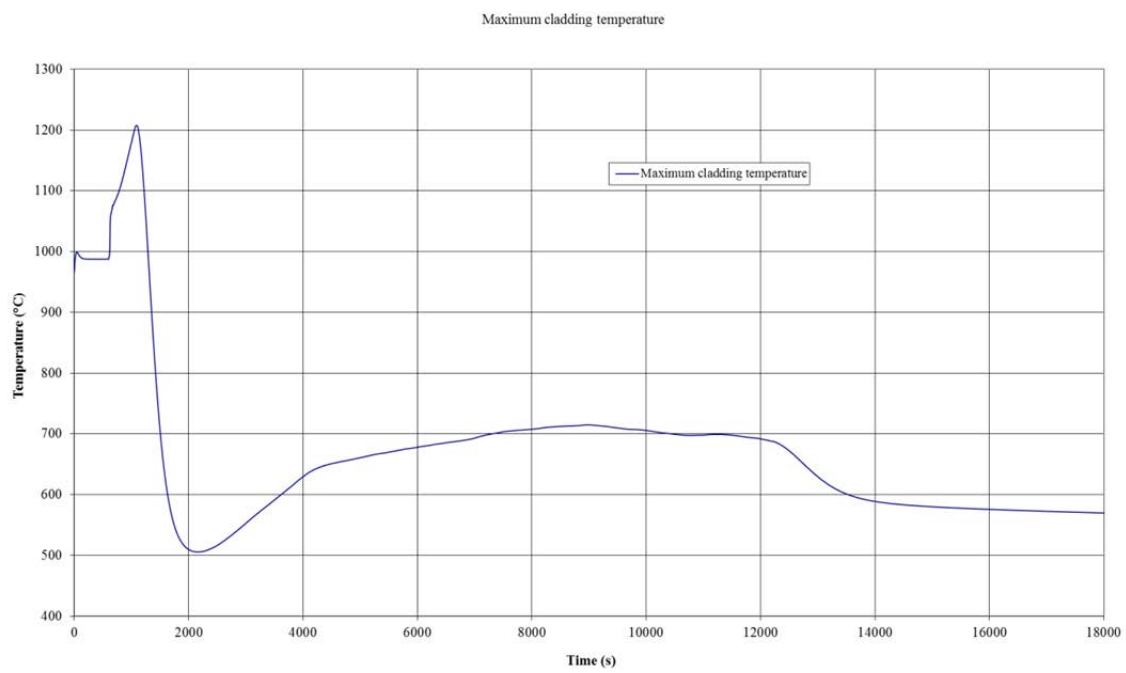


FIG. 147. Clad temperature.

⁶ It is important to note that the fuel "hot spot" varies its location. In steady state, it is located at ~1.6 m from the bottom of core. While during transient, it is located at core exit.

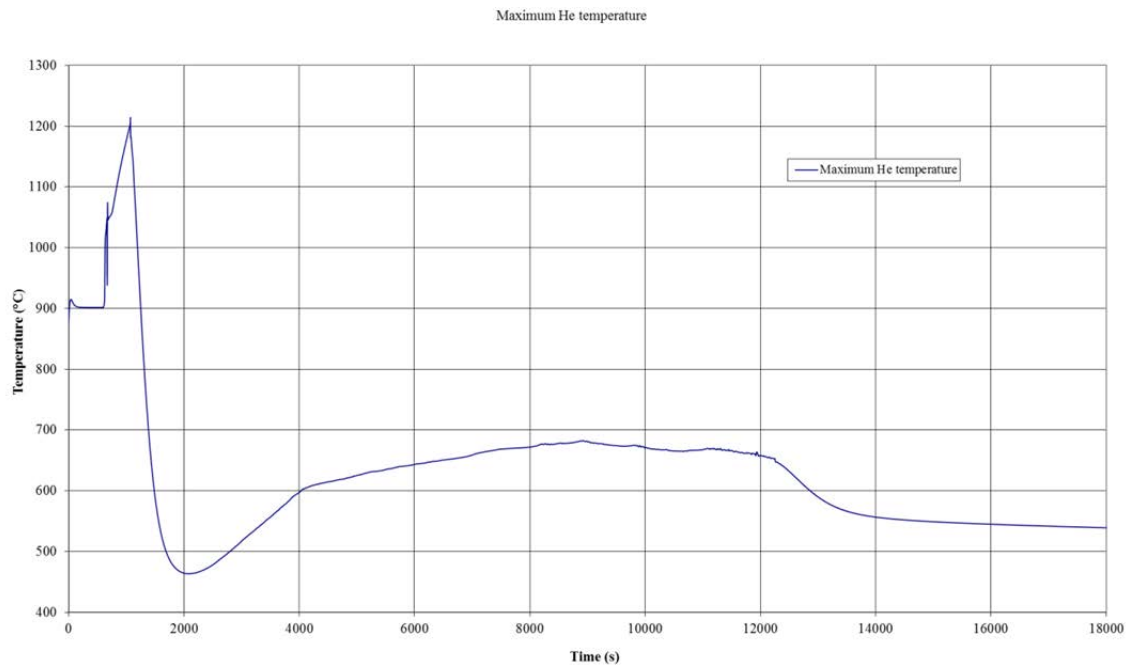


FIG. 148. He temperature at core hot channel exit.

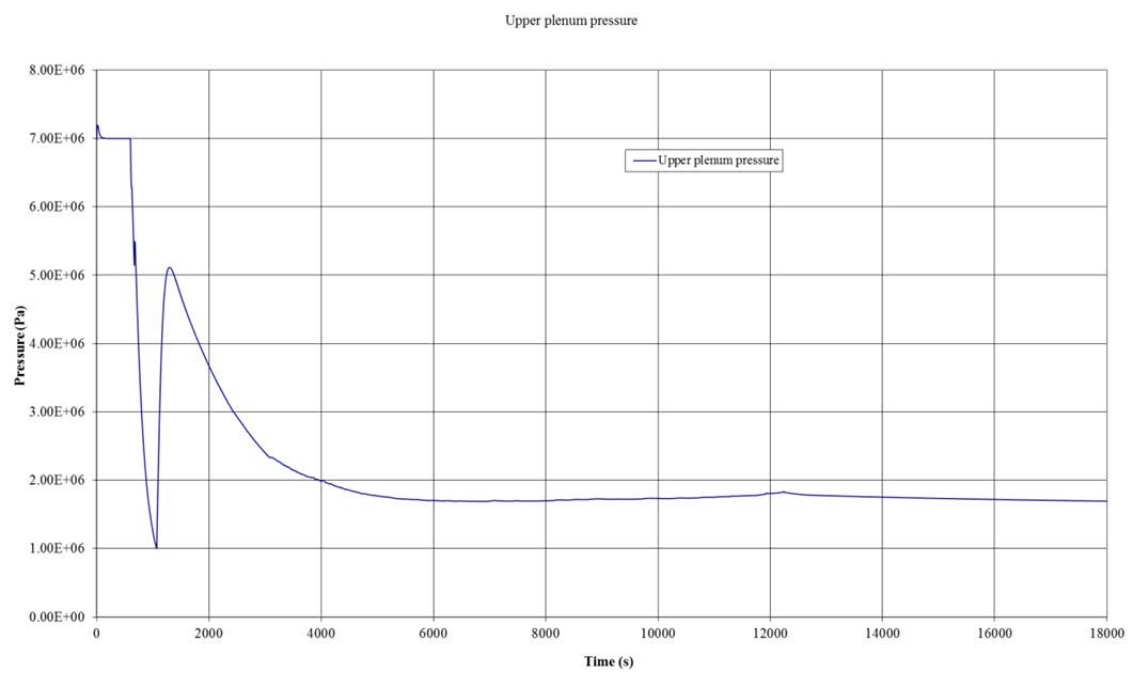


FIG. 149. Upper plenum pressure.

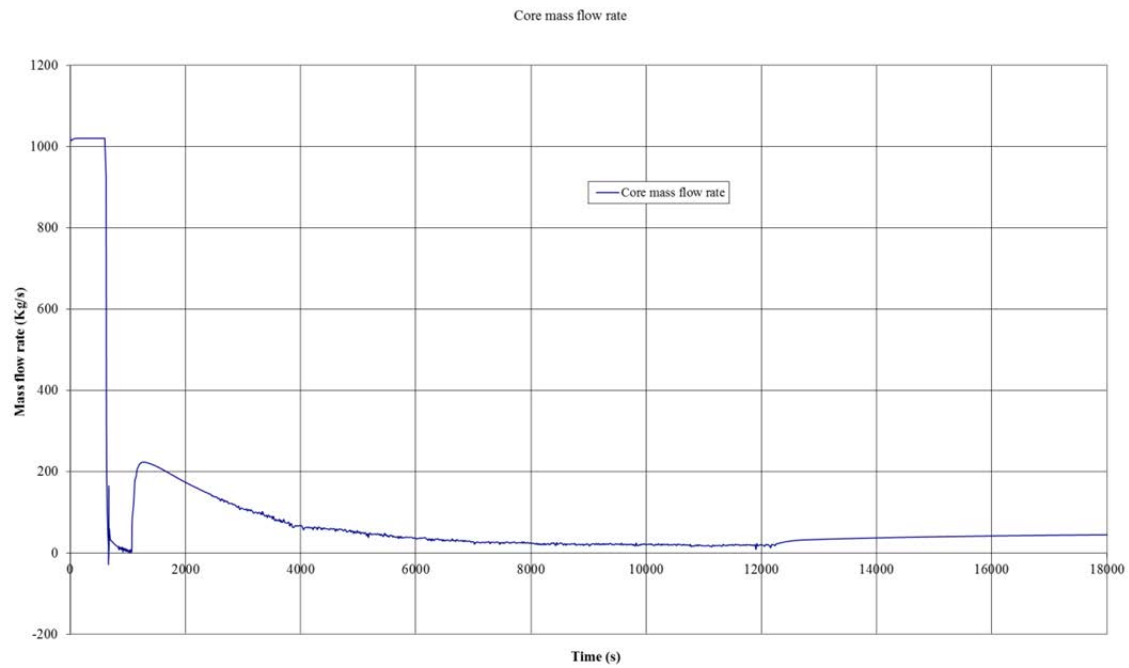


FIG. 150. Core mass flow rate.

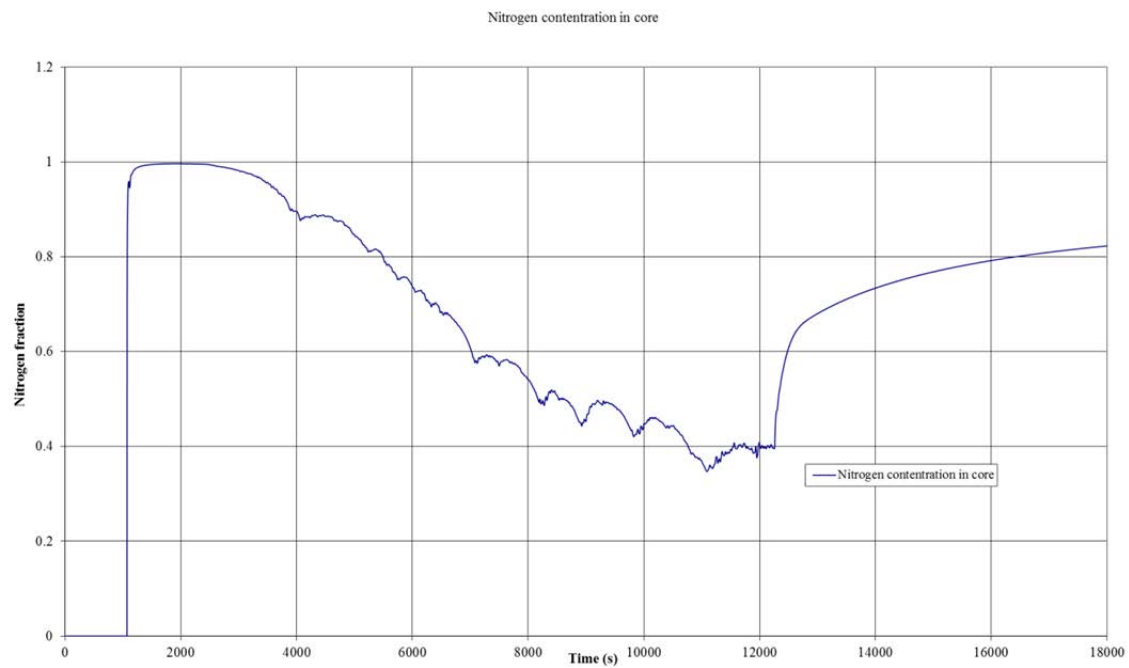


FIG. 151. N2 concentration in core.

Figures 152 to 156 show the DHR parameters during transient; following the opening of valves, after the temperature and the longer pressure transient phase are ended (see above), the Helium side of DHR loops follows the same pressure and temperature evolution of the upper plenum of primary loop in the long term cooling of the system. The DHR He side hot

leg wall, whose temperature has been limited by failure criteria (Table 21), reaches its maximum value after ~11000 seconds from the beginning of the transient. The maximum temperature is ~530 °C, which is well below 850 °C (Fig. 153).

In the secondary DHR water loops, after ~6000 seconds the loops are stabilized at a temperature of 115 °C (Fig. 152) and a mass flow rate of 200 kg/s (Fig. 155). Differently from He loops, which follows the core outlet parameters, the water loops are also directly conditioned by the tertiary heat sink pools. In the pools, temperature slowly rises until saturation value (at atmospheric pressure) is reached after ~12000 seconds, then some vapor starts forming in the pools, and quality slowly starts rising. This causes a local decrease in temperature in the water–water heat exchanger because of enhanced HTC resulting into a better heat removal from the He loop and, ultimately, the core.

Figures 157 and 158 show the close containment pressure distribution and mass flow rate at the break respectively.

From Fig. 159, it can be noticed that once the long term cooling phase has started, the power removed from core, the heat exchanged in He–Water DHR HX and heat transmitted to the final pool are identical. This clearly shows how the system has actually entered a long term safe cooling phase, where all residual decay power generated in the core can be safely removed by only natural circulation means, without the help of any active system, in the case of a LOCA.

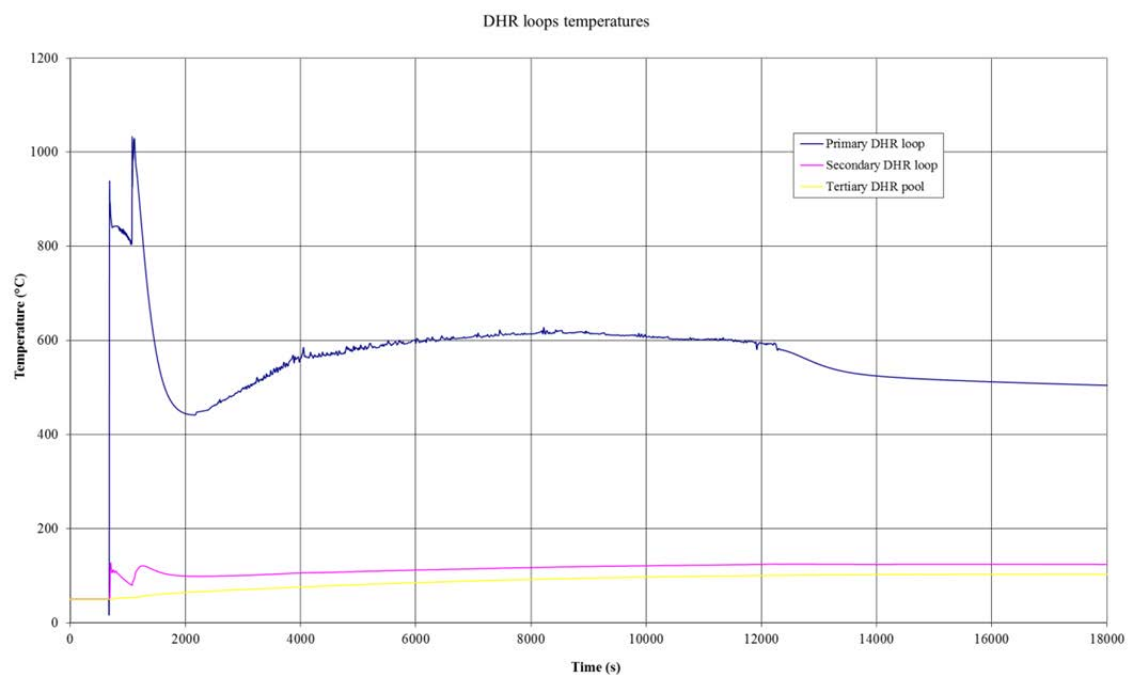


FIG. 152. DHR loops temperature evolution.

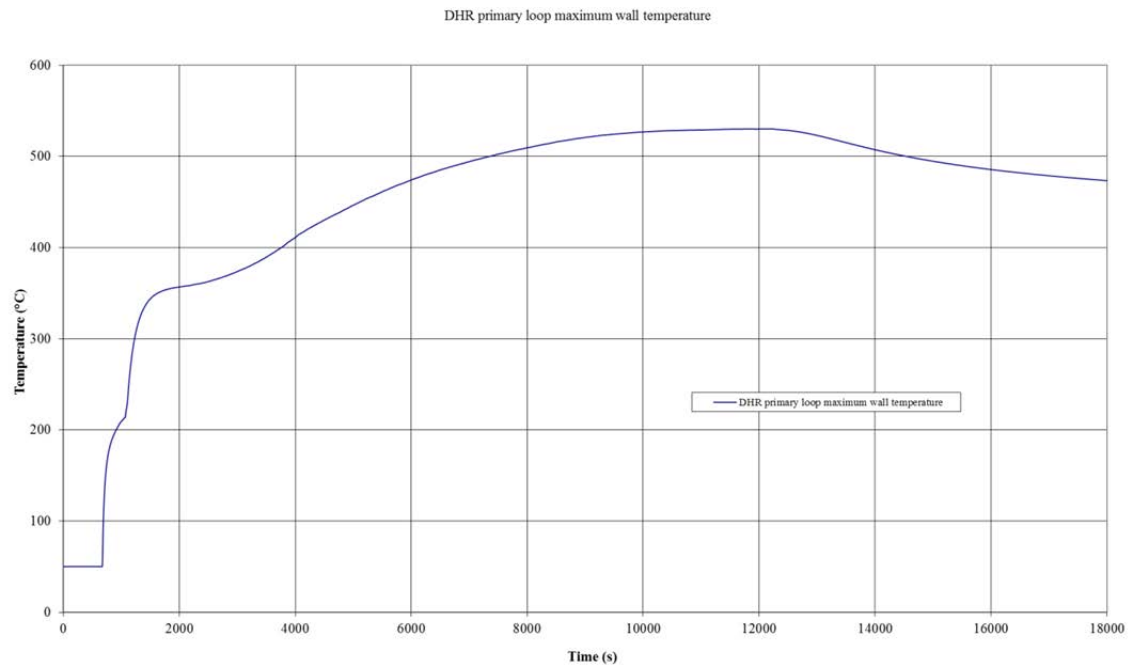


FIG. 153. DHR He loop wall temperatures.

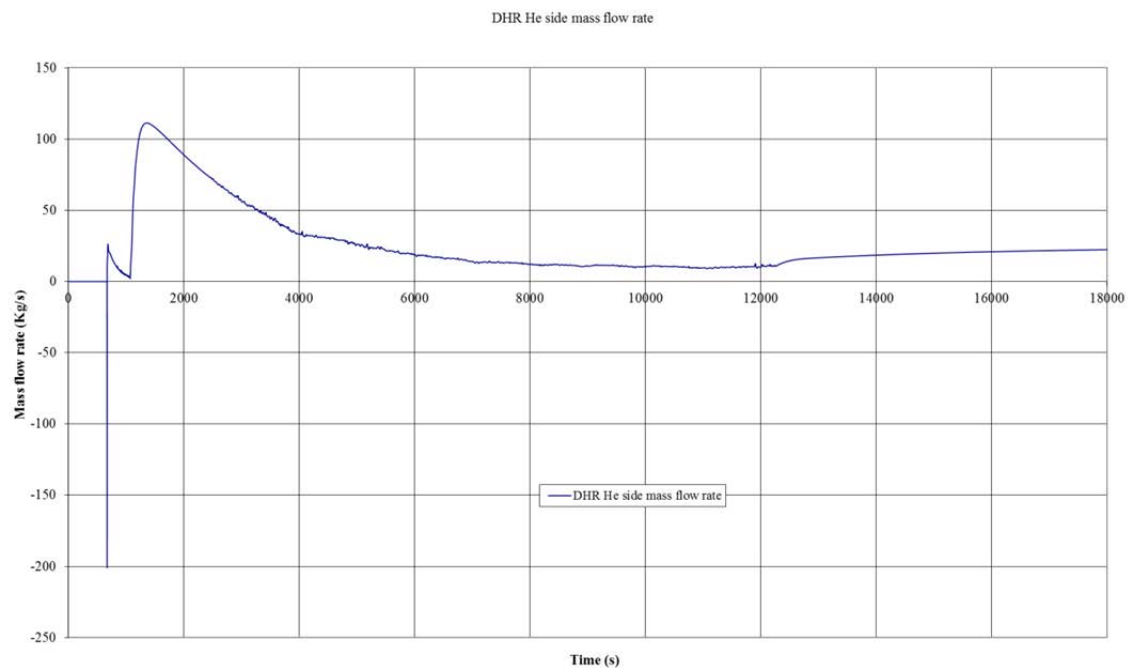


FIG. 154. DHR He side mass flow rate.

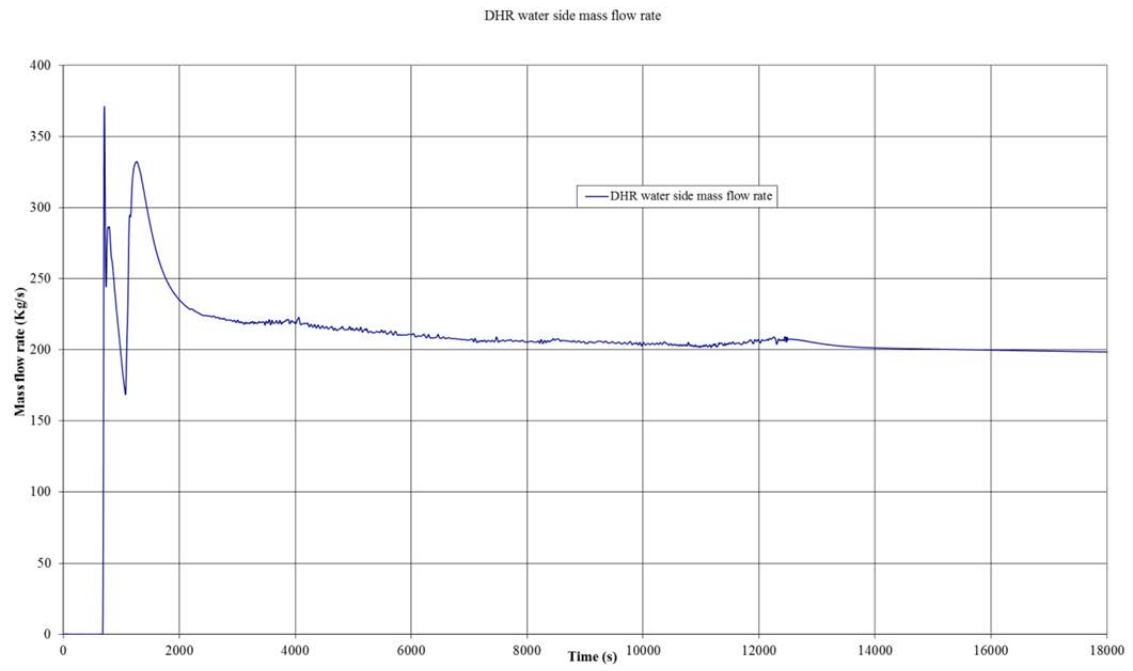


FIG. 155. DHR water side mass flow rate.

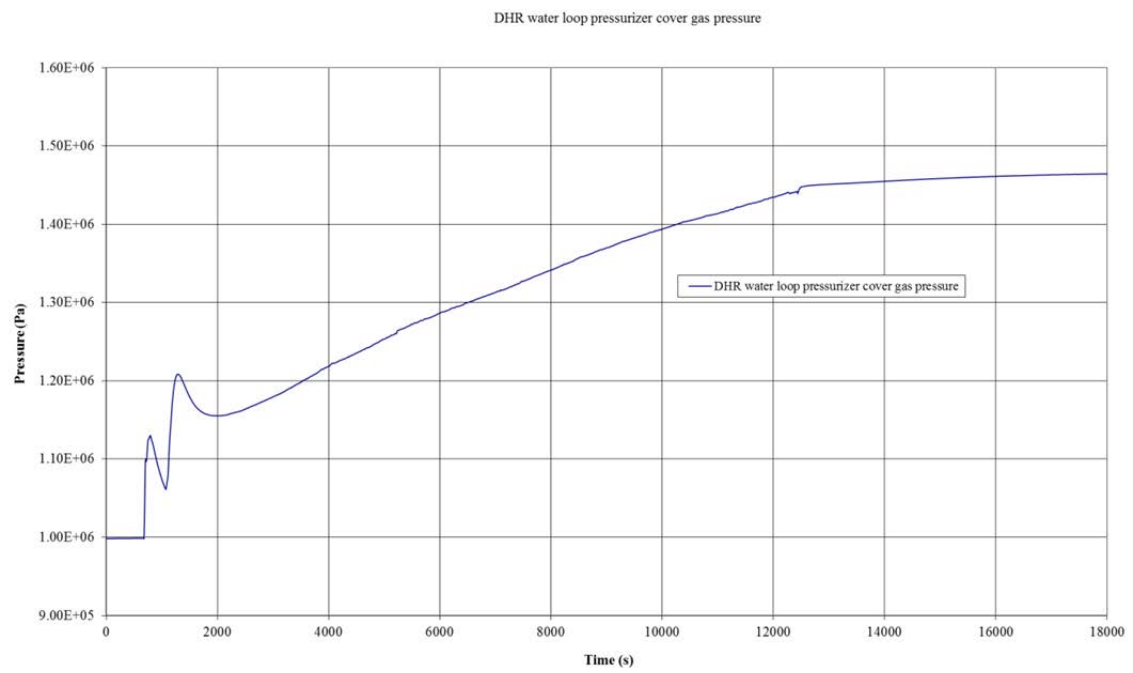


FIG. 156. DHR water side pressurizer cover gas pressure.

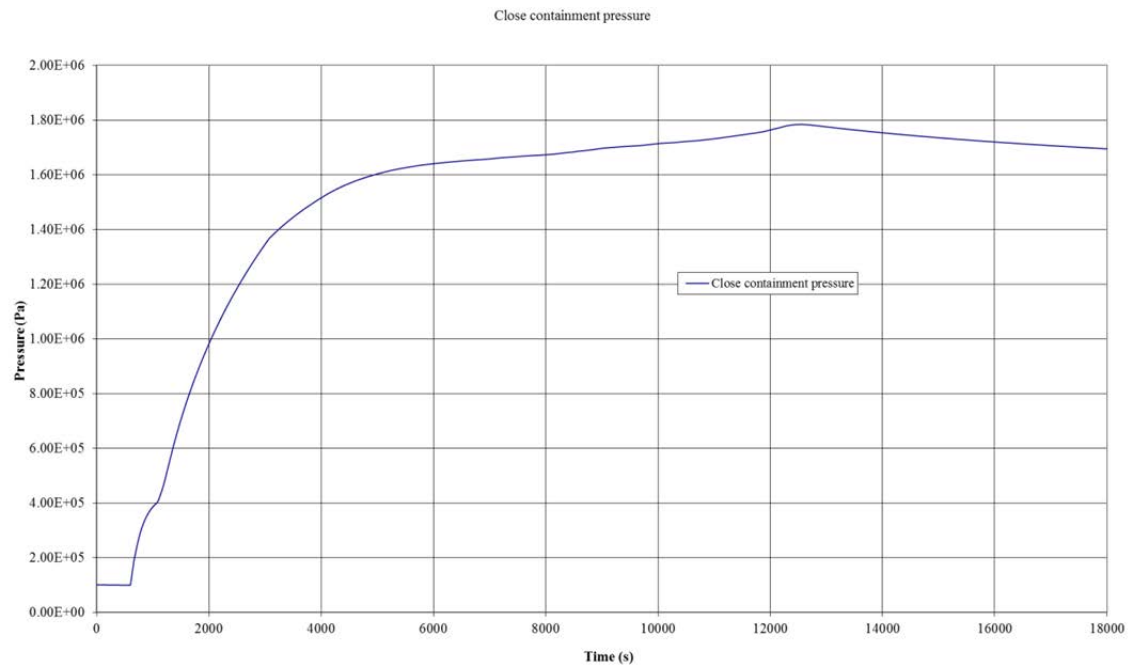


FIG. 157. Close containment pressure.

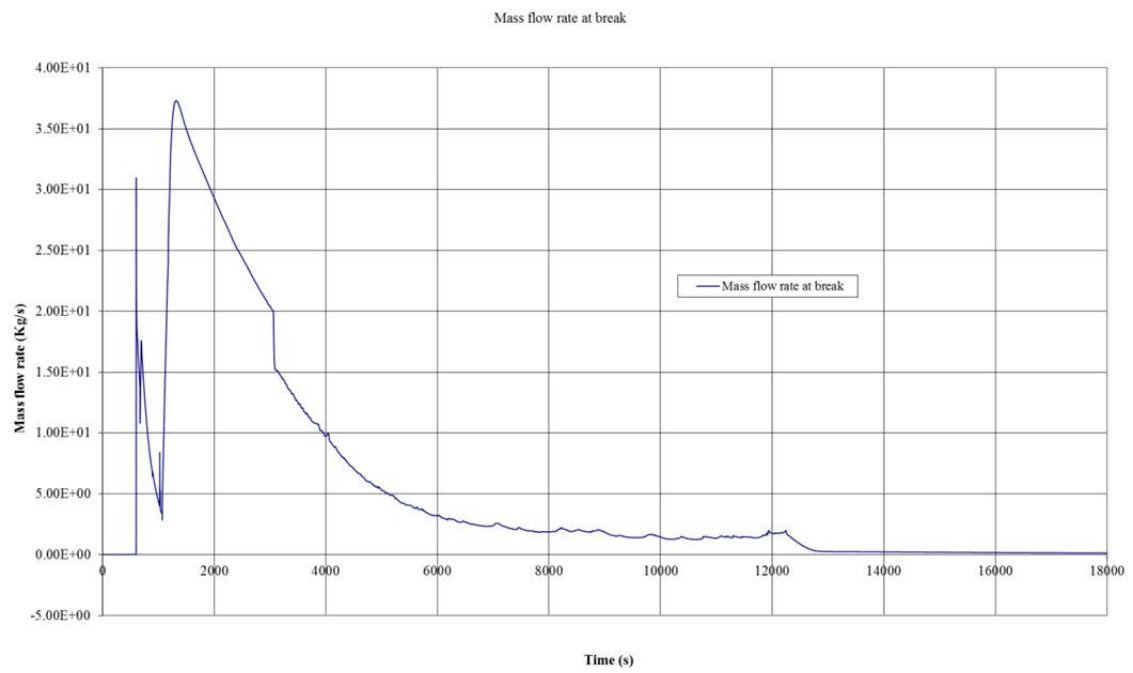


FIG. 158. Mass flow rate at break.

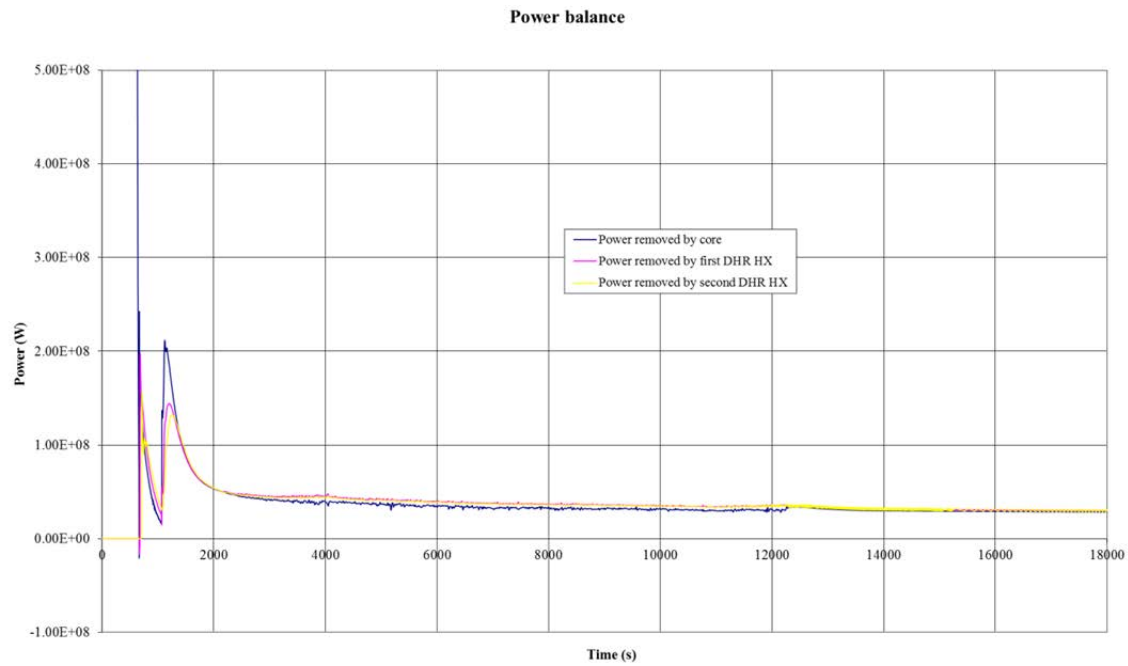


FIG. 159. Power balance during transient.

Table 69 summarizes the LOCA transient failure criteria and the maximum pressures and temperatures obtained during the transient. It can be seen that maximum containment pressure has not satisfied the failure criterion.

TABLE 69. COMPARISON WITH FAILURE CRITERIA

Parameter	Unit	Failure limit	Value obtained from calculation
Maximum DHR structures T	°C	850	530.2
Maximum cladding T (1st peak)	°C	1600	1073.0
Maximum cladding T (2nd peak)	°C	1000	710.0
Maximum He T	°C	1250	1204.7
Maximum containment Pressure	MPa	1.4	1.78

III.2.3. Sensitivity studies

In order to select a series of input parameters to be analyzed in the transient II reliability statistical analysis, a sensitivity analysis has been run.

Starting from the reference LOFA evaluation, two modifications have been made to the system configuration (in the RELAP5 input deck) in order to see the influence and the differences in the main T-H output.

The input parameters that have been studied in the sensitivity analysis are:

- DHR inlet pressure drop K-factor (simulating DHR pump failure): +50%
- DHR HTC in the He-water HT: -10%

These two input parameters have been previously considered in the reliability analysis of the LOFA transient and have high influence on the transient evolution, especially considering the long term cooling phase.

Figures 160 to 164 show the impact of varying the two parameters.

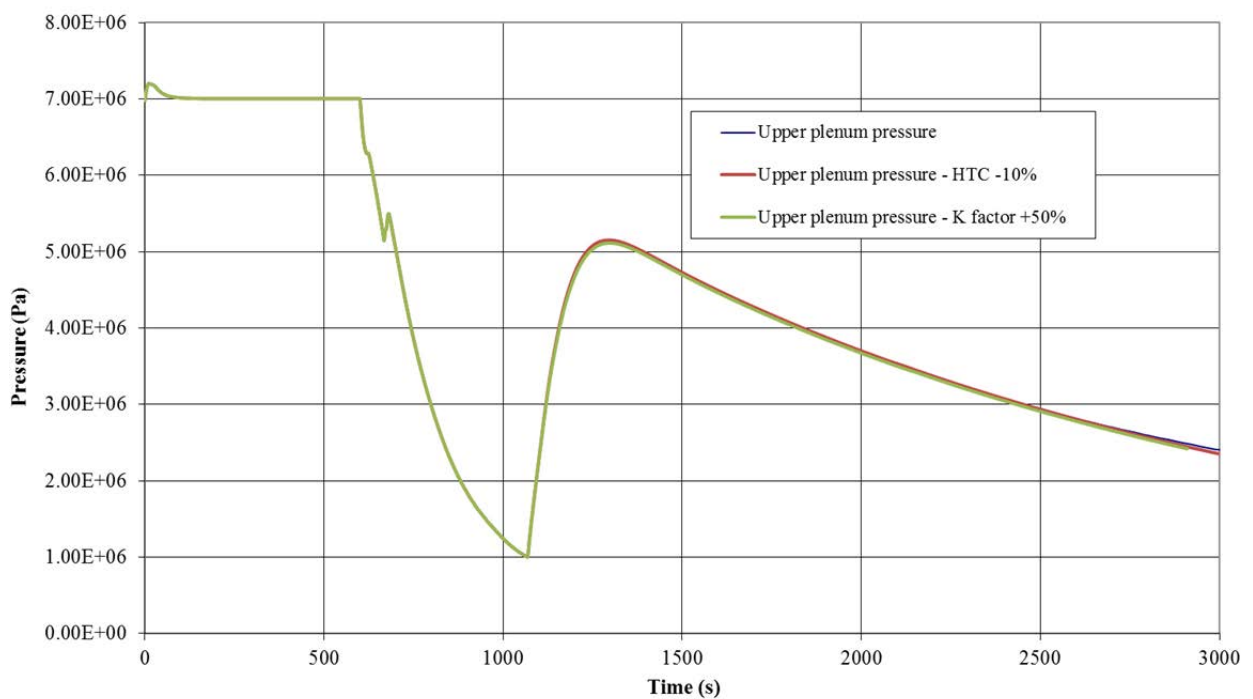


FIG. 160. Upper plenum pressure comparison.

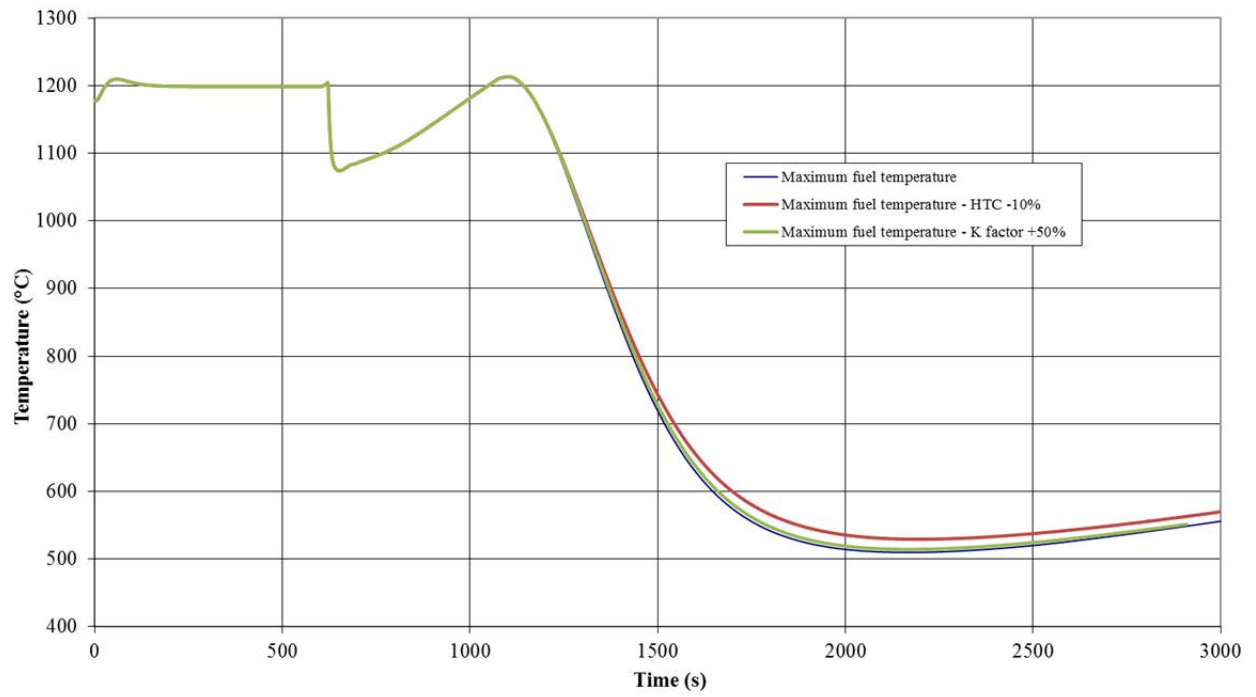


FIG. 161. Fuel maximum temperature comparison.

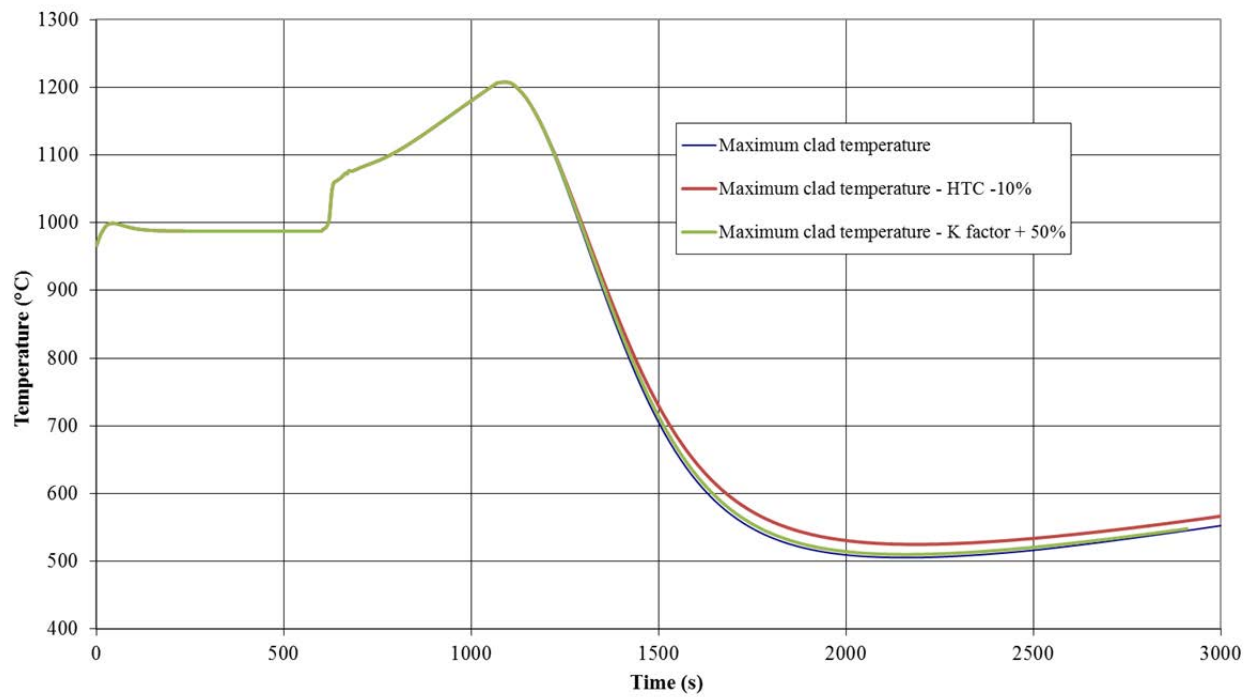


FIG. 162. Cladding maximum temperature comparison.

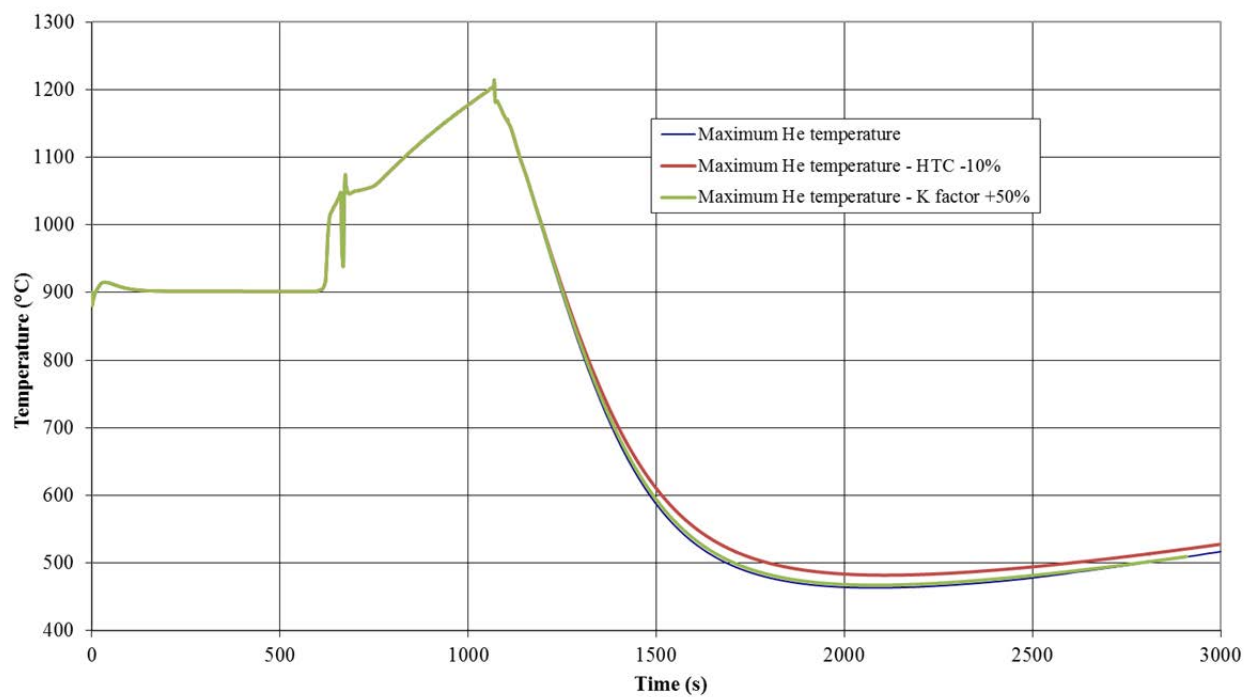


FIG. 163. He maximum temperature comparison.

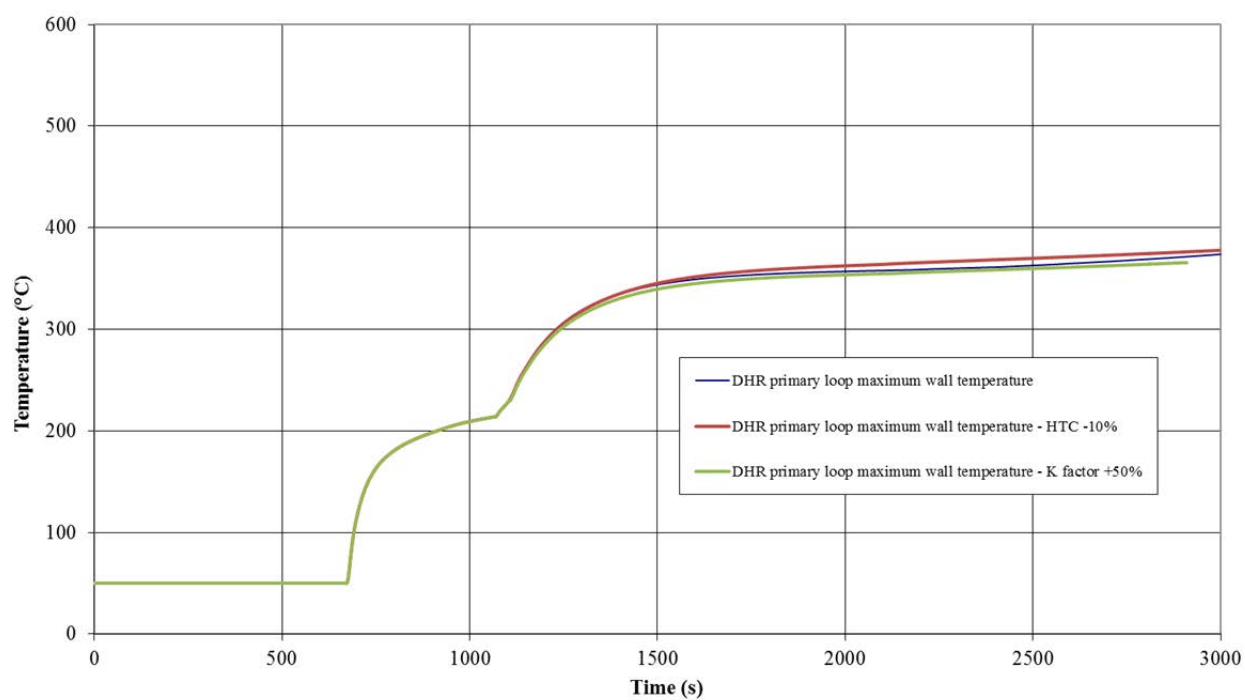


FIG. 164. DHR structures temperature comparison.

It can be noticed that by decreasing the DHR HTC and increasing the pressure loss factor (simulating stopped DHR blower), the T-H transient conditions during the first ~1000 s do not experience any noticeable difference with the reference case.

On the other hand, in the long term cooling phase, the decrease in HTC causes an increase in temperature.

Conclusion

The purpose of this benchmark calculation is to explore the capabilities of the GFR to withstand 21600 seconds (6 hours) from the beginning of the transient event in the accidental conditions specified, reaching a safe long term cooling phase and respecting the specified failure criteria.

A steady state is achieved after 200s, with all T-H parameters being close to their nominal value.

The LOCA transient evolution of main primary system, primary DHR and secondary DHR system T-H parameters (pressures, temperatures, mass flow rates, power exchanged in HXs) are analyzed. Below is the summary of timeline of events during transient evolution:

- (1) 0.0 s: start of transient (break in the cold part of main cross duct);
- (2) 22.0 s: containment pressure > 1.3 bars → reactor scram;
- (3) 80.0 s: start of DHR sequence (core mass flow rate below 3% of nominal value);
- (4) 83.0 s: valves in main loops start to close;
- (5) 91.0 s: valves in DHR loop start to open;
- (6) 96.0 s: DHR sequence is completed;
- (7) 468.0 s: pressure in primary system falls below 1 MPa → N₂ accumulators open.

At this point, the natural circulation (NC) is started and the system is entered into a safe long term cooling phase.

During this long term cooling phase, a low temperature peak is reached after ~8500s. This is important because of the second N₂ pressure peak maximum safety limits, though low in value compared to what the system experiences in the earliest phase of the transient.

Once the long term cooling phase has started, the power removed from the core, the heat exchanged in He–Water DHR HX and heat transmitted to the final pool are identical. This clearly shows how the system has actually entered a long term safe cooling phase, where all residual decay power generated in the core can be safely removed by only natural circulation means, without the help of any active system, in the case of a LOCA.

Also, after considering the results of the LOCA sensitivity analysis, the failure criteria (with the exception of maximum containment pressure, which was not respected in the reference case either) related to temperatures are still satisfied.

REFERENCES

- [1] INTERNATIONAL ATOMIC ENERGY AGENCY, Safety Related Terms for Advanced Nuclear Plant, IAEA-TECDOC-626, IAEA, Vienna (1991).
- [2] D'AURIA, F., GALASSI, G.M., Methodology for the evaluation of the reliability of passive systems, DIMNP, NT 420, University of Pisa, Italy (2000).
- [3] MARQUES, M., PIGNATEL, J. F., SAIGNES, P., D'AURIA, L., MULLER, C., BOLADO-LAVIN, C., KIRCHSTEIGER, C., LA LUMINA, V., IVANOV, L., Methodology for the reliability evaluation of a passive system and its integration into a probabilistic safety assessments, Nuclear Engineering and Design 235 (2005) 2612–2631.
- [4] PAGANI, L.P., APOSTOLAKIS, G.E., HEJZLAR, P., The impact of uncertainties on the performance of passive systems, Nuclear Technology 149 (2005) 129–140.
- [5] NAYAK, A.K., GARTIA, M.R., ANTONY, A., VINOD, G., SINHA, R.K., Passive system reliability analysis using the APSRA methodology, Nuclear Engineering and Design 238 (2008) 1430–1440.
- [6] GLÄSER, H., Experience in application of uncertainty methods and review of methods used in licensing, Exploratory OECD meeting of experts on best estimate calculations and uncertainty analysis, Aix-en-Provence, France, 13–14 May (2002).
- [7] D'AURIA, F., GIANNOTTI, W., Development of a code with internal assessment of uncertainty, Nuclear Technology 131 (2000) 159–196.
- [8] SAATY, T., Mathematical Methods of Operations Research, Dover Publications, Inc. (1988).
- [9] ZIO, E., CANTARELLA, M., CAMMI, A., The analytic hierarchy process as a systematic approach to the identification of important parameters for the reliability assessment of passive systems, Nuclear Engineering and Design 226 (2003) 311–336.
- [10] BASSI, C. & MARQUES, M., Reliability assessment of 2400 MW(th) Gas-cooled Fast Reactor natural circulation Decay Heat Removal in pressurized situations, Science and Technology of Nuclear Installations, Special issue “Natural Circulation in Nuclear Reactor Systems”, 2008 (2008).
- [11] BURGAZZI, L., Passive system reliability analysis: a study on the isolation condenser, Nuclear Technology 139 (2002) 3–9.
- [12] SALTELLI, A., et al., Sensitivity Analysis, John Wiley & Sons (2000).
- [13] RUBINSTEIN, R.Y., Simulations and Monte-Carlo method, Wiley Series in Probability and Mathematical Statistics, J. Wiley & Sons (1981).
- [14] MADSEN, H., et al., Methods of Structural Safety, Prentice Hall (1986).
- [15] RACKWITZ, R., et al., Structural reliability under combined random load sequences, Computers and Structures, 9 (1979) 489–494.
- [16] MELCHERS, R.E., Structural Reliability Analysis and Prediction, J.Wiley & Sons (1999).
- [17] DEVICTOR, N., Advances in methods for uncertainty and sensitivity analysis, Proceedings of the Workshop on Level 2 PSA and Severe Accident Management, OECD/NEA/CSNI/WGRISK, Köln, March (2004).
- [18] MARQUÈS, M., PIGNATEL, J.F., D'AURIA, F., BURGAZZI, L., MÜLLER, C., COJAZZI, G., LA LUMIA, V., Reliability Methods for Passive Safety functions, Proceedings of International Conference on Nuclear Engineering (ICONE-10), Arlington, Virginia, USA April 14–18 (2002).

- [19] LORENZO, G., ZANOCCO, P., GIMENEZ, M., MARQUES, M., IOOSS, B., BOLADO-LAVLN, R., PIERRO, F., GALASSI, G., D'AURIA, F., BURGAZZI, L., Assessment of an isolation condenser of an integral reactor in view of uncertainties in engineering parameters, *Science and Technology of Nuclear Installations*, Article ID 827354 (2011).
- [20] MALO, J.Y. et al., The DHR systems of the GFR, preliminary design and thermal-hydraulics studies, *Proceedings of ICAPP'07, Nice, France* (2007).
- [21] DUMAZ, P., ALLEGRE P., BASSI, C., CADIOU, T., CONTI, A., GARNIER, J.C., MALO, J.Y., TOSELLO, A., "Gas-cooled fast reactors—Status of CEA preliminary design studies" *Nuclear Engineering and Design* 237 (2007) 1618–1627.
- [22] MACKAY et al., Incorporating reliability analysis into the design of passive cooling systems with an application to a gas-cooled fast reactor, *Nuclear Engineering and Design* 238 (2008) 217–228.
- [23] FaultTree+V10.1, Copyright Isograph Reliability Software (1986).
- [24] INTERNATIONAL ATOMIC ENERGY AGENCY, Component Reliability Data for Use in Probabilistic Safety Assessment, IAEA-TECDOC-478, IAEA, Vienna (1988).
- [25] KRZYKACZ, B., HOFER, E., KLOOS, M., A software for probabilistic uncertainty and sensitivity analysis of results from computer models, *Proceedings of PSAM II, San Diego, CA, USA* (1994).

LIST OF ABBREVIATIONS

APSR	Assessment of passive system reliability
CFD	Computational fluid dynamics
CHF	Critical heat flux
Coeff.	Coefficient
COV	Coefficient of variance
CP	Collaborative project
CRP	Coordinated research project
DHR	Decay heat removal
DHRS	Decay heat removal system
ET	Event tree
EU	Europe
FORM	First order reliability method
FT	Fault tree
GFR	Gas cooled fast reactor
He	Helium
HTC	Heat transfer coefficient
HX	Heat exchanger
IHX	Intermediate heat exchanger
INPRO	International Project on Innovative Nuclear Reactors and Fuel Cycles
LHS	Latin hypercube sampling
LOCA	Loss of coolant accident
LOFA	Loss of flow accident
MW	Megawatt
NC	Natural circulation
NCDHR	Natural circulation decay heat removal
OAT	One at a time

PCT	Peak clad temperature
PDF	Probability density function
PSA	Probabilistic safety assessment
R&D	Research and development
RMPS	Reliability methods for passive safety functions
SBO	Station blackout
SORM	Second order reliability method
SRC	Standardized regression coefficient
T-H	Thermohydraulic

CONTRIBUTORS TO DRAFTING AND REVIEW

Castelliti, D.	Nuclear Research Centre (SCK-CEN), Belgium
Khartabil, H.	International Atomic Energy Agency
Marques, M.	Atomic Energy Commission (CEA), France
Nayak, A.K.	Bhabha Atomic Research Centre (BARC), India
Qureshi, K.	International Atomic Energy Agency
Subki, H.	International Atomic Energy Agency

Consultants Meetings

Cadarache, France: 16–17 June 2008
Vienna, Austria: 16–17 June 2009
Cadarache, France: 16–18 February 2010
Vienna, Austria: 23–25 November 2010
Vienna, Austria: 13–15 December 2011



IAEA

International Atomic Energy Agency

No. 22

Where to order IAEA publications

In the following countries IAEA publications may be purchased from the sources listed below, or from major local booksellers. Payment may be made in local currency or with UNESCO coupons.

AUSTRALIA

DA Information Services, 648 Whitehorse Road, MITCHAM 3132
Telephone: +61 3 9210 7777 • Fax: +61 3 9210 7788
Email: service@dadirect.com.au • Web site: <http://www.dadirect.com.au>

BELGIUM

Jean de Lannoy, avenue du Roi 202, B-1190 Brussels
Telephone: +32 2 538 43 08 • Fax: +32 2 538 08 41
Email: jean.de.lannoy@infoboard.be • Web site: <http://www.jean-de-lannoy.be>

CANADA

Bernan Associates, 4501 Forbes Blvd, Suite 200, Lanham, MD 20706-4346, USA
Telephone: 1-800-865-3457 • Fax: 1-800-865-3450
Email: customercare@bernan.com • Web site: <http://www.bernan.com>

Renouf Publishing Company Ltd., 1-5369 Canotek Rd., Ottawa, Ontario, K1J 9J3
Telephone: +613 745 2665 • Fax: +613 745 7660
Email: order.dept@renoufbooks.com • Web site: <http://www.renoufbooks.com>

CHINA

IAEA Publications in Chinese: China Nuclear Energy Industry Corporation, Translation Section, P.O. Box 2103, Beijing

CZECH REPUBLIC

Suweco CZ, S.R.O., Klecakova 347, 180 21 Praha 9
Telephone: +420 26603 5364 • Fax: +420 28482 1646
Email: nakup@suweco.cz • Web site: <http://www.suweco.cz>

FINLAND

Akateeminen Kirjakauppa, PO BOX 128 (Keskuskatu 1), FIN-00101 Helsinki
Telephone: +358 9 121 41 • Fax: +358 9 121 4450
Email: akatilauk@akateeminen.com • Web site: <http://www.akateeminen.com>

FRANCE

Form-Edit, 5, rue Janssen, P.O. Box 25, F-75921 Paris Cedex 19
Telephone: +33 1 42 01 49 49 • Fax: +33 1 42 01 90 90
Email: formedit@formedit.fr • Web site: <http://www.formedit.fr>

Lavoisier SAS, 145 rue de Provigny, 94236 Cachan Cedex
Telephone: + 33 1 47 40 67 02 • Fax +33 1 47 40 67 02
Email: romuald.verrier@lavoisier.fr • Web site: <http://www.lavoisier.fr>

GERMANY

UNO-Verlag, Vertriebs- und Verlags GmbH, Am Hofgarten 10, D-53113 Bonn
Telephone: + 49 228 94 90 20 • Fax: +49 228 94 90 20 or +49 228 94 90 222
Email: bestellung@uno-verlag.de • Web site: <http://www.uno-verlag.de>

HUNGARY

Librotrade Ltd., Book Import, P.O. Box 126, H-1656 Budapest
Telephone: +36 1 257 7777 • Fax: +36 1 257 7472 • Email: books@librotrade.hu

INDIA

Allied Publishers Group, 1st Floor, Dubash House, 15, J. N. Heredia Marg, Ballard Estate, Mumbai 400 001,
Telephone: +91 22 22617926/27 • Fax: +91 22 22617928
Email: alliedpl@vsnl.com • Web site: <http://www.alliedpublishers.com>

Bookwell, 2/72, Nirankari Colony, Delhi 110009
Telephone: +91 11 23268786, +91 11 23257264 • Fax: +91 11 23281315
Email: bookwell@vsnl.net

ITALY

Libreria Scientifica Dott. Lucio di Biasio "AEIOU", Via Coronelli 6, I-20146 Milan
Telephone: +39 02 48 95 45 52 or 48 95 45 62 • Fax: +39 02 48 95 45 48
Email: info@libreriaaeiou.eu • Website: www.libreriaaeiou.eu

JAPAN

Maruzen Company Ltd, 1-9-18, Kaigan, Minato-ku, Tokyo, 105-0022
Telephone: +81 3 6367 6079 • Fax: +81 3 6367 6207
Email: journal@maruzen.co.jp • Web site: <http://www.maruzen.co.jp>

REPUBLIC OF KOREA

KINS Inc., Information Business Dept. Samho Bldg. 2nd Floor, 275-1 Yang Jae-dong SeoCho-G, Seoul 137-130
Telephone: +02 589 1740 • Fax: +02 589 1746 • Web site: <http://www.kins.re.kr>

NETHERLANDS

De Lindeboom Internationale Publicaties B.V., M.A. de Ruyterstraat 20A, NL-7482 BZ Haaksbergen
Telephone: +31 (0) 53 5740004 • Fax: +31 (0) 53 5729296
Email: books@delindeboom.com • Web site: <http://www.delindeboom.com>

Martinus Nijhoff International, Koraalrood 50, P.O. Box 1853, 2700 CZ Zoetermeer
Telephone: +31 793 684 400 • Fax: +31 793 615 698
Email: info@nijhoff.nl • Web site: <http://www.nijhoff.nl>

Swets and Zeitlinger b.v., P.O. Box 830, 2160 SZ Lisse
Telephone: +31 252 435 111 • Fax: +31 252 415 888
Email: info@swets.nl • Web site: <http://www.swets.nl>

NEW ZEALAND

DA Information Services, 648 Whitehorse Road, MITCHAM 3132, Australia
Telephone: +61 3 9210 7777 • Fax: +61 3 9210 7788
Email: service@dadirect.com.au • Web site: <http://www.dadirect.com.au>

SLOVENIA

Cankarjeva Založba d.d., Kopitarjeva 2, SI-1512 Ljubljana
Telephone: +386 1 432 31 44 • Fax: +386 1 230 14 35
Email: import.books@cankarjeva-z.si • Web site: <http://www.cankarjeva-z.si/uvvoz>

SPAIN

Díaz de Santos, S.A., c/ Juan Bravo, 3A, E-28006 Madrid
Telephone: +34 91 781 94 80 • Fax: +34 91 575 55 63
Email: compras@diazdesantos.es, carmela@diazdesantos.es, barcelona@diazdesantos.es, julio@diazdesantos.es
Web site: <http://www.diazdesantos.es>

UNITED KINGDOM

The Stationery Office Ltd, International Sales Agency, PO Box 29, Norwich, NR3 1 GN
Telephone (orders): +44 870 600 5552 • (enquiries): +44 207 873 8372 • Fax: +44 207 873 8203
Email (orders): book.orders@tso.co.uk • (enquiries): book.enquiries@tso.co.uk • Web site: <http://www.tso.co.uk>

On-line orders

DELTA Int. Book Wholesalers Ltd., 39 Alexandra Road, Addlestone, Surrey, KT15 2PQ
Email: info@profbooks.com • Web site: <http://www.profbooks.com>

Books on the Environment

Earthprint Ltd., P.O. Box 119, Stevenage SG1 4TP
Telephone: +44 1438748111 • Fax: +44 1438748844
Email: orders@earthprint.com • Web site: <http://www.earthprint.com>

UNITED NATIONS

Dept. I004, Room DC2-0853, First Avenue at 46th Street, New York, N.Y. 10017, USA
(UN) Telephone: +800 253-9646 or +212 963-8302 • Fax: +212 963-3489
Email: publications@un.org • Web site: <http://www.un.org>

UNITED STATES OF AMERICA

Bernan Associates, 4501 Forbes Blvd., Suite 200, Lanham, MD 20706-4346
Telephone: 1-800-865-3457 • Fax: 1-800-865-3450
Email: customercare@bernan.com • Web site: <http://www.bernan.com>

Renouf Publishing Company Ltd., 812 Proctor Ave., Ogdensburg, NY, 13669
Telephone: +888 551 7470 (toll-free) • Fax: +888 568 8546 (toll-free)
Email: order.dept@renoufbooks.com • Web site: <http://www.renoufbooks.com>

Orders and requests for information may also be addressed directly to:

Marketing and Sales Unit, International Atomic Energy Agency

Vienna International Centre, PO Box 100, 1400 Vienna, Austria
Telephone: +43 1 2600 22529 (or 22530) • Fax: +43 1 2600 29302
Email: sales.publications@iaea.org • Web site: <http://www.iaea.org/books>

INTERNATIONAL ATOMIC ENERGY AGENCY
VIENNA
ISBN 978-92-0-139010-3
ISSN 1011-4289